Investigating the role of Huntingtin in development and disease using the zebrafish model organism

A thesis submitted for the degree of Doctor of Philosophy, January 2007

Amanda Lumsden, B. Sc. (Hons)

School of Molecular and Biomedical Science, Discipline of Genetics,
ARC Special Centre for the Molecular Genetics of Development,
The University of Adelaide

Table of contents

List of figures and tables

Declaration

This work contains no material that has been accepted for the award of any other degree or diploma in any university or other tertiary institution and, to the best of my knowledge and belief, contains no material previously published or written by another person, except where due reference has been made in the text.

I give consent to this copy of my thesis, when deposited in the University Library, being available for loan and photocopying.

Amanda Lumsden

Acknowledgements

There are many people that I wish to thank for making this PhD possible and for offering support along the way.

Firstly, thankyou to the Faculty of Science, and the Centre for Molecular Genetics of Development (CMGD), for granting me a scholarship to support my PhD studies. Thankyou also to the Discipline of Genetics, greater School of Molecular Biosciences, and the CMGD for providing a supportive network of knowledge and resources, and a friendly work environment.

I would like to thank Rob Richards for being a wonderful supervisor and role-model, and for giving me the opportunity to pursue my PhD in the fascinating area of Huntington's disease genetics. Thankyou for your encouragement and support, for discussion of ideas, for giving me the freedom to follow my intuition, and for offering invaluable advice. I would also like to thank all the members of the Richards lab (past and present), for thought-provoking discussions, useful tips at the lab bench, and for being a dynamic and fun bunch of people to work with. I would especially like to thank Donna Crack and Rob for constructive advice during the preparation of this thesis, and Sonia Dayan for helping so much with the qPCR assay; your time and effort was greatly appreciated. I am also grateful to Tanya Henshall, for allowing me to present her beautiful western result in this thesis.

To my co-supervisor, Michael Lardelli, thankyou for introducing me to the wonders of zebrafish. Your help and advice was very much appreciated, especially with the initial assessment of the morphant phenotype, discussions of transgene design and scoring of apoptosis levels. I am also sincerely grateful to all the members of the Lardelli Lab for making me feel welcome in their lab, for generously offering advice, reagents, protocols and assistance, and for in-depth discussions of fish matters. In particular, thanks to Ben Tucker, Svanhild Nornes and especially Simon Wells for performing embryo injections for me, often at short notice!

I am very grateful to several other people that have made valuable contributions to this PhD project: Graham Lieschke, for reassuring discussions regarding the blood phenotype, and for confirming that it was an effect worth pursuing; Tim Cox, for suggesting Prussian blue staining as a means of visualising iron; and Steve (Ped) Pederson (statistics guru and great pal), for assistance with analyses of the qPCR data. Special thanks also to Danielle Simmons and the Lynch lab (at UCI), for allowing me to cite their unpublished findings.

I would also like to acknowledge all those who have kept me sane (ish), on a day to day basis. In particular- to Amanda for frequent coffee break debriefs, and for lending a sympathetic ear in trying times; Sonia, for being a great sounding board for ideas (and for our enjoyable singing sessions in the lab!); Alex (Sasch), for introducing the lab to good ol' Uncle Ernie (Ernest Ranglin), and for constantly surprising me with new nicknames; Edwina and Velta, for helping me draw that 'line in the sand'; and Joan Kelly for great advice on all sorts of matters. Thanks to all the other PhD students also, for moral support!

To my friends outside the department, thanks for being so supportive, and for getting my mind off the PhD every now and then, for brunches, coffees…or something stronger when required! I really appreciated it!

Thanks to all the zebrafish embryos that gave up their lives for science research!

Lastly, a very special thanks goes to my loving family for believing in me, and taking an interest in my project. Thanks for your encouragement, and ongoing support, especially during the writing period. Now I can finally say… "it's finished!!"

Abbreviations

aa:	amino acid
ALAS:	5-aminolevulinic acid synthase (as in ALAS1 and ALAS2)
AP:	alkaline phosphatase
ATP:	adenosine triphosphate
BCIP:	5-bromo-4-chloro-3-indolyl phosphate
bp:	base pairs
BSA:	bovine serum albumin
c-aconitase:	cytosolic aconitase
cDNA:	complementary DNA
CHAPS:	3-[(3-cholamidopropyl)dimethylammonio]-1-propanesulfonate
*c*MO:	control MO
DAB:	3,3-diaminobenzidine
Dcytb:	duodenal cytochrome B
DIC:	(Nomarski) differential interference contrast
DMSO:	dimethyl sulfoxide
DMT1:	divalent metal transporter 1
DNA:	deoxyribonucleic acid
dNTP:	deoxynucleoside triphosphate
dpf:	days post fertilisation
DRPLA:	dentatorubral pallidoluysian atrophy
dUTP:	deoxyuridine triphosphate
EDTA:	ethylenediaminetetraacetic acid
EGFP:	enhanced green fluorescent protein
ELT:	Expand Long Template
ES:	embryonic stem (as in ES cells)
Fe:	iron
GABA:	γ-aminobutyric acid
Hb:	haemoglobin
HD:	Huntington's disease
*hd*MO:	MO antisense to *hd* mRNA (as in *hd*MO1 and *hd*MO2)
hpf:	hours post fertilisation
HPLC:	high performance liquid chromatography
Htt:	Huntingtin
ICM:	intermediate cell mass

IPTG:	isopropyl-β-D-thiogalactopyranoside
IRE:	iron responsive element
IRES:	internal ribosomal entry site
IRP:	Iron responsive protein (as in IRP1 and IRP2)
ISC:	Iron-sulfur cluster
kB:	kilobase pairs
kDa:	kilodalton
LB:	luria broth
m-aconitase:	mitochondrial aconitase
*mc*MO1:	mispair control MO
mL:	millilitre
mM:	millimolar
MO:	morpholino oligonucleotide
MQ:	MilliQ
mRNA:	messenger RNA
NBT:	nitro blue tetrazolium chloride
NEB:	New England Biolabs
ng:	nanogram
nL:	nanolitre
NMDA:	*N*-methyl-D-aspartate
ORF:	open reading frame
pA:	polyadenylation
PBS:	phosphate buffered saline
PBST:	phosphate buffered saline plus 0.1% Tween 20
PCR:	Polymerase Chain Reaction
PNRC:	perinuclear recycling compartment
POD:	peroxidase
qPCR:	quantitative PCR
RNA:	ribonucleic acid
rpm:	revolutions per minute
SAP:	shrimp alkaline phosphatase
SBMA:	Spinobulbar muscular atrophy
SCA:	Spinocerebellar ataxia (as in SCA1, SCA2 etc.)
SOC:	Super Optimal Broth plus glucose (originally for catabolite repression)
SSC:	NaCl (salt)/sodium citrate buffer

TBE:	Tris/boric acid/EDTA buffer
TdT:	Terminal deoxynucleotide transferase
Tf:	Transferrin
TfR:	Transferrin receptor
TMR:	Tetramethylrhodamine (as in TMR red)
TUNEL:	Terminal deoxynucleotide transferase (TdT)-mediated dUTP nick-end labelling
UTR:	untranslated region
UV:	ultraviolet light
YE:	yolk extension
X-Gal:	X-galactoside (5-bromo-4-chloro-3-indolyl -β-D-galactoside; BCIG)

Abstract

Huntington's disease (HD) is a dominantly inherited neurodegenerative disorder of typically mid-life onset, for which there is currently no cure. HD is one of nine neurological disorders caused by the expansion of a CAG trinucleotide repeat that encodes an extended polyglutamine tract within the respective disease proteins (which, in the case of HD, is Huntingtin). Curiously, despite these proteins having mostly widespread patterns of expression in the brain, a specific subset of neurons is preferentially affected in each disease, whilst other neurons also expressing the mutant protein are relatively unaffected. Furthermore, although the expression patterns of these disease proteins often overlap in distribution within the brain, the population of neurons that is most vulnerable differs from one disease to the next. Knowledge of what determines the specificity of neuronal vulnerability is likely to provide insight into the molecular mechanism(s) underlying the pathology in these diseases.

The aim of this work was to use the zebrafish model organism to investigate two factors hypothesised to contribute to the specificity of neuronal vulnerability in HD: 1) region-specific somatic expansion of the disease allele, and 2) disruption of normal Huntingtin (Htt) protein function. The most significant findings of this study resulted from the investigation into the normal function of Htt. Antisense morpholino oligonucleotides were used to specifically knock down Htt expression in early zebrafish development, resulting in a wide variety of developmental defects. Most notably, Htt-deficient zebrafish had pale blood due to a decrease in haemoglobin production, despite the presence of (apparently unavailable) iron within these cells. Provision of additional iron in a bio-available form to the cytoplasm restored haemoglobin production in Htt-deficient embryos. Since blood cells acquire iron via receptor-mediated endocytosis of transferrin, these results suggest a role for Htt in the release of iron from endocytic compartments into the cytosol.

Iron is required for the function of many cellular proteins and enzymes that play key roles in oxidative energy production. Disrupted iron homeostasis and decreased energy metabolism are features of HD pathogenesis that correlate to the major sites of degeneration in the HD brain. The findings of this study raise the possibility that perturbation of normal Htt function (by polyglutamine expansion) may contribute to these defects, thereby providing a novel link between Htt function and specificity of neuronal vulnerability in HD.

Chapter 1: Background

Huntington's disease

Huntington's disease (HD) is a devastating neurodegenerative disorder that is dominantly inherited, and affects approximately 5 to 10 in 100,000 people of European descent (1). The age of onset usually occurs in the late 30's to 40's, but may occur anywhere between childhood and old age. The disease begins insidiously with subtle symptoms and progresses without remission for 15 to 20 years, eventually leading to premature death due to secondary complications. Characteristic features of HD include progressive development of choreiform (sudden, irregular and purposeless) involuntary movements, deterioration of cognitive and intellectual abilities, psychiatric disturbances, and weight loss despite adequate dietary intake. Neurological symptoms are associated with dramatic neuronal cell loss, primarily affecting the striatum and deeper layers of the cerebral cortex. Occasionally the disease presents in the first two decades (juvenile onset HD), in which case neuropathology is more widespread and disease progression is typically more rapid, with more severe symptoms, including rigidity, dementia and epileptic seizures, but little or no chorea. The order in which clinical symptoms manifest differs between HD-affected individuals, even within a given family. Whilst therapeutic drugs can help manage some of the symptoms of HD, currently there are no treatments available to cure or slow the progression of this relentless disease.

Genetics of HD

The gene that is affected in HD (*interesting transcript 15* (*IT15*), or the *HD* gene) was identified in 1993 (2). The *HD* gene encompasses 67 exons spanning 180 kb on chromosome 4p16.3 (2, 3). Structural analysis of the *HD* promoter region is in accordance with *HD* being a housekeeping gene (4). Two alternate transcripts of approximately 10.3 and 13.7 kb that differ only in the length of their 3' untranslated region (5), encode the particularly large huntingtin protein, comprised of ~3144 amino acid residues and having an approximate molecular weight of 348 kDa (2). *HD* gene products are widely expressed in both neural and somatic tissues throughout the body (5-11).

Note that in zebrafish nomenclature, the first letter of Huntingtin is capitalised. Since the current work focuses on the zebrafish homologue, in this thesis dissertation all further references to the Huntingtin protein (Htt) will be capitalised, irrespective of

species, for simplicity. Gene nomenclature will be species-specific (for example, *HD* in human, *Hdh* in mouse, *rhd* in rat, *hd* in zebrafish), or referred to collectively as *HD* gene homologues.

Within the coding region of *HD* exon 1 is a CAG trinucleotide repeat encoding a stretch of consecutive glutamine residues known as a polyglutamine repeat, beginning at residue 18 of the Htt protein (2). The CAG repeat contains no interruptions, and in the normal population is highly polymorphic in length. HD results from the abnormal expansion of this repeat tract to lengths above the normal range. Normal alleles contain between 6 and 39 CAG copies (1), and disease alleles contain copy numbers between 36 and ~250 repeats (1, 12), although alleles containing greater than 80 copies are rare. The overlap between normal and disease ranges (36-39 copies) indicates an intermediate range of reduced penetrance within which some individuals develop HD and others do not (13), whilst alleles containing 40 or more repeats have complete disease penetrance (1). Larger alleles are associated with earlier age of onset, with lengths greater than 55 repeats frequently causing juvenile onset HD. Interestingly, disease duration and clinical presentation appear to be independent of CAG repeat number (14). The expanded repeats are unstable in length and tend to further increase in size upon transmission from one generation to the next (particularly via the paternal germline), leading to an earlier age of onset in subsequent generations - a phenomenon known as ‘genetic anticipation’. The expanded alleles are also commonly unstable within somatic tissues, leading to mosaicism of repeat length within an individual (15).

Whilst repeat number is the best predictor available for estimating age of onset in HD, there is still considerable variability in onset age for any given repeat number, suggesting that other factors influence onset age. An estimated 60% of this variance is due to environmental effects, whilst an estimated ~40% is attributable to genetic modifiers (genes other than the *HD* gene) (16).

HD neuropathology

HD neuropathology is characterised by a striking loss of neurons in the caudate nucleus and putamen of the neostriatum (17), an area deep within the brain, that is part of the basal ganglia. The basal ganglia, (a region that also encompasses the globus pallidus, substantia nigra and subthalamic nucleus) receives information from all parts of the cerebral cortex, and returns inhibitory signals back to the motor cortex, the part of the brain that dictates movement. Normally, smooth, coordinated body motion is maintained by a balance between these inhibitory signals from the basal ganglia, and

excitatory signals from the cerebellum (18). In HD, this balance is disrupted by the loss of striatal neurons, leading to hyperactivity of the motor cortex. Whilst this can explain the involuntary movements associated with HD, it is less clear what determines the cognitive and psychiatric aspects of the disease.

The striatum is predominantly made up of medium spiny projection neurons that utilise the inhibitory neurotransmitter, γ-aminobutyric acid (GABA). The striatum, considered the gateway to the basal ganglia, receives most of its input from the cortex as glutamatergic efferents and sends most of its GABAergic output to the globus pallidus, from where the circuit continues to the thalamus and back to the motor cortex (18). The striatum is also interconnected with the dopamine-rich substantia nigra; the substantia nigra receives GABAergic efferents from the striatum and sends information back to the striatum via dopaminergic projections (Fig. 1.1).

Within the HD striatum, the earliest signs of cell loss appear in the dorsomedial caudate and dorsal putamen, and in the most severe cases, up to 95% of cells in the caudate nucleus are lost (17). However, not all striatal neurons are affected to the same extent; the GABAergic striatal projection neurons are most sensitive to degeneration in HD (17, 19). The gradual and selective depletion of these cells is accompanied by gliosis (17). Affected striatal neurons display abnormal features such as recurvature of dendrites and altered density and morphology of spines (19), suggesting that cellular dysfunction precedes cell death.

Among the GABAergic neurons, the enkephalin-rich neurons projecting to the external segment of the globus pallidus are most sensitive, followed by substance P-rich neurons projecting to the substantia nigra. Substance P-rich neurons projecting to the internal segment of the globus pallidus appear to be the least vulnerable, however in late stages of HD extensive depletion of all striatal projection neurons is seen (20-25) (Fig. 1.1).

Marked reductions in expression of cannabinoid, dopamine and adenosine receptors are evident in the striatum and globus pallidus from very early stages of HD, prior to obvious cell loss (25, 26) and a loss of *N*-methyl-D-aspartate (NMDA) receptors has been observed in putamen samples from HD patients (27), and even in a pre-symptomatic patient (28). That these receptor changes occur prior to major cell loss further supports the idea that neuronal dysfunction precedes cell death.

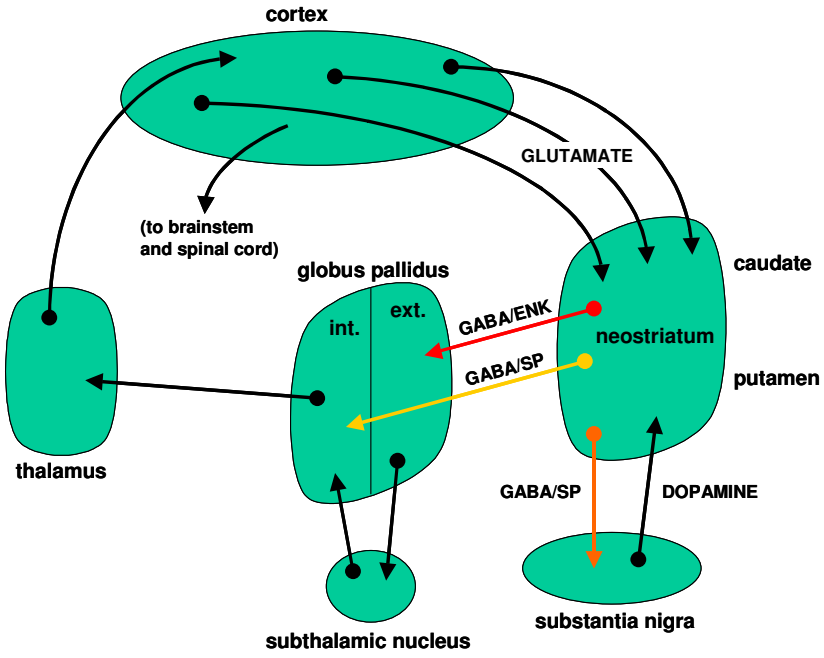

Figure 1.1 The striatal and cortical connections relevant to HD pathology. Adapted from references (18, 29). GABAergic striatal neurons that project to the globus pallidus and substantia nigra are most affected in HD. Of these, the enkephalin (ENK)-rich neurons projecting to the external segment (ext.) of the globus pallidus are most vulnerable (red), followed by substance P (SP)-rich neurons projecting to the substantia nigra (orange), whilst SP-rich neurons projecting to the internal segment (int.) of the globus pallidus (yellow) appear to be the least vulnerable of these projection neurons (refs (20-25)).

Intriguingly, a small subset of neurons that make up only a small percentage of striatal volume is remarkably resistant to degeneration. These neurons include large cholinergic interneurons, and aspiny interneurons containing nicotinamide adenine dinucleotide phosphate diaphorase (NADPH-d), somatostatin and neuropeptide Y (30).

Although HD atrophy is most evident in the striatum, considerable shrinkage and thinning of the cortex is also seen (31, 32). Neuronal loss is observed in the deeper cortical layers (III, V and VI), particularly affecting large pyramidal neurons (33-37). It is unclear whether the cortical neurons die as a consequence of striatal defects or independently in a parallel process.

Whilst the striatum and cortex are most affected in HD, neuronal loss has also been observed in the hypothalamus (38), cerebellum (39-41) and hippocampus (42) and a reduction in size of the amygdala and thalamus have been seen (32). Generally the extent of degeneration is most widespread in severe, juvenile onset cases (39). In summary, a hierarchy of neuronal vulnerability exists in the HD brain, with the most dramatic cell loss evident in the caudate nucleus and putamen of the striatum. One of the most pressing questions in the field of HD research is what determines the selective

vulnerability of the striatum, and in particular, the GABAergic medium spiny projection neurons.

Energetic defects, excitotoxicity and oxidative damage in HD

The mechanism by which expanded Htt initiates the gradual demise of specific neurons is unclear. However, signs of decreased energy metabolism, excitotoxicity and oxidative stress are all evident in the HD brain, and correlate well with affected regions suggesting that these detrimental pathways may contribute to the pathogenic process.

In the HD striatum, decreased glucose metabolism is observed prior to the bulk of cell loss (and clinical symptoms) (43-45), therefore representing one of the earlier events in HD pathogenesis, and further supporting the notion that cellular dysfunction precedes cell loss. Indications of decreased oxidative respiration are evident in this region, including reduced activities of the citrate cycle enzyme, aconitase (46), and mitochondrial respiratory complexes II-IV (47, 48). Consistent with these findings, decreased striatal oxygen consumption (49) and increased lactate concentrations in the basal ganglia and occipital cortex (50, 51) have also been reported. For a more detailed overview of metabolic defects in HD, see reference (52). Currently the underlying cause of these energetic deficits is unknown, however a role for decreased energy metabolism in HD aetiology is suggested by findings that 3-nitroproprionic acid (3-NP) leads to HD-like striatal lesions. 3-NP is an irreversible inhibitor of succinate dehydrogenase (mitochondrial complex II), an important component of the citrate cycle and oxidative phosphorylation pathway. Systemic administration of low doses of 3-NP to animals causes selective striatal lesions associated with decreased ATP levels and elevated lactate concentrations (see for review (53)).

Decreased energy metabolism lowers the threshold at which glutamate, an excitatory amino acid, becomes toxic to neurons (54). The striatum receives most of its input as glutamatergic efferents from the cortex, and it has been proposed that excitotoxicity may be one mechanism by which reduced energy levels could lead to neuronal cell death (52, 55). Excitotoxicity refers to the over-stimulation and consequent damage of neurons by over-activation of excitatory neurotransmitter receptors, and is essentially associated with an excessive increase in intracellular calcium (Ca^{2+}) ions. The hypothesis that excitotoxicity is involved in HD is supported by findings that intracranial injection of other excitatory amino acids such as quinolic acid (a tryptophan metabolite that selectively activates the NMDA receptor) in animals leads to HD-like neuropathology in the striatum, with sparing of aspiny neurons (56-58).

Numerous signs of oxidative stress are also evident in affected areas of the HD brain, including increased lipid peroxidation, greater occurrence of DNA strand breaks and stronger immunohistochemical staining of oxidative damage products (59). The correlation of these markers with sites of pathology suggests that oxidative damage may be another factor contributing to neuronal cell death, although what underlies this oxidative damage has not been elucidated. Several studies have reported abnormal accumulation of iron in HD affected brain regions; either specifically in the striatum (60, 61), or in striatal and globus pallidal tissues (62-64). Due to the potential for iron to generate free radicals, iron accumulation presents a potential cause of oxidative stress. Iron accumulation and oxidative stress are also associated with regions of brain pathology in a number of other neurodegenerative disorders (65). Another possibility is that the oxidative damage observed in the HD brain results from energetic defects, or as a consequence of excitotoxicity (52).

Whilst disrupted energy metabolism, excitotoxicity, oxidative stress and iron accumulation all represent factors that may contribute to HD pathology it remains to be determined which are primary, causative effects and which are secondary events in disease progression. It is also unclear how expanded mutant Htt triggers these effects.

HD is a member of the polyglutamine disease family

HD is the most common of nine neurodegenerative disorders in which the underlying genetic cause is the abnormal expansion of a CAG repeat encoding polyglutamine within in the associated disease protein (Table 1.1). The other members of this group of 'polyglutamine diseases' are spinocerebellar ataxias (SCAs) 1, 2, 3, 6, 7 and 17, dentatorubral pallidoluysian atrophy (DRPLA) and spinobulbar muscular atrophy (SBMA) (66, 67)(Table 1.1). The proteins in which the polyglutamine tracts reside share no other homology and appear to be functionally unrelated. In three of these diseases the repeat resides within proteins whose functions are well established; the androgen receptor in SBMA (68), the α1A subunit of the voltage-dependent P/Q type calcium channel in SCA6 (69), and the TATA-binding protein in SCA17 (66). In the other diseases, the repeats lie within novel genes whose functions are gradually being elucidated. The polyglutamine diseases fall within a broader category of inherited unstable repeat expansion disorders that also encompasses diseases where the repeat lies within non-coding DNA sequence of the affected gene (70).

Polyglutamine disease	Normal (CAG)n	Expanded (CAG)n	Gene product	Protein function	Most affected brain regions
HD	6-39	36-250	Huntingtin	Novel	Striatum, cerebral cortex
SBMA	9-36	38-62	Androgen receptor	Testosterone binding, transcription factor	Anterior horn and bulbal neurons, dorsal root ganglia
DRPLA	6-36	49-88	Atrophin-1	Novel	Cerebellum, cerebral cortex, basal ganglia, Luys body
SCA1	6-44*	39-82	Ataxin-1	Novel	Cerebellar Purkinje cells, dentate nucleus, brainstem
SCA2	15-31^{+}	36-63	Ataxin-2	Novel	Cerebellar Purkinje cells, brainstem, fronto-temporal lobes
SCA3	12-41	55-84	Ataxin-3	Novel	Cerebellar dentate neurons, basal ganglia, brainstem, spinal cord
SCA6	4-18	21-33	CACNA1A	α1A subunit of voltage-dependent P/Q type calcium channel	Cerebellar Purkinje cells, dentate nucleus, inferior olive
SCA7	4-35	37-306	Ataxin-7	Novel	Cerebellum, brainstem, macula, visual cortex
SCA17	27-42	47-55	TATA binding protein	Transcription factor	Striatum, cerebral cortex, thalamus, cerebellar Purkinje cells

Table 1.1 Polyglutamine diseases known to be caused by the expansion of CAG repeat tracts within the coding region of genes encoding unrelated proteins. *Normal SCA1 alleles with greater than 20 repeats are interrupted by 1 to 4 CAT units. $^{+}$Normal SCA2 alleles are frequently interrupted by 1 to 3 CAA units. For references see (12, 13, 66, 67).

Common features of polyglutamine diseases

The underlying genetic cause of HD and other polyglutamine disorders is clearly the expansion of the CAG repeat, however the mechanism by which the resulting polyglutamine repeat exerts its toxicity in each disease is unclear. The diseases share a number of common features, leading to the suggestion that there might be a common unifying pathogenic pathway involved in some, or even all of them. Firstly, despite the affected proteins being apparently unrelated and sharing no common domains outside the polyglutamine tract, all of these diseases are progressive neurodegenerative disorders and have overlapping (although distinct) arrays of clinical symptoms (67).

Secondly, the polyglutamine diseases are inherited in a dominant manner (except SBMA which is X-linked) suggesting that the expanded repeat confers a toxic gain-of-function upon the disease protein. Thirdly, there is a similar disease copy number threshold, with inherited copy numbers less than 35 generally falling in the normal allele range, and copy numbers greater than 40 repeats causing disease (Table 1.1). An exception to this general 'rule' is SCA6 that has a lower pathogenic threshold of 21 repeats. Fourthly, an inverse correlation exists between repeat copy number and age of onset, with juvenile onset cases being associated with the largest repeats. Lastly, these diseases are subject to genetic anticipation due to repeat instability, whereby disease tends to be more severe or have an earlier age of onset in subsequent generations, especially through paternal transmission.

Polyglutamine gain-of-function hypothesis

The common features of polyglutamine diseases suggest that the expanded polyglutamine repeat imparts a toxic function upon the affected protein. Early evidence to support this hypothesis was provided by the first transgenic mouse model of HD (71). These mice express a transgene containing the promoter and first exon of the human *HD* gene with CAG repeats of lengths that would cause juvenile onset HD in humans (115-150 copies). Even though these mice expressed the polyglutamine tract in a severely truncated Htt fragment, they developed progressive HD-like symptoms including involuntary movements, seizures, weight loss and brain atrophy leading to premature death after 3 to 4 months (71). Further evidence that an expanded polyglutamine tract was sufficient to cause a progressive neurological phenotype came from another study, where expression of an expanded polyglutamine tract of 146 repeats within the unrelated mouse *hypoxanthine phospho-ribosyltransferase* gene (that is not associated with polyglutamine diseases or neurodegeneration) was able to produce a similar progressive neurological phenotype involving ataxia, seizures and early death (72). Subsequently, expression of disease length polyglutamine repeats has been shown to cause cellular dysfunction and cell death in all other model systems tested, including nematode (73), zebrafish (74), *Drosophila* (75, 76), yeast (77), and cultured neurons (78), illustrating the intrinsically toxic nature of expanded polyglutamine repeats.

The relationship between repeat copy number and disease onset/severity is also observed in transgenic mouse models of HD (71, 72, 79, 80). In general, larger repeats lead to earlier onset of neurological phenotype, and more premature lethality. The size

of the peptide backbone in which the polyglutamine tracts are expressed also appears to have an effect on this correlation, such that a repeat of given disease length copy number is more toxic when expressed within a short fragment, than in a fragment of greater length (81). This also holds true in a *Drosophila* polyglutamine disease model, where for a given disease-length repeat number, age at lethality is higher when the repeat is expressed in a longer protein context, than it is when it is expressed in a truncated fragment (82).

Inclusions/aggregates: causative, consequential, or innocent bystanders?

Another common feature of the polyglutamine diseases is the presence, within patient tissue, of neuronal inclusions. Such inclusions were first discovered in the nucleus and processes of neurons in expanded exon 1 transgenic mice (83). The finding that these inclusions, which stain positively with antibodies against ubiquitin or the N-terminal of Htt, occurred prior to signs of disease and were absent in brain tissue from mice expressing a similar transgene with only 18 CAG repeats, suggested that these inclusions may play a causative role in the pathogenic process (83). Similar inclusions were subsequently found within neurons and dystrophic neurites in the striatum and cortex of post-mortem human HD brain samples (84, 85), but not in the (relatively unaffected) globus pallidus or cerebellum (86), thus seemingly correlating, at least at the regional level, with the pattern of HD neuropathology. Inclusions have now been found in all other polyglutamine diseases, although whether the inclusions localise to the nucleus, cytoplasm, or both, depends on the polyglutamine disease. The hallmark presence of inclusions in these diseases offered further support to the unifying toxic polyglutamine hypothesis.

At the biochemical level, these inclusions are believed to be due to the propensity for expanded repeat proteins to form insoluble aggregates. *In vitro*, Htt fragments containing repeat lengths greater than 40 are insoluble, whilst fragments containing smaller repeats (in the non-pathogenic range) are soluble (87), thus providing an interesting correlation of this change in solubility with the approximate repeat copy number threshold of polyglutamine disease pathogenesis. Further evidence that expanded polyglutamine tracts alter the physical properties of the host protein is that expanded repeats cause Htt to migrate disproportionately on SDS PAGE gels (88), and alter immunoreactivity with specific monoclonal reagents (89-91)

Investigations into the toxic nature of polyglutamine aggregates and attempts to suppress their formation, however, have yielded conflicting results depending on the

model system and manipulations employed. Consequently there has been much controversy regarding whether the aggregates are indeed pathogenic, whether they are protective against disease, or whether they are merely innocent bystanders in the pathogenic process (for reviews see references (92, 93)). Compelling evidence against aggregates being the initiating pathogenic trigger in these diseases comes from the finding that, at the cellular level, the presence of inclusions does not correlate well with neuronal cell death. Cell death can occur without the formation of inclusions, and inclusions can exist without cell death (93). For example, in the HD striatum, inclusions occur more frequently in large interneurons than in the more affected medium spiny neurons (94). Furthermore, time lapse imagery of cultured neurons using automated microscopy has revealed that cells that form inclusions appear to clear the cytoplasm of mutant Htt, and have a reduced likelihood of dying (78). Whilst aggregates may contribute in some way to polyglutamine disease progression, it appears that they are not the primary pathogenic agent in these diseases.

What determines the specificity of neuronal vulnerability?

Expanded polyglutamine repeats appear to be inherently toxic in nature, with their over-expression causing cellular dysfunction and cell death in all model systems tested. It is thus intriguing that in the human polyglutamine disorders, despite the disease proteins having mostly widespread and overlapping patterns of endogenous expression, only a subset of neurons expressing the mutant protein is most prone to degeneration, while other neuronal cell types also expressing the mutant protein are less affected or relatively spared. For example, in HD, although Htt is expressed throughout the brain, greatest cell loss is found in the striatum and cortex. Furthermore, a different hierarchy of susceptibility to neuronal degeneration exists from one disease to the next (Table 1.1) as reflected in the variable clinical features of these diseases. In SCA1, a disease primarily affecting the cerebellar Purkinje cells, the disease-causing polyglutamine repeat resides in the widely expressed ataxin 1 protein. The fact that ataxin 1 and Htt are each expressed in both the striatal and Purkinje cells, and yet in HD polyglutamine expansion affects the striatum (and not the cerebellum), and in SCA1 polyglutamine expansion affects the cerebellar cells (leaving the striatum relatively unaffected) indicates that it is not simply expression of expanded polyglutamine tracts that causes pathology. What determines the unique specificities of neuronal vulnerability in these and other polyglutamine diseases is likely to be mediated by the different protein contexts in which the polyglutamine tracts reside (95, 96). In support of

this, mouse models of HD in which the expanded repeats are expressed within the context of the full-length Htt protein (79, 80) generally show selective neurodegeneration more closely resembling the human disease than models where the repeats are expressed within a truncated Htt fragment or ectopically within the unrelated HPRT protein (71, 72).

There is increasing evidence that unique attributes of the host proteins are critical for neurodegeneration. For example, in SCA1, neurodegeneration is dependent upon the phosphorylation of a serine residue within the mutant protein, ataxin-1 (97). In SBMA, nuclear translocation of the mutant androgen receptor upon binding of its ligand, testosterone, is required for neurodegeneration (98). In fact this disease, which presents only in males, may actually be dominantly inherited, with females being protected due to their low testosterone levels (99).

In some cases where the normal function of the affected protein is known, there is evidence that polyglutamine expansion causes a disruption of this normal function. For example, in SCA6 the polyglutamine expansion perturbs the function of the calcium channel subunit in which it resides (100, 101), and the symptoms of this disease resemble those of other channelopathies unrelated to polyglutamine (102). Loss of normal protein function is also observed in SBMA, where affected males often show signs of androgen insensitivity due to disrupted function of the androgen receptor (103). However, individuals with a reduction in androgen receptor activity due to non-polyglutamine related mutations do not experience neurodegeneration (104), suggesting that the expanded polyglutamine repeat contributes to the neurodegenerative aspect of the disease.

There are a number of possible pathogenic mechanisms that could hypothetically explain both the dominant inheritance and selective neuronal vulnerabilities of the polyglutamine diseases (95, 96). For example, one possibility is that polyglutamine is the pathogenic agent in some/all of these diseases, but that post-translational processing mediated by unique amino acid sequences of the affected protein (outside of the repeat) are required for the expanded repeat to exert its toxicity. If this were the case then the selective neuronal vulnerability might be due to tissue/cell-specific processing, or alternatively, to particular sensitivity of certain neurons to the processed, polyglutamine-containing peptide. Another possibility is that rather than the polyglutamine repeat itself being toxic, the expanded repeat may alter wildtype protein function, thus perturbing the molecular pathway(s) in which each normally participates, in a dominant manner that is deleterious to the cell. This may be by enhancing or decreasing normal protein function, altering interactions with the protein's normal

binding partners and/or cellular components, or by facilitating novel interactions that have detrimental consequences for the cell. Specificity of neurodegeneration could therefore be determined by the differential sensitivity of neurons to this abnormal function. Given that outside the polyglutamine repeat, the affected proteins appear to be unrelated, this latter hypothesis suggests that the initial event that triggers the disease process would be different in each disease. These gain- and loss-of-function mechanisms are not mutually exclusive. For example it is possible that partial loss or disruption of normal protein function could render certain cells more vulnerable to polyglutamine-mediated toxicity. Conceivably, a different combination of mechanisms may contribute to pathogenesis in each disease. In any case, further knowledge of the normal functions of the proteins associated with these diseases, and the biological processes within which they belong would appear likely to increase our understanding of the pathogenic mechanism(s) involved in these diseases.

Huntingtin function and HD

Htt is a soluble protein of ~3144 amino acids with limited similarity to any other known protein. Although significant advances in knowledge of Htt function have been made in the past thirteen years since the discovery of the *HD* gene, the exact biological function of this protein remains elusive. Htt has been implicated in a large variety of cellular processes including apoptosis, endocytosis, vesicle trafficking, transcriptional regulation, and dendrite formation (See for recent reviews, (105, 106)) but as yet no aspect of its function has been revealed whose disruption (by polyglutamine expansion) could account for the hierarchy of neuronal vulnerability observed in the HD brain.

Ubiquitous expression of HD gene products in the body

Htt protein and mRNA transcript are widely expressed throughout the body with particular enrichment in neural tissues (5-11) and testes (8, 107). Htt expression is not enriched in the striatum, either in the adult brain (6-8, 11, 108), or during foetal development (109), and the disease-causing repeat expansion does not significantly alter the pattern of expression in HD-affected tissue, apart from a reduction of expression in the striatum related to cell loss (6, 11, 88, 108). This suggests that factors other than the expression levels of expanded mutant Htt contribute to the unique pattern of neurodegeneration characteristic of HD. The widespread expression of Htt from early

development to adulthood suggests that this protein plays a ubiquitous role that is not limited to neurons.

Huntingtin is essential for development and plays a pro-survival role

Htt function is essential in development since homozygous inactivation of the *HD* homologue in mouse (*Hdh)* causes embryos to become developmentally delayed and disorganised, leading to embryonic lethality from 7.5 days of gestation, prior to development of the neural system (110-112). The cause of embryonic lethality is not clear, however homozygous null embryos exhibit an increase in the number of cells exhibiting morphological signs of programmed cell death (110, 111) and increased apoptosis has been confirmed using TdT-mediated dUTP-nick-end labelling (TUNEL) (110). These findings suggest that Htt may play a pro-survival role. This is supported by an *in vitro* study in which transfected cells were protected from apoptotic stress by over-expressing wildtype Htt (113). Another study suggests that a deficit in the transport of maternal nutrients into the developing blastocyst across the visceral endoderm is responsible for the early lethality (114).

In contrast to the knockout mouse phenotype, hemizygous mice with only a single active *Hdh* allele ($Hdh^{+/-}$) are born and develop similarly to wildtype littermates in two mouse models (110, 111). In a third model, hemizygous mice display cognitive deficits and enhanced motor activity (112), associated with neuronal cell loss in the basal ganglia but sparing the striatum (115). Notably, it is possible that the aberrant phenotype/neuropathology in this latter model may be caused by a dominant negative effect of expression of a 20 kDa N-terminal fragment of Htt resulting from the genetic inactivation method employed (112). The fact that signs of a progressive HD-like phenotype were not observed in hemizygous mice (at least within the time frames examined) suggests that expansion of the polyglutamine tract does not cause HD simply by inactivating the normal function of the affected allele. Furthermore human subjects with a hemizygous deletion spanning the *HD* gene do not develop HD symptoms (116), and individuals homozygous for an expanded allele do not display embryonic lethality, but instead are born, undergo normal development and have a phenotype similar to heterozygotes (117, 118). Thus it would appear that the HD mutation does not cause disease through haplo-insufficiency or a dominant negative loss of function although the possibility that partial loss, or alteration, of function contributes to disease pathogenesis cannot be ruled out.

A hypomorphic *Hdh* allele that was serendipitously created during the generation of a knock-in mouse model of HD, expresses Htt at approximately one third of wildtype

levels (91). Mice homozygous for this hypomorphic allele exhibit severe cranial and brain abnormalities, leading to death around the time of birth. Whilst this hypomorphic allele actually contains 50 CAG repeats (within the pathogenic range in humans), the developmental abnormalities described in this mouse model are unlikely to be due to the expanded repeat because mice expressing this expanded allele at wildtype levels had no developmental phenotype (91). Taken together these Htt deficiency studies indicate a dose-dependent response to Htt levels in development, such that 50% levels (in hemizygotes) are sufficient for normal development, but levels less than 50% have dire detrimental consequences.

In an effort to circumvent the early lethality of homozygous inactivation and observe later effects of Htt deficiency, one group engineered a mouse model that allowed conditional inactivation of the *Hdh* gene postnatally in the forebrain and testis (119). Postnatal inactivation of *Hdh* expression caused cellular dysfunction and cell loss in these regions, and the neural atrophy was associated with motor phenotypes and premature death (119). This indicates that Htt is essential for the viability of neurons (and testicular function), although results from an *in vitro* study suggest that Htt is not required for the differentiation of embryonic stem cells into functional neurons (120). Additionally, Htt-deficient embryoid body cells (derived from $Hdh^{-/-}$ embryonic stem cells) can differentiate into haematopoietic progenitors, but Htt appears to be required for their subsequent proliferation and survival (121).

In another study designed to bypass the lethality that results from homozygous inactivation of the *Hdh* gene, chimeric mouse embryos (created by the injection of knockout ($Hdh^{-/-}$) embryonic stem cells into wildtype host blastocysts) were allowed to develop to adulthood and then colonisation of the $Hdh^{-/-}$ cells within the brain was examined (122). Whilst $Hdh^{-/-}$ neurons were found to be distributed throughout the brains of these chimeric animals, they occurred 5 to 10 times more frequently in the hypothalamus, midbrain and hindbrain than the telencephalon and thalamus. These findings indicate that Htt-deficient neurons are able to survive in the adult mouse brain to some extent, but suggest that certain neuronal cell types may be more dependent upon Htt function for proliferation/survival than others. Interestingly, the striatum lies within the (less colonised) telencephalon, suggesting that striatal neurons may be more susceptible to a slight loss of wildtype function in HD than other areas of the brain.

Evidence suggesting that perturbation of normal Htt protein function might contribute to HD pathogenesis

Detrimental consequences of the expression of expanded Htt have been shown to be exacerbated on a background of reduced wildtype Htt levels, whilst increased expression of wildtype Htt appears to counter the effects of expanded mutant Htt (123-125). The ability of wildtype Htt to modulate the effects of expanded Htt suggests that disruption of Htt function may play a role in HD pathology. Furthermore, the colonisation study described earlier in which *Hdh*$^{-/-}$ embryonic stem cells showed decreased survival/proliferation in the mouse forebrain in comparison to other brain regions (122), suggests that perturbation of Htt function may contribute to the specificity of HD neurodegeneration.

Intracellular localisation of Htt, and the effect of Htt depletion on organellar distribution

At the intracellular level, Htt is mostly found in the cytoplasm where it is concentrated in the perinuclear region (126, 127), although it has also been detected in dendrites and nerve endings (128, 129) and within the nucleus (130-133). The Htt protein associates with various cellular structures and organelles including the plasma membrane, clathrin-coated and non-coated vesicles, endosomes, endoplasmic reticulum, Golgi complex, mitochondria, and microtubules (9, 126, 128, 134-138). This wide variety of associations and lack of distinct compartmentalisation does not make the role of Htt immediately clear.

In one study, a panel of markers and antibodies was used to observe the effect of Htt deficiency on the distribution of organelles in *Hdh*$^{-/-}$ mouse embryonic stem cells (139). This study revealed a requirement of Htt for the correct distribution of nucleoli, transcription speckles, mitochondrial clusters, endoplasmic reticulum, Golgi complex and recycling endosomes. Moreover, the levels of transferrin receptor were up-regulated in *Hdh*$^{-/-}$ cells, and further investigation showed that Htt levels were increased in wildtype cells in response to iron chelation. These findings implicated Htt in a variety of processes including RNA biogenesis, intracellular trafficking and iron homeostasis (139).

Functional clues from evolutionary conservation

Some insight into the function of Htt and the biological pathway(s) in which it interacts may be gained from studying its phylogenetic profile (Figure 1.2). Homologues

of the *HD* gene have been identified in vertebrates from fish to man (2, 140-144). A putative homologue has been isolated in the invertebrate, *Drosophila melanogaster* (fly) (145), and partial sequences similar to the C-terminal region of vertebrate Htt have been identified in the ascidian *Halocynthia roretzi* (sea squirt, a basal chordate), and echinoderms *Strongylocentrotus purpuratus* and *Heliocidaris erythrogramma* (sea urchins, basal deuterostomes) (146). A predicted protein (Accession No: AAS38622) with similarity to human Htt has been found in *Dictyostelium discoideum* (soil-dwelling amoeba), thus existing prior to the protostome/deuterostome divergence and representing the earliest homologue identified so far. A gene with similarity to the *HD* gene has not been identified in either *Saccharomyces cerevisiae* (yeast) or *Arabidopsis thaliana* (thale-cress plant). Interestingly, *Caenorhabditis elegans* (nematode worm) also does not appear to have a homologue, which suggests that Htt was lost in the divergence of this lineage.

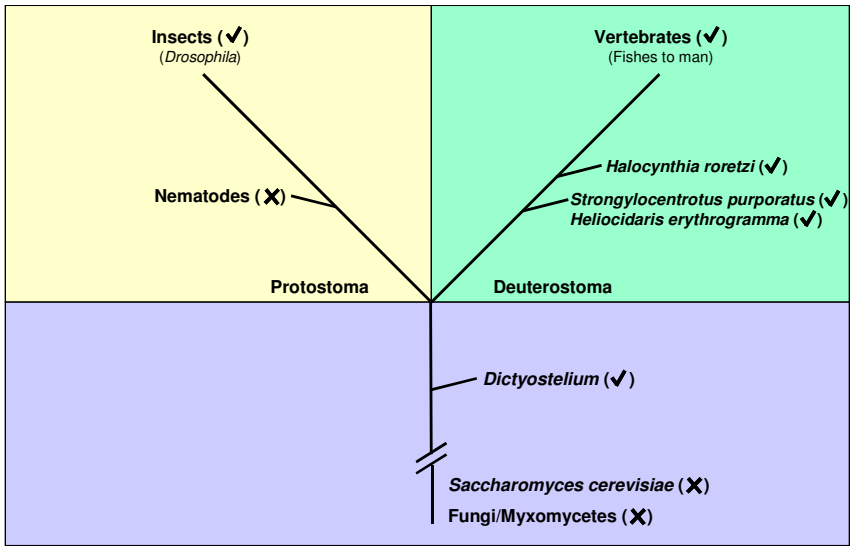

Figure 1.2 Phylogeny showing the evolutionary conservation of the *HD* gene. Adapted from reference (105). Ticks and crosses indicate presence or absence of an *HD* homologue.

The phylogenetic profile of the *HD* gene suggests that Htt may be involved in a biological pathway that is conserved in vertebrates and insects, but not in yeast, nematode or plants. This particular pattern of evolutionary conservation is shared by the NF-κB/Rel/dorsal family of transcription factors, leading one research group to investigate a possible role for Htt in this pathway (147). *Drosophila* Htt was found to associate, and enter the nucleus, with dorsal in a *Drosophila* S2 cell over-expression

system. In human HeLa cell extracts, NF-κB (p50 subunit) was also found to co-immunoprecipitate with human Htt, hinting at a potential cross-species conservation of function (147). The NF-κB/Rel/dorsal proteins regulate a range of biological processes such as neuronal survival, haematopoiesis and innate immunity, thereby implicating Htt in these pathways. Another pathway that is conserved in insects and vertebrates but has recently been reported to have been completely lost in the divergence of the nematode lineage is the haem biosynthesis pathway (148). A functional relationship of Htt with this pathway has not yet been investigated.

Expression pattern of *HD* gene homologues

Embryonic expression of mRNA transcripts encoding Htt has been detected in human, rodent, zebrafish, *H. roretzi*, *H. erythrogramma* and *Drosophila* (107, 109, 111, 114, 141, 145, 146). *In situ* mRNA hybridisation studies (performed on rodents and early chordates) have revealed ubiquitous and uniform expression in early developmental stages (107, 111, 114, 146). In adulthood, *HD* (and *Hdh*, *rhd*) gene products are ubiquitously expressed in neural and non-neural tissues in man and rodents, with particular enhancement in the brain (5-11). Similarly, Htt has been detected in the adult zebrafish head but not body tissue (141). In the basal chordate *H. roretzi*, HrHd mRNA is expressed in neural and mesodermal tissues in late developmental stages (146). Interestingly, in the basal deuterostome *H. erythrogramma*, expression of HeHd mRNA after metamorphosis (juvenile stage) is limited to mesodermal tissues, and is not detected in ectodermal tissue (including nerve cell-types) (146). This finding raises the possibility that neural Htt expression is a novel feature that has arisen in chordate organisms (146).

Huntingtin protein structure and sequence homology

At the N-terminal of the primary amino acid sequence of human Htt (Fig. 1.3) lies the polyglutamine repeat (beginning at residue 18), as previously mentioned. A stretch of consecutive glutamines is present in Htt in mouse (142, 144), rat (107), miniature pig (140), zebrafish (141) and pufferfish (143), but not in *Drosophila* (145) or *Dictyostelium* Htt proteins, suggesting it is a feature of vertebrate Htt proteins (Fig. 1.4). Amongst the vertebrate homologues, polyglutamine repeat length ranges in size from 4 repeats in fishes to up to 39 copies in (non-HD) human (Figure 1.4), with repeat polymorphisms

occurring in human and swine (140). Copy numbers of disease-causing lengths have only been found in humans.

Immediately C-terminal to the polyglutamine repeat lies a proline-rich domain ((149), and see Fig. 1.3) that mediates protein-protein interactions (106). Many proteins with glutamine and proline-rich domains have been shown to be involved in transcriptional regulation (150). The proline-rich domain is found only in mammalian homologues (Fig. 1.4), indicating that if it does play a role in the function of mammalian Htt, this aspect of its function is not conserved in lower vertebrates.

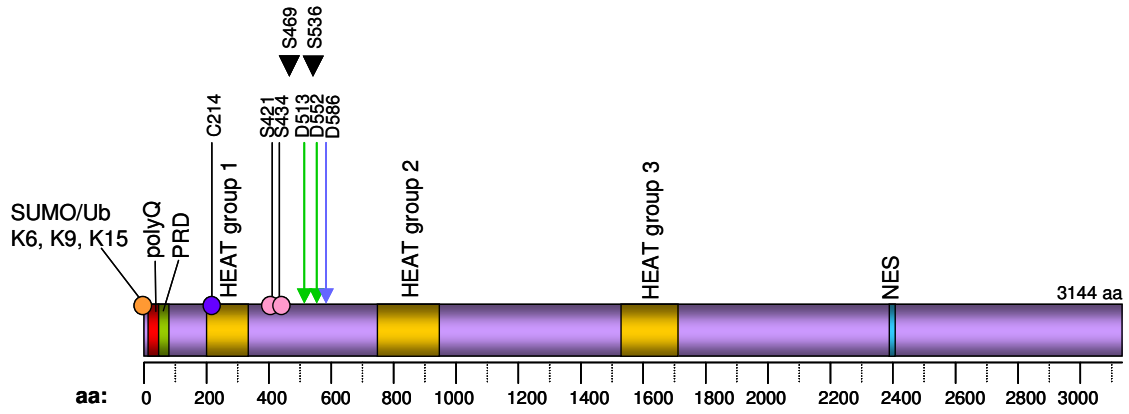

Figure 1.3 Schematic illustration of the amino acid sequence of Huntingtin. Adapted from reference (105). PolyQ indicates the polyglutamine tract (red), which is followed by the proline-rich domain (PRD; green). The gold regions indicate the 3 main clusters of HEAT repeats. Cleavage sites for caspase-3 (green arrows) and caspase-6 (blue arrow) are indicated, and their amino acid positions are shown. Calpain cleavage sites are indicated by black arrowheads and their amino acid positions are shown. The orange circle indicates the position where three lysine residues are SUMOylated (SUMO) and/or ubiquitinated (Ub) (amino acid positions indicated). The blue circle indicates the position at which Htt is palmitoylated and the pink circles represent phosphorylation sites (amino acid positions shown). NES is the nuclear export sequence. aa, amino acid.

Another feature of Htt is the presence of HEAT repeats. HEAT repeats (named after the four proteins in which they were originally found; **H**untingtin, **e**longation factor 3, the **A** subunit of protein phosphatase 2A, and **T**OR1) are ~40 residues in length and divergent in sequence.(151). They are predicted to form α-helical structures, and they mediate protein-protein interactions (for example, (147)). Other proteins containing HEAT repeats are involved in cytoplasmic and nuclear transport processes, microtubule dynamics and chromosome segregation (152).

Three main clusters of HEAT repeats have been identified within the N-terminus half of the Htt protein (Fig. 1.3) (151). The first and third cluster of HEAT repeats, that

each contains three consecutive repeat units, are positioned from amino acid residues 205 to 329 and 1534 to 1710, respectively, within the human Htt sequence. The second region contains four consecutive repeats that are positioned between residues 745 and 942 (151). A total of 36 putative HEAT repeats have been identified in human Htt, spanning the entire length of the protein (147). HEAT repeats are conserved in other vertebrates (106, 147) and are also present in *Drosophila* Htt (147) suggesting that interactions mediated by these repeats may be evolutionarily conserved.

Htt also contains a functionally active nuclear export signal (NES) near the C-terminus (^{2397}IIISLARLPL^{2406}) (Fig. 1.3). The NES sequence shows a high degree of conservation throughout vertebrates (153), suggesting that this signal might be important for the function of Htt.

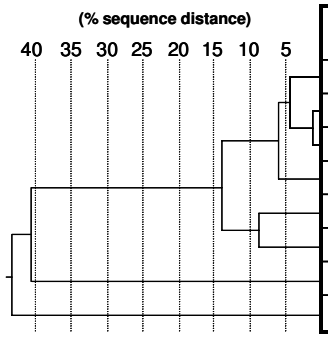

	Identity to human Htt	Protein length (aa)	Polyglutamine tract	PRD	HEAT repeats
Human	100%	3144	**Yes** (6-36Q)	**Yes**	**Yes**
Mouse	90.1%	3120	**Yes** (7Q)	**Yes**	**Yes**
Rat	90.1%	3110	**Yes** (8Q)	**Yes**	**Yes**
Pig	87.8%	3139	**Yes** (17-18Q)	**Yes**	**Yes**
Zebrafish	70.2%	3121	**Yes** (4Q)	No	**Yes**
Pufferfish	58.2%	3148	**Yes** (4Q)	No	**Yes**
Amoeba	10.6%	3095	No	No	ND
Fruit Fly	10.5%	3584	No	No	**Yes**

mammals

vertebrates

Figure 1.4 Conservation of Huntingtin homologues from various species. The phylogenetic tree and calculation of percentage identity to human Htt are based on sequence pair differences using the Clustal method. The NCBI accession numbers of the sequences used are as follows: human (*Homo sapiens*) NP_002102; mouse (*Mus musculus*) NP_034544; rat (*Rattus norvegicus*) P51111; miniature pig (*Sus scrofa*) NP_999129; zebrafish (*Danio rerio*) NP_571093; pufferfish (*Takifugu rubripes*) P51112; amoeba (*Dictyostelium discoideum*) AAS38622; fruit fly (*Drosophila melanogaster*) AAD51369. Conservation of the polyglutamine tract, proline-rich domain (PRD), and HEAT repeats within each Htt homologue is indicated. Other abbreviations: aa, amino acids; ND, not determined; Q, glutamine.

Post-translational modifications of Huntingtin

The Htt protein is subject to various kinds of post-translational modification (Fig. 1.3). Within the first 17 amino acids are three lysine residues (K6, K9 and K15) that compete as substrates for ubiquitination and/or SUMOylation (154). Htt is also palmitoylated at cysteine residue C214 by Htt interacting protein, HIP14 (palmitoylated proteins are often involved in vesicle trafficking) (155, 156). Other modification sites include two phosphorylation sites at serine residues S421 and S434 (157, 158), two

caspase-3 cleavage sites at aspartate residues D513 and D552 (^{510}DSVD^{513} and ^{549}DLND^{552}) (159) a caspase-6 cleavage site at D586 (^{583}IVLD^{586}) (160) and calpain cleavage sites at serine residues S469 and S536 (^{468}SSS^{470} and ^{535}VSA^{537}) (161, 162).

The contribution of Htt proteolysis (by caspases and calpains) to normal cellular function is not clear, however reduction of caspase and calpain activities decreases the proteolysis and toxicity of expanded mutant Htt, and delays various aspects of disease progression in cellular and animal models (160, 162-164). Phosphorylation of Htt has been shown to reduce the cleavage of this protein by caspases (158), and protect against the toxicity of expanded Htt in cell culture (157). Interestingly, within the normal human brain, the extent of Htt phosphorylation differs from region to region (at least of residue S421), with lowest levels seen in the striatum, intermediate levels in the cortex, and highest levels in the cerebellum (165), thus inversely correlating with regional susceptibility to degeneration in HD. This raises the possibility that decreased Htt phosphorylation in the striatum and cortex could permit greater caspase cleavage and generation of toxic N-terminal fragments of expanded Htt in HD.

Interacting partners implicate Htt in a diverse range of biological processes

Numerous Htt-interacting proteins have been identified, in yeast-2-hybrid screens, co-immunoprecipitation studies, or by extraction from Htt-positive aggregates (Table 1.2). The majority of yeast-2-hybrid experiments have used N-terminal fragments of Htt as bait, since interactions that may be enhanced or decreased by the polyglutamine repeat expansion in HD are considered to be more likely to interact with the N-terminus of Htt. Furthermore, in one study no interactors were identified when an internal segment or C-terminal segment of Htt was used as bait (166). Using alternative methods, two proteins have been found to interact with regions of Htt other than the N-terminus: the previously mentioned NF-κB (147), and a 40 kDa Huntingtin-associated protein, HAP40 (167). Htt interactors are involved in many different biological processes including endocytosis, vesicle transport, apoptosis, cell signalling, transcriptional regulation and morphogenesis (Table 1.2) (106), suggesting that Htt may play a complex role involving a wide variety of biological processes. Due to the large size and multiple interactions of Htt and the presence of HEAT repeats in its sequence, it has been proposed that Htt may act as a scaffold that coordinates many different processes (106). Many of the interactions are altered by the expansion of the polyglutamine tract (as indicated in Table 1.2). However, identification of these interactors has not yet provided any clues as to the regional specificity of HD pathology.

Interacting protein	Method of identification	PolyQ length dependence	Region of Htt involved	Function	Refs
α-adaptin C/HYP-J	Y2H, human testis	Yes (↓)	NT (aa 1-550)	Endocytosis	(166)
Akt/PKB	Phosphorylation assay	No	S421	Kinase	(157)
CA150	Y2H, *C. elegans*	No	Not known	Transcriptional activator	(168)
CBP	GST-pull down	Yes (↑)	NT (aa 1-588)	Transcriptional co-activator with acetyltransferase activity	(169, 170)
CIP4	Y2H, *C. elegans*	Yes (↑)	NT (aa 1-152)	cdc42-dependent signal transduction	(171)
CtBP	Co-IP	Yes (↓)	PLDLS motif (aa 182-186)	Transcription factor	(130)
FIP-2/HYPL	Y2H, human testes	Not known	NT (aa 1-550)	Cell morphogenesis	(166, 172)
GASP2	Y2H, Co-IP	Yes (↑)	NT (aa 1-90)	Membrane receptor degradation	(173)
GIT1	Y2H, Co-IP	Not known	NT (aa 1-170)	Membrane trafficking	(174)
Grb2	Co-IP	Not known	PRD	Growth factor receptor binding protein	(175)
HAP1	Y2H, rat brain	Yes (↑)	NT (aa 171-230)	Membrane trafficking	(176)
HAP40	Isolation from inclusions	Yes (↑)? (Increased intracellular co-localisation)	CT	Endosome motility	(167, 177)
HIP1	Y2H, human brain	Yes (↓)	NT (aa 1-540)	Endocytosis, pro-apoptotic	(178, 179)
HIP2/ hE2-25K	Y2H, human brain	No	NT (aa 1-540)	Ubiquitin conjugating enzyme	(180)
HIP14/HYP-H	Y2H, human brain, human testes	Yes (↓)	NT (aa 1-550)	Palmitoyl transferase, protein trafficking	(156, 166, 181, 182)
N-CoR	Y2H, rat brain	Yes (↑)	NT (aa 1-171)	Nuclear receptor co-repressor	(183)
NF-κB	Co-IP	Not known	HEAT repeats	Transcription factor	(147)
p53	Isolation from inclusions	No	PRD	Transcription factor	(169)
PACSIN1/syndapin 1	Y2H	Yes (↑)	PRD	Endocytosis, synaptic vesicle recycling	(184)
PSD-95	Co-IP	Yes (↓)	PRD	Synaptic scaffolding protein	(185)
RasGAP	Co-IP	Not known	PRD	Ras GTPase activating protein	(175)
SH3GL3/endophilin 3	Y2H, human brain	Yes (↑)	PRD	Endocytosis	(186)
Sin3a	Isolation from inclusions	Yes (↑)	NT (aa 1-171)	Transcriptional repressor	(169)
Sp1	GST pull down; Y2H	Yes (↑)	NT (aa 1-171)	Transcription factor	(187, 188)
TAFII-130	Y2H interaction	No	NT (aa 1-480)	Transcription factor	(188)

Table 1.2 Selected Huntingtin-interacting proteins. Modified from reference (106) to include additional information. Abbreviations: aa, amino acid; Akt, identified in AKT virus; CA150, co-activator 150; CBP, cAMP-response-element-binding protein; CIP4, Cdc42-interacting protein 4; Co-IP, Co-immunoprecipitation; CT, C-terminus; CtBP, C-terminal-binding protein; FIP2, for 14.7K interacting protein; GASP2, G protein-coupled receptor associated sorting protein 2; GIT1, G protein-coupled receptor kinase-interacting protein 1; Grb2, growth factor receptor-binding protein 2; GST, glutathione S-transferase; HYP-J Htt yeast protein-J; HYP-L, Htt yeast protein-L; HAP1, Htt-associated protein1; HAP40, Htt-associated protein-40; HIP1, Htt interacting protein-1; HIP2, Htt interacting protein 2; HIP14, Htt-interacting protein-14; HYP-H, Htt-yeast partner-H; HPY-L, Htt-yeast partner-L; N-CoR, nuclear receptor co-repressor; NT, N-terminal; PACSIN1, protein kinase C and casein kinase substrate in neurons1; PKB, protein kinase B; PRD, proline-rich domain; PSD-95, postsynaptic density-95; RasGAP, Ras GTPase activating protein; S421, Serine 421 (Akt consensus phosphorylation site); SH3GL3, SH3-containing Grb2-like protein 3; Sp1, specificity protein1; TAFII-130, TATA-binding protein (TBP)-associated factor; Y2H, yeast two-hybrid; (↑), stronger interaction with mutant Htt; (↓), weaker interaction with mutant Htt.

Somatic instability and HD

Another mechanism proposed to account for the specificity of neuronal vulnerability in HD is brain region-specific somatic instability. Somatic instability has been observed in many polyglutamine diseases (15, 189-192) and could contribute to the pathogenesis in these diseases by further expanding the length of the CAG/polyglutamine repeat in the inherited disease allele, above a copy number threshold that renders it toxic to cells (193)(Fig. 1.5). According to this model, the more repeats an individual inherits, the fewer years it would take for gradual somatic expansion to raise the repeat copy number in the disease allele above that critical pathogenic threshold. In theory, the areas of the brain with the greatest instability would reach the pathogenic threshold first. For this model to account for the specificity of neuronal vulnerability in polyglutamine diseases, region-specific somatic instability would have to correlate to the spatially restricted pattern of neurodegeneration in each of the diseases, with the specificity somehow mediated by repeat context.

The somatic expansion model offers a potential explanation for the inverse correlation between inherited CAG copy-number and age of onset in polyglutamine diseases, since the higher the inherited copy number, the less time it would take to reach the pathogenic threshold (Fig 1.5). Furthermore, it would be consistent with pathology being more widespread when inherited repeat copy numbers are higher, since all cells would be closer to the pathogenic threshold from birth.

Somatic instability correlates to sites of neurodegeneration in HD

In the Huntington's disease brain, somatic instability has been observed most significantly in the regions showing the greatest neuropathological involvement such as the basal ganglia and cerebral cortex, whilst the cerebellum, which is rarely affected in HD, shows limited repeat instability (15). This instability appears to be age-related since no mosaicism was observed between various tissues of a foetus carrying an expanded HD allele (194). Age-dependent somatic instability of the disease allele has also been demonstrated in a number of mouse models of HD (195-198). In 2000, Kennedy and Shelbourne reported on the somatic instability in a knock-in mouse model of HD, containing an expanded CAG repeat of between 72 and 80 copies within one of the endogenous *Hdh* alleles (197). In these heterozygous mice ($Hdh^{Q72\text{-}80}/Hdh^{Q7}$), instability of the inherited disease allele ($Hdh^{Q72\text{-}80}$) was expansion-biased, and was most pronounced in the striatum, with repeat lengths that increased in an age-dependent manner.

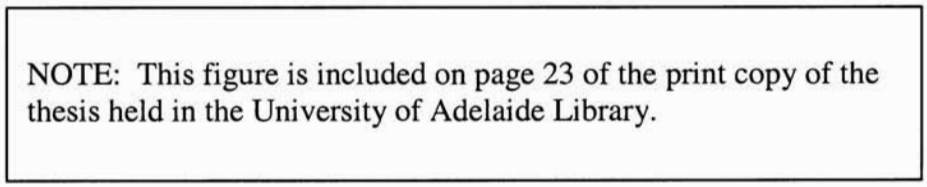

Figure 1.5 Model for the relationship between inherited repeat copy number and age at the onset of symptoms. Taken with permission from reference (193). The time taken (*t*) for the repeat to reach a critical copy number threshold by means of incremental increases in repeat copy number would be determined by the inherited (germline) copy number (green arrows) at birth (*n*). The greater is *n* the shorter is *t*. Time taken (*t*) to reach a disease-causing copy number is inversely proportional to 'starting' copy number (*n*), $t = k/n$ (where *k* is determined by the repeat context).

By using a small pool PCR amplification technique the authors provided the first quantitative analysis of expanded allele length and frequency; expansion of the disease allele above the inherited copy number was observed in more than 80% of cells in the striatum, whilst only low to medium levels of instability were observed in non-neural tissues and other brain regions (197). In 2003, the same authors and their colleagues showed that the extent of somatic instability in these mice correlated with decreasing performance on a rotarod test for motor coordination (199). They also used small pool PCR to analyse repeat instability in post-mortem human brain samples from patients that had died either before predicted age of onset of HD (no visible signs of neuropathology), or at late stage HD. Vast expansions of the disease allele, most strikingly in the striatum and cortex, were observed in pre-HD samples, whilst in the late stage HD brain, in which severe striatal atrophy was evident, there was a notable absence of largest expansion sizes (199). These results suggest that cells with the greatest repeat size were lost first, consistent with the general correlation between larger repeat lengths and disease severity.

Loss of stabilising repeat interruptions in SCA1 and SCA2 disease alleles

Interestingly, SCA1 and SCA2 alleles in the upper normal range contain repeat interruptions, which are known to have a stabilising effect on trinucleotide repeat tracts (200), and are not present in the expanded disease alleles (67). The CAG tract in normal SCA1 alleles (6-44 repeats) with more than 20 repeats are interrupted by 1 to 4 CAT units (encoding histidine), but expanded disease alleles (39-82 repeats) contain a contiguous CAG repeat sequence. Similarly, the CAG tract in normal SCA2 alleles (15-31 repeats) is frequently interrupted by one to three CAA units (encoding glutamine like CAG), which are not present in the expanded disease alleles (36-57 repeats). The effect of CAT interruptions on somatic repeat stability in SCA1 was examined by comparing size heterogeneity of alleles from an unaffected individual with allele sizes of 30 and 39 repeats, and an affected individual with 29 repeats (normal allele) and 40 repeats (one of the smallest disease causing alleles described) (192). Both alleles of the unaffected individual, and the smallest (normal) allele of the affected individual were interrupted by at least one CAT repeat. However, the SCA1 disease allele of 40 repeats was uninterrupted. When low copy genomic analysis was used to examine instability in peripheral blood cells from these individuals, all the interrupted alleles were stable, but in contrast, prominent heterogeneity of allele size was observed in the SCA1 allele with 40 uninterrupted repeats (192). The finding that an interrupted normal SCA1 allele of 39 repeats was somatically stable, whilst an uninterrupted SCA1 allele that was only one repeat unit larger in size (40 repeats) was markedly unstable and pathogenic, is consistent with the hypothesis that somatic instability contributes to disease pathogenesis.

Interruptions in SCA1 disease alleles delay the age of SCA1 disease onset

In further support of the somatic instability hypothesis, rare SCA1 alleles exist that have repeat copy numbers in the disease range, but contain CAT interruptions (89, 201-203). In these cases, the presence of these interruptions appears to delay SCA1 symptoms beyond the age of onset that would normally be predicted for that repeat length. One explanation for this is that the repeat interruptions in these large SCA1 alleles delay the age of onset by hindering somatic expansion of the SCA1 allele, thus increasing the time it takes for the repeat to expand above the pathogenic threshold. It should also be noted, however, that since the CAT interruptions encode histidine residues, they would therefore lead to interruptions in the polyglutamine tract, potentially rendering the expanded protein less toxic (as will be discussed at the end of Chapter 3).

This study

Insight into what determines the unique specificities of neuronal vulnerability in HD, and other polyglutamine diseases, is likely to increase our understanding of the underlying pathogenic mechanism(s) at play in these disorders. The aim of this work was to investigate two factors hypothesised to play a role in mediating the specificity of HD pathology; tissue-specific somatic expansion of the CAG repeat, and disruption of normal Htt function. The zebrafish (*Danio rerio*) model organism was selected for use in these experiments, as it was hoped that the novel attributes of this model system would provide new insight into these research areas, and that the outcomes would complement previous studies performed using other models.

Zebrafish (*Danio rerio*) as a model system

The zebrafish system provides a useful vertebrate model in which to study early developmental genetics. Large numbers of embryos are produced from a tank of adult fish in a single breeding session, providing sufficient numbers for multiple time-points to be analysed throughout development. The embryos are large, transparent and develop externally, facilitating non-invasive observation of developing embryonic structures under a light microscope. Embryogenesis progresses rapidly from the 1-cell zygote stage (0 hours post fertilisation; hpf) through a series of well-defined stages (Fig. 1.6) (204). By 26-28 hpf embryos have established a heartbeat and circulation of blood cells, and by ~72 hpf, the early larva has hatched from its protective encasement (chorion) and displays food-seeking and active avoidance behaviours (204, 205). Zebrafish have a reasonably short generation time, reaching sexual maturity after 3 to 4 months.

The zebrafish *HD* gene homologue (*hd*)

The zebrafish *HD* gene homologue, *hd*, encodes a Huntingtin (Htt) protein of 3121 amino acid residues that is 70% identical to human Htt (141). Many features of human Htt are conserved in the zebrafish homologue, including the polyglutamine tract (4 consecutive glutamine residues) and HEAT repeats (106, 147). In accordance with human and rodent expression, zebrafish Htt has been detected at high levels in late embryonic development and in the adult head (141).

Period	hpf	Description
Zygote 1-cell	0	The newly fertilised egg through the completion of the first zygotic cell cycle.
Cleavage 2-cell to 64-cell	0.75	Cell cycles 2 to 7 occur rapidly and synchroniously.
Blastula 128-cell to 30% epiboly	2.25	Rapid, metasynchronous cell cycles
Gastrula 50% epiboly to bud stage	5.3	Morphogenetic movements of involution, convergence, and extension from the epiblast, hypoblast, hypoblast, and embryonic axis; through the end of epiboly.
Segmentation 1-somite to 26-somite	10	Somites, pharyngeal arch primordia and neuromeres develop; primary organogenesis; earliest movements; the tail appears.
Pharyngula Primordium-5 to high pec stage	24	Body axis straightens from its early curvatures about the yolk sac; circulation, pigmentation, and fins begin development.
Hatching Long-pec	48	Completion of rapid morphogenesis of primary organ systems; cartilage development in head and pectoral fin; hatching occurs asynchronously.
Early larva	72	Swim bladder inflates; food seeking and active avoidance behaviours.

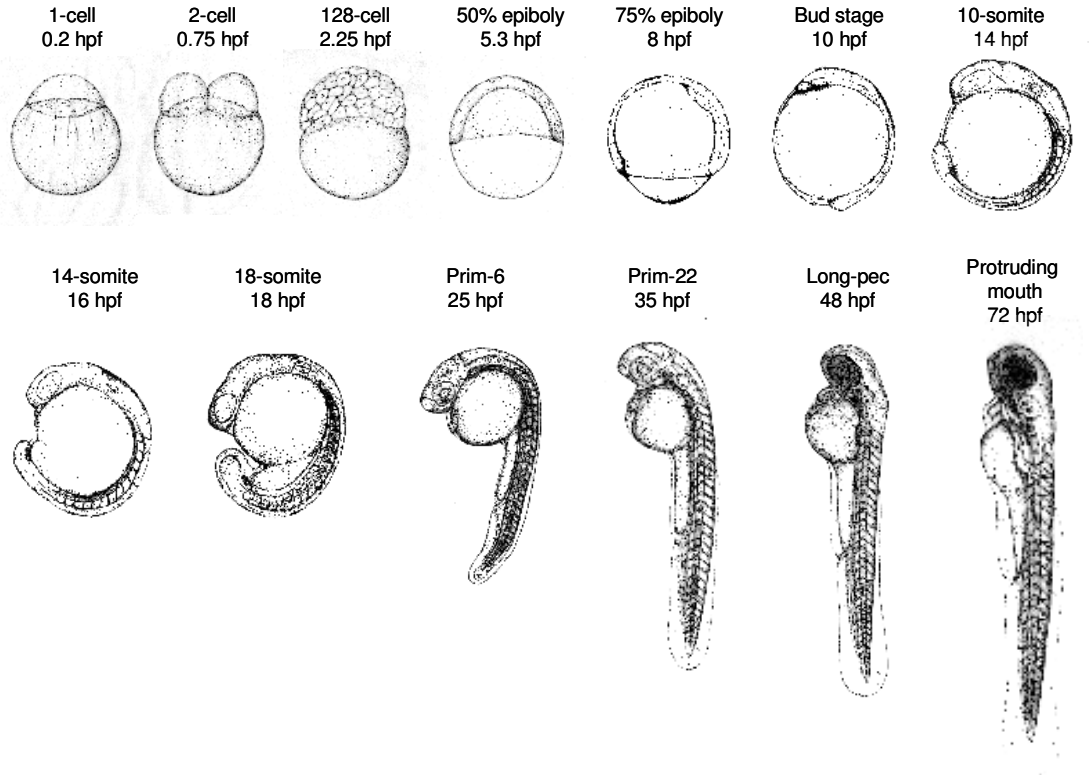

Figure 1.6 Stages of early zebrafish development. Table and selected images taken from (204). Abbreviatons: hpf, hours post fertilisation; pec, pectoral; Prim, primordium.

Research aim 1: Investigation of the role of somatic instability in HD

Given the regionally specific and age-related somatic expansion that has been observed in a knock-in mouse model of HD and also in the human disease (15, 197, 199), the first part of this work was aimed at directly addressing the question of whether somatic instability contributes to the age of onset and/or disease severity in HD by developing transgenic zebrafish lines expressing CAG repeats with and without stabilising interruptions. This part of the study yielded some beneficial outcomes, but the work was not seen to completion largely due to the fact that during the course of this study, new data published by others cast reasonable doubt on the somatic instability hypothesis (206, 207), as discussed at the end of Chapter 3. Consequently, more focus was then placed on the second aim of this work (below).

Research aim 2: Investigation of the normal role of Htt in development

Previously, lack of a viable mouse model of Htt deficiency has limited investigation of Htt function *in vivo*. Here a novel approach was taken by using antisense methodology (morpholinos) to transiently 'knock down' *hd* gene function in early zebrafish development. The level of inhibition is dependent upon the dose of morpholinos administered, thus allowing the effects of partial Htt depletion to be investigated. The main goal of this part of the study was to investigate the effects of Htt-deficiency in zebrafish, in the hope that characterisation of the resulting phenotypes might provide further insight into the biological role of Htt, and offer clues as to the specificity of neuronal vulnerability in HD. Initial characterisation of Htt-deficient zebrafish (described in Chapter 4), suggested a role for Htt in iron metabolism. This role was further investigated, as described in Chapter 5. Finally, in Chapter 6, the significant outcomes of this work are discussed in the context of Huntington's disease.

Chapter 2: Materials and methods

Materials

Bacterial strains

DH5α: F', *f80, lacZΔM15, recA1, endA1, gyrA96, thi-1, hsdR17, (r_K-, M_K+), supE44, relA1, deoR, Δ(lacZYA-argF)U169*. Chemically competent cells were prepared by S. Dayan and electrocompetent cells were prepared by D. Crack.

One shot® Top10 chemically competent *E. coli* cells (Invitrogen).

All cells were stored in 50 µl or 200 µl aliquots at –80°C

Growth media

Bacterial media:
All bacterial media were prepared with distilled and deionised water and sterilised by autoclaving, except heat labile reagents, which were filter-sterilised. Where indicated, ampicillin (SIGMA) was added from a sterile stock solution to the media after autoclaving.

Luria broth (LB): 1% (w/v) bactotryptone, 0.5% yeast extract, 1% NaCl, pH 7.0.
Supplemented with ampicillin (100 µg/mL).

Luria agar (L-agar) plates: LB with 1.5% (w/v) bactoagar supplemented with ampicillin (100 µg/mL). If selection for loss of β-galactosidase activity was required (blue/white transformant selection), 56 µL of 100 mM IPTG (SIGMA) and 40 µL of 20 mg/mL X-Gal (Promega) were applied to the plate surface prior to spreading of bacteria.

SOC: 2% bactotryptone, 0.5% yeast extract, 10 mM NaCl, 2.5 mM KCl, 10 mM $MgCl_2$, 10 mM $MgSO_4$, 20 mM glucose.

Zebrafish embryo medium:
Embryo medium was prepared with sterile liquid stock solutions and MQ water. $NaHCO_3$ was added last, as a powder.

Embryo medium: 13.72 mM NaCl, 0.54 mM KCl, 0.025 mM Na_2HPO_4, 0.044 mM K_2HPO_4, 1 mM $CaCl_2$, 1 mM $MgSO_4$, 0.035% (w/v) $NaHCO_3$.

Buffers and solutions

Commercially obtained:

Ferroject iron dextran injectable solution:	Swift and Company Ltd
Formaldehyde Solution (40%):	AnalaR (MERCK Pty Ltd)
Hydrogen peroxide (30%):	SIGMA
Tween 20 Solution (10%):	Bio-Rad Laboratories (Hercules, CA)

Laboratory prepared:

Agarose gel loading dye (6 ×):	30% glycerol, 0.2% (w/v) bromophenol blue, 0.2% (w/v) xylene cyanol.
Formaldehyde (4%):	4% formaldehyde (diluted from 40%) in 1× PBS.
Hybridisation buffer:	50% formamide (deionised), 5× SSC, 2% Blocking Reagent (Boehringer Mannheim), 0.1% Tween-20, 0.5% CHAPS, 50 µg/mL yeast RNA, 5 mM EDTA, 50 µg/mL heparin.
PBS:	7.5 mM Na_2HPO_4, 2.5 mM NaH_2PO_4, 145 mM NaCl.
PBST:	1× PBS, 0.1% Tween 20.
o-dianisidine stain:	40% ethanol, 0.01 M sodium acetate (pH 4.5), 0.6 mg/mL *o*-dianisidine, 0.65% H_2O_2 (added fresh immediately prior to use).
Prussian blue stain:	Whole embryos: 1 part 5% (w/v) potassium ferrocyanide and 1 part 5% (~0.5 M) HCl, combined immediately prior to use. Isolated blood cells: 3 parts 1% HCl and 1 part 2% potassium ferrocyanide combined immediately prior to use.
Sodium citrate buffer:	0.1% (w/v) sodium citrate, 0.1% Triton X-100, 1× PBS.
SSC (20×):	1.75% (w/v) NaCl, 0.88% (w/v) sodium citrate, pH 7.0.
TBE (20×):	1.8 M Tris, 1.8 M boric acid, 0.05 M EDTA, pH 8.3

Chemical reagents

All chemical reagents were of analytical grade, or of the highest grade obtainable.

Compounds

CHAPS:	SIGMA
Potassium ferrocyanide:	SIGMA
o-dianisidine:	SIGMA
Bovine Serum Albumin (BSA), dessicate:	SIGMA
Agarose (DNA Grade):	Progen Biosciences

Enzymes and indicators

Enzymes

Pfu DNA polymerase:	Stratagene
Pfu Turbo DNA Polymerase:	Stratagene
Proteinase K:	SIGMA
Restriction endonucleases:	New England Biolabs
Shrimp Alkaline Phosphatase (SAP):	USB
SP6 RNA Polymerase:	Roche
SuperScript II™ RNase H^- Reverse Transcriptase:	Invitrogen
T4 Polynucleotide Kinase, 3' phosphatase free:	Roche
T4 DNA Ligase:	Roche
T4 DNA Polymerase:	New England Biolabs
T7 RNA Polymerase:	Roche
Taq Polymerase:	Invitrogen
ABI Prism™ Dye Terminator Cycle Sequencing Ready Reaction Mix:	Perkin-Elmer

Indicators and antibodies

BCIP:	Roche
Digoxigenin-11-UTP:	Roche
NBT:	Roche
SigmaFast™ DAB/urea tablets:	Sigma-Aldrich
Anti-digoxigenin-AP, Fab fragments	Roche

Kits

Expand Long Template (ELT) PCR System:	Roche
GENECLEAN® II Kit:	Qbiogene
GenElute™ Plasmid Miniprep Kit:	SIGMA
In Situ Cell Death Detection Kit, POD:	Roche
In Situ Cell Death Detection Kit, TMR red:	Roche
PCR Purification Kit:	QIAGEN
pGem®-T Vector System I:	Promega
QIAGEN® Plasmid Midi Kit:	QIAGEN
QIAprep® Spin Miniprep Kit:	QIAGEN
QIAshredder™:	QIAGEN
QuikChange® Site-Directed Mutagenesis Kit:	Stratagene
RNeasy® Mini Kit :	QIAGEN

Plasmids

Commercial plasmids

pGem®-T:	Promega
pCS2+:	D. Turner, The University of Michigan (208)
pIRES2-EGFP:	BD Biosciences Clontech

notch2 (notch6) clone

BJ1:	M. Lardelli, The University of Adelaide (209)

DNA oligonucleotides

DNA oligos were synthesised and purified by GeneWorks Pty Ltd (Thebarton, SA). Oligos used for cloning or *in vitro* mutagenesis were purified by HPLC. Oligos used for PCR amplification and sequencing were obtained at the standard PCR grade.

Oligo sequences are given in the 5' → 3' direction. Sequence complementary to the template is underlined. Restriction sites in non-complementary 5' additions are shown in bold. Not all restriction sites were utilised in this study. Bases that anneal to, or create, coding sequence are grouped in the open reading frame of that sequence (except for the quantitative PCR primers). F, forward primer; R, reverse primer.

Amplification of *hd* ORF(1-1503):
ZHD.F7+*Eco*RI: CTGAT**GAATTC**C ATG GCC ACC ATG GAG AAG CTA A
ZHD.R7+*Xba*I: GACTG**TCTAGA**TGACATCTGGTTGGCATCGGTT

Amplification of *hd* exon 1 and flanking sequences:
ZHD.F3+*Bam*HI: GTCGC**GGATCC**CGTGCTATCAACTACCTTCAGA
ZHD.R3+*Eco*RI: GACCG**GAATTC**ACATCAGTTCAGCACTCA CTG T

In vitro mutagenesis to create a *Kpn*I site within *hd* CAG repeat:
ZHD.QC.F1: CTA AAA TCA TTC CAG GTAC CAG CAG CAA GGC CCG CTG TC
ZHD.QC.R1: GA CAG CGG GCC TTG CTG CTG GTAC CTG GAA TGA TTT TAG

Amplification of *hd* promoter region (~1.2 kB) and first 15 bp of *hd* ORF (*Nco*I site in italics):
ZHD.F8+*Sph*I: GAT**GCATGC**TGACCTACCATCCCATCTGAGA
ZHD.R8+SacII: GTA**CCGCGG** CT*C CAT GG*T GGC CAT TTTAACAGAAG

Addition of myc tag sequence (italics) and stop codon (TAG) to 3' end of *hd* exon 1:
ZHD.R9+MTtag: CTA *CAA ATC TTC TTC AGA AAT CAA CTT TTG TTC* CTG TTT CTG GAC GA

Oligos that anneal to create a double-stranded DNA 30mer of pure CAG repeat sequence and were also used for PCR-based expansion of pure repeat sequences:
$(CAG)_{10}$: CAG CAG CAG CAG CAG CAG CAG CAG CAG CAG
$(CTG)_{10}$: CTG CTG CTG CTG CTG CTG CTG CTG CTG CTG

Oligos that anneal to create a double stranded DNA 30mer of CAG/CAA mixed repeat sequence and were also used for PCR-based expansion of mixed repeat sequences:
$(CAG/CAA)_{10}$: CAG CAA CAA CAG CAA CAG CAG CAA CAA CAG
$(CTG/TTG)_{10}$: CTG TTG TTG CTG CTG TTG CTG TTG TTG CTG

Amplification of *EGFP* ORF and polyadenylation (pA) signal from pIRES2-EGFP:
pI2EGFP.F2: TGGCCACAACC ATG GTG AGC AA
pI2EGFP.F4+*Sac*I: AG**GAGCTC** ATG GTG AGC AAG GGC GAG GA
pI2EGFP.R2+*Nco*I: GT**CCATGG**ACAAACCACAACTAGAATGCA

Amplification of IRES-EGFP-pA region from pIRES2-EGFP:
pI2EGFP.F3+*Sac*II: GATCA**CCGCGG**TCTAGATCTCGAGCTCAAGCTTCGA

Colony PCR screening, and sequencing:
M13F: GTAAAACGACGGCCAG
M13R: CAGGAAACAGCTATGAC

Quantitative PCR (primers are complementary to exonic sequence, and each primer pair flanks an intron near the 3' end of the respective transcript):
DrTfR1aF: AATCGCATTATGAGGGTGGAA
DrTfR1aR: GGGAGACACGTATGGAGAGAGC

DrTfR1bF: AAGAATAGTGACCTGGAAGACATGG
DrTfR1bR2: AATGAGACGTAAGGAGAGAGGAAATT

acta1F: TGCCCAGAGGCCCTGTT
acta1R: ACCGCAAGATTCCATACCCA

Morpholino oligonucleotides

Morpholino oligos (MOs) were designed and synthesised by GeneTools (LLC Ore.). Oligo sequences are given in the 5' → 3' direction.
MO sequences antisense to the zebrafish *hd* gene mRNA transcript:
*hd*MO1: GCCATTTTAACAGAAGCTGTGATGA
(+5 to -20 with respect to the start of the *hd* ORF, initiation codon underlined).

*hd*MO2: GATATAATCTGATCGGAGATAGGGT
(-22 to -46 with respect to the start of the *hd* ORF).

Standard negative control MO with no known target in zebrafish:
*c*MO: CCTCTTACCTCAGTTACAATTTATA

Mispair control MO representing *hd*MO1 with 5 base alterations (lower case):
*mc*MO1: GCgATTTcAACAcAAcCTGTcATGA

Methods

DNA manipulation

Standard molecular genetic techniques were performed as described in (210).

Annealing oligonucleotides

To generate double-stranded, blunt-ended DNA fragments for cloning, equimolar quantities of two complementary single-stranded oligos were combined in MQ water such that each oligo was at a concentration of 100 ng/µL and then the mixture was heated to 95°C and cooled slowly to room temperature. The 5' ends were then phosphorylated using T4 polynucleotide kinase in the supplied kinase buffer (50 mM Tris-HCl, 10 mM $MgCl_2$, 5 mM dithiothreitol, pH 8.2) supplemented with 1 mM ATP, for 30 minutes at 37°C. The resulting double-stranded DNA fragments were then ready for ligation.

Restriction enzyme digestion of DNA

Digests were carried out as suggested by the manufacturer's instructions. When digested DNA was to be used for cloning, reactions were terminated by heat inactivating the enzyme where possible. In the case of enzymes that were not able to be heat inactivated (such as *Kpn*I), digested DNA was purified by agarose gel electophoresis and gel extraction.

Dephosphorylation of vector DNA

Vector DNA to be used for cloning was dephosphorylated, after linearisation by restriction enzyme digestion, by adding 1-2 units of SAP to the digestion reaction, and incubating at 37°C for 1 hour. Afterwards, SAP was heat inactivated by incubating at 65°C for 15 minutes.

Blunting of 3' overhangs generated by KpnI digestion

Vector DNA linearised by *Kpn*I was dephosphorylated, then the 3' overhangs were removed by T4 DNA polymerase (due to its 3' → 5' exonuclease activity) in the supplied 1× NEB buffer 2 (10 mM Tris-HCl, 50 mM NaCl, 10 mM $MgCl_2$, 1 mM dithiothreitol, pH 7.9) supplemented with 100 µM dNTPs (100 µM of each dNTP) and 50 µg/mL BSA (NEB). The reaction was undertaken at 12°C for 20 minutes and then the DNA was purified using the Qiagen PCR Purification Kit according to the manufacturer's instructions, except that the DNA was eluted in MQ water rather than buffer in the final step.

Purification of DNA from agarose gels

DNA bands excised from agarose gels were purified using the GENECLEAN® II Kit, according to the manufacturer's instructions. MQ water was used in the final elution step, rather than buffer.

Ligations

Ligations of PCR-generated products into pGem-T were carried out using the manufacturer's instructions. For other ligations, DNA fragments to be ligated were placed in a mix (total volume 10-20 µL) containing 1-2 units of T4 DNA ligase and 1× ligation buffer. All ligation reactions were incubated at room temperature (22°C) for at least 16 hours.

Transformation of bacteria

In general, transformation of *E. coli* with plasmid DNA was performed by heat shock, using chemically competent DH5α cells. When higher efficiency was required, transformation was performed by electroporating electrocompetent DH5α cells, or by heat shock using One shot® Top10 cells.

Transformation by heat shock

Chemically competent cells were thawed on ice (from –80°C), and 50 µl added to 2-5 µL of each ligation reaction. The mixture was incubated on ice for 20 minutes, heat-shocked for 45-50 seconds at 42°C and then returned to ice for 2 minutes. 450 µl LB were added, and the mixture was inverted gently. The cells were incubated for 1 hour at 37°C then pelleted for 30 seconds at 6,500 rpm. 400 µl of the supernatant was removed, and the cells were gently resuspended in the remaining LB, plated onto L-agar plates with appropriate supplements, and incubated at 37°C overnight.

Transformation by electroporation

Ligated DNA was first purified as follows. Ligase was inactivated by incubating the ligation reaction at 65°C for 10 minutes. Ligation volume was made up to 50 µL with MQ water and 500 µL of *n*-butanol was then added. After vortexing for 5 seconds, the reaction was centrifuged at 12,000 rpm for 10 minutes. The DNA pellet was retained, dried, and resuspended in 10 µL of MQ water. Typically, 5 µL was then used for electroporation.

For transformation, electrocompetent cells were thawed at room temperature, added to ligation reaction mixture and incubated on ice for 1-2 minutes. Cells were then transferred to an ice-cold 2 mm electroporation cuvette and electroporated in a Bio-Rad *E. coli* Pulser set to 2,500 V, 25 mFD capacitance and Capacitance Extender set to 500 mFD. The cells were immediately flushed from the cuvette with 1 ml of SOC, and the suspension incubated at 37°C for 1 hour. Cells were then pelleted for 5 mins at 2,500 rpm, then 800 ml of the supernatant was removed, and the cells gently resuspended in

the remaining SOC. The cells were then plated onto L-agar plates with appropriate supplements, and incubated at 37°C overnight.

Isolation of plasmid DNA from bacteria

Small-scale preparation of plasmid DNA was performed using the GenElute Plasmid Miniprep Kit and large-scale preparation was performed using the Qiagen Plasmid Midi Kit. For each procedure the manufacturer's instructions were followed, except that MQ water was used instead of buffer in the final elution step so that the DNA samples could be made more concentrated by evaporation, if required, using a SpeedVac Concentrator (SAVANT).

Agarose gel electrophoresis

Molten 1% agarose dissolved in 0.5× TBE and containing ethidium bromide was poured onto a glass plate or into a plastic gel-cast (sealed at each end with masking tape) and set with well combs in place. The gel was submerged in 0.5× TBE in an electrophoresis tank. DNA samples were mixed with agarose loading buffer and loaded into wells alongside a well containing DNA markers of known size (1 Kb Plus DNA Ladder (Invitrogen)). DNA was size-separated by applying 40-120V to the tank, and was visualised by UV light exposure, using Gel-Doc™ apparatus (Bio-Rad).

PCR amplification of DNA

All PCR reactions were cycled in an MJ Research PTC-200 Peltier Thermal Cycler. For amplification of PCR products < 500 bp in length, "File21" PCR conditions were used, and "Longfile21" cycling conditions were used for products larger that 500 bp (see below, under "Cycling conditions"). Special conditions were used for PCR-based expansion of repeat sequences as described in section below entitled "PCR-based expansion of pure and interrupted repeats".

PCR amplification of DNA to be used in cloning steps

PCR amplification for cloning was generally performed using the Expand Long Template (ELT) PCR System since the DNA polymerase mix provided in this kit has proofreading activity, but also adds 3' A-overhangs that facilitate cloning into pGem-T. For a given primer pair, three PCR reactions were set up, using ELT buffers 1, 2 and 3, respectively, according to the manufacturer's guidelines. PCR products were visualised by agarose gel electrophoresis to see which reaction resulted in the purest and most

abundant PCR product. The appropriate band was then excised, gel purified, and used for cloning. For PCR amplification of the first 1.5 kB of the *hd* ORF, Taq polymerase was used, according to the manufacturer's guidelines.

Colony PCR

Each selected transformant colony was transferred, using a sterile toothpick, to a master plate (L-agar plus Ampicillin) then into a 10 µL PCR reaction mix containing 0.25 units of Taq polymerase, 1× supplied polymerase buffer, 0.2 mM dNTPs, 2 mM $MgCl_2$ and 2.5 ng/µL of each primer (M13F and M13R).

Cycling conditions

File21: 10 cycles of 94°C (30 seconds), 60°C (30 seconds), 72°C (30 seconds), 25 cycles of 94°C (30 seconds), 55°C (30 seconds), 72°C (30 seconds), and finally, 72°C for 10 minutes.

Longfile21: As for 'File21', except the time allowed for extension (72°C) in the cycling steps was lengthened to 90 seconds.

In vitro site-directed mutagenesis

Primers for the site-directed mutagenesis were designed following the instructions provided in the QuikChange Site-Directed Mutagenesis kit (Stratagene). The reaction was carried out in a 50 µL volume. To each reaction the following was added: 5 µL of 10× Pfu reaction buffer, 200 ng double-stranded DNA template, 125 ng forward primer (ZHD.QC.F1), 125 ng reverse primer (ZHD.QC.R1), 1 µL of 10mM dNTP mix (10 mM each dNTP), 5 µL DMSO and MQ water to a final volume of 49 µL. 1 µL Pfu Turbo DNA polymerase (2.5 units/µL) was added last. The reaction was cycled in an MJ Research PTC-200 Peltier Thermal Cycler, as follows: 150 seconds at 95°C, then 30 cycles of 30 seconds at 95°C, 60 seconds at 55°C and 20 minutes at 68°C. The parental (non-mutated) DNA was digested by adding 1 µL of *Dpn* I (20 units) to the reaction, and incubating at 37°C for 4 hours. 1 µL of this digest reaction was then transformed by heat shock into DH5α cells and transformants were screened by digesting colony PCR products with *Kpn*I to see whether the introduced restriction site was present. The introduced mutation was further confirmed using sequencing analysis.

PCR-based expansion of pure and interrupted repeats

The repeat tracts in plasmids *hd*ex1$(CAG)_{23}$ and *hd*ex1$(CAG/CAA)_{14}$ were expanded using an adaptation of a previously described method for introducing repeat expansions into CAG-repeat-containing genes (211), that also proved successful for expanding the interrupted repeat.

Expansion of CAG repeats

Preparation and execution of PCR1: 100 ng of *hd*ex1$(CAG)_{23}$ plasmid was linearised downstream of the repeat by the restriction enzyme *BseR*I in a 10 µL reaction volume. A 1/100 dilution of this reaction was made, and 2 µL (2 ng) were used for PCR1 in a total reaction volume of 20 µL, using primers ZHD.F3+*Bam*HI and $(CTG)_{10}$, each at a final concentration of 2.5 ng/µL. The reaction also contained 2 mM dNTPs, 1 unit of Pfu DNA polymerase, and 1× Pfu buffer. The PCR reactions were carried out using cycling conditions described previously (211). Since the trinucleotide repeat primer could anneal at various positions overlapping the template repeat sequence, PCR products with variable and increased repeat length were generated.

Preparation and execution PCR2: 100 ng of *hd*ex1$(CAG)_{23}$ plasmid was linearised upstream of the repeat by the restriction enzyme *Msc*I in a 10 µL reaction volume. Dilution and PCR amplification was carried out as for PCR1 except that primers $(CAG)_{10}$ and ZHD.R3+*Eco*RI were used.

Preparation and execution of PCR3, and re-cloning of expanded products back into pGem-T: 1 µL of PCR1 and 1 µL of PCR2 were combined with 18 µL MQ water. The DNA species were denatured at 94ºC for 5 minutes, and annealed at 65ºC for 2 minutes. The reaction volume was then increased to 50 µL with the addition of 2 mM dNTPs, 1× Pfu buffer (final concentrations) and 2.5 units of Pfu DNA polymerase, and hybrid DNA species were elongated for 5 minutes at 72ºC to reconstitute the unique sequences flanking the repeat. Only hybrids formed between the sense strand from PCR1 and the antisense strand from PCR2 could be extended by the polymerase, each acting as both a primer and a template for the other. Also, since the expanded repeats at the 3' end of each DNA species can anneal to each other in various positions overlapping the repeat at the 3' end of the complementary strand, further repeat expansion could occur in this step. A 1/50 dilution was then prepared from this sample, and 5 µl was used as template for PCR reaction 3 (PCR3), designed to amplify the successfully reconstituted products. Additionally this reaction contained external primers ZHD.F3+*Bam*HI and ZHD.R3+*Eco*RI (3 ng/µL each), dNTPs (0.5 mM), 0.75 µl of ELT

enzyme and 1× ELT buffer 2 in a 50 µL total reaction volume. Since the original template was cut between these primers by restriction enzymes *BseR*I or *Msc*I (prior to PCR1 and PCR3, respectively) amplification of the original sequence was avoided. This reaction yielded products ranging in size from ~400 bp (the original size) to >5 kb viewed as a smear on an agarose gel. DNA products migrating in the size range of 650 to 1,000 bp (predicting repeat lengths of 80 to 200 repeats) on an agarose gel were excised in a single block, purified, and ligated back into pGem-T. Transformants were screened by colony PCR to identify expanded clones that were then sequenced to determine the exact repeat copy number.

Expansion of CAG/CAA mixed repeat

Expansion of the interrupted repeat in plasmid *hd*ex1$(CAG/CAA)_{14}$ was achieved in the same manner as described above for the pure repeat, except that primers ZHD.F3+*Bam*HI and $(CAG/CAA)_{10}$ were used for PCR1 and primers $(CTG/TTG)_{10}$ and ZHD.R3+*Eco*RI were used for PCR2. The design of the mixed repeat primers allows them more than one possible annealing site, and the expansion procedure resulted in a spread of product sizes similar to that obtained with the pure repeat.

Automated sequencing

DNA was sequenced using the ABI PRISM® BigDye™ v3.0 Terminator Ready Reaction Cycle Sequencing Kit with AmpliTaq™ DNA polymerase, FS (Applied Biosystems). Typically a sequencing reaction contained 500 ng of purified double-stranded template DNA, 20 ng of primer, 4 µL of BigDye Terminator mix (half the amount suggested by manufacturers) and MQ water up to a 20 µL volume. Reactions were performed using an MJ Research PTC-200 Peltier Thermal Cycler, with the following conditions: 25 cycles of 96°C for 30 seconds, 50°C for 15 seconds and 60°C for 4 minutes. Afterwards, the samples were purified as follows. Extension products were precipitated for 15 minutes at room temperature (~22°C), following the addition of 80 µL of 75% isopropanol to each sample. Precipitated DNA was pelleted by centrifugation for 20 minutes at 13,000 rpm and the supernatant was carefully removed by pipetting. The pellet was washed by briefly vortexing in 250 µL of 75% isopropanol. After 5 minutes of centrifugation the supernatant was carefully removed, and the pellet was air-dried. Running of Dye Terminator gels was conducted by the Sequencing Centre at the Institute of Medical and Veterinary Science, and the output was returned as a Macintosh®-compatible chromatogram file that was then analysed using SeqMan II™ software.

RNA extraction from zebrafish embryos and preparation of cDNA

RNA extraction

RNA was prepared from a frozen sample of 100 zebrafish embryos (72 hours post fertilisation) as follows. The tissue was thawed, homogenised with an eppendorf pestle in guanidine thiocyanate-containing "RLT" buffer from the RNeasy Mini Kit, and filtered through a QIAshredder column to remove most of the insoluble debris. The flow-through was centrifuged at maximum speed to pellet any particulate matter, and the supernatant was transferred to a new tube. The DNA was precipitated by adding an equal volume of ethanol, and then the RNA was extracted from the sample using the RNeasy Mini Kit according to the manufacturer's instructions.

Preparation of cDNA

To obtain cDNA from extracted RNA, reverse transcription was performed using SuperScript II RNase H^- Reverse Transcriptase according to the manufacturer's instructions.

Generation of DNA constructs not containing repeats

*hd*ORF(1-1503): The first 1503 bp of zebrafish *hd* open reading frame (ORF) was amplified from total cDNA using primers ZHD.F7+*Eco*RI and ZHD.R7+*Xba*I, and cloned into pCS2+ (208) as an *Eco*RI/*Xba*I fragment (not shown diagrammatically).

hd(1.2):EGFP: The published zebrafish *hd* cDNA sequence (141); Genbank accession no AF052603) was used to perform a BLAST search of the Sanger Centre Zebrafish Sequencing Project genomic DNA database in order to obtain additional 5' sequence. A region of DNA sequence spanning ~1.2 kb 5' to, and including, the first 15 nucleotides of the *hd* ORF was amplified from zebrafish genomic DNA using primers ZHD.F8+*Sph*I and ZHD.R8+*Sac*II and was ligated into pGem-T. A region containing the *EGFP* ORF and SV40 polyadenylation (pA) signals was amplified from pIRES2-EGFP (Clontech) using primers pI2EGFP.F2 and pI2EGFP.R2+*Nco*I, and ligated in frame as a *Nco*I fragment downstream of the *hd* sequence, utilising the *Nco*I sites spanning both the fourth codon of the *hd* ORF, and the start codon of *EGFP*. A schematic illustration of this construct is shown in chapter 3 (Fig. 3.1 C).

Sequencing of this plasmid revealed 3 nucleotides within the *hd* 5' sequence that differed from the published sequence (141). Relative to the translation start site (+1), these were G→C (-558), A→G (-529), and T→C (-223). While it is possible that these alterations could have been introduced by DNA polymerase during PCR amplification,

the error rate for the polymerase enzyme mix used (from the ELT System; 4.8×10^{-6}) is not sufficient to account for the observed variation (3 in 1227 nucleotides). Since the laboratory zebrafish strains used in this study are not inbred, sequence variation is expected, and therefore these alterations are likely to be polymorphisms.

Generation of repeat-containing constructs

Isolation of hd exon 1 and preparation to receive repeats

A region containing the ORF of the zebrafish *hd* exon 1 (99 bp), flanked by 250 bp of 5' sequence and 18 bp of intron 1, was PCR amplified from zebrafish genomic DNA using primers ZHD.F3+*Bam*HI and ZHD.R3+*Eco*RI. This product was ligated into the pGem-T vector in the forward orientation with respect to the vector sequence (Fig. 2.1 A).

The four consecutive glutamine residues comprising the 'polyglutamine tract' in zebrafish Htt are encoded by the sequence $(CAG)_3CAA$. In order to facilitate the expansion of this tract to pathological length, site-directed mutagenesis was performed (using primers ZHD.QC.F1 and ZHD.QC.R1) to introduce 4 bases (*GTAC*) between the first and second CAG repeat, creating a *Kpn*1 restriction site (Fig 2.2; method adapted from (212)). A successful clone was selected by screening transformants using colony PCR methods (vector primers M13F and M13R), and digesting the products with *Kpn*1. Incorporation of the 4 bases was confirmed by sequencing (Fig. 2.1 B). In preparation for the insertion of expanded repeat sequences, this vector was linearised with *Kpn*1, dephosphorylated, and treated with T4 DNA polymerase to remove the resulting 3' overhangs, providing a blunt-end insertion point into which the various repeats could be ligated, in frame with the zebrafish *hd* ORF (Fig. 2.2).

Introduction of pure and interrupted repeats of modest length

To introduce initial modest expansions into the repeat tract, two pairs of complementary oligo 30mers were used. The oligos of the first pair, for creating uninterrupted repeats, were 5'- $(CAG)_{10}$ and 5'- $(CTG)_{10}$. The oligos of the second pair, for creating interrupted repeats, were 5'- CAG CAA CAA CAG CAA CAG CAG CAA CAA CAG and 5'- CTG TTG TTG CTG CTG TTG CTG TTG TTG CTG (referred to as $(CAG/CAA)_{10}$ and $(CTG/TTG)_{10}$, respectively). Each pair of oligos was annealed to create blunt-ended units of 10 triplet repeats. These 10-repeat units were phosphorylated, and ligated into the blunted *Kpn*1 site of *hd* exon 1. Resulting transformants were screened by colony PCR methods to identify expanded clones, and selected clones were sequenced to identify those with inserts the correct orientation. In most cases, only a single 10 repeat

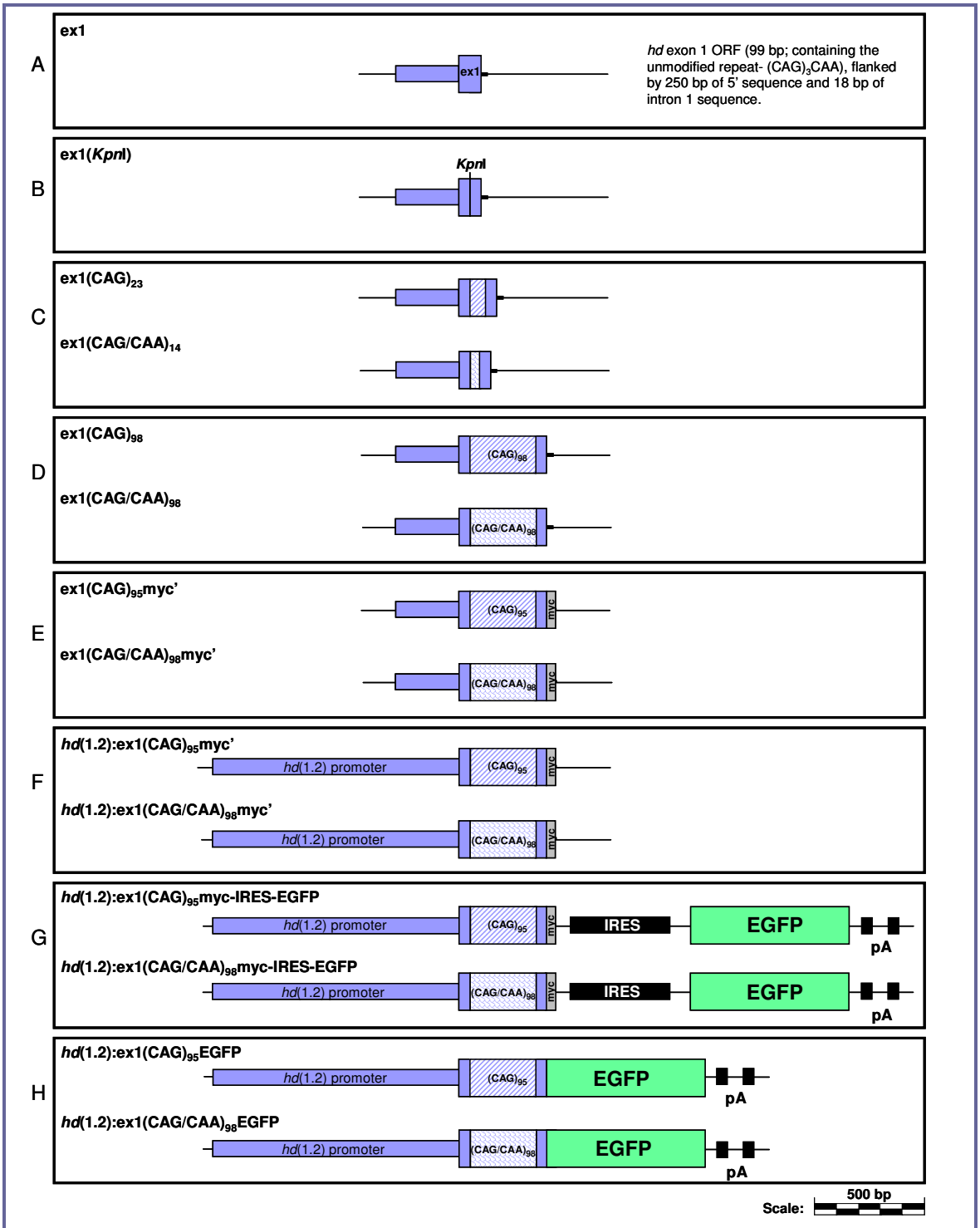

Figure 2.1 Schematic diagram illustrating the sequential steps (A-H) involved in the generation of repeat-containing contructs (G and H), as referred to in the main text. All inserts lie within the bacterial cloning vector, pGem-T. Inserts are in the same orientation as that of the pGem-T vector sequence, except where indicated by an apostrophe (**E** and **F**) in which case the insert is in the reverse orientation. Purple block colour represents sequence derived from the zebrafish *hd* gene. Purple striped and paved patterns indicate pure and mixed repeat sequences, respectively, that were inserted into the *Kpn*I site. The EGFP ORF is indicated in green. Positions of the IRES and polyadenylation (pA) signals (black) and myc tag (grey) are indicated.

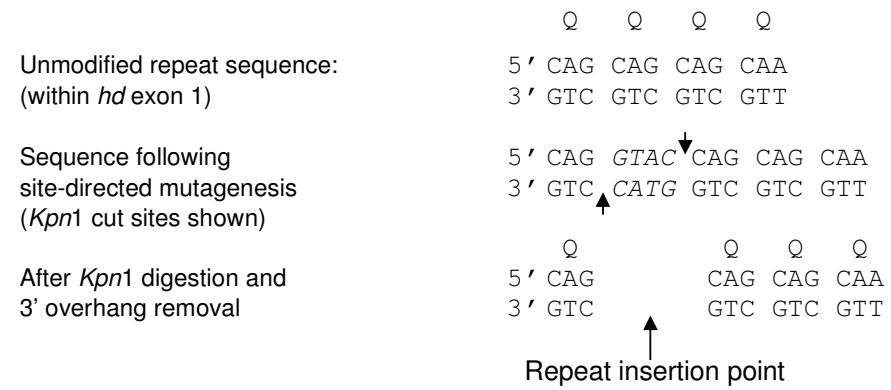

Figure 2.2 Introduction of a *Kpn*I site into the *hd* polyglutamine-encoding region, to facilitate the insertion of longer repeat sequences. CAG and CAA codons each encode glutamine (Q).

unit was incorporated. However, for the pure repeat, one transformant contained two 10-repeat units ligated in tandem, resulting in a vector containing a total of 23 CAG repeats (plasmid ex1(CAG)$_{23}$). For the interrupted repeat, a transformant with a single 10-repeat (mixed) insertion was selected (plasmid ex1(CAG/CAA)$_{14}$; Fig. 2.1 C).

Further expansion of pure and interrupted repeats to pathogenic lengths

The repeat tracts in these plasmids were further expanded using a previously described method for introducing repeat expansions into CAG-repeat-containing genes (211), that also proved successful for expanding the interrupted repeat. The strategy is described in the section of this Chapter, entitled 'PCR-based expansion of pure and interrupted repeats'.

Expanded plasmid DNA was transformed into *E. coli* and transformants were analysed by colony PCR methods. For the pure repeat, 27/43 screened transformants yielded products that appeared to have increased in size above the original length, as visualised by agarose gel DNA electrophoresis. For the interrupted repeat, 16/29 screened transformants had increased in size. Selected transformants with predicted repeat lengths of 80 to 100 triplets were sequenced, and clones ex1(CAG)$_{98}$ and ex1(CAG/CAA)$_{98}$ were selected for further cloning steps (Fig. 2.1 D). The configuration of CAG and CAA triplets in these clones are shown in Table 2.1.

Clone	Repeat sequence
ex1(CAG)$_{98}$	CAG | (CAG)$_{95}$ | CAGCAGCAA
ex1(CAG/CAA)$_{98}$	CAG | (CAGCAACAACAGCAACAG)$_{15}$CAGCAACAACAG | CAGCAGCAA

Table 2.1 Configuration of CAG and CAA triplets within the repeat sequence in expanded exon 1 clones *hd*ex1(CAG)$_{98}$ and *hd*ex1(CAG/CAA)$_{98}$. Vertical bars represent the boundaries between endogenous *hd* gene sequence and additional repeat sequence.

Fusion of myc tag sequence

Sequence encoding a 10 amino acid myc tag and stop codon (TAG) were added to the 3' end of each of the expanded *hd* exon 1 ORFs by PCR amplification using primers ZHD.F3+RS and ZHD.R9+MTtag. The PCR products were ligated back into pGem-T, and clones in which the insert had integrated in the reverse orientation were selected by restriction analysis. Sequencing of selected clones revealed sequence alterations within the pure repeats in 3/3 clones that were analysed. In two clones, repeat length was unchanged but 1 or 2 nucleotide substitutions had occurred (C→T in 2 cases, G→A in one case) despite the use of ELT DNA polymerase mix that has proofreading activity. In the third clone, the CAG repeat had contracted from 98 to 95 triplets, but there were no nucleotide substitutions so this clone (*hd*ex1(CAG)$_{95}$myc') was chosen for further steps. For the interrupted repeat, one clone was sequenced and the integrity of the repeat sequence was conserved. This clone was named *hd*ex1(CAG/CAA)$_{98}$myc' (Fig. 2.1 E).

Addition of the hd(1.2) promoter region

In the next step, the myc-tagged exon 1 fragments were placed downstream of the *hd*(1.2) promoter region. First the promoter region was amplified from genomic DNA using primers ZHD.F8+*Sph* and ZHD.F3+*Bam*HI, and ligated into pGem-T (not shown diagrammatically). A transformant with the promoter fragment in the reverse orientation was selected. Each myc-tagged expanded exon 1 fragment was subsequently inserted downstream of the promoter as a *Nco*I fragment. The resulting clones were named *hd*(1.2):ex1(CAG)$_{95}$myc' and *hd*(1.2):ex1(CAG/CAA)$_{98}$myc' (Fig. 2.1 F).

Addition of EGFP reporter as a bi-cistronic sequence

A fragment containing the IRES sequence, *EGFP* ORF and two pA signals was PCR amplified from the eukaryotic expression vector pIRES2-EGFP, using primers pI2EGFP.F3+*Sac*II (*Sac*II site not subsequently used) and pI2EGFP.R2+*Nco*I. This product was ligated into pGem-T and a clone containing the insert in the forward orientation was selected (IRES-EGFP; not shown). Sequence analysis revealed a nucleotide within the IRES region that differed from the published vector sequence

(Clontech). This G→A variation was subsequently found in the parent vector (pIRES2-EGFP) at nucleotide position 1146, and was thus disregarded, as the vector is known to successfully express EGFP.

The *hd*(1.2):ex1(CAG)$_{95}$myc and *hd*(1.2):ex1(CAG/CAA)$_{98}$myc fragments were each released from pGem-T and ligated as *Sph*I/*Sac*II fragments, upstream of the IRES in vector IRES-EGFP. The resulting clones were named *hd*(1.2):ex1(CAG)$_{95}$myc-IRES-EGFP and *hd*(1.2):ex1(CAG/CAA)$_{98}$myc-IRES-EGFP (Fig. 2.1 G).

Addition of EGFP reporter as a fusion protein

Another set of plasmids was created in which the *EGFP* ORF was fused in frame to the 3' end of the expanded *hd* exon 1 fragments (the last 4 codons of *hd* exon 1 were lost in doing so). First the *EGFP* ORF and pA signals were first PCR amplified from the pIRES2-EGFP vector using primers pI2EGFP.F4+*Sac*I and pI2EGFP.R2+*Nco*I, and the resulting product was ligated into pGem-T. A clone containing the insert in the forward orientation was then selected, enabling the insert to be released with the *Sac*I restriction enzyme. The myc-IRES-EGFP-pA region was removed from bi-cistronic vectors *hd*(1.2):ex1(CAG)$_{95}$myc-IRES-EGFP and *hd*(1.2):ex1(CAG/CAA)$_{98}$myc-IRES-EGFP using *Sac*I (utilising an endogenous *Sac*I site that cuts 4 codons upstream from the 3' end of *hd* exon 1, and a unique site within the pGem-T vector), and was replaced with the EGFP-pA *Sac*I fragment, creating fusion vectors *hd*(1.2):ex1(CAG)$_{95}$EGFP and *hd*(1.2):ex1(CAG/CAA)$_{98}$EGFP (Fig. 2.1 H).

Zebrafish maintenance and staging

Zebrafish were maintained at 28.5°C under standard conditions as described (213). Developmental stages were determined by using both hours post fertilisation (hpf) and morphological features (204).

Zebrafish embryo fixation

Zebrafish embryos were fixed by placing them in 4% formaldehyde (in 1× PBS) at 4°C for at least 16 hours. Embryos 22 hpf and older were manually dechorionated prior to fixation so that they would not be fixed out of shape. Embryos of earlier time-points were dechorionated either before or after fixation since their shape was not restricted by the chorion.

Whole-mount *in situ* hybridisation of mRNA

Generation of probes

For synthesis of labelled RNA probe antisense to *hd* mRNA, template vector *hd*ORF(1-1503) was linearised at the 5' *Cla*I site and transcribed with T7 RNA polymerase in the presence of digoxigenin-labelled UTP. *notch2* (*notch6*) probe was prepared by linearising vector BJ1 with *Bam*HI and transcribing with T3 RNA polymerase in the presence of digoxigenin-labelled UTP.

Whole-mount in situ hybridisation

Pre-treatment and hybridisation of whole-mount zebrafish embryos was performed as described (214). Proteinase K was used at a concentration of 10 µg/mL in PBST, to further permeabilise embryos aged 36 hpf (5 minutes) and 48 hpf (10 minutes). The hybridisation buffer used is as listed earlier in this chapter. AP-conjugated anti-digoxigenin antibody and BCIP/NBT substrate were used for probe detection, as described (214). Embryos were stored in 80% glycerol for microscopy and photography.

Embryo microinjection conditions and solution concentrations

All MOs were solubilised in MQ water to create 2 mM stocks. Prior to microinjection, MO stock samples were diluted to the required concentration, in MQ water. For all experiments involving microinjection, zebrafish embryos were injected into the cytoplasm at the 1-cell stage using an MPPI-2 Pressure Injector (Applied Scientific Instrumentation Inc.).

In preparation for experiments involving the injection of DNA, vector DNA was linearised (*Xmn*I) and purified using the QIAquick PCR Purification Kit. DNA injections for experiments described in Chapter 3 (mosaic expression of EGFP constructs) were performed either by S. Nornes or myself, and typically involved the injection of ~5 nL of DNA sample at a concentration of 40 pg/µL.

Experiments involving the use of MOs (described in Chapters 4 and 5) were performed by B. Tucker, S. Nornes, S. Wells or myself, as indicated in Table 2.2. The MO doses administered in different experiments are also detailed in Table 2.2. For iron-rescue experiments, Ferroject iron dextran injectable solution (Swift and Company Ltd) (referred to here as iron-dextran) was co-injected as indicated (Table 2.2).

Chapter	Experiment	MO sample concentration (mM)	Approximate injection volume (nL)	MO dose (ng)	Co-injected sample concentrations
4	EGFP knockdown[a]	0.5	5	21.3	*hd*(1.2):EGFP (40 pg/nL)
4	Western[a] (T. Henshall)	0.5	5	21.3	-
4	Initial assessment[b]	0.25 0.5 1.0	5 5 5	10.6 21.3 42.3	- - -
4	Low dose assessment[c]	0.1	5	4.3	-
4	Dose response[c]	0.05 0.1 0.15	5 5 5	2.1 4.3 6.4	- - -
4	Pigment quantification[d]	0.1	7.5	6.4	-
4	TUNEL (POD)[d]	0.5	5	21.3	-
4 4	TUNEL (TMR red)[c,a]	0.5 0.2	5 5	21.3 8.5	- -
5	Initial *o*-dianisidine assessment[d]	0.5	2	8.5	-
5	Prussian blue (whole-mount)[a]	0.2	5	8.5	-
5	Prussian blue (isolated blood cells)[d]	0.5	2	8.5	
5	Iron rescue experiment 1[a] Iron rescue experiment 2[d]	0.2 0.5	5 2	8.5 8.5	iron-dextran (20 ng/nL) iron-dextran (25 ng/nL)
5	Assessment of effect of iron-dextran on *hd*MO function[d]	0.2	5	8.5	*hd*(1.2):EGFP (40 pg/nL) iron-dextran (40 ng/nL)
5	Assessment of *tfr1a* and *tfr1b* transcript levels by qPCR[d] (S. Dayan)	0.5	2	8.5	

Table 2.2 Details of injection volumes and concentrations used in MO studies. Injections were performed by *a*: S. Nornes, *b*: B. Tucker, *c*: A. Lumsden (myself), or *d*: S. Wells, as indicated.

Detection and analysis of apoptosis in zebrafish whole-mount embryos

Preparation of tissue

Zebrafish embryos were fixed in 4% formaldehyde. To facilitate reagent penetration, tissue was permeabilised as previously described (215). Briefly, embryos were dehydrated in a graded ethanol series (50, 70, 95, 100%, 20 minutes in each), followed by 10 minutes in acetone at –20°C. After a rinse in PBS embryos were further permeabilised in sodium citrate buffer for 15 minutes and rinsed twice in PBS.

Detection of apoptotic cells

The fragmented DNA of apoptotic cells was labelled by TUNEL (terminal deoxynucleotide transferase (TdT)-mediated dUTP nick-end labelling) using either the POD (peroxidise) or TMR (tetramethylrhodamine) red In Situ Cell Death Detection Kit

(Roche), according to the instructions of the manufacturer. For the POD (peroxidase) kit, PBS-dissolved SigmaFast DAB/urea (H_2O_2) tablets (Sigma-Aldrich) were used as the peroxidase substrate. In negative control experiments, embryos were treated in an identical manner except that the TdT enzyme was omitted from the labelling incubation. No staining was observed in these embryos. Embryos were equilibrated in 80% glycerol at 4ºC prior to microscopy (in the dark for TMR red-labelled embryos).

Scoring criteria

The level of apoptosis in embryos stained using the TMR red In Situ Cell Death Detection Kit was analysed using fluorescent microscopy (See below in section entitled 'Microscopy'). The embryos depicted as 'low' and 'high' in Chapter 4 (Table 4.1) were designated as standards for classing the embryos. Those with a similar, or lower level of apoptosis than that in the 'low' standard embryo were classed as 'low', and those with a similar or higher level than that in the 'high' standard embryo were classed as 'high'. Embryos with a level of apoptosis between the 'low' and 'high' standards were classed as 'medium'. Classification was performed by M. Lardelli, who was unaware of the injection status of the embryos.

Histochemical staining of haemoglobin

Staining of whole embryos

Haemoglobin activity was detected in whole embryos by performing *o*-dianisidine staining, essentially using methods previously described (216). Live embryos were placed in *o*-dianisidine stain for 15 minutes in the dark (the embryos die within the first 10 seconds). After incubation, the stain was removed and embryos were rinsed 2-3 times with MQ water. Embryos were post-fixed in 4% formaldehyde and stored in 80% glycerol for microscopy.

Scoring criteria

Each stained embryo was observed under the microscope at 10× and 20× magnification, such that individual blood cells (stained with *o*-dianisidine) were clearly visible on the yolk ball. Within any given embryo, the intensity of staining was similar in most blood cells. Embryos were scored based on whether the blood cells exhibited weak or strong *o*-dianisidine staining.

Histochemical staining of ferric iron

Staining of whole embryos

For detection of ferric iron in whole zebrafish embryos, a 3,3-diaminobenzidine (DAB)-enhanced Prussian blue staining method was used, as follows. Fixed embryos were immersed in a freshly prepared working solution containing 2.5% potassium ferrocyanide and 0.25 M HCl, for 30 minutes at room temperature, then rinsed 3 times in PBST. Potassium ferrocyanide reacts with ferric ions in the embryo, producing ferric ferrocyanide (Prussian blue). In preparation for stain enhancement, endogenous peroxidase activity was quenched by incubating the embryos in 0.3% H_2O_2 (in methanol) for 20 minutes at room temperature. Following two rinses in PBST, embryos were incubated for 7 minutes in DAB substrate using PBS-dissolved SigmaFast DAB/urea (H_2O_2) tablets (Sigma-Aldrich). Ferric ferrocyanide catalyses the H_2O_2-mediated oxidation of DAB, producing a reddish brown colour. Finally embryos were rinsed 3 times in PBST, and stored in 80% glycerol for microscopy.

Isolation and staining of blood cells

Live embryos (33 hpf) were placed in a solution of PBS, containing tricaine (anaesthetic). Blood cells were released by cardiac puncture onto a poly-L-lysine coated slide. Embryo debris was carefully removed with tweezers and blood cells were allowed to settle and adhere to the slide for 30 minutes. The cells were then fixed in 4% formaldehyde (in PBS) for 30 minutes. Ferric iron was detected using a DAB-enhanced Prussian blue staining method similar to that used for whole embryos described above, with a few modifications, as follows. Cells were incubated in a working solution of 0.5% potassium ferrocyanide and 0.75% HCl (conditions previously used for staining blood cells (217)) for 30 minutes. The cells were then rinsed 3 times in PBST. Endogenous peroxidase activity was quenched by incubating the cells in 0.3% H_2O_2 (in methanol) for 20 minutes. Following two rinses in PBST, embryos were incubated for 4 minutes in DAB substrate using PBS-dissolved SigmaFast DAB/urea (H_2O_2) tablets (Sigma-Aldrich). Finally, cells were rinsed 3 times in PBST, and air-dried before being covered with 80% glycerol and a coverslip for microscopy.

Microscopy

Whole live embryo images

For live embryo images, a Nikon TE300 inverted microscope was used, with bright field optics. Black and white images were captured using a Photometrics Coolsnap fx black and white digital camera and Digital Optics V++ precision digital

imaging system software. Colour images (of circulating blood in the heart) were captured using Nikon COOLPIX 995 digital camera and image colour was optimised using Adobe Photoshop 6.0 software.

mRNA in situ hybridisations

For mRNA *in situ* hybridisation images, a Zeiss Axiophot microscope was used with DIC (Nomarski differential interference contrast) optics. Images were captured using a Fujix HC1000 digital 3CCD colour camera and Fujix Photograb imaging software. Image collages were compiled using Adobe Photoshop 6.0 software.

EGFP fluorescence

For EGFP fluorescence images, a Nikon TE300 inverted microscope was used in conjunction with UV excitation. Images were captured using a Photometrics Coolsnap fx black and white digital camera and Digital Optics V++ precision digital imaging system software. Contrast was adjusted and green colour was added to the images using Adobe Photoshop 6.0 software.

TUNEL staining of apoptotic cells

For images of embryos TUNEL-labelled with POD, a Zeiss Axiophot microscope was used with DIC (Nomarski differential interference contrast) optics. For images of embryos TUNEL-labelled with TMR red, a Nikon TE300 inverted microscope was used in conjunction with UV excitation. Images were captured using a Photometrics Coolsnap fx black and white digital camera and Digital Optics V++ precision digital imaging system software. Red colour was added to the images using Adobe Photoshop 6.0 software.

Prussian blue staining

Images of Prussian blue-stained whole embryos and isolated blood cells were obtained using a Zeiss Axiophot microscope. For whole embryos, staining was visualised using bright field optics, and DIC (Nomarski) optics was used to aid the identification of blood cells in the intermediate cell mass. Staining of isolated blood cells was observed using bright field optics. All images were captured using a Fujix HC1000 digital 3CCD colour camera and Fujix Photograb imaging software. Colour and contrast were optimised using Adobe Photoshop 6.0 software.

Quantitative PCR

The following procedures were carried out by S. Dayan, according to the instructions of the manufacturers. Total RNA was extracted from zebrafish embryos (approximately 30 embryos per sample) using the RNeasy mini kit (QIAGEN). From this RNA, cDNA was synthesised using Superscript II RNase H^- Reverse Transcriptase (Invitrogen). Quantitative PCR (qPCR) was performed on an ABI 7000 sequence detection system (Applied Biosciences), using the relative standard curve method for quantification, as described by the manufacturers. The primers used to detect *tfr1a*, *tfr1b* and *acta1* transcripts are listed in the appropriate section of this chapter. Primers for *tfr1a* and *tfr1b* were designed by S. Dayan, and *acta1* primers were designed by T. Henshall, using Primer Express software (Applied Biosystems).

Chapter 3: Investigation of the role of somatic instability in HD pathogenesis, and progress towards a transgenic zebrafish model of HD

Introduction

In most polyglutamine diseases, including HD, the disease-causing expanded repeat is unstable in length. Upon transmission from one generation to the next (particularly via the paternal germline), these expanded repeats tend to further increase in size, leading to an earlier age of onset in subsequent generations. The disease alleles are also commonly unstable within somatic tissues, leading to mosaicism of repeat length within an individual. The current views on potential mechanisms of germline and somatic repeat instability are discussed in a recent review (218).

It has been proposed that somatic instability may play a role in the pathogenesis of CAG/polyglutamine repeat diseases, whereby the repeat length increases with age (above the inherited copy number) until reaching a certain pathogenic threshold, above which it becomes toxic to cells (193). This model is in agreement with inherited CAG copy number being inversely related to age of onset in these diseases, since the more repeats an individual inherits, the fewer years it would take for gradual somatic expansion to raise the repeat copy number in the HD allele above that critical disease causing length.

Interestingly, in the human HD brain (15), and in a mouse knock-in model of HD (197), somatic instability has been observed most significantly in the regions showing the greatest neuropathological involvement (such as the basal ganglia and cerebral cortex), whilst the cerebellum, which is rarely affected in HD, shows limited repeat instability;. This correlation gave rise to the suggestion that somatic expansion may contribute to HD pathogenesis and to the specificity of neurodegeneration in this disorder.

Research aim

The objective of this study was to investigate the contribution of somatic instability to age of onset and disease severity in an animal model of HD. The intended strategy was to generate transgenic zebrafish that would express the *hd* gene containing either a pure CAG repeat of disease-causing length, or an interrupted repeat tract of comparable length, comprised of a mixture of CAG and CAA codons. The CAA codon also encodes glutamine, therefore the repeat tract would be interrupted only at

the nucleotide level, whilst not affecting the polyglutamine tract at the protein level. As interruptions are known to have a stabilising effect on trinucleotide repeats, it was expected that the CAA triplets would hinder somatic expansion and allow the effects that this has on neuropathology and on age of onset to be assessed.

Rationale behind transgene design

In the design of the transgenes to be used in this study, care was taken in deciding 1) the protein context in which to express the repeat, 2) the appropriate repeat length to use, 3) what promoter to use to drive expression, and 4) what reporter gene to use. The rationale behind the decisions made in transgene design is outlined below. The resulting expression vectors that were generated (as described in Chapter 2, Materials and methods), and used in the experiments presented in this chapter, are illustrated schematically in Figure 3.1.

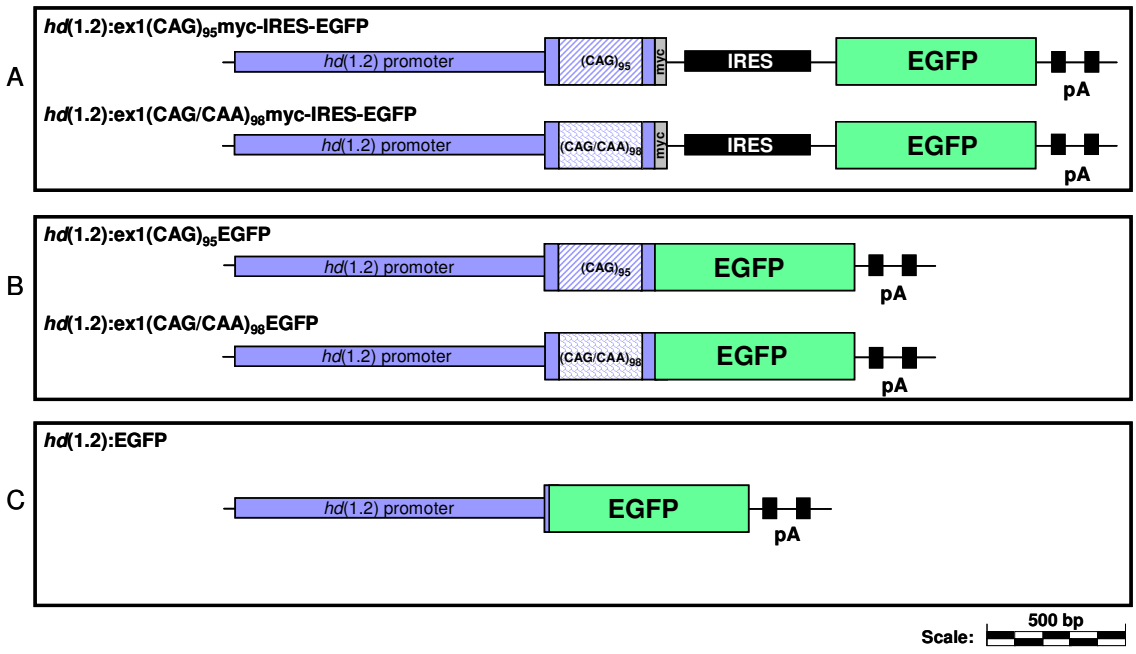

Figure 3.1 Schematic representation of the expression vectors used in experiments described in this chapter. All constructs are driven by a 1.2 kb fragment of zebrafish *hd* 5' DNA sequence, and contain 2 polyadenylation signals at the 3' end. Purple block colour represents sequence derived from the zebrafish *hd* gene. (**A** and **B**) Pure $(CAG)_{95}$ (striped pattern) and mixed $(CAG)_{98}$ (paved pattern) expanded repeats were incorporated into the *hd* exon 1 open reading frame (ORF). Expanded *hd* exon 1 sequences were linked to the *EGFP* ORF (green) either (**A**) bi-cistronically (separated by an IRES), or (**B**) so as to create a fusion protein. In (**A**), sequence encoding a single myc tag was incorporated in frame at the 3' end of the exon 1 fragments. (**C**) Reporter construct *hd*(1.2):EGFP encodes a fusion protein comprised of the first 3 amino acids of Htt (Met-Ala-Thr) followed by EGFP.

Context of the repeat

Since the isolation of the human *HD* gene in 1993 (2), numerous mouse models of HD have been generated that replicate many of the symptoms of the human disease (summarised in (219, 220)). The models differ in various ways including whether the expanded repeat is introduced into the endogenous *Hdh* gene (knock-in models), within a truncated cDNA fragment as a transgene, or within a YAC genomic fragment containing the whole gene (and others). Expression levels of the disease allele vary depending on the promoter used, and the number of integrated copies of the transgene. In general, the larger the repeat, and the shorter the fragment in which it resides, the more severe the outcome. However, the models in which the mutation resides within full-length Htt (such as the knock-in models and the YAC transgenic mice) show selective neuronal cell loss that more closely resembles HD pathogenesis than models in which a short fragment is used. Given the apparent importance of repeat context in determining specificity of HD neurodegeneration, it would be ideal to express the repeat in the context of the full-length gene. Currently the technology is not available to make a knock-in model in zebrafish, therefore a transgenic approach was taken. Transgenes were created that would express the expanded repeats within an exon 1 fragment of the zebrafish *hd* gene (similar to the widely recognised R6/2 model that expresses exon 1 of the human *HD* gene containing an expanded repeat (71)). Although expression of the exon 1 fragments may not lead to region-specific neurodegeneration it would still be possible to study the effects of instability on age of onset and disease severity.

Promoter selection

In an effort to express the transgene in a similar spatial and temporal pattern to the endogenous *hd* gene it is preferable to drive the transgene using the endogenous promoter. In the R6/2 mouse model, ubiquitous transgene expression is driven by ~1 kb of human DNA sequence upstream of the *HD* open reading frame (71). However, it was unclear whether a mammalian *HD* promoter would be effective for driving expression in zebrafish. Therefore a 1.2 kb region of the zebrafish *hd* upstream sequence was tested for its ability to drive reporter gene expression and was found to be suitable for driving transgene expression (as will be described in the 'Results' section).

Strategy for expanding the hd CAG repeat tract

As in the mouse and human Htt proteins, the polyglutamine tract in zebrafish Htt begins at amino acid 18 (141) but is comprised of only 4 consecutive glutamine residues (encoded by the sequence $(CAG)_3CAA$), and is not polymorphic in length. Expanded alleles containing 70 and 140 repeats have exhibited somatic instability in

mouse models of HD (195-197, 199), so the aim was to achieve lengths within this range. Previously described methods for introducing trinucleotide repeats into endogenous genes and for expanding existing repeat regions (211, 212) were adapted for use in this study. Pure (CAG) and interrupted (CAG/CAA) repeats encoding ~100 glutamine residues were achieved (as described in Chapter 2, Materials and methods).

Reporter gene configurations

Since zebrafish embryos are transparent and develop externally, a reporter gene encoding a fluorescent protein is a particularly useful tool for screening live embryos for transgene expression and the enhanced green fluorescent protein (EGFP) was chosen for this study. The constructs were designed in two ways. In one pair of constructs, EGFP was co-expressed downstream of the mutant Htt fragment from a single bi-cistronic mRNA transcript, by use of an internal ribosomal entry site (IRES) (Fig. 3.1 A). In the other pair, EGFP was expressed as a fusion protein, attached near the carboxy terminus of the mutant Htt exon 1 fragment (Fig. 3.1 B). Each design had advantages and disadvantages and it was not initially clear which would be the most useful. As a fusion protein, the advantage was that fluorescence would indicate the actual presence and location of the mutant Htt peptide, but there was a risk that extending the length of the mutant Htt peptide (by fusing to EGFP) would diminish the pathogenic effects of the repeat. By co-expressing EGFP and the mutant Htt fragment from a bi-cistronic transcript (separated by IRES sequence), the presence of EGFP would indicate expression of the mutant fragment, whilst not diminishing its pathogenic effects. However, it was unclear whether the IRES (routinely used in mammalian expression studies) would function efficiently enough in zebrafish to facilitate EGFP expression. Therefore a single myc-tag (10 amino acids) was fused to the carboxy terminus of the mutant Htt fragment (in the bi-cistronic constructs) so that anti-myc antibodies could be used to assess whether or not the mutant fragment was being expressed, in the absence of visible EGFP fluorescence. Two polyadenylation signals were included at the 3' end of all transgenes to aid mRNA processing.

Results

Evaluating the efficacy of DNA sequence upstream of the *hd* ORF as a suitable transgene promoter

To determine whether DNA sequence upstream of the *hd* open reading frame (ORF) would provide a suitable promoter to drive transgene expression, the normal pattern of *hd* gene expression was first examined by *in situ* hybridisation. This expression pattern was then compared to the expression pattern seen when a 1.2 kB fragment of sequence upstream of the *hd* ORF was used to drive expression of EGFP using vector *hd*(1.2):EGFP (Fig. 3.1 C).

Normal distribution of hd mRNA in the developing zebrafish embryo

Whole-mount *in situ* hybridisation was performed on zebrafish embryos of various developmental stages from 1-cell to 48 hours post fertilisation (hpf) using an antisense probe prepared from the first 1.5 kb of *hd* ORF. Expression of *hd* transcript was detected in all stages examined (Fig. 3.2). At the 1-cell stage, before the onset of zygotic transcription (which begins between 2.3 and 5.3 hpf (221)), *hd* mRNA was apparent at a high level and is therefore maternally supplied (Figure 3.2 A). The distribution of transcript was uniform during gastrulation (Fig. 3.2 B), but as development progressed, expression decreased in non-neural tissues and became stronger in the head (Fig. 3.2 C-F). At 36 hpf, expression was also increased in the intermediate cell mass (ICM; the major site of early haematopoiesis; Fig. 3.2 E), above basal levels observed throughout the trunk and tail (Fig. 3.2 E). Expression in the ICM was examined more closely, and will be described in Chapter 5. At 48 hpf, *hd* mRNA was expressed highly in the head (Fig. 3.2 F), branchial arch primordium, and developing pectoral fins (not shown), whilst basal levels persisted in the trunk and tail (Fig. 3.2 F). The early expression of the *hd* gene in zebrafish development is consistent with mammalian expression studies (107, 111, 114).

hd promoter-driven expression of EGFP in transgenic zebrafish embryos

A region of genomic DNA sequence spanning ~1.2 kb 5' to, and including, the first 15 nucleotides of the *hd* ORF was ligated in frame with, and upstream of, the *EGFP* ORF (and two SV40 polyadenylation signals) in the bacterial cloning vector, pGem-T (Promega) to create plasmid *hd*(1.2):EGFP (Fig. 3.1 C).

Wildtype embryos that were injected with *hd*(1.2):EGFP (Fig 3.3 A) exhibited fluorescence due to mosaic EGFP expression which was first detected throughout the blastoderm at 8 hpf (12 hpf shown in Fig. 3.4 A,B). Expression persisted throughout early development (Fig. 3.4 C-H) and could still be observed in a similar distribution, 8 days post fertilisation (not shown). Mosaic expression was observed in neurons, muscle fibres (myotubes), and cells of the eye, developing heart and pectoral fins although the extent of mosaic expression varied from embryo to embryo. After onset of circulation (26-28 hpf), it was not uncommon to also see the occasional circulating blood cell fluorescing. Whilst expression was mosaic, the distribution of cells expressing EGFP was comparable to the ubiquitous distribution of endogenous *hd* gene expression that was shown by mRNA *in situ* hybridisation (Fig. 3.2).

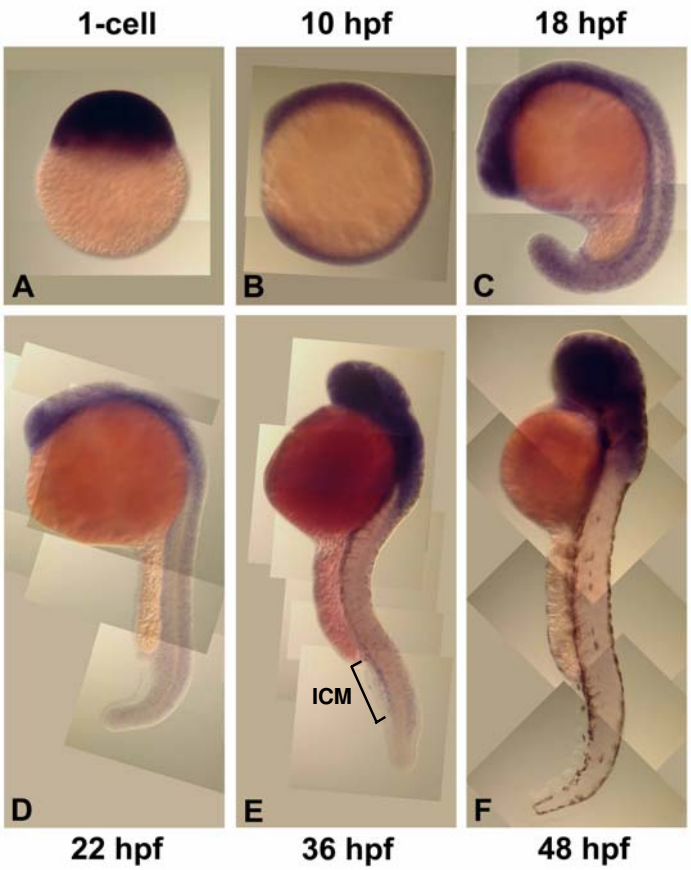

Figure 3.2 Whole-mount *in situ* hybridisation of *hd* mRNA (stained purple) in early zebrafish development. (**A**) Zebrafish *hd* transcript was detected at the 1-cell stage, prior to the onset of zygotic expression, and is therefore maternally deposited. (**B**) Distribution was uniform throughout gastrulation (10 hpf shown). (**C**-**F**) From 18 to 48 hpf expression became stronger in the head, and weaker in the trunk/tail. At 36 hpf, transcript was detected in the haematopoietic **ICM** region (**E**). In images (**E**) and (**F**), dark brown melanophores are visible.

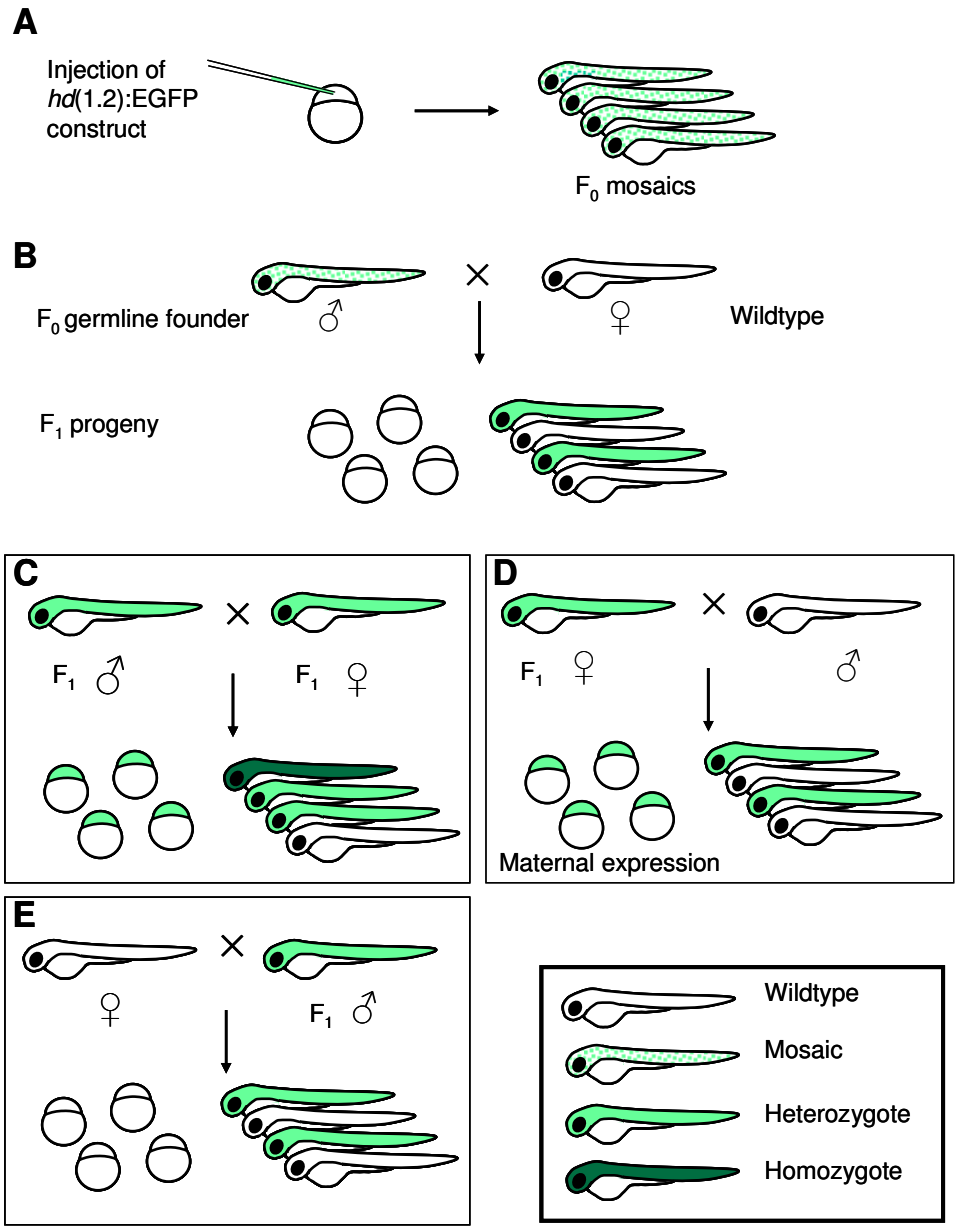

Figure 3.3 Diagram summarising the creation and breeding of *hd*(1.2):EGFP transgenic zebrafish. (**A**) Injection of the *hd*(1.2):EGFP construct at the 1-cell stage produced F_0 founder embryos that expressed EGFP mosaically. (**B**) A single F_0 germline founder (male) was identified that produced transgenic embryos amongst the progeny (F_1) of a pairwise mating with a wildtype female. No EGFP expression was observed in F_1 embryos prior to zygotic expression. (**C**) The progeny of a self-cross between male and female F_1 transgenics exhibited maternal expression of EGFP. After this faded, embryos could be identified as having either similar expression to F_1 embryos, stronger expression, or no expression, putatively representing heterozygous, homozygous and wildtype embryos, respectively. (**D**) Maternal expression of EGFP was evident in the progeny of a pairwise mating between an F_1 transgenic female and a wildtype male. Once this faded, embryos could be identified as being transgenic (heterozygote), or non-transgenic (wildtype) embryos. (**E**) A pairwise mating between an F_1 transgenic male and a wildtype female produced transgenics in the progeny, with no EGFP expression prior to zygotic expression.

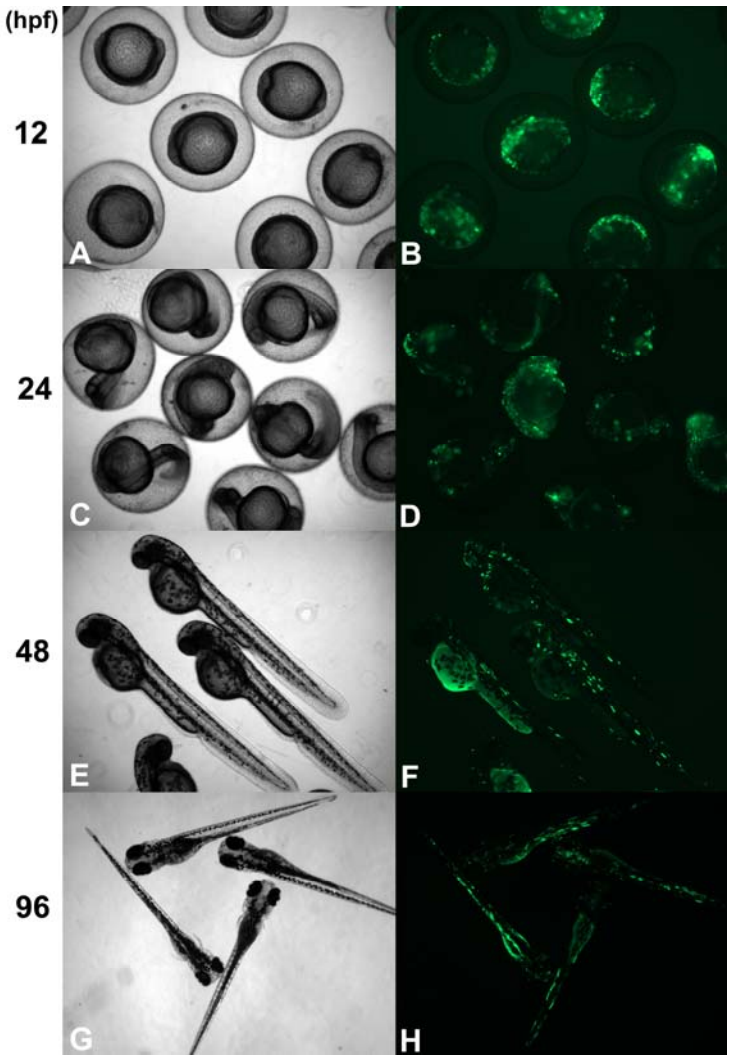

Figure 3.4 Mosaic *hd* promoter-driven expression of EGFP in live F_0 embryos at various developmental stages. Embryos were injected with plasmid *hd*(1.2):EGFP at the 1-cell stage and observed at 12, 24, 48 and 96 hpf. Bright field (**A**, **C**, **B** and **G**) and UV illuminated (**B**, **D**, **F** and **H**) images of the same embryos are shown. Note that at 24 hpf, embryos are particularly active, therefore some embryos are not in the same position within the chorion in (**C**) as they are in (**D**).

The *hd*(1.2):EGFP plasmid was injected into ~1100 wildtype embryos (founder (F_0) embryos) over a number of injection sessions, of which ~350 survived to 24 hpf (Fig. 3.3 A). In the interest of minimising progeny-screening efforts, F_0 embryos expressing EGFP were sorted into 'high' and 'low' expression groups, and these groups were raised in separate tanks. Highly expressing embryos (for example, see Fig 3.5) generally expressed EGFP in cells of at least two tissue types (most typically in neurons and muscle cells) and sometimes also expressed EGFP in a few blood cells, the eye, and/or the pectoral fin buds.

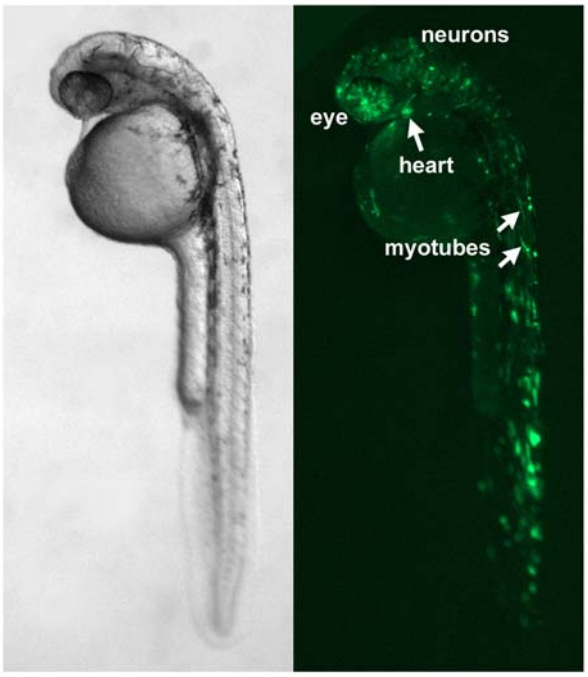

Figure 3.5 Example of an F_0 zebrafish embryo exhibiting a high level of mosaic *hd* promoter-driven EGFP expression in neurons, myotubes and cells of the eye and heart at 30 hpf. Bright field (left) and UV illuminated images of the same embryo are shown.

At the time this work was performed, a high rate of embryo attrition was experienced, with the majority of embryos (both injected and uninjected) failing to survive past a 14-day critical period. Consequently only 13 embryos survived to adulthood (>3 months). Eight of these had been classed as highly expressing embryos (2 females, 6 males), and were therefore screened preferentially for germline transmission; the reasoning being that embryos with a wider distribution of expression would have a greater chance of the transgene having also integrated into the germline. In a clutch of F_1 embryos collected from this tank of highly expressing F_0 adults, EGFP expression was detected in 24 out of 160 embryos, indicating germline integration of the *hd*(1.2):EGFP construct in at least one of these F_0 fish (Fig. 3.3A). To identify the germline founder fish, pairwise crosses were performed between F_0 transgenic fish and wildtype mates. A single germline founder (male) was identified, that produced 38% transgenic progeny overall from 3 clutches (17/39, 8/43, 74/180, the denominator representing the number of fertilised embryos in the clutch) (Fig. 3.3B). Expression was easily detectable at 36 hpf, but not at 24 hpf, and persisted at 6 days post fertilisation. The distribution of EGFP fluorescence in the F_1 generation was ubiquitous and relatively uniform throughout the head, trunk and tail, and also in the lens of the eye (a characteristic that made transgenic embryos easy to recognise amongst non-transgenic siblings) (Fig 3.6).

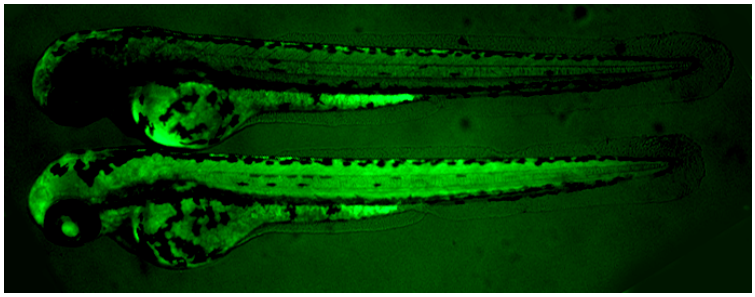

Figure 3.6 Ubiquitous *hd* promoter-driven expression of EGFP in a transgenic F_1 embryo (lower) compared to a wildtype sibling (upper) shown at 62 hpf.

Transgenic F_1 embryos collected from crosses between the founder germline transgenic male and wildtype females were subsequently raised to adulthood and were either self-crossed to each other or out-crossed to wildtype fish. Interestingly, when F_1 embryos were self-crossed (Fig. 3.3 C), all of the resulting embryos expressed a high level of EGFP in the blastocyst from the 1-cell stage, indicating maternal product deposition (Fig. 3.7).

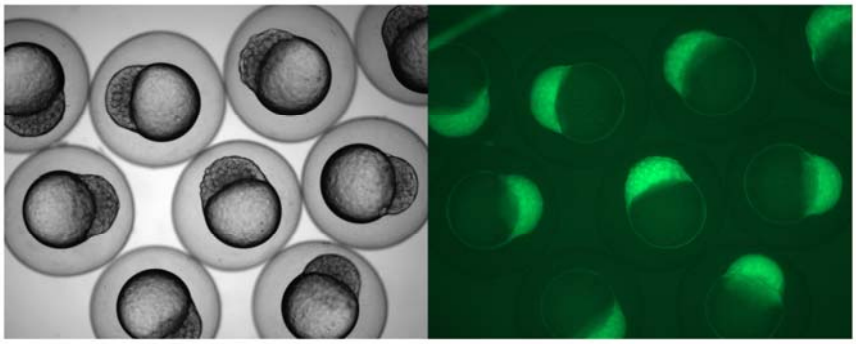

Figure 3.7 Maternal expression of EGFP in the progeny (F_2) of a self-cross between a pair of F_1 transgenic fish. Bright field (left) and UV illuminated images shown of 128-cell stage embryos (2.25 hpf).

By 3 days post fertilisation, fluorescence from the maternal product had faded and the embryos could be separated into 3 groups, based on their level of (zygotic) EGFP expression. The intensity of fluorescence at this time was either identical to F_1 transgenic embryos, more intense than F_1 transgenic embryos, or not detectable, putatively representing heterozygotes, homozygotes and non-transgenics, respectively (Fig. 3.3 C). As expected, when female F_1 embryos were mated to wildtype males, all F_2 embryos fluoresced at the 1-cell stage (Fig. 3.3 D), but when male F_1 embryos were

mated to wildtype females, no maternal product was detected, and like in the F_1 embryos derived from the male germline founder, fluorescence was best detected after 36 hpf (Fig. 3.3 E).

Unfortunately failure of one of the water circuitry systems in our zebrafish facility resulted in the loss of this transgenic line, and no additional germline transgenic founders were identified amongst the remaining 5 less highly expressing mosaic founder fish. However the results that were achieved indicated that the 1.2 kb *hd* promoter fragment contains *cis* elements that are sufficient to promote maternal and zygotic expression reminiscent of endogenous *hd* gene expression. Therefore, this fragment was deemed suitable for driving expression of the repeat constructs.

Conserved *HD* promoter elements identified by *in silico* analysis

Since 1.2 kb of 5' sequence from the *hd* gene was able to drive ubiquitous and maternal expression, a comparative promoter analysis was performed (*in silico*) to identify transcription factor binding sites within this 1.2 kb region that are conserved in other vertebrate *HD* gene promoters. The rationale was that evolutionary conservation of a binding site would increase the chance that this site was a functional regulatory element, and knowledge of the type of gene responses regulated by the corresponding transcription factors may provide insight into the biological pathway(s) in which Htt acts, thus complementing the investigation into Htt function (Chapters 4 and 5).

The MatInspector search engine (222) was used to identify putative transcription factor binding sites within 1.2 kb of genomic DNA sequence immediately upstream of the translation start codon, from human, rat, mouse, pufferfish and zebrafish, and the resulting lists were compared. Two transcription factors were found to have at least one putative binding site in all vertebrates examined: 5'TG3'-interacting factor (TGIF), and 'cooperates with myogenic proteins 1' (COMP1) (Table 3.1). Interestingly, in each species, one TGIF and one COMP1 site occurred in close proximity of each other, on opposing strands, and within 400 bp of the start of translation. In human, rat, mouse and pufferfish, the TGIF site occurred on the positive stand and the COMP1 site on the negative strand, and the two sites were overlapping. In zebrafish, the sites occurred on the opposite strands with respect to other species, and were adjacent to each other, but not overlapping (Table 3.1 (bold text) and Fig. 3.8). The presence of these sites (albeit in altered configuration) in these diverse species suggests that TGIF and COMP1 may perform some conserved function in the regulation of *HD* gene expression.

The TGIF and COMP1 target sites identified here lie upstream of (but in close proximity to) a previously identified region of high homology between rat, mouse and human *HD* promoter sequences (between positions –56 and –206 in the rat *rhd* promoter) that was found to be both necessary and sufficient to drive expression of a reporter gene in neural and somatic cell lines (223).

	Position	Strand	Core similarity	Matrix similarity	Sequence
TGIF					
CONSENSUS					*nnntGTCAnnn*
Human	**-238 to -228**	**+**	**1.000**	**1.000**	**ggctGTCAatc**
Rat	**-226 to -216**	**+**	**1.000**	**1.000**	**cgctGTCAatt**
Mouse	**-226 to -216**	**+**	**1.000**	**1.000**	**gcctGTCAatt**
Pufferfish	-1139 to -1129	+	1.000	1.000	agctGTCAaac
	-1018 to -1008	-	1.000	1.000	ccctGTCAgaa
	-358 to -348	**+**	**1.000**	**1.000**	**tcatGTCAatc**
Zebrafish	-773 to -763	-	1.000	1.000	ttatGTCAgat
	-334 to -324	**-**	**1.000**	**1.000**	**tcctGTCAaaa**
COMP1					
CONSENSUS					*nnwtsATTGrcrrsranmrrnnn*
Human	**-246 to -224**	**-**	**1.000**	**0.870**	**gcatgATTGacagccctagcctg**
Rat	**-234 to -212**	**-**	**1.000**	**0.804**	**gcagaATTGacaagcggatgctg**
Mouse	**-234 to -212**	**-**	**1.000**	**0.797**	**gcagaATTGacaggcggatgcgt**
Pufferfish	**-366 to -344**	**-**	**1.000**	**0.908**	**tcttgATTGacatgagaaccgac**
	-333 to -311	-	1.000	0.827	ttttgATTGgctactgagtttga
Zebrafish	-562 to -540	-	1.000	0.801	aatatATTGgcaaatatacccta
	-323 to -301	**+**	**0.826**	**0.794**	**gttttATTAaccggaaatacag**

Table 3.1 Putative TGIF and COMP1 binding sites occurring within 1.2 kb upstream of the *HD* ORF in human, rat, mouse, pufferfish and zebrafish. Consensus binding sequences for each transcription factor are shown in italics. The core sequence of each binding site is capitalised. The most informative positions within the binding sequence are indicated in red. Core and matrix similarities (calculated by MatInspector, as described (222)) are shown (maximum = 1.000). Positions given are relative to the translation start site (+1). In each organism, one TGIF site and one COMP1 site overlap (or lie adjacent to each other), on opposing strands; these sites are indicated in bold, and are also illustrated in Figure 3.8.

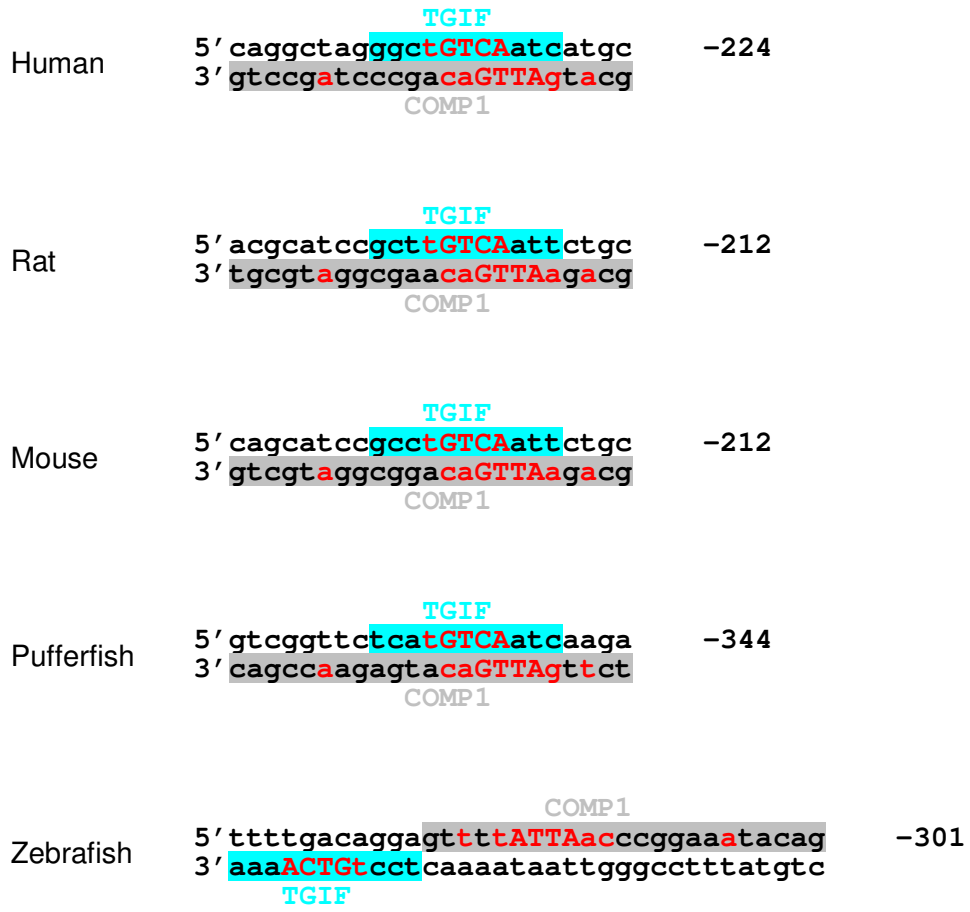

Figure 3.8 Location of overlapping/adjacent putative TGIF and COMP1 binding sites within vertebrate *HD* promoters. TGIF binding sites are indicated in blue, COMP1 sites are indicated in grey. The core sequence of each binding site is capitalised, and the most informative positions are indicated in red. Positions given are relative to the translation start site (+1).

Mosaic expression of repeat constructs

Given that the 1.2 kb *hd* promoter was sufficient for driving ubiquitous expression, and that EGFP was a useful reporter under this promoter, the promoter and EGFP DNA sequences were incorporated into the repeat constructs (as described in Chapter 2, Materials and methods) to produce two pairs of constructs: one pair with EGFP expressed bi-cistronically downstream of the expanded exon 1 fragments (Fig 3.1 A), and one pair with EGFP expressed as a fusion to the carboxy terminus of the expanded exon 1 fragments (Fig 3.1 B). One of each pair of constructs had a pure expanded repeat of $(CAG)_{95}$ within exon 1, and the other had an interrupted repeat; $CAG(CAG(CAA)_2CAGCAACAG)_{15}CAG(CAA)_2(CAG)_3CAA$.

When the IRES-containing vectors (Fig. 3.1 A) were injected into 1-cell zebrafish embryos, EGFP expression was detectable in a proportion of embryos at 10 hpf, but expression was weaker than the expression seen when the *hd*(1.2):EGFP construct was injected. After 24 hours, minimal, if any, cells exhibited fluorescence (not shown). Altering vector concentration and injection volume did not improve this outcome. It is likely that the poor fluorescence was due to inefficient IRES-mediated translation of the EGFP reporter, rather than death of cells expressing the expanded repeats (and EGFP), since another laboratory also experienced difficulty driving fluorescent reporter gene expression in zebrafish embryos using an IRES sequence (B. Key, personal communication). Additionally, around the time of these experiments, Miller and colleagues (2005) reported having successfully expressed expanded polyglutamine repeats (fused to green fluorescent protein; GFP) in zebrafish embryos using similar methods, and mosaic expression was evident at 24 hpf (74).

When the expanded Htt-EGFP fusion constructs were injected, mosaic EGFP expression was evident at 10 hpf, in a pattern indistinguishable from embryos injected with the *hd*(1.2):EGFP construct. Expression persisted at 48 hpf (Fig. 3.9), and was still evident after 6 days.

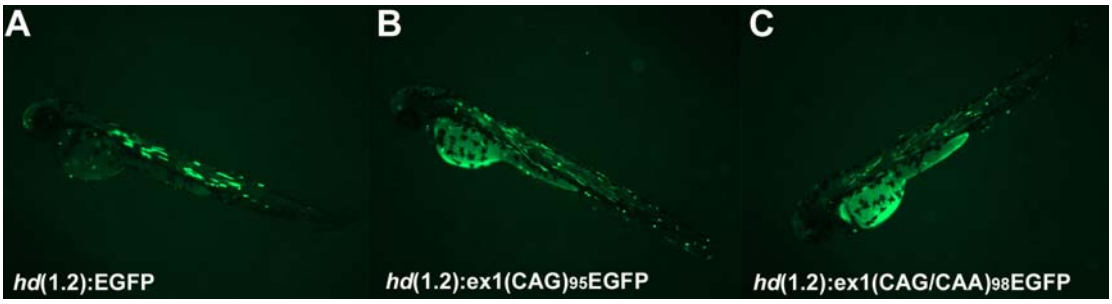

Figure 3.9 Mosaic expression of expanded Htt-EGFP fusion constructs in zebrafish embryos. Embryos injected at the 1-cell stage with expanded Htt-EGFP constructs *hd*(1.2):ex1$(CAG)_{95}$EGFP (B) or *hd*(1.2):ex1$(CAG/CAA)_{98}$EGFP (C), exhibit a similar pattern of mosaic transgene expression to *hd*(1.2):EGFP (A), shown at 48 hpf.

Discussion

The primary aim of this work was to address the question of whether somatic instability contributes to the age of onset and/or disease severity in HD. The approach was to develop transgenic zebrafish lines expressing expanded CAG repeats with and without stabilising interruptions, and assess differences in phenotype severity.

Towards this aim, constructs were generated that express an N-terminal fragment of zebrafish Htt housing a polyglutamine tract of ~100 repeats encoded by either pure CAG repeat sequence, or by a mixture of CAG and CAA codons. Expression was driven by 1.2 kb of *hd* 5' sequence. This sequence was first shown to be able to promote ubiquitous (and maternal) expression of EGFP in a similar distribution to the normal pattern of *hd* gene expression, and at levels high enough to be able to visually detect EGFP fluorescence in mosaic and germline transgenic embryos. In order to detect transgenic expression of the repeat constructs, EGFP was used as a reporter, integrated either bi-cistronically using an IRES, or as a fusion protein at the carboxy terminus of the mutant Htt fragments.

The expanded Htt-EGFP fusion constructs (Fig. 3.1 B) were able express EGFP mosaically in injected zebrafish embryos, at a level sufficient to facilitate visual screening of transgene expression. This was not the case for the IRES constructs (Fig. 3.1 A). The next step would have been to make several transgenic lines from the expanded Htt-EGFP fusion constructs, and assess them for phenotypes analogous to those found in other model systems such as 1) behavioural/motor abnormalities, 2) reduced lifespan, 3) aggregate formation and 4) neuropathology, and then compare the severity of these phenotypes in the pure (CAG) versus interrupted (CAG/CAA) repeat lines. Small pool PCR (197), or laser dissection and single-cell PCR amplification (191) would have been appropriate techniques for the assessment of somatic expansion, allowing correlations between phenotype severity and somatic instability to be assessed.

In case the Htt-EGFP fusion constructs did not produce obvious disease phenotypes within the lifespan of the zebrafish (~3 years), the IRES constructs could be further assessed for their use as an alternative strategy for the creation of transgenics, since disease length polyglutamine tracts are generally more pathogenic when expressed within shorter peptide sequences than longer sequences (81, 82). Anti-myc antibodies could be used to assess whether the expanded Htt-myc fusion proteins are expressed in the IRES constructs, despite the absence of visible EGFP fluorescence. If the expanded Htt-myc fusion proteins are expressed, these constructs could be used to create transgenic fish. Germline transgenics would be able to be identified in the F_1 generation by taking fin cuttings and screening by PCR-based methods for the presence of the transgene.

Progress of this work was delayed by a number of unforeseen technical difficulties. Recent upgrade of the zebrafish facility has overcome these and will increase the success of future transgenesis work. However, this investigation was

discontinued, largely due to new data published by others that cast doubt on the somatic instability hypothesis (see below).

Recent evidence against the somatic instability hypothesis

During the course of this study Watase and colleagues (2003) published some work that cast doubt on the hypothesis of a causative role for somatic expansion in polyglutamine disease pathology (206). The authors assessed the instability of an expanded *Sca1* allele (154 CAG repeats) in a knock-in mouse model of SCA1 by performing small-pool PCR amplification on DNA obtained from various neural and non-neural tissues (in a manner comparable to that employed by Kennedy and Shelbourne for examining somatic instability in HD knock-in mice (described earlier) (197)). This SCA1 model recapitulates many features of the human disease, including specific loss of cerebellar Purkinje cells and cells of the brainstem (224). However, Watase and colleagues found that somatic instability did not correlate with the areas of greatest pathology. They observed the greatest instability in the striatum, with moderate instability in other brain regions except for the cerebellum, in which the disease allele was relatively stable (206). Thus, in the affected regions, cell loss was observed without somatic expansion, and in the striatum, somatic expansion was observed without any cell loss.

The instability profile is similar to that which was observed in the HD knock-in mouse model by Kennedy and Shelbourne (197), suggesting that rather than somatic instability being correlated to affected regions in different polyglutamine diseases, the striatum appears to possess properties that result in greater repeat instability than that of other brain regions. Whilst it cannot be ruled out that somatic instability makes some contribution to HD pathogenesis, it appears that somatic instability is not the primary determinant of specificity of neurodegeneration in the polyglutamine diseases.

Other evidence that originally supported the somatic instability hypothesis was that in expanded SCA1 alleles (of human SCA1 subjects), the unusual presence of CAT interruptions suppress the onset of SCA1 symptoms beyond the age predicted for a given repeat length (89, 201-203). It was hypothesised that the presence of these interruptions might hinder somatic instability, thereby delaying onset of the disease. However, this is unlikely to be the case, since the findings of Watase and colleagues in the SCA1 mouse (206) suggest that somatic instability does not play a role in SCA1 pathogenesis. The CAT interruptions encode histidine, and therefore interrupt the repeat tract at the protein level as well as at the DNA level. These interruptions have

been reported to alter the conformation of polyglutamine tracts (89), and reduce their propensity to aggregate (207). Therefore it is conceivable that SCA1 disease onset is suppressed in these cases because the histidine interruptions within the polyglutamine tract reduce the toxicity of the mutant ataxin-1 protein.

Given the delays due to technical difficulties, and the new findings contradicting the hypothesis being tested, it was decided not to continue with this work, but to concentrate on the second research aim - the investigation of normal Htt function - as this project was producing some promising findings by this stage (Chapters 4 and 5).

Positive outcomes

Although the initial somatic instability hypothesis was not addressed in this work, a number of beneficial outcomes were generated that complement the work that will be described in Chapters 4 and 5.

The distribution of *hd* transcript in whole zebrafish embryos during developmental stages was determined using mRNA *in situ* hybridisation. *hd* transcript was detected prior to the onset of zygotic expression and is therefore maternally deposited. Uniform distribution of transcript was detected throughout the embryo in early development, but expression was later decreased in non-neural tissues and became more highly expressed in the head in later developmental stages. This pattern of zebrafish *hd* mRNA distribution is consistent with the early uniformity (107, 111, 114) and subsequent down-regulation in non-neural tissues (107) of *Hdh* and *rhd* mRNA transcript levels in rodent development. A large scale *in situ* hybridisation screen has been performed previously by Thisse *et al.* (225), the results of which are accessible from the Zebrafish Information Network (http://zfin.org). By comparison with this screen, the general pattern of *hd* expression in development was found to be similar to that of ubiquitous housekeeping genes, normally associated with the maintenance of a basal cellular function (226). The early expression of the *hd* gene in zebrafish development also indicated that this gene would be an ideal candidate for the morpholino knockdown studies.

The expanded repeat-containing constructs (particularly the EGFP fusion constructs) generated in this study will be useful for future generation of transgenic zebrafish models of HD. The *hd*(1.2):EGFP reporter construct generated for this work also proved useful in the morpholino studies presented in Chapters 4 and 5, since this construct contains the morpholino target sequences (5' to and spanning the *hd* translation start site) and was therefore able to be used as a tool for demonstrating the

effectiveness of *hd*-directed morpholinos at binding their target sequences and preventing protein translation.

A cross-species promoter comparison revealed two transcription factors, TGIF and COMP1, that each has a conserved putative binding site within 400 bp of the start of translation in human, rat, mouse, pufferfish and zebrafish *HD* promoter sequences. COMP1 is a DNA-binding factor that was identified by its ability to interact with muscle-specific transcription factor, myogenin (227). Whilst this factor is largely uncharacterised, COMP1 binding sites have been found to be common amongst glycolytic and respiratory chain genes (228), suggesting that this factor may play a role in the regulation of genes involved in energy metabolism.

TGIF is a transcriptional repressor that was originally isolated by its ability to bind the retinoid X receptor (RXR)-responsive element found in the promoter of the cellular retinol-binding protein II gene (229). In this promoter, the binding elements for RXR and TGIF overlap, and the two factors exhibit mutually exclusive binding *in vitro* (229). TGIF also binds to DNA sequence from the promoter of the D_{1A} gene that encodes the predominant striatal dopamine receptor (230). A positive transcriptional regulator, Meis2, binds an overlapping site on the complementary strand. TGIF competes with Meis2 for binding to DNA at these overlapping sites, and D_{1A} gene expression appears to be differentially regulated by TGIF and Meis2 in various cell types (230).

TGIF mRNA is expressed in a variety of tissues, and appears to be most abundant in proliferative and differentiating cell lineages (229, 231). Given that TGIF is a negative regulator of transcription, it is interesting that *TGIF* mRNA is barely detectable in the brain, where the *HD* gene is most highly expressed (229). The *TGIF* gene is, however, expressed in defined regions of the brain during developmental stages (231), and is likely to play a critical role in brain development since loss-of-function mutations in the *TGIF* gene lead to holoprosencephaly, a human birth defect caused by incomplete cleavage of the foetal forebrain (232).

The finding that putative TGIF and COMP1 binding sites overlap in human, rat, mouse and pufferfish *HD* promoters raises the possibility that these factors might compete for binding to DNA and differentially regulate *HD* gene expression. However, if this were to be the case, then the regulatory mechanism may differ in zebrafish since although the putative COMP1 and TGIF binding sites are adjacent to each other, they do not appear to overlap. Furthermore, the respective DNA strands on which each site occurs in zebrafish are opposite to that of the other vertebrate promoters.

Whilst the evolutionary conservation of TGIF and COMP1 binding sites in vertebrate *HD* gene promoters is not sufficient evidence to indicate transcriptional

function conclusively, the existence of these conserved sites puts forward TGIF and COMP1 as interesting candidate regulatory proteins for future experimental verification. If these are indeed true binding sites, further understanding of the gene responses regulated by TGIF and COMP1 may offer further insight into the biological role of Htt.

Chapter 4: Developmental defects associated with Htt deficiency in zebrafish embryos

Introduction

Huntingtin (Htt) is a ubiquitously expressed protein that is essential for embryonic viability, but as yet its function and the biological process in which it is involved remain unclear. Expansion of a polyglutamine tract within the N-terminus of the Htt protein leads to the neurodegenerative disorder, Huntington's disease. However, it is yet to be determined whether the expanded repeat tract causes disease by attributing a toxic novel function to the Htt protein, by disrupting normal Htt function, or by a combination of both. Elucidation of the role of Htt and the biological pathway in which it is involved are therefore likely to further our understanding of HD pathogenesis.

In a novel approach towards investigating Htt function, antisense morpholino oligonucleotides (MOs) are used in this study to transiently inhibit, or 'knock down' *hd* gene expression during early zebrafish development. Given the early expression of the *hd* gene in zebrafish embryos (Chapter 3), and that in mouse studies, *Hdh* inactivation causes major developmental defects and embryonic lethality (110-112), it was hypothesised that depletion of Htt protein levels in zebrafish embryos using MOs would have a detrimental effect on embryonic development and produce phenotypes that would provide insight into the normal role of Htt.

MOs are synthetic 25mer oligos that are commonly used to knock down genes of interest in the zebrafish model system. When specifically targeted to mRNA 5' leader sequences or spanning the AUG translational start site, MOs inhibit translation by annealing to the transcript and physically preventing ribosomal binding (233). MOs can be injected at any time during the first few cleavage steps, at which stage they are able to diffuse between cells of the blastocyst. However, due to fact that *hd* mRNA is maternally deposited (Chapter 3), all MO injections in this study were performed at the 1-cell stage in order to prevent translation as early as possible. The non-degradable nature of MOs means that after initial injection into embryos knockdown lasts until the MOs become too diffuse to have any further effect (approximately 2-3 days, depending on MO concentration and the abundance of target transcript).

Past investigations of Htt function *in vivo* have been somewhat limited by the lack of a viable mouse model of Htt deficiency. Mouse *Hdh*$^{-/-}$ null embryos gastrulate but fail to neurulate and rapidly degenerate causing lethality prior to birth, between 7.5 and 10 days of gestation (110-112). A major advantage of using the zebrafish/MO system is

that zebrafish produce optically transparent embryos that develop externally, allowing the morphological effects of Htt knockdown to be observed in live embryos, non-invasively, under the microscope. Furthermore, the MO method of gene knockdown enables the extent of inhibition to be adjusted by modifying the dose of MOs administered.

Results

Preparation for MO experiments

To identify any polymorphisms or nucleotides differing from the published *hd* gene sequence (141) to be avoided when designing *hd*-specific MOs, a genomic region spanning the *hd* translation start site was PCR amplified and sequenced. No nucleotide variations were found within the target vicinity. Two non-overlapping MOs (*hd*MO1 and *hd*MO2) antisense to the *hd* 5' untranslated region and translation initiation codon (Fig. 4.1), were subsequently designed by and purchased from Gene Tools (LLC, Ore), in addition to a standard negative control morpholino (*c*MO) that lacks specificity to zebrafish transcripts. In later studies (Chapter 5) a mispair control morpholino (*mc*MO1; representing *hd*MO1 with 5 base modifications out of 25, see Materials and methods) was also used. Neither of the control MOs produced any morphological defects upon injection into 1-cell stage zebrafish embryos at the concentrations used in this study.

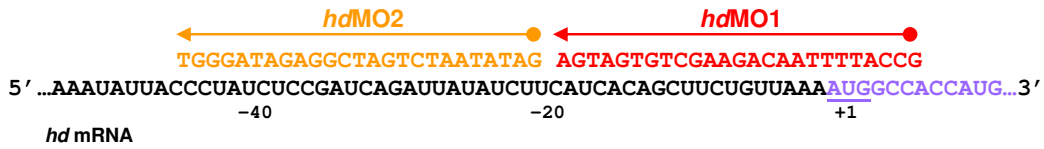

Figure 4.1 Positions within the *hd* mRNA sequence targeted by antisense morpholinos *hd*MO1 (red) and *hd*MO2 (orange) are shown relative to the translation start site (+1; start codon underlined). *hd* ORF sequence is indicated in purple.

Initial optimisation of MO injection conditions

The manufacturers of MOs (Gene Tools) suggest injecting up to 10 nL of 1.0 mM MO into the zebrafish oocyte (1-cell embryo). At the time this study commenced, colleagues in the Lardelli laboratory were using an injection volume of ~5 nL and MO sample concentration of 1.0 mM to successfully knock down their gene of interest, so these measurements were used as a guide. In initial trials for this study, an injection volume of ~5 nL, and MO sample concentrations of 1.0, 0.5 and 0.25 mM were used,

equating to approximately 42.5, 21.3 or 10.6 ng of MO per embryo. Upon first assessment, it appeared that 21.3 ng was the best dose to use for characterisation of the consequences of Htt deficiency (see below), as this dose produced a greater number of obvious morphological phenotypes (in the *hd*MO-injected groups) than the lower dose (10.6 ng). The highest dose (42.5 ng) produced the same phenotypes as 21.3 ng, but the embryos were more severely affected and it was reasoned that using the higher dose might increase the risk of encountering non-specific effects.

Different volumes and concentrations of MOs were used at various times throughout this study, as summarised in Table 2.2 (Chapter 2). Therefore, MO dose will be given in 'ng' in order to simplify comparisons between experiments.

Evaluation of morphological defects in Htt-deficient embryos

For initial phenotypic characterisation of the morphant phenotype, a 21.3 ng dose of MOs was injected into 1-cell zebrafish embryos that were then examined throughout early development in comparison to *c*MO-injected and uninjected embryos. The same spectrum of phenotypes was produced using either *hd*MO1 or *hd*MO2, indicating specificity of Htt knockdown. In general however, the effects of *hd*MO1 were slightly stronger than *hd*MO2 suggesting that *hd*MO1 (targeting the translation initiation codon) is more effective at inhibiting translation of the *hd* mRNA transcript than the more 5' morpholino, *hd*MO2.

Early in development, throughout gastrulation, somitogenesis and early neurulation (formation of the neural plate, neural keel and notochord), *hd*MO-injected embryos appeared similar to *c*MO-injected embryos. By 18 hpf, *hd*MO-injected embryos often exhibited slight growth delay (Fig. 4.2 A-C). Brain necrosis was evident at this time, and this persisted at 24 hpf when it was also evident that the brain ventricles had not enlarged like they had in control embryos (Fig. 4.2 Q-S). At 26 hpf (Fig. 4.2 D-F) the yolk extension (YE) was notably thinner than in control embryos and had totally disappeared in most *hd*MO-injected embryos by 48 hpf (Fig. 4.2 G-K). At this stage, *hd*MO-injected embryos were shorter, and had delayed or paler pigmentation of melanophores, small head and eyes, and pale or colourless blood. In more severely affected embryos, the tail was often twisted and/or truncated (Fig. 4.2 I and K). By 96 hpf, the melanophores had developed in colour, but were obviously disrupted in their patterning along the length of the body (Fig. 4.2 L-P). The body was also thinner than control embryos, and appeared necrotic. At this stage the *hd*MO-injected embryos appeared to have poorly formed jaw and branchial arch structures and the swim bladder

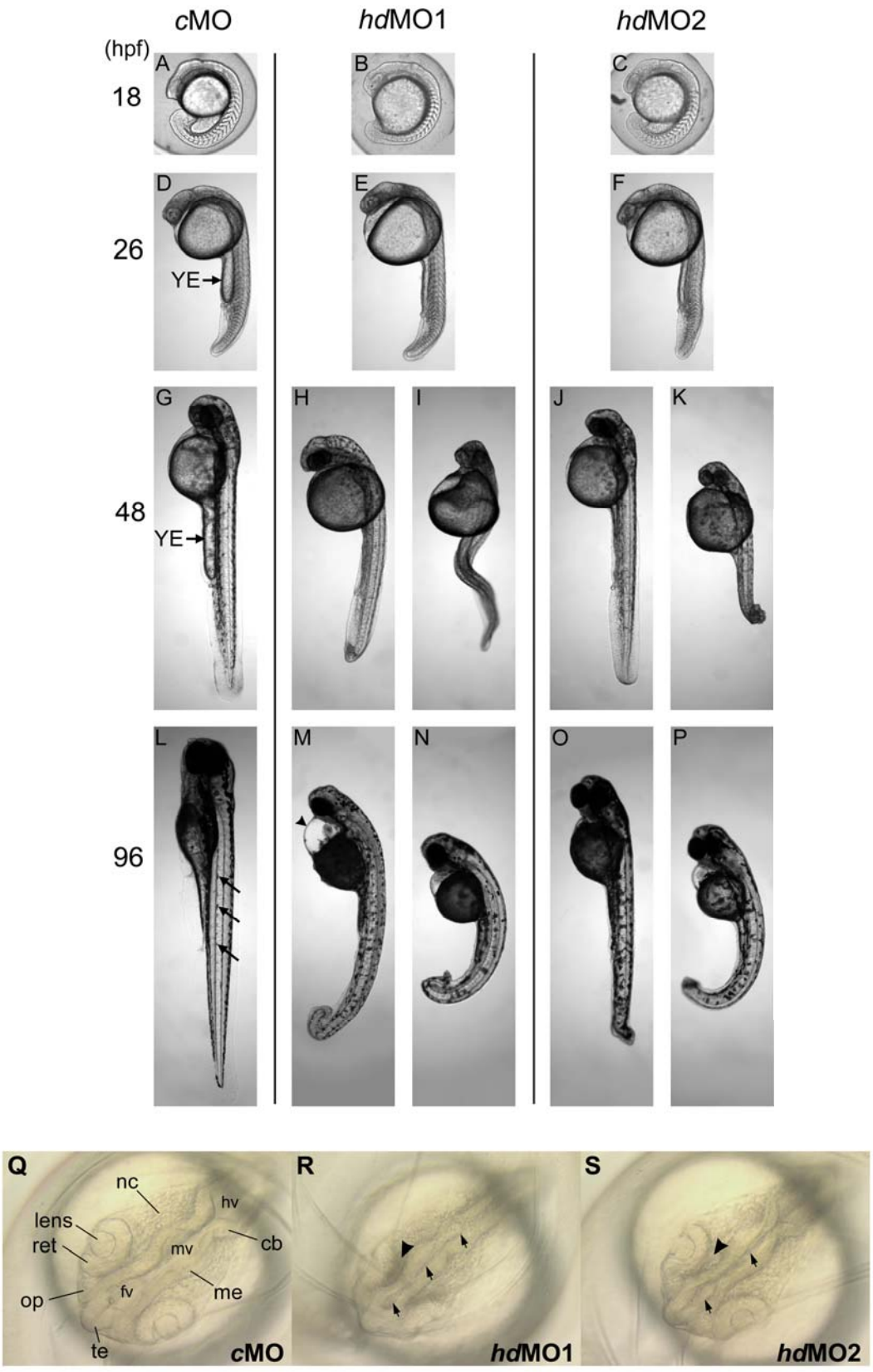
cMO
hdMO1
hdMO2
(hpf)
18
26
48
96
A
B
C
D
E
F
G
H
I
J
K
L
M
N
O
P
YE
YE
Q
R
S
nc
hv
lens
ret
mv
cb
op
fv
me
te
cMO
hdMO1
hdMO2

Figure 4.2 Morphological appearance of Htt-deficient zebrafish embryos. Zebrafish embryos injected with 21.3 ng of *c*MO (**A**, **D**, **G**, **L**, **Q**), *hd*MO1 (**B**, **E**, **H**, **I**, **M**, **N**, **R**) or *hd*MO2 (**C**, **F**, **J**, **K**, **O**, **P**) were examined at various developmental stages. The *c*MO group show normal embryonic development (**A**, **D**, **G**, **L**). At 18 hpf, *hd*MO-injected embryos exhibit slight developmental delay (**B**, **C**). At 26 hpf, the yolk extension (**YE**) is pronounced in the control embryos (**D**) but thinner in Htt-deficient embryos (**E**, **F**). At 48 hpf, *hd*MO-injected embryos lack the YE and have delayed pigmentation and small eyes (**H**-**K**) in comparison to control embryos (**G**). The more strongly affected embryos exhibit tail abnormalities such as curling (**I**) or truncation (**K**). By 96 hpf, Htt-deficient embryos have small head and eyes (**M**-**P**), and the normal alignment of melanophores along the trunk (**L**, arrows) is disrupted (**M**-**P**). Pericardial oedema is often seen (for example, **M,** arrowhead). The more severely affected embryos are shorter and ventrally curved (**N**, **P**). Htt-deficient embryos exhibit brain necrosis (**R**, **S**; arrowhead) and failure to enlarge ventricles (**R**, **S**; arrows) compared to *c*MO embryos (**Q**) shown here at 24 hpf. Visible regions of the brain are labelled in (**Q**): cb, cerebellum; hv, hindbrain ventricle; fv, forebrain ventricle; me, mesencephalon; mv, midbrain ventricle; nc, neural crest; op, olfactory placode; ret, retina; te, telencephalon. Images **A**-**P** are lateral views of live embryos that were manually dechorionated. Images **Q**-**S** are dorsal views of live embryos within their chorion.

had not inflated as it had in *c*MO-injected embryos by this time. *hd*MO-injected embryos also appeared to be less responsive to touch stimuli (such as being poked with a needle). These phenotypes were often accompanied by pericardial oedema (swelling around the heart; Fig. 4.2 M). Very few (if any) *hd*MO-injected embryos survived to 8 days post fertilisation (dpf).

Assessing the effectiveness of *hd*-targeted MOs

Knockdown of reporter protein expression

The finding that both *hd*MO1 and *hd*MO2 produce the same spectrum of phenotypes supports these effects being specifically due to Htt deficiency. To further test the effectiveness of the MOs at binding the *hd* mRNA transcript and blocking downstream translation, the *hd*(1.2):EGFP construct (described in Chapter 3) was used. This construct contains ~1.2 kb of DNA sequence 5' to, and including, the first 9 nucleotides of the *hd* ORF (encompassing the *hd* morpholino target sequences), fused in frame to the *EGFP* ORF encoding enhanced green fluorescent protein. Injection of *hd*(1.2):EGFP vector DNA into zebrafish embryos at the 1-cell stage, resulted in strong fluorescence at 10 hpf due to mosaic EGFP expression (100%, *n* = 45, Fig. 4.3 A). Co-injection of *c*MO with *hd*(1.2):EGFP did not affect EGFP expression (100%, *n* = 28, Fig. 4.3 B), but co-injection of a mixture of *hd*(1.2):EGFP and either *hd*MO1 or *hd*MO2 (21.3 ng) inhibited EGFP expression (*hd*MO1: 0%, *n* = 39; *hd*MO2: 0%, *n* = 27, Fig. 4.3 C and D). These results show that both *hd*MO1 and *hd*MO2 are each able to bind their *hd*-specific target sequence and prevent downstream translation.

Knockdown of endogenous Htt protein (performed by T. Henshall)

In conjunction with the EGFP knockdown experiment described above, antibodies raised (in rabbit) against the N-terminus (first 17 amino acids) of zebrafish Htt were also used to confirm a reduction in endogenous Htt levels by western analysis. This complementary experiment was performed in our laboratory by T. Henshall, and is reported here only for the purpose of project completeness. Embryos were injected at the 1-cell stage with *c*MO or *hd*MO1 (21.3 ng), and extracts were prepared from these and wildtype uninjected embryos after 48 hpf. Western blot analysis using the antisera showed that Htt was greatly reduced in embryos injected with *hd*MO1 compared to uninjected or *c*MO-injected embryos (Figure 4.3 E).

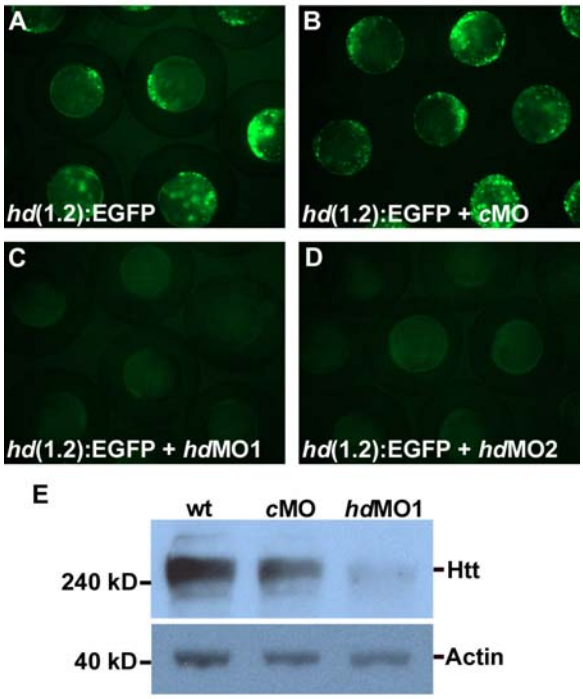

Figure 4.3 Knockdown of an EGFP reporter and endogenous Htt levels by *hd*-targeted morpholinos. To test the effectiveness of the *hd*MOs at binding their *hd* target sequences and blocking downstream translation, the *hd(1.2)*:EGFP reporter construct (driven by DNA sequence upstream from the zebrafish *hd* coding region that encompasses the *hd*MO target sequences) was used. **(A)** Injection of *hd(1.2)*:EGFP at the 1-cell stage, resulted in strong fluorescence at 10 hpf due to mosaic EGFP expression. **(B)** This expression was unaffected when *hd(1.2)*:EGFP was co-injected with 21.3 ng of *c*MO. Co-injection of *hd(1.2)*:EGFP with 21.3 ng of *hd*MO1 (**C**) or *hd*MO2 (**D**) inhibited EGFP expression. **(E)** T. Henshall used antibodies raised against the N-terminus of zebrafish Htt to confirm a reduction in endogenous Htt levels; Western blot analysis of Htt expression in lysates prepared from 48 hpf embryos showed that Htt is markedly reduced in embryos injected with 21.3 ng of *hd*MO1 in comparison to uninjected, or *c*MO-injected embryos. Actin loading control also shown.

The effect of Htt deficiency on apoptosis levels

Htt knockdown produced a large range of developmental defects. As a starting point towards characterising the Htt-deficient embryos, apoptosis levels were assessed, since an increased number of apoptotic cells have been observed in mouse *Hdh*$^{-/-}$ knockout mice using the TdT-mediated dUTP-nick-end labelling (TUNEL) assay (110). A pro-survival role for Htt is also supported by the finding that *in vitro*, transfected cells are protected from various apoptotic stressors by over-expressing wildtype Htt (113).

For initial assessment of apoptosis in zebrafish by TUNEL, embryos injected with *hd*MO1 (21.3 ng), and wildtype uninjected embryos were fixed at 24 hpf, and stained using the POD (peroxidase) In Situ Cell Death Detection Kit (Roche), used previously by Cole and Ross (2001) for the characterisation of apoptosis in zebrafish development

(215). At this time-point, a high level of apoptosis was evident both in uninjected and *hd*MO-injected embryos (Fig. 4.4). The staining also appeared to be superficial, even though methods were employed to permeabilise the embryos prior to staining (see Chapter 2, Materials and methods, and reference (215)). The pattern of apoptosis was disrupted and less organised in the morphant embryos compared to the control group, thus making it difficult to assess whether there was more apoptosis occurring in the morphant embryos.

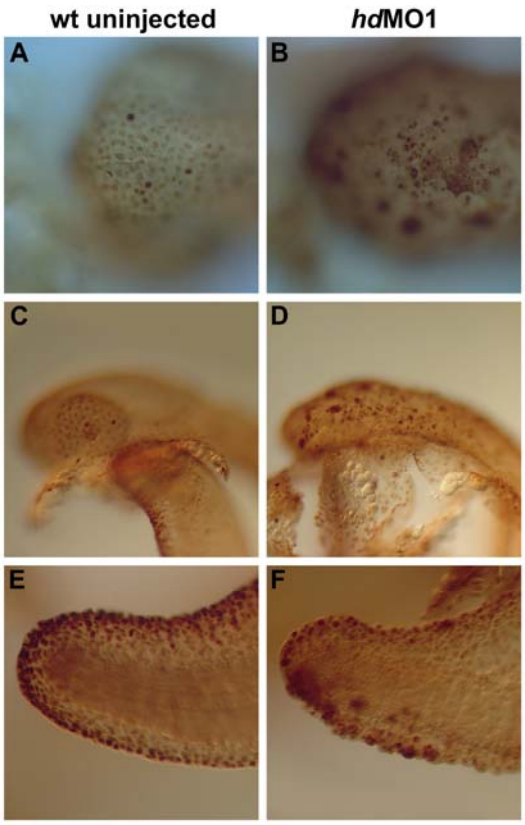

Figure 4.4 The normal pattern of apoptosis is disrupted in Htt-deficient embryos at 24 hpf. Apoptotic cells (stained red/brown) was detected by TUNEL (POD) in wildtype uninjected embryos (**A**, **C**, **E**) and embryos injected with 21.3 ng of *hd*MO1 (**B**, **D**, **F**). In uninjected embryos, a regular distribution of apoptosis was observed on the dorsal surface of the head (**A**), in the eye, as seen in a lateral view of the head (tail also visible) (**C**), and in the tail (**E**). The normal distribution of apoptotic cells in these regions was perturbed in Htt-deficient embryos (**B**, **D**, **F**). In images **A**-**D**, rostral is to the left.

In order to reduce background levels of apoptosis, embryos were examined at 19 hpf, a stage when normal levels of apoptosis are relatively low in the developing zebrafish (215) so an increase in apoptosis could be more easily observed.

Embryos injected with *hd*MO1 or *c*MO (21.3 ng) and uninjected embryos were TUNEL-stained at 19 hpf using the POD kit. As expected, levels of apoptosis were minimal in all of the uninjected embryos (Fig. 4.5 A). However, a greater number of

apoptotic cells were observed in embryos in both the *c*MO and *hd*MO1 groups (Fig. 4.5 B and C) compared to the uninjected embryos, suggesting that apoptosis was being induced to some extent by the injection process itself, or as a non-specific effect of using a relatively high morpholino dose. There was a lot of heterogeneity within each of the *c*MO and *hd*MO1 groups regarding apoptosis levels, with some embryos showing near wildtype levels of staining.

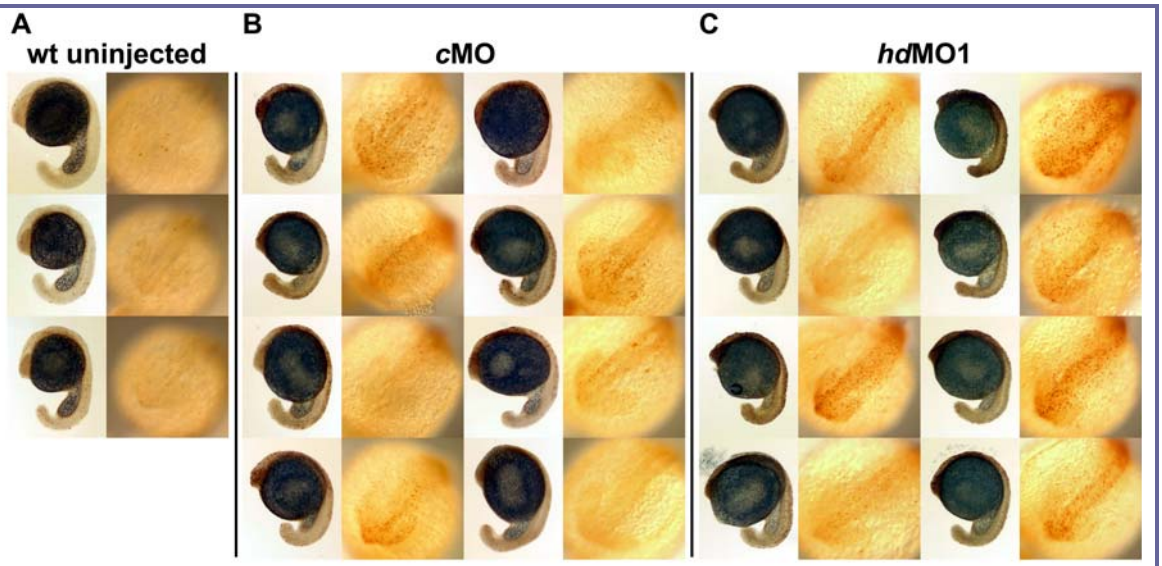

Fig 4.5 Heterogeneous levels of apoptosis amongst embryos injected with *c*MO or *hd*MO1 in comparison to minimal levels in uninjected embryos at 19 hpf. Lateral (left) and dorsal (right) views of 3 representative wildtype uninjected embryos (**A**), 8 randomly selected *c*MO-injected embryos (**B**), and 8 randomly selected *hd*MO1-injected embryos (**C**), stained using TUNEL (POD) to detect apoptotic cells. Unfortunately, the images of wildtype embryos were taken without the use of the microscope condenser, whilst the condenser was employed for *c*MO and *hd*MO1 images. However, whilst this resulted in increased brightness of the yolk ball in the injected groups (**B** and **C**), the red/brown staining of the apoptotic cells is clearly visible under both microscope conditions. Minimal apoptosis was observed in all uninjected embryos (**A**). Increased apoptosis was observed in a proportion of embryos in the *c*MO (**B**) and *hd*MO1 (**C**) groups.

Apoptosis was also examined using the TMR red In Situ Cell Death Detection Kit (Roche). Embryos injected with either *hd*MO1 or *c*MO (21.3 ng) and wildtype embryos were fixed at 19 hpf, stained using the TMR red kit, and examined by fluorescence microscopy. Apoptosis levels were semi-quantitatively evaluated by classifying embryos using the embryos depicted in Table 4.1 as 'low' and 'high', as designated standards; those embryos with a level of apoptosis similar to or lower than that seen in the 'low' standard embryo were classed as 'low', and those with a level similar to or higher than that in the 'high' standard embryo were classed as 'high'. Embryos with a level of apoptosis between the 'low' and 'high' standards were classed as 'medium'. Classification was performed by M. Lardelli, who was unaware of the injection status of

	Low	Medium	High	
	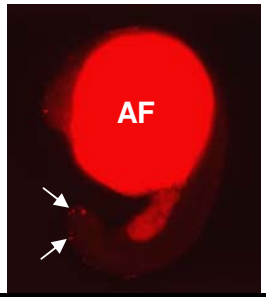	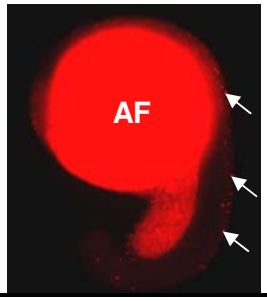	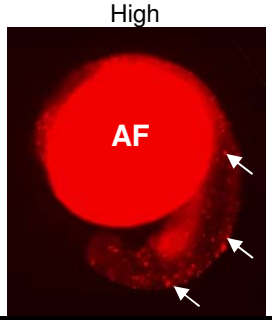	
A MO dose: 21.3 ng				Total *n*
wt uninjected	24 (49%)	25 (51%)	0	49
*c*MO	2 (6.7%)	20 (66.7%)	8 (26.6%)	30
*hd*MO1	1 (3%)	29 (87.9%)	3 (9.1%)	33
B MO dose: 8.5 ng				Total *n*
wt uninjected	20 (55.6%)	16 (44.4%)	0	36
*c*MO	13 (30.9%)	27 (64.3%)	2 (4.8%)	42
*hd*MO1	3 (8.1%)	32 (86.5%)	2 (5.4%)	37

Table 4.1 Quantification of apoptosis levels at 19 hpf in uninjected embryos and embryos injected with either *c*MO or *hd*MO1. Apoptosis was detected using TUNEL (TMR red) and classification was performed as described in the main text (and see Chapter 2, Materials and methods). Signal in the yolk is autofluorescence (**AF**). Examples of individual apoptotic cells are indicated with arrows. Injected embryos received a 21.3 ng MO dose (**A**), or 8.5 ng MO dose (**B**).

the embryos. Category allocation was done by visual estimation rather than cell-counting, using fluorescence microscopy.

The data indicated that in both the *c*MO and *hd*MO1 groups, there was a similar shift in distribution from the 'low' category into the higher categories in comparison to the uninjected group (Table 4.1 A). Therefore, consistent with earlier results using the POD kit, this suggested that the process of MO injection, or non-specific effects of this MO concentration, were causing an increase in apoptosis.

Background levels of apoptosis in the injected groups were decreased by using a lower MO dose of 8.5 ng. Classification was performed by M. Lardelli, in the same manner, and using the same standards as in the previous experiment. Using 8.5 ng of MOs, the proportion of embryos (19 hpf) with a low level of apoptosis decreased from 55% (uninjected) to 30.9% in the *c*MO group indicating a slight shift in distribution towards the 'medium' and 'high' apoptosis categories in response to injection of *c*MO. In the *hd*MO1-injected group the proportion of embryos with a 'low' level of apoptosis was

markedly reduced to 8.1%, one quarter of the *c*MO value, indicating an even greater shift (particularly from the 'low' to 'medium' category) in the *hd*MO1-injected group. A Chi-squared contingency comparison confirmed that the number of 'low' classed embryos was significantly decreased in the *hd*MO1 group in comparison to the *c*MO-injected group ($p < 0.03$). These results are consistent with previous findings of increased apoptosis in *Hdh*$^{-/-}$ knockout mouse embryos (110), and suggest conservation of the pro-survival role of Htt.

Pale blood and thin yolk extension phenotypes occur in the absence of other morphological defects, using a low *hd*MO dose

To look for further clues as to the function of Htt, the morphant phenotype was examined in more detail. Since Htt deficiency had such a global effect on zebrafish development it was difficult to ascertain which aspects of the morphant phenotype were primary effects of Htt depletion and which were secondary consequences. To address this, embryos were injected with *hd*MO1 or *c*MO using a lower dose of 4.3 ng (5 nL of 0.1 mM MO), and were closely monitored during development.

At 19.5 hpf (and stages prior to this time), *hd*MO1-injected embryos were indistinguishable from embryos in the control group. The somites were forming in the correct chevron shape, the notochord looked normal, the yolk extension looked normal as it began to extend caudally from the yolk ball, and the tails were beginning to twitch intermittently, like the *c*MO group. In all *hd*MO1-injected embryos the brain compartments appeared to be forming correctly, the otic capsule (ear) was visible, and the eyes looked normal, with both the lens and retina visible.

By 25 hpf, the head and brain of the embryos in the *hd*MO1 group looked similar to control embryos. Brain necrosis was not evident as it had been when the higher concentration (21.3 ng) of *hd*MOs was administered. The first morphological defect observed was a notable decrease in the width of the yolk extension that was evident at this stage (similar to Fig. 4.2 E and F).

At 26 hpf, prior to the onset of circulation, *hd*MO1 embryos were thrashing their tails like the control group. In response to each thrash of the tail, large, round, colourless blood cells could be seen moving through the vasculature in both groups. Many of these cells were visible in the intermediate cell mass (ICM; the main site of early haematopoiesis) in the ventral tail region. Within the next hour, the heart started to beat, slowly and irregularly at first, and then becoming regular, and blood began to pulse around the early vasculature. At this stage, the only morphological difference was the thinner yolk extension in *hd*MO-injected embryos compared to controls.

After 48 hours, the *hd*MO-injected embryos appeared generally healthy and were the same length as control embryos. Their head, eyes, somites and notochord looked similar to control embryos. The pectoral fin buds had formed and the distribution of pigment cells looked normal. All *hd*MO1-injected and control embryos had established good circulation by this time and blood cells could be seen circulating through the intersegmental blood vessels and brain as well as through the main axial vessels. However, whilst the blood cells in control embryos had developed a reddish colour by this stage, the blood cells in the *hd*MO1-injected embryos were pale, or even colourless. The yolk extension was still thin.

At 56 hpf the thin yolk extension and pale blood phenotypes persisted. Pericardial oedema was observed in a small proportion (3 out of 34) of *hd*MO1-injected embryos. By 72 hpf (3 dpf), *hd*MO1-injected embryos looked generally healthy despite having a thin yolk extension and pale blood. The pale blood phenotype was best observed by looking at the heart where the blood cells are concentrated in number (Fig 4.6). At this time the pectoral fins had developed, and embryos in both groups were spending more time upright than on their sides, due to the inflation of the swim bladder.

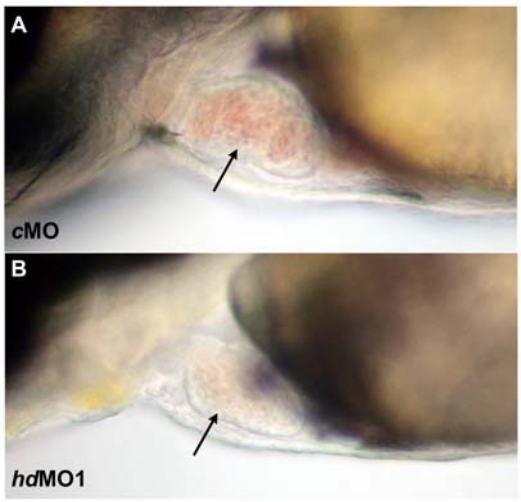

Figure 4.6 Htt-deficient embryos have a pale blood phenotype. Blood flowing through the heart (arrows) of 72 hpf embryos treated with 4.3 ng of *c*MO (**A**) or *hd*MO1 (**B**). The blood of Htt-deficient embryos is pale (**B**), in comparison to the red blood of control embryos (**A**). Lateral view shown, rostral to the left.

At 5 dpf, many of the circulating blood cells in embryos of both groups appeared to be the lentiform shape of differentiated erythrocytes rather than the round basophilic shape of the immature pro-erythroblasts. In the *hd*MO-injected embryos, the erythroid cells had developed some red colouration but overall the blood appeared paler than in the control group.

In summary, many phenotypes that were evident using the higher *hd*MO dose of 21.3 ng such as brain necrosis, small head and eyes, pericardial oedema, body curvature and failure to inflate the swim bladder were not common using the lower dose of 4.3 ng. That the thin yolk extension and pale blood phenotypes presented in the absence of other phenotypes indicates that they are not secondary consequences of these other phenotypes, and are therefore more likely to be primary effects of Htt depletion.

Phenotypic frequencies are responsive to *hd*MO dose modifications

Next a dose-response relationship between *hd*MO concentration and the frequency of occurrence of various phenotypes was assessed. Embryos were injected either with *hd*MO1, *hd*MO2, or *c*MO using doses of 2.1, 4.3 or 6.4 ng. The frequency of occurrence of evident phenotypes (pale blood, thin yolk extension and tail curvature) was then recorded at 48 hpf (Table 4.2). The tail curvature scored here was mild arching of the tail (either dorsally or ventrally), or a wave at the tip of the tail (not shown), and was not as severe as the curling observed using the 23.1 ng dose described earlier. The pale blood phenotype was assessed visually, by observing the colour of the blood passing through the heart under the microscope. The 'thin YE' classification included embryos that had either a thin YE or no YE at all.

From the resulting data it was evident that the phenotypes associated with Htt deficiency presented with a hierarchy of penetrance. Pale blood was the most common defect, followed by the thin yolk extension phenotype. Tail curvature was the least frequent of these phenotypes, occurring only with the highest dose (6.4 ng). These 3 phenotypes were cumulative; pale blood was often observed without other phenotypes, but a thin yolk extension was rarely observed without the co-presence of pale blood, and tail curling was rarely seen without the co-presence of both thin yolk extension and pale blood. To illustrate this further, out of a total of 187 embryos injected with either *hd*MO1 or *hd*MO2 in this set of experiments, 54 embryos had a thin yolk extension, and of these, 51 also exhibited pale blood. Similarly, 13 out of 14 embryos that exhibited tail curling also had a thin yolk extension and pale blood.

The frequency of occurrence of each phenotype increased in an *hd*MO-dose-dependent fashion, and these phenotypes were not observed in *c*MO-injected embryos. Consistent with earlier observations using the 21.3 ng dose, the phenotypes occurred with a higher frequency amongst *hd*MO1-injected embryos than *hd*MO2-injected embryos.

MO dose:	2.1 ng			4.3 ng			6.4 ng		
	*hd*MO1	*hd*MO2	*c*MO	*hd*MO1	*hd*MO2	*c*MO	*hd*MO1	*hd*MO2	cMO
Pale blood	0	0	0	25 (71%)	24 (56%)	0	25 (96%)	24 (96%)	0
Thin YE	1 (3%)	0	0	12 (34%)	8 (19%)	0	17 (65%)	16 (64%)	0
Pale blood & thin YE	0	0	0	12 (34%)	6 (14%)	0	17 (65%)	16 (64%)	0
Tail curve	0	0	0	0	0	0	12 (46%)	2 (8%)	0
Pale blood & thin YE & tail curve	0	0	0	0	0	0	12 (46%)	1 (4%)	0
Not affected	28 (97%)	29 (100%)	13 (100%)	9 (26%)	17 (40%)	16 (100%)	1 (4%)	1 (4%)	28 (100%)
Total *n*	29	29	13	35	43	16	26	25	28

Table 4.2 Dose-dependent effect of *hd*MO1 and *hd*MO2 on phenotypes associated with Htt deficiency in zebrafish embryos at 48 hpf.

Failed swim bladder inflation

The swim bladder of the fish is an air-filled sac that is inflated or deflated in order to maintain neutral buoyancy at various water depths (234) and is also used as an auditory organ for sound production and detection. Initial bladder inflation normally occurs at approximately 84 hpf in the zebrafish (235).

The embryos observed at 48 hpf in the dose-response study described above were also observed at 5 dpf. At this time the majority of embryos that had been injected with 6.4 ng of *hd*MO1 or *hd*MO2 had not inflated their swim bladder, and were lying on their side (Fig. 4.7 B), whilst *c*MO-injected embryos were all floating upright without exception (Fig. 4.7 A). This phenotype of failed swim bladder inflation was not apparent in embryos injected with lower doses of 4.3 or 2.1 ng of *hd*MO1 or *hd*MO2.

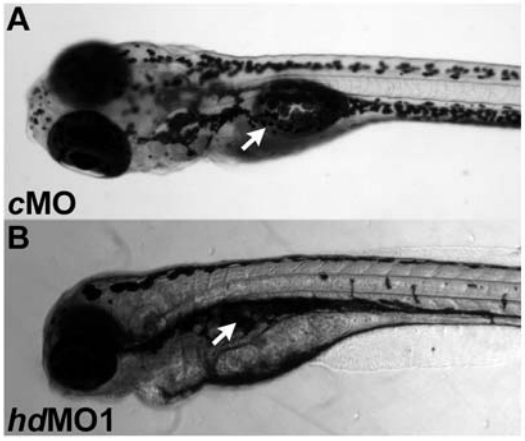

Figure 4.7 Swim bladder inflation is impaired in Htt-deficient embryos. The swim bladder (arrow) is inflated by 5 dpf in control embryos injected with 6.4 ng of *c*MO (**A**), but often fails to inflate in embryos treated with 6.4 ng of *hd*MO1 or *hd*MO2 (**B**; representative *hd*MO1-treated embryo shown).

Disruption of melanophore alignment at 96 hpf

From 24 hpf of zebrafish development, dark brown pigment cells called melanophores migrate from the head, extending ventrally across the yolk ball and caudally along the length of the body, reaching the tip of the tail by 42 hpf (204). By 96 hpf, a subset of these melanophores aligns centrally at the level of the horizontal myoseptum of the somites. These melanophores later converge to form the central stripe in the adult zebrafish.

One of the phenotypes of Htt-deficiency initially observed using the 21.3 ng *hd*MO dose was a disruption in the alignment of melanophores along the central axis at 96 hpf (Fig. 4.2 L-P). Rather than aligning along the central axis, they appeared enlarged, and in a haphazard distribution throughout the trunk/tail. Melanophores are derived from the neural crest, so this disruption raised the possibility that Htt may play a role in neural crest pathways. However, it was unclear whether or not the disrupted pigment patterning was a secondary consequence of the overall tissue disorganisation that was evident at this high dose.

To explore this phenotype further, embryos were injected with 6.4 ng of *hd*MO1, *hd*MO2, or *c*MO and the patterning of melanophores was examined at 48 and 96 hpf. At 48 hpf the melanophores appeared along the entire length of the tail in Htt-deficient embryos, similarly to control embryos (Fig. 4.8 A and B). By this stage, a few melanophores at the rostral end of the tail had begun to align to the horizontal myoseptum in control embryos (Fig. 4.8 A; arrow) but not in Htt-deficient embryos (Fig. 4.8 B). At 96 hpf, melanophores were centrally aligned in control embryos (Fig. 4.8 C; arrows) but this alignment was disrupted in *hd*MO-injected embryos (Fig. 4.8 D; arrows).

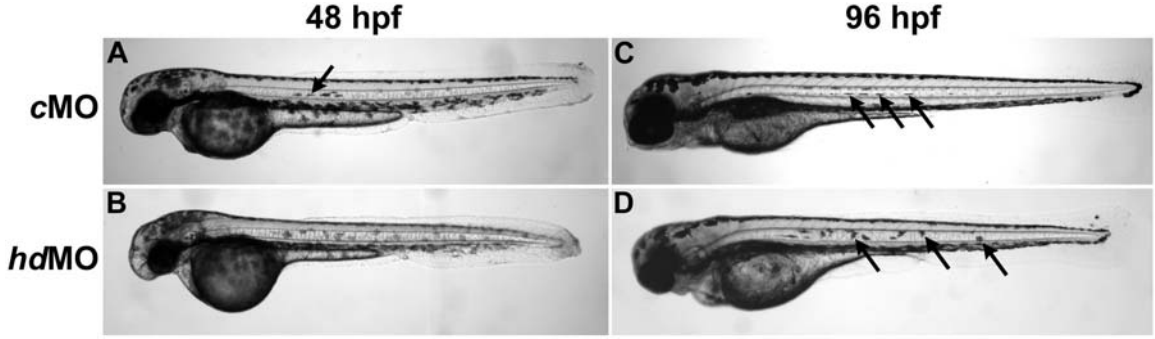

Figure 4.8 Alignment of melanophores to the horizontal myoseptum is disrupted in Htt-deficient embryos. Distribution of melanophores in embryos injected with 6.4 ng of *c*MO (**A**, **C**) or *hd*MO (**B**, **D**) was examined at 48 hpf (**A**, **B**) and 96 hpf (**C**, **D**). Since *hd*MO1 and *hd*MO2 produced the same result, representative examples of *hd*MO-injected embryos are shown in **B** and **D**. At 48 hpf, melanophores have migrated along the length of the tail in control (**A**) and Htt-deficient embryos (**B**), and have begun to centrally align to the horizontal myoseptum in control embryos (**A**; arrow). At 96 hpf the normal alignment of melanophores along the central axis (**C**; arrows) is disrupted in Htt-deficient embryos (**D**; arrows).

To quantify this phenotype, embryos were classed as having disrupted pigmentation if melanophores were not centrally aligned along the central axis (Table 4.3). Pigment disruption was seen in 78% of *hd*MO1-injected embryos (*n* = 53/68) and 82% of *hd*MO2-injected embryos (*n* = 77/94), whilst no disruption was observed in *c*MO-injected embryos (0/100).

	Normal 	Disrupted 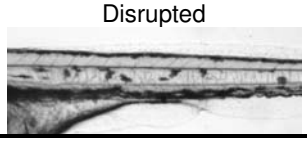	Total *n*
*c*MO	100 (100%)	0	100
*hd*MO1	53 (78%)	15 (22%)	68
*hd*MO2	77 (82%)	17 (18%)	94

Table 4.3 Quantification of pigment disruption at 96 hpf in embryos injected with cMO, *hd*MO1 or *hd*MO2. Classification was performed as described in the main text. Data was pooled from 3 experiments. MO dose was 6.4 ng per embryo.

The failure of melanophores to line up along the central axis was not due to an absence of the horizontal myoseptum (to which the melanophores normally align), as this feature was visible in *hd*MO-injected embryos when viewed using Nomarski (differential interference contrast) microscopy (not shown).

Discussion

It has previously been shown that homozygous inactivation of the *Hdh* gene in 3 mouse models leads to embryonic lethality after 7.5 days of gestation (110-112). The effect of Htt deficiency is first evident during gastrulation, when although the three germ layers are formed, development is retarded. These embryos fail to neurulate and rapidly degenerate without forming nodes, notochord or somites. These effects are accompanied by an increased level of apoptotic cell death in the embryonic ectoderm (110). Whilst these studies indicate the importance of Htt during development, the severity of the knockout phenotype has made elucidation of the exact function of Htt difficult using these models.

The aim of this work was to transiently knock down Htt levels in zebrafish embryos using antisense MOs, and to look for developmental consequences that could offer novel clues as to the function of Htt. The external development and optical transparency of zebrafish embryos facilitated the visualisation of a variety of morphological phenotypes associated with Htt deficiency. These included pale blood,

thin yolk extension, disrupted melanophore patterning, failure to inflate the swim bladder, tail curling, small head and eyes, disrupted jaw/branchial structures, pericardial oedema and reduced touch sensitivity. The same spectrum of phenotypes was produced by either of two independent, non-overlapping *hd*MOs, and none of these phenotypes were observed in *c*MO-injected embryos, indicating that they are specific effects of Htt depletion. The use of TUNEL methodology also indicated an increased level of apoptosis in Htt-deficient embryos, consistent with previous findings in mouse (110).

The morphological effects of Htt knockdown in zebrafish manifested later in development than in the mouse knockout models, even though *hd*MOs were administered at the 1-cell stage. Using a relatively high MO dose of 21.3 ng, stages of gastrulation, somitogenesis and early neurulation (formation of the neural plate, neural keel and notochord) appeared to occur normally in Htt-deficient zebrafish embryos, unlike null mouse embryos. The earliest sign of abnormal morphology in the morphants was brain necrosis, first evident 14 to 18 hours post fertilisation.

The delayed/less severe effect of Htt deficiency in zebrafish is likely to be due to incomplete saturation of *hd* mRNA transcripts by *hd*MOs, as suggested by the incomplete knockdown of Htt observed in the western analysis performed by T. Henshall (Fig. 4.3 E). It is also possible that some translation of *hd* mRNA may occur prior to *hd*MO injection, given that a high level of maternally deposited *hd* transcript is present in 1-cell embryos (Chapter 3). The ability to knock down *hd* gene function incompletely is an advantage of using the MO system, since embryos are able to survive to later stages of development and MO dose can be adjusted to observe more subtle effects of Htt deficiency.

Knockdown of Htt levels in zebrafish revealed a requirement of Htt in multiple developmental processes, and provided a variety of morphological phenotypes that had investigative potential for further study of Htt function. Each of these phenotypes was considered in the context of the current literature and information available on the Zebrafish Information Network website (ZFIN; http://zfin.org/), to determine which aspect would be most informative to pursue further.

Pale blood phenotype

Of all the morphological defects observed in Htt-deficient embryos, the pale blood phenotype occurred most frequently, and (at the lowest concentrations) often presented in the absence of other visible defects suggesting that it is a primary effect of

Htt deficiency. Pale or 'hypochromic' blood is also observed in mutant zebrafish strains with deficits in haemoglobin production (236, 237) and is often caused by a disruption in iron metabolism (238-240). This was particularly interesting since wildtype Htt has been implicated in haematopoiesis and iron homeostasis in cultured cells (121, 139), and also in the transport of nutrients such as iron across the visceral endoderm from maternal to embryonic tissues in the mouse foetus (114).

Thin yolk extension, and other phenotypes common to mutant strains with defects in housekeeping genes

After pale blood, the thin yolk extension phenotype was the next most common phenotype of Htt deficiency. Whilst the yolk extension initially forms correctly by protruding caudally from the yolk ball (18 hpf), it becomes thinner by 24 hpf and often disappears completely.

A search of the mutant zebrafish gene database listed on the ZFIN website revealed 34 mutant strains that also exhibit a thin yolk extension phenotype. In general the mutations affect ubiquitous genes with essential housekeeping functions such as those encoding polymerases, ribosomal proteins, RNA processing factors and translation initiating factors (see Appendix A). Other phenotypes that are observed in Htt-deficient embryos such as brain necrosis, pericardial oedema, enlargement of melanophores and failure to inflate the swim bladder are also common amongst these mutant strains, suggesting that these phenotypes are symptoms of general cellular dysfunction. Therefore, these phenotypes are likely to be secondary consequences of Htt-deficiency, and may not be particularly informative regarding the specific role of Htt. However, the presence of these phenotypes in Htt morphants is consistent with Htt having an important housekeeping function.

Phenotypes suggesting neural crest involvement

Some of the phenotypes associated with Htt knockdown in zebrafish suggest that neural crest pathways are affected by Htt deficiency. Pigment cells and craniofacial structures are derivatives of the neural crest (241) and are affected in Htt-deficient embryos. The small head and poorly formed branchial/jaw structures observed in Htt-deficient zebrafish might be analogous to craniofacial abnormalities that have been observed previously in mouse embryos/pups expressing less than 50% of normal Htt levels from a hypomorphic allele (91).

However, since the phenotypes of small head and enlarged melanophores observed in Htt-deficient embryos are common amongst strains with defects in housekeeping genes, these neural crest-related phenotypes may be secondary consequences of cellular dysfunction, and thus may not be the most informative phenotypes for ascertaining the role of Htt.

Increased apoptosis

Htt has been implicated as a pro-survival protein, largely due to the findings that an increased level of apoptotic cell death is observed in knockout mice (110), and wildtype Htt can protect cells from apoptosis caused by stress (113). Consistent with these previous findings, a general increase in apoptosis was observed in Htt-deficient zebrafish embryos, suggesting conservation of this aspect of Htt function.

Characterisation of this phenotype was complicated by variable background levels, since the injection process itself appeared to induce apoptosis to some extent. Furthermore, vast heterogeneity of apoptosis levels was observed among any given batch of injected embryos.

A limitation of the TUNEL methods used here is that the staining appeared to be somewhat restricted to the surface layer of embryos. In future experiments it may be useful to stain tissue sections, or to use an alternate method of cell death detection that has greater tissue penetrance, such as acridine orange staining of live embryos (242).

Failed inflation of the swim bladder

Htt-deficient zebrafish embryos often fail to inflate the swim bladder. Interestingly, haemoglobin oxygen transport is involved in swim bladder inflation in adult fish, and functional ablation of haemoglobin (by chemical modification with phenylhydrazine) significantly impairs initial swim bladder inflation in zebrafish embryos, suggesting an involvement of haemoglobin in this process (235). The pale blood phenotype of Htt-deficient embryos suggested a defect in haemoglobin function in these embryos. It was therefore thought possible that the impaired bladder inflation in Htt-deficient embryos might be a secondary consequence of reduced haemoglobin function. However, contradicting this argument, zebrafish genetic mutant strains that have pale blood due to a reduction in haemoglobin levels have not been reported as having any defects in swim bladder inflation (236, 237).

In any case, the loss-of-swim bladder phenotype was considered a late effect in relation to other phenotypes, and is observed in housekeeping gene mutants as mentioned above. This phenotype is therefore most likely to be a secondary effect of Htt-deficiency and was not investigated further in this study.

Conclusion

Of all the phenotypes associated with Htt knockdown in zebrafish embryos, the pale blood phenotype appeared to be the most informative for investigating Htt function. Pale blood was observed at low doses of *hd*MO, below the threshold required to visualise any other morphological phenotypes, and is thus likely to be one of the primary consequences of Htt depletion. This phenotype also suggested a requirement for Htt in haemoglobin production, which is interesting given that previous studies support a role for Htt in iron transport and homeostasis (114, 139).

Intriguingly, there is evidence of iron misregulation in HD. Patients exhibit numerous signs of disrupted iron homeostasis such as decreased serum ferritin levels (243, 244), increased striatal iron accumulation (60) and a significant increase in basal ganglia ferritin levels early in HD progression (63, 64). Regional iron accumulation is a suspected cause of pathology in a number of other neurodegenerative diseases due to the potential for iron to generate reactive oxygen species. In view of the possibility that the pale blood phenotype in Htt-deficient zebrafish embryos may be caused by a disruption in iron metabolism, thereby hinting at a potential link between normal Htt function and specificity of HD pathology, this aspect of the Htt morphant phenotype was further investigated, as described in the next chapter.

Chapter 5: Identification of a role for Huntingtin in intracellular iron compartmentalisation

Introduction

In the previous chapter, a blood phenotype was identified as a primary consequence of Huntingtin (Htt) knockdown in zebrafish embryos. Whilst similar numbers of blood cells were observed in Htt morphant and wildtype embryos, the cells appeared pale or even colourless in comparison to the redness of wildtype blood cells. This suggested that Htt-deficient blood cells had a decreased capacity to produce haemoglobin, the oxygen-carrying haemoprotein that gives erythrocytes their characteristic red colour. In this chapter, the pale or 'hypochromic' blood phenotype of erythroid cells was further characterised in the hope that the findings would identify a function for Htt that would be applicable to all Htt-expressing cells.

Haemoglobin (Hb) is a tetramer of subunits each comprised of a globular protein (globin) and a prosthetic haem group containing a single iron atom (245). Thus a reduction in functional Hb could be caused by a disruption in either cytoplasmic globin synthesis, regulation/initiation of mitochondrial haem biosynthesis, or iron transport and compartmentalisation. Mutagenesis screens for defects in early zebrafish haematopoiesis (236, 237) have generated a number of strains with hypochromic blood, due to mutations affecting one of these 3 processes (238-240, 246-249). A previous study into the effect of Htt deficiency on mouse haematopoiesis demonstrated that Htt was not essential for differentiation of embryoid body cells (derived from *Hdh*$^{-/-}$ embryonic stem cells) into haematopoietic progenitors, but was required for their subsequent proliferation and survival (121). Notably, β globin expression (embryonic βH-1 and adult β) was not reduced in these Htt-deficient haematopoietic cells (121), suggesting that the hypochromia phenotype in Htt-deficient zebrafish was unlikely to be caused by globin deficiency. Since Htt has been implicated in intracellular iron homeostasis (139), and in the transport of iron from maternal to embryonic tissues (114), it was hypothesised that Htt deficiency was causing hypochromia due to some perturbation of the iron pathway.

As an introduction to this work, a review of early zebrafish haematopoiesis, iron homeostasis, haem and Hb production, and previously characterised hypochromic zebrafish mutants will be given.

Primitive zebrafish haematopoiesis

As in all vertebrates, zebrafish haematopoiesis occurs in two successive waves: 'primitive' and 'definitive' (205). Whilst definitive haematopoiesis gives rise to cells of all haematopoietic lineages, the first, primitive wave of haematopoiesis produces predominantly erythroid cells. It is this period of haematopoiesis that was examined in the current study. The site of primitive zebrafish erythropoiesis is the intermediate cell mass (ICM), analogous to the extraembryonic yolk sac blood islands in mammals and birds. The zebrafish ICM is located in the ventral trunk region, bordering the yolk extension, and arises from the convergence (at the ventral midline) of two parallel bands of lateral mesoderm (Fig. 5.1). By the completion of ICM formation at approximately 19 hours post fertilisation (hpf), approximately 300 large, round, basophilic cells morphologically identifiable as proerythroblasts are present within this region (205). These cells begin to circulate through the vasculature at 24-26 hpf. The primary function of these cells is to produce Hb.

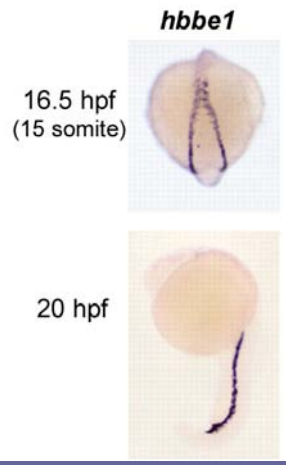

Figure 5.1 Position of the intermediate cell mass (ICM) in developing zebrafish embryos, highlighted by the erythroid-specific distribution of *haemoglobin beta embryonic-1* (*hbbe1*) mRNA. Dorsal (16.5 hpf) and lateral (20 hpf) views shown.

These images were taken from Wingert *et al*, 2004, reference (238), and are shown here to illustrate the position of the ICM.

Iron homeostasis

For most organisms, iron is an essential element for cellular function, acting as a vital co-factor in numerous haemoproteins (such as Hb) and non-haem iron-requiring proteins and enzymes. However, unless appropriately chelated, high levels of iron can be toxic, primarily due to its potential to generate reactive oxygen species (250). Therefore, tight regulatory mechanisms have evolved that maintain a fine balance between iron deficiency and overabundance, in order to meet cellular iron requirements (251).

Iron is acquired via dietary absorption through the intestinal lining into the bloodstream where it is subsequently transported throughout the body to sites of utilisation and storage (252). Since the body has only limited physiological means of

getting rid of excess iron, iron homeostasis is maintained by regulatory feedback between body iron needs and intestinal iron absorption. For reference, an overview of the pathway of iron acquisition is illustrated in Figure 5.2.

Absorption of iron

Dietary iron can be taken up into duodenal enterocytes either in an inorganic form or as haem (252). Non-haem iron is transported across the apical surface of enterocytes by the divalent metal transporter, DMT1 (also known as DCT1 or Nramp2) (253, 254). Since DMT1 transports only divalent ions, the ferric reductase duodenal cytochrome B (Dcytb) aids in the conversion of any ferric iron to its ferrous form (255). The uptake of haem iron is less well characterised, however HCP 1 (haem carrier protein 1) has recently been proposed as the transporter responsible for this (256) (not shown in Fig. 5.2). Haem absorbed into the enterocytes is degraded and the released iron follows the same path as iron acquired from non-haem sources (252).

The plasma membrane iron exporter, ferroportin 1 (240), mediates the release of iron from the enterocytes across the basolateral membrane into the plasma, and is thought to act in conjunction with the membrane-bound ferroxidase, hephaestin (257). Once in the plasma, extracellular iron is bound tightly, but reversibly by the glycoprotein, transferrin (Tf) (251). Tf maintains ferric iron in a soluble and non-toxic form and enables its transport throughout the body between sites of absorption, storage and utilisation.

Iron-loaded Tf (but not iron-free apo-Tf) is specifically recognised by the Tf receptor (TfR) on the cell surface (251). Two TfR types have been described (TfR1 and TfR2). The first discovered and most characterised of these is TfR1 (258), which is expressed by all iron-requiring cells and is much more abundant than TfR2 that is predominantly expressed in the liver (259). Binding of iron-loaded Tf to the TfR initiates clathrin-mediated endocytosis of the receptor/ligand complex into endocytic vesicles that rapidly lose their clathrin coat and fuse to early endosomes (260). Acidification of these endosomes by the vacuolar (V)-ATPase proton pump (261) facilitates the disassociation of ferric iron from the Tf/TfR complexes. Steap3 has recently been identified as the endosomal ferrireductase responsible for converting ferric iron to its ferrous state (262), allowing its transport across the endosomal membrane into the cytosol via DMT1 (263), the same transporter expressed in the duodenal enterocyte. Iron free apo-Tf/TfR complexes are then recycled back to the cell surface, where the extracellular pH releases apo-Tf from the TfR, making each available for re-use (Fig. 5.2 A).

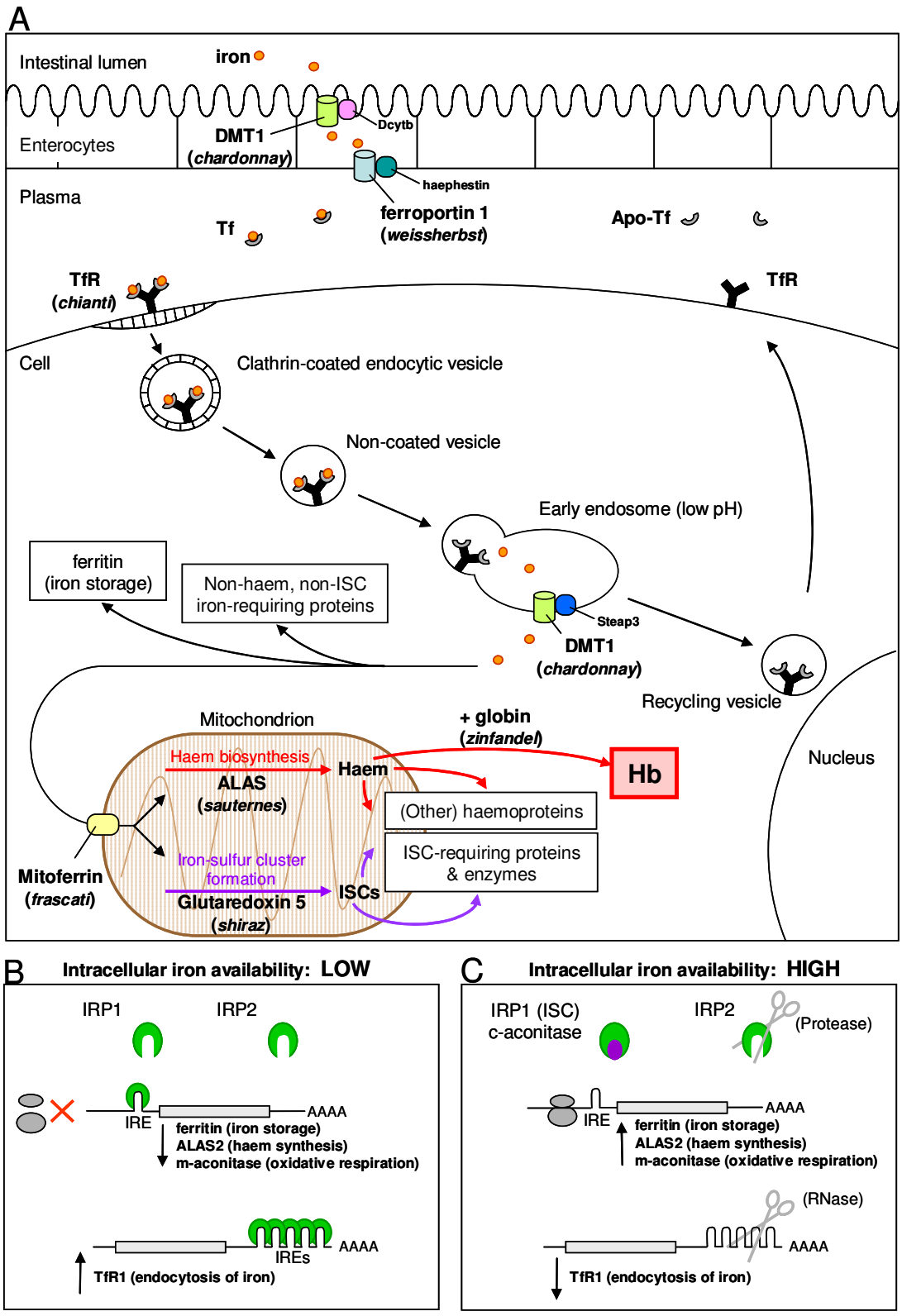
A
Intestinal lumen
iron
Enterocytes
DMT1
(chardonnay)
Dcytb
haephestin
ferroportin 1
(weissherbst)
Plasma
Tf
Apo-Tf
TfR
(chianti)
TfR
Cell
Clathrin-coated endocytic vesicle
Non-coated vesicle
Early endosome (low pH)
ferritin
(iron storage)
Non-haem, non-ISC
iron-requiring proteins
Steap3
DMT1
(chardonnay)
Recycling vesicle
Mitochondrion
+ globin
(zinfandel)
Haem biosynthesis
ALAS
(sauternes)
Haem
Hb
(Other) haemoproteins
Iron-sulfur cluster
formation
ISC-requiring proteins
& enzymes
Mitoferrin
(frascati)
Glutaredoxin 5
(shiraz)
ISCs
Nucleus
B
Intracellular iron availability: LOW
IRP1
IRP2
IRE
AAAA
ferritin (iron storage)
ALAS2 (haem synthesis)
m-aconitase (oxidative respiration)
IREs
AAAA
TfR1 (endocytosis of iron)
C
Intracellular iron availability: HIGH
IRP1 (ISC)
c-aconitase
IRP2
(Protease)
IRE
AAAA
ferritin (iron storage)
ALAS2 (haem synthesis)
m-aconitase (oxidative respiration)
(RNase)
AAAA
TfR1 (endocytosis of iron)

Figure 5.2 Diagram illustrating the key proteins involved in iron acquisition, and the regulation of homeostatic responses to cellular iron availability by IRE-IRP interactions.
(**A**) Iron is absorbed from the intestinal lumen into enterocytes via divalent metal transporter **DMT1** (aided by **Dcytb**) and is transported through basal membrane into the plasma via **ferroportin 1** (aided by **hephaestin**) (ref. (252)). In the plasma, iron is bound by **transferrin** (**Tf**). Binding of iron-loaded Tf to **TfR** on the plasma membrane of cells initiates clathrin-mediated endocytosis of the receptor/ligand complex into **endocytic vesicles** that lose their clathrin coat and fuse to **early endosomes** (ref. (260)). The decreased internal pH of the early endosome causes iron to disassociate from apo-Tf/TfR, facilitating its release into the cytoplasm via **DMT1,** aided by **Steap3**; (refs (262, 263)). Iron-free apo-Tf/TfR complexes are recycled back to the cell surface for re-use. Once released iron enters the mitochondria (**Mitoferrin** is the proposed solute carrier responsible for this, at least in erythroid cells; ref. (246)) where it is incorporated into **haem** and **iron-sulfur clusters** (**ISCs**). Haem synthesis is initiated by **ALAS** (ALAS2 is the erythroid-specific isoform) (ref. (264)). Haem is then utilised by mitochondrial and cytoplasmic haemoproteins (ref. (252)). In erythroid cells, most haem is utilised (in conjunction with **globin**) as **haemoglobin** (**Hb**). **ISCs** are important co-factors in many mitochondrial and cytoplasmic proteins and enzymes (refs (265, 266)). **Glutaredoxin 5** is required for ISC formation (ref. (249)). Iron is also utilised by a number of **non-haem, non-ISC, iron-requiring proteins** such as hydroxylases (ref. (267)). Excess iron not immediately required for cellular use is stored in the intracellular iron storage molecule, **ferritin** (ref. (268)).

(**B**) In conditions of **low iron availability**, iron regulatory proteins **IRP1** and **IRP2** translationally regulate expression of a number of proteins by binding to iron response elements (**IREs**) in the target transcripts, either in the 5' UTR to inhibit translation (in the case of **ferritin**, **ALAS2** and **mitochondrial (m-) aconitase**) or the 3' UTR to stabilise the transcript and increase translation (in the case of **TfR1**) (refs (251, 252)). (**C**) However, in conditions of **high iron availability**, **IRP1** exists in its ISC-bound (non IRE-binding) form as cytosolic **(c-) aconitase**, and **IRP2** is degradation prone. Consequently, translation of **ferritin**, **ALAS2** and **m-aconitase** is permitted, and the **TfR1** is down-regulated due to mRNA transcript degradation (refs (251, 252).

In previously characterised hypochromic zebrafish mutants (discussed later in this chapter), Hb production is disrupted due to mutations affecting zebrafish orthologues of **DMT1** (***chardonnay***), **ferroportin 1** (***weissherbst***), **TfR1** (***chianti,*** affecting the erythroid-specific *tfr1a* gene), **Mitoferrin** (***frascati***), **ALAS2** (***sauternes***), **Glutaredoxin 5** (***shiraz***) and **globin** (***zinfandel***) (refs (238-240, 246-249)).

Once in the cytoplasm, iron is available for utilisation by non-haem iron-requiring proteins (such as aromatic amino acid hydroxylases (267)), or for mitochondrial haem biosynthesis and iron-sulfur cluster (ISC) formation (Fig. 5.2 A). Haem and ISCs are important co-factors in many mitochondrial and cytoplasmic proteins and enzymes. In addition to Hb, other haemoproteins include myoglobin, respiratory cytochromes, oxygenases, peroxidases, nitric oxide synthase and guanylate cyclase (252). ISC-requiring proteins and enzymes include mitochondrial and cytosolic aconitases, and components of mitochondrial respiratory complexes I, II and III (265, 266).

Iron storage

Surplus iron that is not immediately required for cellular use is sequestered within the intracellular iron storage protein, ferritin. Ferritin is a hollow shell-like structure (comprised of 24 subunits of heavy (H) and light (L) chains) that can accommodate up to 4500 ferric ions (268). Different cell types typically contain varying levels of ferritin depending on their function and iron requirement. Erythroid cells have a very high iron requirement, containing the majority of the body's iron within Hb. Ferritin is not normally expressed in these cells, as imported iron is quickly utilised in Hb production. Most iron is stored in the hepatocytes of the liver, and in reticuloendothelial macrophages (252).

Haem biosynthesis

Haem biosynthesis is a multi-step pathway requiring eight nuclear encoded enzymes (see for review (269)). The pathway begins and terminates in the mitochondria, but intermediate steps take place in the cytosol. The first step is catalysed by 5-aminolevulinic acid synthase (ALAS). Two ALAS isoforms exist; ALAS1, a housekeeping isoform, and ALAS2 that is erythroid specific. In the final step of haem synthesis, a ferrous ion is inserted into protoporphoryn IX, catalysed by ferrochelatase in the mitochondria (269). Haem is then utilised in mitochondrial haemoproteins such as respiratory cytochromes, or is transported into the cytosol to be incorporated into other cellular haem-requiring proteins such as Hb and myoglobin in the blood and muscle, respectively.

Composition of haemoglobin

The haemoglobin (Hb) molecule is a tetramer composed of two α-globin subunits and two β-globin subunits, each coordinated with a prosthetic haem group. Haem is a heterocyclic porphyrin ring containing a single iron atom that, in its divalent (Fe^{2+}, or ferrous) form, is responsible for the binding of oxygen (245).

Regulation of cellular iron homeostasis by the IRP/IRE system

The expression levels of many proteins involved in iron homeostasis are regulated post-transcriptionally by the presence of 'iron responsive elements' (IREs) in the untranslated regions (UTRs) of mRNAs encoding these proteins (251, 252)(Fig 5.2 B and C). When cellular iron levels are depleted, iron responsive proteins IRP1 and IRP2 are activated to bind to the stem-loop structure formed by the IRE motif. Whether the IREs lie in the 5' or 3' UTR of a particular mRNA determines whether IRP binding results in translational silencing, or transcript stabilisation, respectively.

Expression of TfR1 (but not TfR2) and ferritin (both H and L chains) is reciprocally regulated by the IRP-IRE system (Fig. 5.2 B and C). In low iron conditions, the interactions of IRPs with five IREs in the 3' UTR of TfR1 mRNA stabilises the transcript which would otherwise be sensitive to ribonuclease degradation. This mRNA stabilisation results in the up-regulation of TfR1 expression levels, leading to an increase in TfR-mediated iron uptake. In the case of ferritin mRNA, the IRP-IRE interaction in the 5' UTR inhibits translation, resulting in decreased ferritin synthesis. Conversely, in iron-replete cells IRP1 and IRP2 are inactivated, allowing TfR1 mRNA degradation and ferritin mRNA translation to occur. As a result, iron uptake is reduced, and excess intracellular iron is able to be sequestered within ferritin.

Other proteins whose expression is also regulated by the IRP/IRE system include ALAS2 and mitochondrial aconitase (m-aconitase) (Fig. 5.2 B and C). Incompletely characterised IREs have also been found in ferroportin 1 and DMT1 mRNAs.

Iron regulatory proteins (IRPs)

IRP1 and IRP2 both bind IREs in conditions of iron deficiency but not in iron replete cells, and thus act as cellular iron sensors (Fig. 5.2 B and C). The two proteins share some homology, but their activity is differentially regulated (251, 252). In iron-replete cells, IRP1 assembles an ISC to become enzymatically active as cytosolic aconitase (c-aconitase), an enzyme involved in the citrate cycle. In this form it is unable

to bind IRE sequences. Iron starvation conditions result in the disassembly of the ISC, and IRP1 regains IRE-binding activity. In contrast, IRP2 is subject to proteasomal degradation in iron-replete cells, but is synthesised *de novo* and is stable under conditions of iron deficiency (or hypoxia).

Hypochromic mutants generated previously in zebrafish haematopoietic screens

The zebrafish has been identified as an ideal model organism in which to study early haematopoiesis (205). The transparency of zebrafish embryos allows the observation of the relative number and colour of blood cells from onset of circulation. The blood cells generally resemble those of other vertebrates. Hb in erythroid cells has the typical $\alpha_2\beta_2$ quaternary structure of higher vertebrates, and the pathways of iron transport and haem biosynthesis are well conserved.

Two chemical mutagenesis screens for defects in primitive zebrafish haematopoiesis have generated over 40 mutant strains comprising 26 complementation groups. These groups are categorised as having either no red blood cells (bloodless mutants), progressive anaemia (decreasing numbers of pigmented blood cells), hypochromic anaemia (blood cells having reduced pigmentation and decreasing blood count), or photosensitive blood cells that autofluoresce and lyse upon light exposure (236, 237).

The blood phenotype of Htt morphants described in Chapter 4 resembles the mutants in the category with hypochromic anaemia of which there are currently 9 (236, 237, 246). Decreased Hb production was confirmed in these mutants, by *o*-dianisidine or diaminofluorene staining. Seven of the hypochromic mutant loci including *chardonnay*, *chianti*, *frascati*, *sauternes*, *shiraz*, *weissherbst* and *zinfandel* have been mapped by positional cloning, to genes required for Hb production (238-240, 246-249), as described below (and see Fig. 5.2 A).

The *weissherbst* hypochromic mutation mapped to the gene encoding ferroportin 1, that as well as being required for absorption of iron from the gut, was also found to be required in early zebrafish development for absorption of iron from the maternally supplied yolk stores, into the bloodstream (240). Mutations in *dmt1* are responsible for hypochromia in *chardonnay* mutants (239). In zebrafish, gene duplication has given rise to two isoforms of TfR1: an erythroid specific isoform encoded by *tfr1a* and a ubiquitously expressed isoform encoded by *tfr1b*. In *chianti* mutants, hypochromia is caused by a mutation in the erythroid specific *tfr1a* gene (238). Hypochromia in *frascati* mutants is caused by mutation of the *mitoferrin* gene, which

encodes a mitochondrial solute carrier protein (of the SLC25 family). Mitoferrin is essential for erythroid haem synthesis due to its role in importing iron into the mitochondria (246). Mutations in *alas2* (encoding alas2, responsible for catalysing the first step in erythroid haem biosynthesis) are responsible for *sauternes* hypochromia (247). The *shiraz* hypochromic mutation mapped to the *grx5* gene, encoding glutaredoxin 5, a mitochondrial protein that is required for ISC formation in the erythroid lineage (249). In *shiraz* mutants, lack of ISC assembly prevents the shift of IRP1 from its IRE-binding form to its non-IRE-binding (c-aconitase) form. Consequently, IRP-IRE binding in the 5' UTR of *alas2* mRNA inhibits translation, thus preventing haem biosynthesis and Hb production. The *zinfandel* hypochromic mutation maps in close proximity to the major zebrafish globin locus and perturbs expression of all six known zebrafish embryonic globin genes (248). This mutation is suspected to cause a regulatory defect, since no coding mutations were detected within closely linked embryonic globin genes.

Zebrafish mutations affecting enzymes downstream of alas2 in the haem biosynthesis pathway, such as uroporphyrinogen decarboxylase (270) and ferrochelatase (271), cause photosensitivity rather than hypochromia. The erythrocytes in these mutants autofluoresce and lyse due to the increased accumulation of toxic haem precursors. This effect was not observed in *hd*MO-injected embryos.

The *hd* gene would not be identified in haematopoietic mutant screens such as those described above, since mutants with only blood-specific phenotypes were characterised, and Htt-deficient embryos display a wide range of phenotypes in addition to pale blood (Chapter 4). The hypochromic mutant strains described above have only minor additional phenotypes (for example cardiomegaly), if any, during development, and affect genes that are predominantly or exclusively expressed in the erythroid lineage (in the ICM; Fig. 5.1) or in the peripheral layer surrounding the yolk, in the case of iron transporter, ferroportin 1. Since the *hd* gene is ubiquitously expressed (Chapter 3), it was hoped that characterisation of the hypochromia phenotype would reveal a global role for Htt that would apply to all Htt-expressing cells.

Results

Expression of *hd* mRNA in zebrafish erythroid tissue

Zebrafish embryos hybridised with *hd* mRNA probe were re-examined with a focus on the ICM, to see if *hd* is normally expressed in erythroid cells that manufacture

Hb, as this would be consistent with Htt having a role in these cells. *hd* mRNA was detected ubiquitously throughout the tail, including the ICM at 22 hpf, prior to the onset of circulation of erythroid cells (Fig. 5.3 B). Expression is shown here in comparison to *notch2* expression, which is detected in somites but is notably absent in the ICM (Fig. 5.3 A). Expression of *hd* mRNA was also detected in the posterior ICM at 36 hpf (Fig 3 G), at higher levels than the rest of the tail. At this time the majority of circulating cells are of the erythroid lineage, although haematopoietic activity in the ICM tissue is not exclusively erythroid by this time (205). Consistent with the expression of *hd* mRNA in the ICM, *Hdh* gene products have also been detected in a range of mouse haematopoietic tissues (121).

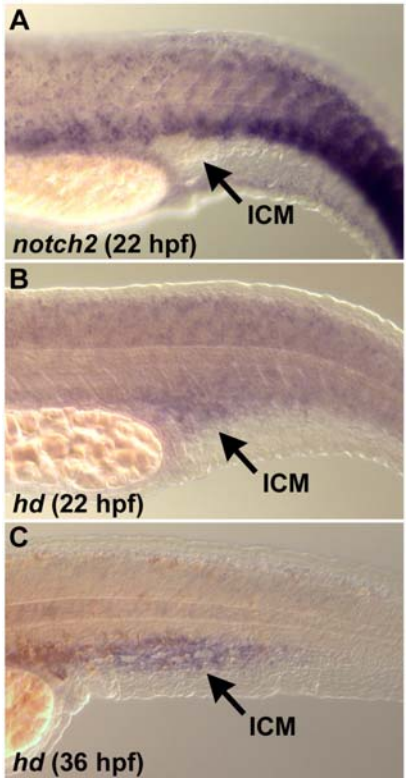

Figure 5.3 Detection of *hd* mRNA expression in the ICM. In comparison to *notch2* mRNA expression that is not detected in the ICM at 22 hpf (**A**), *hd* mRNA is expressed in the ICM (and throughout the tail) at 22 hpf (**B**). At 36 hpf *hd* mRNA expression is increased in the posterior ICM above basal expression throughout the rest of the tail (**C**).

Transient suppression of haemoglobin production in response to Htt knockdown

The hypochromic appearance of the blood in Htt-deficient embryos (Chapter 4) was not due to a lack of red blood cells since similar cell numbers were seen circulating in Htt-deficient and wildtype embryos (Fig. 5.4 A and B). Rather, the blood cells were lacking red pigment (Chapter 4, Fig. 4.6). Whilst the colour of embryonic erythroid cells gives a general indication of Hb levels, *o*-dianisidine staining is a more sensitive and definitive method for detecting Hb. The basis of this assay is that Hb catalyses the

H_2O_2-mediated oxidation of *o*-dianisidine, producing a dark red stain in Hb-positive cells.

To assess Hb levels in Htt morphant zebrafish, embryos were injected with 8.5 ng of *hd*MO1 or *c*MO, and were collected at 33 or 72 hpf for o-dianisidine staining (see Chapter 2, Materials and methods). At 33 hpf, a marked reduction in Hb production was observed in the blood cells of Htt-deficient embryos (Fig. 5.4 G and H) when compared to control embryos (Fig. 5.4 C and D). Very weak staining was detectable in the blood cells of the Htt morphants at this stage, however, confirming that the general low level of staining was not due to an absence of these cells. By 72 hpf all morphant zebrafish exhibited strong *o*-dianisidine staining in the blood, similar to control embryos (Fig. 5.4 I and J, compared to E and F), indicating that suppression of Hb production was transient.

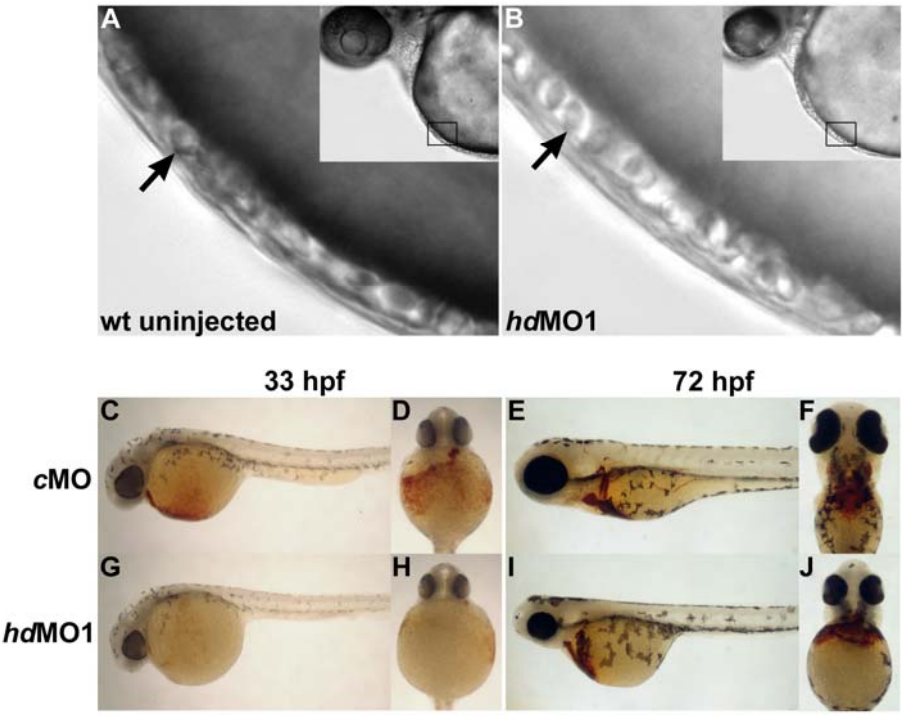

Figure 5.4 Transient suppression of Hb production in response to Htt knockdown. Similar numbers of blood cells are visible circulating across the yolk of wildtype uninjected embryos (**A**) and embryos injected with 8.5 ng *hd*MO1 (**B**) at 36 hpf. Boxed area in the insets indicates the magnified region. Arrows indicate an example of a single blood cell in each image. Hb production was detected by *o*-dianisidine staining in zebrafish embryos injected with 8.5 ng of *c*MO (**C**-**F**) or *hd*MO1 (**G**-**J**). At 33 hpf, Hb production was suppressed in *hd*MO1-injected embryos (lateral, **G**; and ventral, **H**, views of a representative embryo) in comparison to *c*MO-injected embryos (**C**, **D**). By 72 hpf, Hb levels in *hd*MO1-injected embryos (**I**, **J**) returned to a level similar to *c*MO-injected control embryos (**E**, **F**).

Iron staining in whole mount embryos and isolated blood cells

In the zebrafish embryo, iron is absorbed from maternally derived stores in the yolk (240) and erythroid cells endocytose iron from the plasma as transferrin (Tf) via the Tf receptor (TfR) (238). To investigate the possibility that the decrease in Hb levels could be due to a disruption in iron transport, DAB-enhanced Prussian blue staining was used to detect the presence of ferric ions in morphant and control embryos ((114), and see Chapter 2, Materials and methods) in order to assess any differences in iron distribution.

The basis of this iron staining procedure is that potassium ferrocyanide in the substrate reacts with ferric ions in the embryo, producing ferric ferrocyanide (known as Prussian blue due to its colour). Staining is enhanced by the addition of DAB since ferric ferrocyanide catalyses the oxidation of DAB, producing a reddish brown colour that is easier to detect. The use of Prussian blue staining in zebrafish has not previously been described. Therefore the method was first tested on wildtype embryos of various developmental stages from 1-cell to 48 hpf. Staining was easily visible when enhanced with DAB, and revealed the ubiquitous presence of ferric iron throughout the developing embryo at all stages examined (not shown).

Iron staining was then performed at 36 hpf, on wildtype embryos and embryos injected with 8.5 ng of *hd*MO1. Ferric iron was detected throughout the animal (non-yolk) part of Htt-deficient embryos at a level at least the same, and in many cases higher, than in wildtype embryos (Fig. 5.5 A and B). In wildtype embryos ferric iron was also present in the yolk syncytial layer (the peripheral layer that surrounds the embryonic yolk sac, just below the yolk membrane) presumably representing the yolk iron stores (100%, n = 52/52; Fig. 5.5 A, arrow). Embryos injected with *hd*MO1 frequently lacked staining in this region (Fig. 5.5 B, arrow), with only 54% staining positively in the yolk syncytial layer (n = 32/59). All of the *hd*MO1-injected embryos that lacked iron staining in the yolk syncytial layer also had a thin yolk extension. These results indicated that hypochromia was not due to impaired uptake of iron from the maternally derived yolk stores into the embryo.

Blood cells visible in the ventral tail region of morphant embryos (predominantly of the erythroid lineage at this stage) stained positively for ferric iron suggesting that iron was able to enter the Htt-deficient blood cells (Fig. 5.5 C-F). Furthermore, blood cell staining in the Htt morphants appeared stronger than in wildtype embryos. To examine blood iron staining more closely, embryos were injected with 8.5 ng of *hd*MO1 or *mc*MO1 (mispair control MO; see Chapter 2, Materials and methods), and blood cells

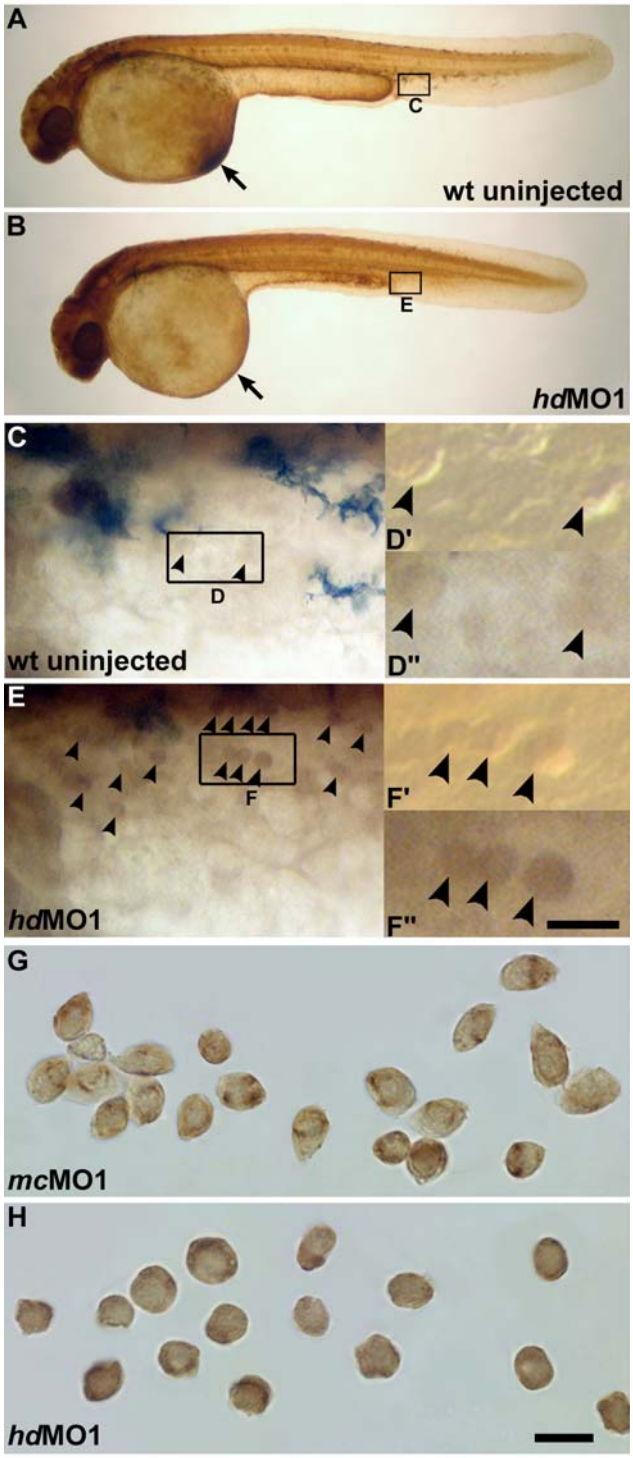

Figure 5.5 Histochemical staining for ferric iron, detected by DAB-enhanced Prussian blue staining (reddish brown). Histochemical ferric iron staining was examined in 36 hpf wildtype embryos (**A**, **C**, **D'**, **D"**) and embryos injected with 8.5 ng of *hd*MO1 (**B**, **E**, **F'**, **F"**). Ferric iron was detected throughout wildtype (**A**) and Htt-deficient (**B**) embryos. Ferric iron present in the yolk syncytial layer in wildtype embryos (**A**, arrow) was frequently absent in *hd*MO1-injected embryos (**B**, arrow). Blood cells visible in the ventral tail region of *hd*MO1-injected embryos (**E**, arrowheads) appeared to stain more strongly for ferric iron than blood cells in wildtype embryos (**C**). At higher magnification, round basophilic blood cells identified by Nomarski optics (**D'** and **F'**, arrowheads) stained positively for ferric iron, as viewed using bright-field optics (**D"**, **F"**, arrowheads). Blood cells extracted at 33 hpf from embryos injected with 8.5 ng of *hd*MO1 (H) appeared to contain at least as much ferric iron as blood cells from *mc*MO1-injected control embryos (G). Scalebars represent 10 μM.

were extracted by cardiac puncture at 33 hpf, for enhanced Prussian blue staining. As mentioned above, the Prussian blue staining procedure detects ferric iron (Fe^{3+}). This is the stable state of iron in most of its biological complexes (including when it is bound to Tf). Hb, however, utilises ferrous iron so Prussian blue stain should not detect iron in Hb. Ferric iron was detected both in control and Htt-deficient blood cells, and the

staining appeared to be stronger in Htt-deficient cells (Fig. 5.5 G and H). Since erythrocytes acquire iron exclusively via TfR-mediated endocytosis of Tf (238), this placed the disruption of Hb production downstream of TfR-mediated endocytosis of iron in the Htt-deficient blood cells.

Rescue of hypochromia and thin yolk extension phenotypes by provision of iron to the cytoplasm

Following the detection of iron within the blood cells of Htt-deficient embryos, it was hypothesised that Htt may be required for rendering this intracellular iron available for cellular use (perhaps by facilitating iron release from endocytic vesicles). If this were the case, then provision of bio-available iron to the cytoplasm ought to bypass the need for Htt, and thereby rescue the hypochromic phenotype of Htt-deficient embryos.

A 'targeted rescue' experiment was therefore performed, based on a technique used to rescue the hypochromic phenotype of *chianti* zebrafish. In *chianti* mutants, hypochromia is caused by a mutation in the gene encoding the blood specific isoform of the TfR1 gene, *tfr1a*, resulting in the inability of blood cells to absorb iron (as Tf) from the plasma (238). Hb production is restored in these embryos by injection of iron-dextran into the cytoplasm at the 1-cell stage such that all cells of the developing *chianti* embryos contain bio-available iron in the cytoplasm, hence circumventing the need for *trf1a* function (238).

To test whether provision of bio-available iron to the cytoplasm would restore Hb production in Htt-deficient embryos, iron-dextran was co-injected with 8.5 ng of *hd*MO1 at the 1-cell stage. Uninjected control embryos, *hd*MO-injected embryos, and embryos co-injected with *hd*MO1 and 100 ng iron-dextran were stained with *o*-dianisidine at 33 hpf (Fig. 5.6 A-F) and were scored with regards to Hb production and yolk extension (YE) status (Fig. 5.6 G, Experiment 1). All wildtype embryos (n = 20/20) had a normal YE and exhibited robust Hb staining. The number of embryos with normal Hb levels was reduced to 14% ($n_{(0+3)}$= 3/22) in *hd*MO1-injected embryos, and co-injection of iron-dextran rescued to 62% ($n_{(11+2)}$= 13/21) (bracketed numbers indicate the quadrants added (see Fig 5.6 G) to achieve the n value, which is shown as a fraction of the total). Interestingly, iron supplementation also rescued the YE phenotype from 5% normal YE in morphants ($n_{(0+1)}$= 1/22) to 71% normal YE ($n_{(11+4)}$= 15/21) in the rescue group (Fig. 5.6 F).

Similar results were achieved in a second rescue experiment (Fig. 5.6 G, Experiment 2), this time using greater population numbers, and using *mc*MO1-injected embryos as the control group. The MO dose was 8.5 ng as in the previous experiment,

however the dose of iron-dextran used for the rescue was halved (50 ng). All control embryos (*mc*MO1-injected) had a normal YE and robust Hb staining (n = 47/47). The number of embryos with normal Hb levels was reduced to 20% ($n_{(2+8)}$= 10/49) in *hd*MO1-injected embryos, and co-injection of iron-dextran rescued to 66% ($n_{(19+10)}$= 29/44). Only 6% of *hd*MO1-injected embryos had a normal YE ($n_{(2+1)}$= 3/49), and iron supplementation was able to increase the number of embryos with a normal YE to 48% in the rescue group ($n_{(19+2)}$= 21/44). These results support the hypothesis that Htt is required to render intracellular iron available for cellular utilisation.

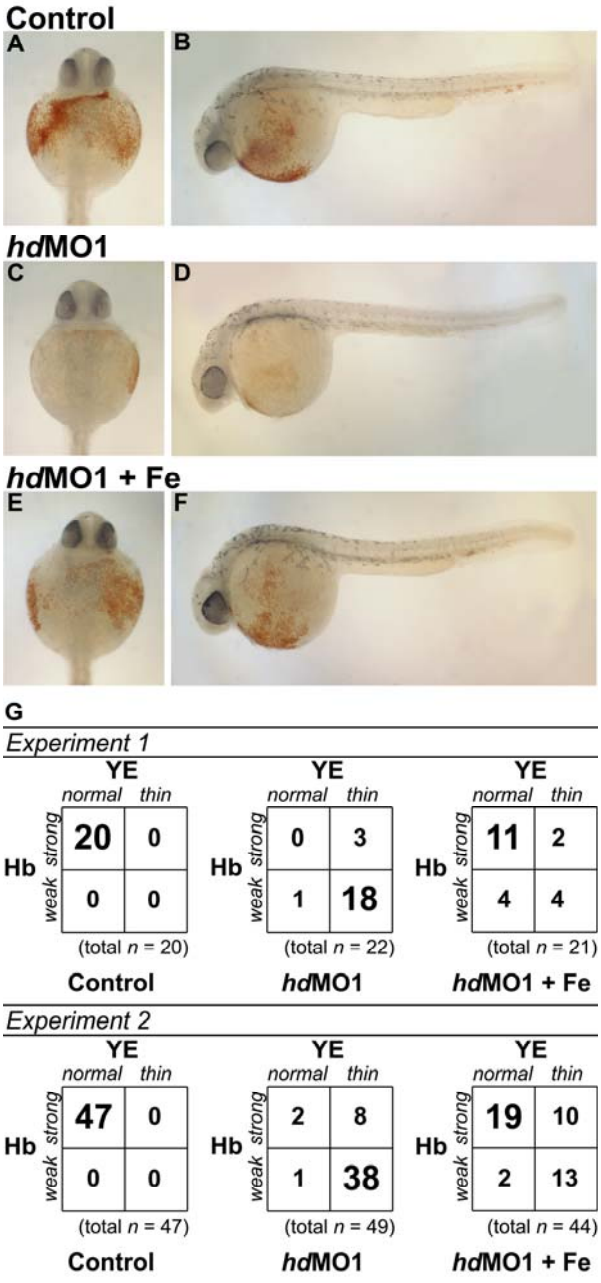

Figure 5.6 Provision of iron to the cytoplasm rescues hypochromia and reduced yolk extension phenotypes in Htt-deficient embryos. Detection of Hb (by *o*-dianisidine) in 33 hpf embryos that were either uninjected (control) (**A**, lateral; **B**, ventral), injected with 8.5 ng of *hd*MO1 (knockdown) (**C**, **D**) or both *hd*MO1 and iron-dextran (Fe; rescue) (**E**, **F**). Representative embryos are shown. The thin yolk extension (YE) of Htt-deficient embryos (**D**) is restored to normal size in iron-supplemented embryos (**F**). (**G**), Raw data from iron rescue experiments. In both experiments, *hd*MO1 dose was 8.5 ng. In **Experiment 1**, control embryos were uninjected; and 100 ng of iron-dextran was co-injected with *hd*MO1 in the rescue group. In **Experiment 2**, control embryos were injected with 8.5 ng of *mc*MO1, and 50 ng of iron-dextran was co-injected with *hd*MO1 in the rescue group.

Morpholino effectiveness is not diminished by iron-dextran treatment

To ensure that iron-dextran did not decrease *hd*MO1 function, the *hd*(1.2):EGFP reporter construct (used to demonstrate *hd*MO-mediated translation knockdown in Chapter 4) was co-injected with 8.5 ng of either *c*MO, *hd*MO1, or both *hd*MO1 and iron-dextran (200 ng). All *c*MO + *hd*(1.2):EGFP embryos exhibited mosaic EGFP expression at 10 hpf (*n* = 29/29). No fluorescence was observed in either the *hd*MO1 + *hd*(1.2):EGFP embryos (*n* = 0/20) or *hd*MO1 + *hd*(1.2):EGFP + iron-dextran embryos (0/18), indicating that the ability of *hd*MO1 to bind the *hd* target sequence and prevent translation was not inhibited by the presence of iron-dextran (not illustrated).

Htt-deficiency leads to an increase in TfR1 mRNAs

The results presented so far suggest that although iron is detected within the blood cells of Htt-deficient embryos, this iron is unavailable for cellular use, hence the decrease in Hb production. To further validate this model, quantitative PCR (qPCR) methodology was used to examine the levels of TfR1 mRNA transcripts in Htt-deficient and control embryos. Since cells typically respond to iron starvation by up-regulating expression of TfR1 (251), it was predicted that levels of TfR1 mRNAs would be increased in Htt-deficient embryos. As mentioned earlier in this chapter, two differentially expressed paralogues of the TfR1 gene exist in zebrafish: *tfr1a* (erythroid specific) and *tfr1b* (ubiquitously expressed) (238). Levels of *tfr1a* and *tfr1b* transcripts were both examined in the experiments described here.

This experiment was performed three times. On each occasion, embryos injected with 8.5 ng of *hd*MO1 or *mc*MO1 (mispair control MO), as well as wildtype uninjected control embryos were collected at 33 hpf. Subsequent sample preparation and qPCR were then carried out by S. Dayan, a senior research assistant in the Richards laboratory. Each qPCR reaction was performed in triplicate to take into account any apparatus error or pipetting inaccuracies. Levels of *tfr1a* and *tfr1b* transcripts were normalised to transcript levels of *acta1* (Accession No. NM_131591), a housekeeping gene encoding actin alpha 1. All data values can be found in Appendix B of this thesis. Normalised *tfr1a* and *tfr1b* triplicate values from the three independent experiments are represented graphically in Figure 5.7. One *hd*MO1/*tfr1b* value was considered to be an obvious outlier from the rest of the data (indicated in Fig. 5.7 B, and see Appendix B) and was excluded from further statistical analyses. One *hd*MO1/*acta1* value was omitted for the same reason, prior to calculation of normalised receptor values (see Appendix B).

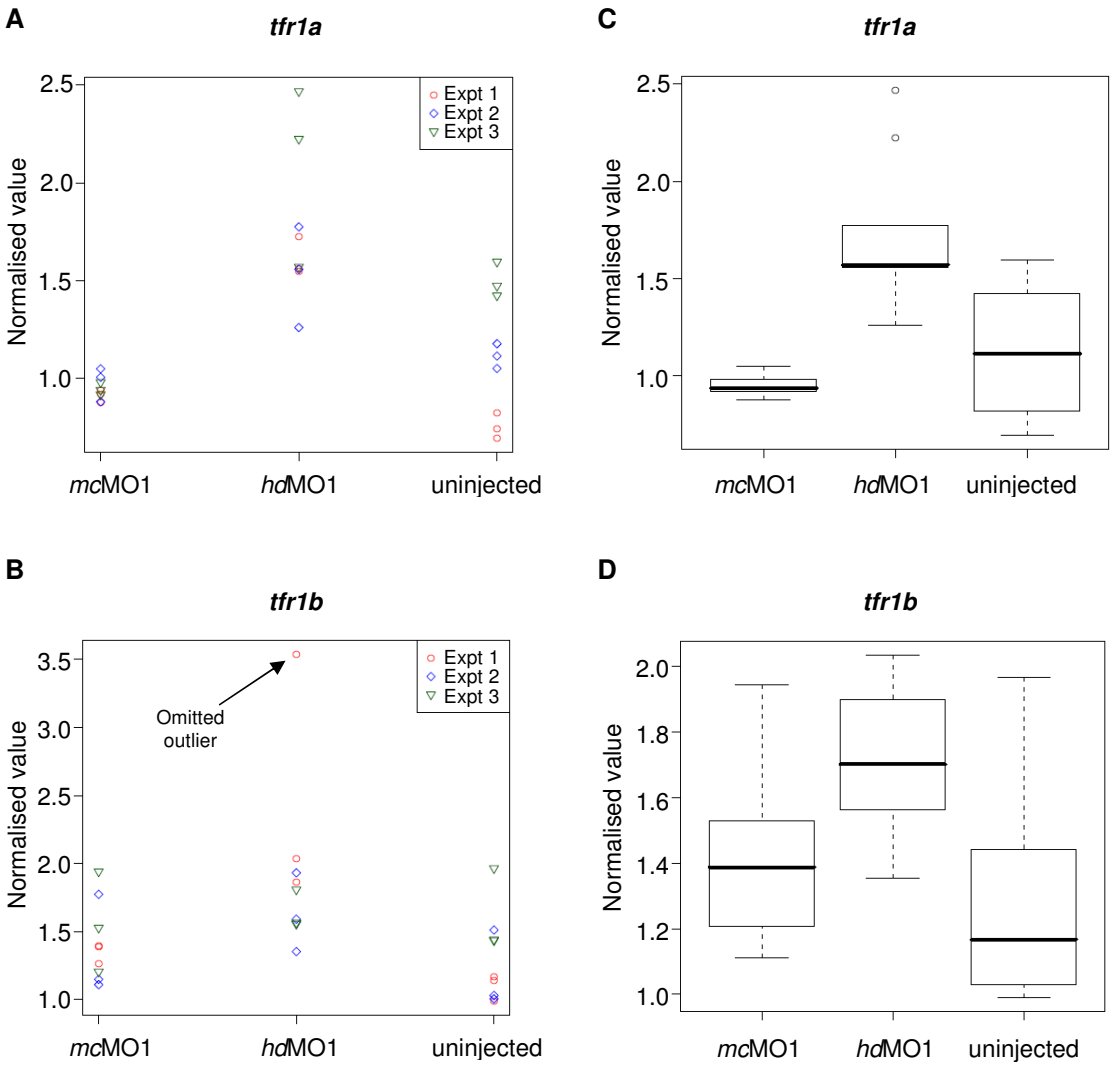

Figure 5.7 Levels of *tfr1a* and *tfr1b* transcripts are increased in response to Htt knockdown. Quantitative PCR was used to compare the levels of *tfr1a* (**A**, **C**) and *tfr1b* (**B**, **D**) transcripts in zebrafish embryos injected with either *mc*MO1 or *hd*MO1, and uninjected embryos. Levels of *tfr1a* and *tfr1b* transcripts were normalised to the level of *acta1* transcript. Normalised triplicate values from three independent experiments are graphically represented for *tfr1a* transcript levels (**A**) and *tfr1b* transcript levels (**B**). A data point that was considered an outlier is indicated (**B**). In (**C** and **D**) the same data shown in (**A** and **B**), excluding the outlier, is represented in box-plot format. The 'box' contains the middle 50% of the data (with the upper and lower edges representing the 75th and 25th percentiles, respectively), the 'horizontal line' within the box represents the median value. The dotted lines, or 'whiskers', indicate minimum and maximum data values for each embryo class, unless data points extend further than 1.5 times the inter-quartile range, in which case these values are represented as individual points, as in (**C**).

Increased levels of TfR1 transcripts were observed in *hd*MO1-treated embryos in each of the experiments. However, there was some variability in the actual values generated from one experiment to the next (Fig. 5.7 A and B). This may be due to slight

inconsistencies in morpholino dose, or age of embryos at collection, for example, although care was taken to keep these variables as constant as possible. Student *t* tests were performed (by S. Pederson) on the collated data to assess the statistical significance of the results. These showed that in *hd*MO1-injected embryos, the level of erythroid specific *tfr1a* transcript was significantly increased in comparison to *mc*MO1-injected ($p<0.0002$) and uninjected ($p<0.002$) embryos. Furthermore, the level of ubiquitous *tfr1b* transcript was also significantly increased in *hd*MO-injected embryos in comparison to *mc*MO1-injected ($p=0.032$) and uninjected ($p<0.008$) embryos.

These results provide strong support for cellular iron starvation in Htt-deficient embryos. Additionally, the increased level of ubiquitously expressed *tfr1b* transcripts in these embryos provides evidence that the role of Htt in intracellular iron compartmentalisation is not limited to erythroid cells.

Discussion

Htt is involved in the intracellular compartmentalisation of iron

One of the primary effects of Htt knockdown in zebrafish embryos is pale, or hypochromic blood. The aim of the work presented in this chapter was to investigate the cause of this hypochromia, in order to gain insight into the normal function of Htt. Characterisation of this phenotype revealed a requirement for Htt in intracellular iron compartmentalisation and/or transport. Production of Hb was decreased in Htt-deficient blood cells despite the presence of iron within these cells, and provision of additional iron in a bio-available form to the cytoplasm restored Hb production (Fig. 5.8). This indicates that the intracellular iron present in Htt-deficient blood cells is unavailable for cellular use. The increased level of erythroid-specific *tfr1a* transcript observed in Htt-deficient embryos supports this model by suggesting that the availability of iron within the blood cells is compromised.

Since erythroid cells acquire iron solely via TfR-mediated endocytosis (238), these findings suggest a role for Htt in the release of iron from endocytic compartments. The majority of cell types (at least in vertebrates) acquire iron via the Tf/TfR endocytic pathway. Since Htt is ubiquitously expressed, it is likely that the role of Htt in this pathway is applicable to all cells that acquire iron in this manner. The finding that the ubiquitous *tfr1b* transcript is up-regulated in response to Htt knockdown supports this. Furthermore, provision of bio-available iron was able to rescue the thin yolk extension

phenotype, a phenotype not normally associated with hypochromic blood, but rather with global cellular dysfunction.

Another finding was that Htt-deficient embryos often appeared to have exhausted their maternally derived yolk iron stores (Fig. 5.5 B). Given the indications of cellular iron starvation in these embryos (such as decreased Hb production and increased TfR1 transcripts), it is likely that the depleted iron stores are a response to embryonic iron starvation. The results of this study suggest that Htt-deficiency disrupts cellular iron acquisition downstream of TfR-mediated endocytosis, leading to cellular iron deficiency, and the accumulation of unavailable iron.

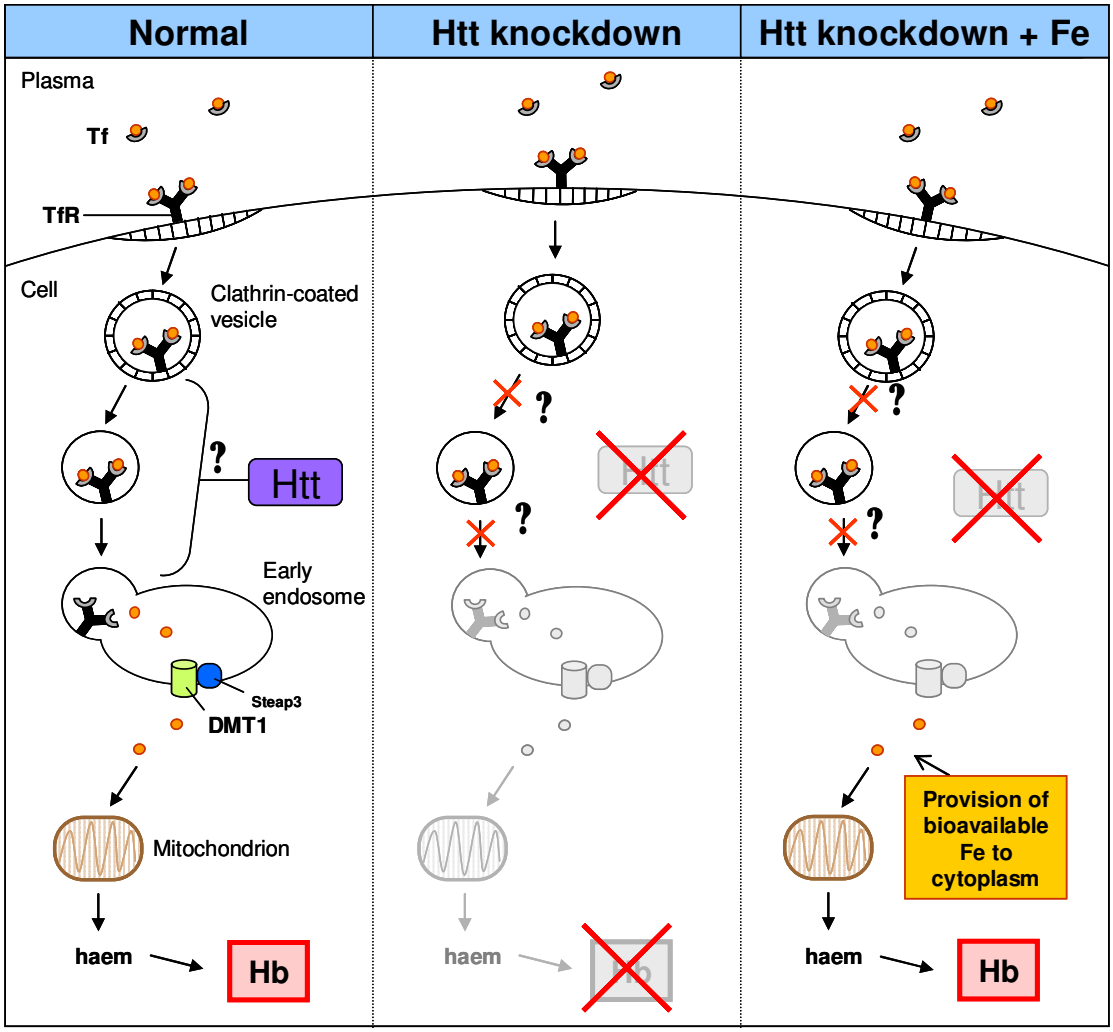

Figure 5.8 Schematic model illustrating how disruption of Hb production in Htt-deficient zebrafish blood cells is rescued by provision of bio-available iron (iron-dextran) to the cytoplasm. In the absence of Htt, iron endocytosed by the Tf/TfR pathway is not available for utilisation in Hb. Supplementing the cytoplasm with bio-available iron (iron-dextran) restored Hb production, suggesting a role for Htt in the release of iron from endocytic compartments.

What is the role of Htt in iron transport/compartmentalisation?

According to the current model of cellular TfR cycling (251, 252), binding of iron-loaded Tf to TfR on the plasma membrane initiates clathrin-mediated internalisation of the Tf/TfR complex into early endocytic vesicles. These vesicles rapidly lose their clathrin coat and are transported towards the perinuclear recycling compartment (PNRC), fusing with early endosomes along the way. The decreased internal pH of the early endosome disassociates iron from apo-Tf/TfR, facilitating its release into the cytoplasm for cellular utilisation. Once this has occurred, iron-free apo-Tf/TfR complexes are able to be redirected from the PNRC back to the cell membrane for re-use (Fig. 5.2).

As previously mentioned, erythroid cells acquire iron for Hb production solely by TfR-mediated endocytosis (238). Therefore, a likely explanation for intracellular iron not being available for Hb production in Htt-deficient cells is that this iron has not been released from endocytic vesicles, suggesting a role for Htt in the targeting/transport/fusion of iron-containing endocytic vesicles to early endosomes.

Further studies are required in order to elucidate the exact role of Htt in the Tf/TfR recycling pathway but known interactions and properties of Htt support a role for Htt in vesicle/endosome dynamics. Htt associates with clathrin-coated and non-coated vesicles, and endosomes (9, 127, 128, 135, 136, 177), and co-fractionates with TfR in density gradient studies (9, 136). Many proteins that interact with Htt are involved in clathrin-mediated endocytosis, such as HIP1 (178, 179), α-adaptin C (166), SH3GL3 (186), PACSIN1 (184) and HIP14 (181) and Htt also interacts with the plasma membrane directly, via a lipid-binding domain located within the N-terminus (137).

Previously, in a survey for differences in intracellular organelle distribution between wildtype and *Hdh*$^{-/-}$ mouse embryonic stem (ES) cells, Hilditch-Maguire and colleagues (2000) observed a disrupted distribution of TfR-positive recycling endosomes in the absence of Htt (139). More specifically, TfR immunostaining revealed a reduction of recycling endosomes in the PNRC, and a vast increase in signal throughout the cytoplasm in *Hdh*$^{-/-}$ cells. The authors also showed that when stimulated to take up FITC-labelled Tf by treatment with the iron chelator deferoxamine mesylate (DM), *Hdh*$^{-/-}$ cells endocytosed FITC-Tf into early endosomes but only weak signal was observed in the perinuclear region in comparison to wildtype cells. These findings indicate that Htt is not required for the cellular uptake of Tf/TfR into endocytic vesicles (consistent with the current findings), and also suggest that subsequent Tf/TfR trafficking from early endocytic vesicles to the PNRC is perturbed in the absence of Htt. Transport of Tf/TfR to the PNRC is microtubule-dependent, since the microtubule

disrupting agent nocodazole decreases this transport (272, 273) and leads to dispersion of the PNRC throughout the cytoplasm (274).

Htt associates with microtubules (126, 128, 134) and is also concentrated in the perinuclear region of cells (126, 127). These findings are consistent with Htt having a role in the microtubule-dependent transport of vesicles and endosomes through the recycling pathway. Furthermore, Htt has been implicated in microtubule-mediated vesicle transport due to an interaction of Htt with dynactin subunit $p150^{Glued}$, via HAP1 (275, 276). Both HAP1 and Htt are transported in neurons (135). A role for Htt in vesicle transport is also supported by findings that over-expression of wildtype Htt enhances microtubule-mediated trafficking of vesicles containing brain-derived neurotrophic factor (BDNF; (277)) and RNAi knockdown of *Drosophila* Htt reportedly disrupts axonal vesicle trafficking in *Drosophila* (278).

Recently Htt has been shown to interact with the small GTPase Rab5 on early endosomes, via Htt binding partner, HAP40 (177). This is an interesting finding since Rab5 is a key regulator of the targeting and fusion of endocytic vesicles to early endosomes, and the attachment of endosomes to, and transport along microtubules (279), thus supporting a role for Htt in these processes. However, the Htt/HAP40/Rab5 interaction appears to negatively regulate the attachment of endosomes to, and transport along microtubules, by favouring the attachment of endosomes to actin rather than microtubules (177). The significance of the Htt/HAP40/Rab5 interaction in terms of endocytic vesicle-endosome fusion and iron release is unclear.

Htt is a large protein containing multiple HEAT motifs and has been proposed to act as a scaffold structure facilitating multiple interactions (106). Based on current knowledge of Htt function and the findings presented in this study, it appears likely that Htt plays an integral role in the progressive transport of Tf/TfR cargo through early endocytic, early endosomal, and recycling compartments.

How do the current findings compare to previous implications of Htt in iron transport and homeostasis?

A link between Htt function and iron homeostasis was previously demonstrated by Hilditch-Maguire and colleagues (139). In addition to their findings of disrupted Tf/TfR distribution in $Hdh^{-/-}$ ES cells as discussed above, the authors also showed using immunoblot analyses, that in response to iron starvation, wildtype ES cells up-regulated Htt levels ~4.5 fold above the level observed in untreated cells. This is consistent with the current proposal that Htt is required for cellular iron acquisition.

In the same study, Hilditch-Maguire *et al* (2000) also showed that TfR protein levels were elevated in *Hdh*$^{-/-}$ ES cells in comparison to wildtype cells (139), which is consistent with the increases in *trf1a* and *tfr1b* transcripts observed in Htt-deficient zebrafish embryos, presented in this chapter. The authors showed that the level of TfR protein was increased ~4.2 fold in *Hdh*$^{-/-}$ ES cells with respect to wildtype levels and this was comparable to the increase in TfR expression that wildtype ES cells exhibited in response to iron starvation (~3.9 fold) (139). Their findings are consistent with a model whereby Htt deficiency causes a shortage of bio-available iron in the cytoplasmic iron pool, as suggested by the results of the current study, presented in this chapter.

In another study, Dragatsis and colleagues (1998) showed that in *Hdh*$^{-/-}$ mouse embryos, transport of iron from the maternally derived extraembryonic tissue into the epiblast was disrupted at the level of the nutritive visceral endoderm (114). The normal function of the visceral endoderm is to take up maternal proteins and other nutrients from extraembryonic tissue (by endocytosis), and digest them in lysosomes to provide nutrition to the developing embryo. In *Hdh*$^{-/-}$ embryos, ferric iron was taken up into the visceral endodermal cells (at embryonic day E7.5), but subsequent transport of iron into the epiblast was disrupted, and at E8.5 the iron detected in the visceral endoderm appeared be concentrated in "small vesicles or granules" in comparison to the cytoplasmic distribution in wildtype embryos (114). Whilst this finding tends to support the current proposal that Htt is required for the release of iron from endocytic vesicles, caution needs to be taken in this interpretation since the mechanism of iron uptake in this tissue is not fully understood and appears to differ from the typical TfR recycling pathway of other cell types; ferric iron bound to maternal Tf is endocytosed by visceral endodermal cells, but apparently in a non-TfR-mediated manner, since this receptor is not expressed by the visceral endoderm (280). The mechanism of iron release is unclear, but rather than being recycled, maternal Tf appears to be degraded in lysosomes (281). It is likely that iron is then presented to the embryo bound to Tf since Tf is synthesised endogenously in the visceral endoderm (282), and TfR is expressed by the receiving embryonic tissues (280).

The findings presented in this thesis (using the zebrafish model organism) both validate and complement these previous findings of others, and extend the understanding of Htt's role in the iron pathway. It is also interesting to note that Htt-deficient zebrafish embryos share phenotypic features with embryos that lack either of the two differentially expressed isoforms of TfR1; whilst genetic mutation of the blood-specific *tfr1a* gene causes blood hypochromia in *chianti* mutants, morpholino knockdown of the ubiquitously expressed isoform (*tfr1b*) results in small head and eyes,

brain necrosis and thin YE (238) indicating that all of these phenotypic features of Htt-deficient embryos can result from cellular iron starvation.

Conclusion

Iron is essential for cellular function, acting as a vital cofactor for numerous proteins and enzymes, many of which play pivotal roles in energy metabolism. The results of this study show that knockdown of Htt leads to cellular iron deficiency, and an accumulation of intracellular iron in a form that is unavailable for cellular use. Disrupted iron homeostasis and decreased energy metabolism are features of HD pathogenesis, and correlate well to the major sites of degeneration in the HD brain, however, the cause of these defects has not yet been established. The experimental results presented here raise the possibility that perturbation of normal Htt function (by polyglutamine expansion) may contribute to these defects, therefore providing an intriguing and novel link between Htt function and specificity of neuronal vulnerability in HD. This will be discussed further in the final chapter.

Chapter 6: Final discussion

Introduction

Thirteen years have passed since the underlying genetic cause of Huntington's disease (HD) was determined to be the expansion of a CAG trinucleotide repeat within the coding region of exon 1 of the *HD* (or *IT15*) gene (2). This genetic abnormality results in an extended polyglutamine tract within the N-terminus of the encoded protein, Huntingtin. HD is one of nine neurodegenerative diseases caused by expansion of CAG repeats encoding polyglutamine in their respective, otherwise apparently unrelated proteins. However, the mechanism(s) by which polyglutamine expansion leads to pathogenesis in these so-called 'polyglutamine diseases' has remained elusive.

The two most pressing questions regarding these diseases are 1) why, despite the affected proteins having widespread patterns of endogenous expression, only a particular subset of neurons is most prone to degeneration while other neuronal cell types also expressing the mutant protein are less affected or relatively spared; and 2) why although the disease proteins have overlapping patterns of expression the subset of neurons most susceptible to degeneration is different in each disease. Insight into what determines the unique specificities of neuronal vulnerability is likely to increase our understanding of the pathogenic mechanism(s) at play in these diseases.

In HD, although the expanded Htt allele (like wildtype Htt) is expressed throughout the brain, neuropathology is most striking in the striatum, where medium spiny γ-aminobutyric acid (GABA)-utilising neurons that project to the substantia nigra and globus pallidus are gradually, and selectively, lost. Neurons in the deeper layers of the cerebral cortex are also particularly vulnerable. The aims of this work were to investigate two factors hypothesised to contribute to the specificity of HD neurodegeneration; region-specific somatic expansion of the CAG repeat, and disruption of normal Htt function.

Investigation of the contribution of somatic instability to HD pathogenesis

In brain samples from human HD patients and a knock-in mouse model of HD, somatic instability of the disease allele has been observed specifically in the striatum (15, 197), leading to the hypothesis that somatic expansion may play a role in HD pathogenesis. The first part of this work was aimed at directly addressing the question of whether somatic instability contributes to the age of onset and/or disease severity in

HD by developing transgenic zebrafish lines expressing CAG repeats with and without stabilising CAA interruptions (Chapter 3).

The expression pattern of the zebrafish *hd* gene was determined using mRNA *in situ* hybridisation. Maternally deposited transcript was detected at the 1-cell stage and after the onset of zygotic expression, transcript was detected uniformly during early development, and ubiquitously (but most highly in the brain) in later developmental stages. A 1.2 kb fragment of DNA sequence upstream of the *hd* ORF was found to be sufficient to drive maternal expression and ubiquitous zygotic expression of a reporter (EGFP) in transgenic zebrafish embryos, and was deemed suitable for driving expression of the repeat transgenes. Pure (CAG) and mixed (CAG/CAA) repeats encoding ~100 glutamine residues were incorporated into the ORF of *hd* exon 1, and these fragments were linked to the *EGFP* coding sequence, either bi-cistronically, or so to encode a fusion protein. Whilst limited EGFP expression was produced by the bi-cistronic constructs in mosaic founders, successful and persistent EGFP fluorescence was seen in mosaics expressing the fusion constructs.

This work was not seen to completion, largely due to new published data that cast doubt on the somatic instability hypothesis (206, 207). However, the fusion construct containing a pure expanded CAG repeat, *hd*(1.2):ex1$(CAG)_{95}$EGFP, will be useful in future studies, for generating a transgenic zebrafish model of HD in which an expanded N-terminal fragment of zebrafish Htt (with a C-terminal EGFP tag), is expressed under the control of the zebrafish *hd* promoter sequence.

An additional outcome of this work was the identification of putative binding sites for two transcription factors (TGIF and COMP1) that are conserved in the *HD* promoter in human, rat, mouse, zebrafish and pufferfish. If these are indeed true binding sites, increased understanding of the gene responses regulated by these factors may offer further insight into the biological role and transcriptional regulation of Htt.

Investigation into the normal function of Htt in development

The proteins affected in polyglutamine diseases have widespread and overlapping patterns of expression, yet different neuronal subsets are most vulnerable in each disease. It is therefore likely that unique aspects of each of these proteins (outside the polyglutamine tract) contribute to this specificity. The second aim of this study was to use the zebrafish model organism to investigate the effects of Htt deficiency in early development, to look for novel insights into Htt function that might offer clues as to the specificity of neuronal vulnerability in HD.

Transient knockdown of Htt using specifically targeted antisense morpholino oligonucleotides (MOs) led to a wide variety of developmental defects (Chapter 4). Many of these were found to be common amongst zebrafish strains with mutations in housekeeping genes (such as small head and eyes, thin yolk extension, disrupted melanophore alignment, pericardial oedema and failed swim bladder inflation), suggesting that they result from general cellular dysfunction. Htt-deficient embryos also frequently exhibited increased apoptosis, consistent with previous findings in *Hdh* knockout mice (110). Most significantly, Htt-deficient zebrafish had hypochromic blood, a phenotype common to zebrafish strains with defects in haemoglobin (Hb) production (236, 237).

Further characterisation of this phenotype revealed a requirement for Htt in rendering intracellular iron available for cellular utilisation (Chapter 5). More specifically, production of haemoglobin (Hb) was decreased in blood cells of Htt-deficient embryos, despite the presence of intracellular iron, and provision of additional iron in a bio-available form to the cytoplasm restored Hb production. Since erythroid cells acquire iron solely via TfR-mediated endocytosis (238), these findings suggest a role for Htt in the release of iron from endocytic compartments. As a further validation of this proposal, the level of erythroid-specific TfR1 mRNA transcript (*tfr1a*) was found to be increased in Htt-deficient embryos as would be predicted if the availability of iron within these cells were compromised.

The role of Htt in the Tf/TfR cycle is potentially applicable to all cells that acquire iron via this pathway (which is the majority of cell types, including neurons), consistent with the ubiquitous expression pattern of Htt. In support of this, Htt knockdown was found to lead to an increased level of the ubiquitous TfR1 transcript (*tfr1b*). Furthermore, provision of bio-available iron also rescued the thin yolk extension phenotype, a phenotype that is symptomatic of global cellular dysfunction. A further indication of iron starvation in Htt-deficient embryos was the finding that maternal iron stores in the yolk appeared to be exhausted in these embryos.

Iron is essential for cellular function, acting as a co-factor for numerous proteins and enzymes, many of which play key roles in energy metabolism. Since defects in energy metabolism and iron homeostasis are characteristics of HD pathology that correlate well to sites of neurodegeneration, the findings of the current study therefore offer a plausible link between perturbation of normal Htt function, and the specificity of HD neurodegeneration.

Activities of iron-requiring proteins/enzymes are decreased in HD

There are several aspects of HD pathogenesis that could be attributed to iron deprivation. Activity of the citrate cycle enzyme, aconitase, is dramatically reduced in HD-affected brain regions with levels as low as 8% in the caudate, 27% in the putamen, and 52% in the cerebral cortex (46). The activities of mitochondrial (m-) and cytosolic (c-) aconitase are regulated by iron levels. Firstly, both are iron-sulfur cluster (ISC)-requiring proteins, and secondly, in conditions of low iron availability, c-aconitase disassembles its ISC and becomes active as iron responsive protein, IRP1, which binds to, and inhibits translation of m-aconitase mRNA (See Fig. 5.2, in the previous chapter). In support of the hypothesis that decreased iron availability could be responsible for the reduction of aconitase activity, iron-deprivation has been shown to cause a striking reduction in the activity of both m- and c-aconitases in rats fed an iron-deficient diet (283).

In addition to aconitase, decreased activities of mitochondrial respiratory chain complexes II, III and IV have also been observed selectively in HD-affected brain regions (46-48) and decreased complex I activity has been recorded in muscle from HD patients (284). Each of these complexes (I-IV) contain subunits that require iron for their function; complex I (NADH dehydrogenase), complex II (succinate dehydrogenase), and complex III (cytochrome c reductase) require the assembly of ISCs, and complexes II, III and IV (cytochrome c oxidase) utilise haem (266).

Levels of serum ferritin are also decreased in HD patients (243, 244). This is a common indication of iron deficiency reflecting a reduction in body iron stores (285). Additionally, decreased Hb levels have been observed in male HD patients (243).

Defects in energy metabolism in HD could be explained by decreased activity of iron-requiring proteins and enzymes

Many findings are suggestive of decreased aerobic respiration in HD. These include elevated production of lactate in the basal ganglia and occipital cortex (50, 51), increased lactate/pyruvate ratio in cerebrospinal fluid (286), decreased oxygen consumption in the striatum (49) and diminished oxidative ATP synthesis in the skeletal muscle of HD patients and pre-symptomatic mutation carriers (287, 288). Additionally, energy production (ATP:ADP ratio) is decreased in lymphoblastoid cell lines derived from human HD patients, and is inversely correlated to repeat length (289).

These energetic defects could be explained by a reduction of iron availability. Aconitase is a catalytic enzyme required in the citrate cycle, and mitochondrial

complexes are involved in electron transport/respiration. The citrate cycle and electron transport chain are the major components of the oxidative respiration process. Since aconitase and complexes I-IV require iron for their function, decreased iron availability is therefore likely to lead to a decrease in oxidative respiration.

Interestingly, similar energetic defects to the ones described in HD have been observed in human cells (K-562, erythroid derived) subjected to iron deprivation, including diminished activities of aconitase and succinate dehydrogenase (complex II), decreased mitochondrial oxygen consumption and raised lactate production (290). Additionally, these iron-deprived cells showed an increase in glycolysis (290) presumably to compensate for the decrease in oxidative respiration. Similarly, studies using various HD mouse models have revealed significant elevations in glucose utilisation throughout the forebrain prior to pathological changes or symptoms, in a manner dependent on polyglutamine repeat length and gene dosage (52, 291, 292). In contrast (although there is one report of raised cortical glucose metabolism in pre-symptomatic HD gene-carriers (293)), most human studies have reported decreased glucose metabolism in the basal ganglia and cerebral cortex of symptomatic HD patients (294, 295) and asymptomatic at-risk HD subjects (43-45). However, one of the mouse models (*Hdh*^{Q111} knock-in) that had elevated glucose utilisation in pre-symptomatic stages was also examined at a later stage when signs of neuropathology were evident. In these older mice, a decrease in glucose utilisation was observed specifically in the striatum, suggesting that earlier examination of human HD subjects may also reveal an increase in glucose metabolism (52). The findings from the mouse studies are consistent with a model whereby an early increase in glucose utilisation is a widespread cellular response to an impairment of normal Htt function, and the decreased utilisation in the striatum in later stages of disease is due to specific cellular dysfunction (as suggested in (52)).

Altered iron distribution in the HD brain and in other neurodegenerative disorders

Another sign of disturbed iron homeostasis in HD is the altered distribution of iron in the HD brain. A number of studies have reported abnormal accumulation of iron specifically in the striatum of post-mortem HD brain samples (60-62). Furthermore, quantitative studies of ferritin iron in live HD subjects have revealed significantly more iron within ferritin in the caudate, putamen and globus pallidus of HD patients (in comparison to healthy controls) even in early symptomatic stages of disease (63, 64). Due to the ability of iron to catalyse free radical reactions, it is thought likely that the

accumulation of iron may contribute to the oxidative damage that is evident in HD-affected brain regions (63).

It seems almost paradoxical that the affected region of the HD brain exhibits signs of both iron deficiency (as described earlier) and iron accumulation. However, within the striatum and frontal cortex of the HD brain, ferric iron (Fe^{3+}) and ferritin appear to accumulate in microglial cells, rather than in neurons themselves (Simmons *et al*, 2006, unpublished observations, cited with permission). It may be possible that iron accumulates in the microglia in response to neuronal iron deficiency caused by perturbation of Htt's normal role in the Tf/TfR pathway. Further understanding of brain iron homeostasis and the role of the microglia in this balance may offer an explanation for this phenomenon.

HD is one of a growing list of neurodegenerative disorders associated with iron accumulation in the respective regions of pathology. Others include neuroferritinopathy, Friedreich's ataxia, neurodegeneration with brain iron accumulation (NBIA; formerly Hallervorden-Spatz syndrome), Parkinson's disease and Alzheimer's disease (65). Neuroferritinopathy and Friedreich's ataxia are examples of monogenic diseases in which the affected protein has a known role in iron homeostasis.

Neuroferritinopathy is a rare, adult-onset neurodegenerative disorder that presents similarly to HD but is caused by dominant negative mutations in ferritin L, one of the two ferritin subunits (296, 297). These mutations appear to affect protein folding and stability of ferritin, although the mechanism by which these mutations lead to disease is unclear (298). Like HD, neuroferritinopathy is associated with low serum ferritin levels, accumulation of iron and ferritin in the basal ganglia, oxidative stress and signs of mitochondrial dysfunction (297).

Friedreich's ataxia is a relatively common autosomal recessive neurodegenerative disorder (affecting spinal cord and peripheral neurons) that is associated with mitochondrial accumulation of iron and oxidative stress (299). Friedreich's ataxia is caused by the expansion of a GAA trinucleotide repeat (within the first intron of the *FRDA* gene) that impairs transcription, leading to reduced expression of frataxin protein. Frataxin is a mitochondrial protein involved in ISC formation and accordingly, reduced activities of ISC enzymes (respiratory complexes I, II and III, and aconitase) have been observed in affected patient tissues (300). Furthermore, the lack of frataxin (and therefore ISCs) appears to cause c-aconitase to revert to its IRE-binding form as IRP1, as suggested by decreased c-aconitase activity and increased IRP1-IRE binding in affected tissue from a mouse model of Friedreich's ataxia (301). This shift is

likely to be responsible for modulated expression of IRP-regulated proteins, such as the increased TfR levels observed in human patients (302).

Further advancements in understanding of the sequence of events leading to pathology in these and other iron-related neurodegenerative disorders, may offer insight into HD pathology, and vice versa.

How could perturbation of Htt function contribute to dominant, iron-related phenotypes in HD?

HD is not caused by a total loss of function of the affected allele, since mice in which one *Hdh* allele is completely inactivated (*Hdh*$^{+/-}$), and a human subject with a translocation interrupting one normal *HD* allele, do not develop HD symptoms (3, 110, 111). Furthermore, HD patients that are homozygous for an expanded disease allele do not exhibit the embryonic lethality of *Hdh* knockout mice, but instead survive birth, and develop essentially as normal until the onset of symptoms (117, 118). Therefore, in order for a disruption of Htt function to be responsible for the defects in iron homeostasis observed in HD, the expanded polyglutamine tract would have to alter Htt function in a manner that causes dominant, detrimental consequences in the Tf/TfR pathway. Whilst it is unclear whether the embryonic lethality of *Hdh* knockout (*Hdh*$^{-/-}$) mice is solely attributable to disruption of iron transport, demonstrations that a single allele expressing expanded Htt is functionally sufficient to rescue *Hdh*$^{-/-}$ mice from embryonic lethality (91, 123, 125) suggest that the polyglutamine expansion allows expanded Htt to retain at least some of its normal function, presumably including its role in the iron pathway.

The expanded polyglutamine tract could disrupt the Tf/TfR pathway by altering the affinities of Htt for its normal binding partners, and/or by facilitating novel interactions that have detrimental consequences on the Tf/TfR pathway. The interactions of Htt with many binding partners involved in endocytic and vesicle trafficking pathways are modulated by polyglutamine expansion. For example, interactions of Htt with endocytic proteins HIP1 (178) and α-adaptin-C (166) are decreased by polyglutamine expansion, and the interaction of Htt with vesicle trafficking protein HAP1 is increased (176). Furthermore, the association of Htt with microtubules via HAP1 and p150^{Glued} is reduced in the presence of expanded Htt (277), as is the efficiency of vesicle trafficking (29, 177, 277, 278, 303). Additionally, HAP40 is up-regulated in HD, leading to striking co-localisation of Htt, HAP40 and Rab5 on early endosomes, an interaction that favours the binding of endosomes to actin rather than

microtubules (177). Based on the evidence for interrupted vesicle transport in the presence of expanded Htt, it is appealing to speculate that the transport of iron-containing vesicles to acidic endosomes for iron release could be perturbed in HD.

Support for the possibility that Htt's role in the iron pathway is altered in HD is provided by the results of a study by Trettel and co-workers (2000) in which the levels and distribution of TfR in cultured striatal cell lines (ST*Hdh*$^{Q111/Q111}$ and ST*Hdh*$^{Q111/Q7}$) established from a knock-in mouse model of HD (304) were examined (305). Increased TfR levels were observed in ST*Hdh*$^{Q111/Q111}$ and ST*Hdh*$^{Q111/Q7}$ cell lines in comparison to wildtype ST*Hdh*$^{Q7/Q7}$ cells, suggesting that expression of expanded Htt results in an up-regulation of the Tf/TfR pathway in these cells (305). This is consistent with the hypothesis that the normal function of Htt in the iron pathway is perturbed by polyglutamine tract expansion, leading to decreased iron availability. In ST*Hdh*$^{Q111/Q111}$ and ST*Hdh*$^{Q111/Q7}$ cells, TfR signal was increased in the perinuclear recycling compartment (PNRC), in comparison to wildtype cells. Similarly, FITC-Tf accumulated in the PNRC in uptake experiments (305). Since release of iron from Tf/TfR appears to be required for the recycling of Tf/TfR back to the plasma membrane (306, 307), the accumulation of Tf and TfR in the PNRC is also consistent with the hypothesis that iron release is impaired in the presence of expanded Htt. Notably, the fact that increased TfR levels and altered distribution of TfR and Tf were observed in heterozygous ST*Hdh*$^{Q111/Q7}$ cells indicates that perturbation of the Tf/TfR cycle is a dominant effect of expanded Htt (305).

Are expanded N-terminal Htt fragments sufficient to disrupt the TfR pathway?

The widely used R6/2 transgenic mouse model of HD expresses an expanded polyglutamine tract within a severely truncated Htt fragment (encoded by *HD* exon 1) (71). Interestingly, this model recapitulates some of the signs of disrupted energy metabolism and iron homeostasis observed in the human disease. For example, R6/2 mice show decreased activities of iron-requiring enzymes aconitase and mitochondrial complex IV (308), and an early accumulation of ferritin in striatal microglia (D. Simmons, unpublished observations, 2006). This therefore raises the question of whether unique sequence(s) within the N-terminal of Htt are sufficient to recruit the mutant Htt fragment to the Tf/TfR pathway and disrupt iron transport.

Why are iron-related phenotypes particularly evident in the striatum/basal ganglia in HD?

It seems likely that tissues and cells with the greatest iron requirement would be most affected by a decrease in iron availability, since they would be presented with the greatest challenge to maintain cellular iron requirements. The striatum (primarily affected in HD) is part of the basal ganglia, which is the most iron-rich area of the brain (309), suggesting a high iron requirement in this region.

Furthermore, the striatum may be a region of the brain that is particularly vulnerable to decreased energy levels, as suggested by findings that systemic administration of 3-nitroproprionic acid (3-NP; an irreversible inhibitor of succinate dehydrogenase (complex II)) to animals leads to selective striatal degeneration, associated with decreased ATP levels, elevated lactate concentrations, and HD-like motor abnormalities (53).

Conclusion

In this study, the zebrafish model organism has been used to examine the effects of Htt deficiency in early development, in order to gain new insight into the normal function of Htt. The most significant outcome of this work is the finding that Htt knockdown leads to cellular iron deficiency and the accumulation of unavailable iron in the cell. Htt appears to act downstream of TfR-mediated endocytosis of iron, thus implicating Htt in the release of iron from endocytic compartments into the cytosol.

Iron is vital for the function of many cellular proteins and enzymes that play primary roles in energy metabolism. Since defects in iron homeostasis and energy metabolism are features of HD pathogenesis, the results of the current study raise the possibility that these defects are dominant effects of a perturbation (by the expanded polyglutamine tract) of Htt's normal role in the iron pathway. Furthermore, since iron accumulation and defects in energy metabolism are most pronounced in sites of HD neurodegeneration, these findings provide a novel link between perturbation of normal Htt function, and the specificity of neuronal vulnerability in HD.

Appendix A

Biological process or function	Genetic mutations causing thin yolk extension phenotype
Ribosome structure and biogenesis	*laminin receptor 1 (ribosomal protein SA)(lamr1^{hi1479})* *ribosomal protein L6 (rpl6^{hi3655b})* *ribosomal protein L7-like 1 (rpl7l1$^{hi1793)}$* *ribosomal protein L11 (rpl11$^{hi3820b)}$* *ribosomal protein L14 (rpl14^{hi823})* *ribosomal protein L19 (rpl19^{hi1987})* *ribosomal protein L28-like (rpl28l^{hi3893})* *ribosomal protein, large, P1(rplp1^{hi3653b}, rplp1^{hi3988})* *EBNA1 binding protein 2-like (ebna1bp2l^{hi3625a})* *DEAD box polypeptide 27 (ddx27^{hi1086a})* *DEAD box polypeptide 56 (ddx56^{hi3073})* *HEAT repeat containing 1(heatr1^{hi3028}, heatr1^{hi932})*
Replication	*topoisomerase (DNA) II alpha (top2a^{hi3635})* *polymerase (DNA directed), alpha (pola^{hi1146})*
Transcription and RNA processing	*polymerase (RNA) I polypeptide A (polr1a^{hi3639})* *polymerase (RNA) II (DNA directed) polypeptide G-like (polr2gl^{hi3685})* *TWIST neighbour (twistnb^{hi2573a})* *DEAH box polypeptide 16 (dhx16^{hi4049})* *splicing factor 3b, subunit 1(sf3b1^{hi3394a})* *splicing factor 3b, subunit 5* (*sf3b5^{hi2271}*) *poly A binding protein, cytoplasmic 1 a (pabpc1a^{hi3202b})* *pleiotropic regulator 1 (plrg1^{hi1902} , plrg1^{hi3174a})*
Translation	*eukaryotic translation initiation factor 3, subunit 4 delta(eif3s4^{hi3663})* *eukaryotic translation initiation factor 4A, isoform 1A (eif4a1a^{hi2596})*
Cell adhesion	*bystin-like (bysl)*
Cytokinesis	*epithelial cell transforming sequence 2 oncogene* (*ect2^{hi3820}*)
Protein folding	*chaperonin containing TCP1, subunit 3 (cct3^{hi383a} cct3^{h1867})*
Pyrimidine biosynthesis	*carbamoyl-phosphate synthetase 2, aspartate transcarbamylase, and dihydroorotase* (*cad^{hi2694}*)
rRNA processing	*fibrillarin (fbl^{hi2581})*
Ubiquitination	*F-box protein 5 (fbxo5^{hi2648})*
Unknown function	*chromosome 13 open reading frame 22-like (c13orf22l^{hi3662})* *GTP binding protein 4 (gtpbp4^{hi2345})* *mak16-like homolog (mak16l^{hi1055a}, mak16l^{hi3960})* *nucleolar protein 5 (nol5^{hi3118})*

Zebrafish genetic mutant strains that have a thin yolk extension phenotype similar to Htt-deficient embryos, have defects in housekeeping genes. Mutant alleles are shown in brackets. All mutant strains listed here were generated in an insertional mutagenesis screen for genes that are essential for early zebrafish development (310). Phenotypes such as brain necrosis, pericardial oedema, enlargement of melanophores and failure to inflate the swim bladder are also common amongst these mutant strains.

Appendix B

Experiment 1	*acta1*		*tfr1a*		*tfr1b*	
	raw value	average	raw value	normalised	raw value	normalised
*mc*MO1	1.16		1.12	0.936	1.51	1.262
	1.26	1.197	1.05	0.877	1.67	1.396
	1.17		1.10	0.919	1.66	1.387
*hd*MO1	1.24		1.90	1.545	2.29	1.862
	1.22	1.230	1.92	1.561	2.25	2.033
	(2.06)*		2.12	1.724	(4.35)*	-
uninjected	1.11		0.80	0.746	1.26	1.167
	1.07	1.080	0.89	0.820	1.07	0.991
	1.06		0.75	0.694	1.23	1.140

* Bracketed values were omitted from further analyses.

Experiment 2	*acta1*		*tfr1a*		*tfr1b*	
	raw value	average	raw value	normalised	raw value	normalised
*mc*MO1	2.20		1.83	0.880	3.69	1.774
	2.08	2.080	2.09	1.005	2.39	1.149
	1.96		2.18	1.050	2.31	1.111
*hd*MO1	2.32		2.96	1.260	3.18	1.353
	2.35	2.350	4.17	1.774	4.54	1.932
	2.38		3.66	1.557	3.74	1.591
uninjected	1.92		2.42	1.177	2.12	1.031
	1.73	2.057	2.29	1.113	2.07	1.006
	2.52		2.16	1.050	3.11	1.512

Experiment 3	*acta1*		*tfr1a*		*tfr1b*	
	raw value	average	raw value	normalised	raw value	normalised
*mc*MO1	1.81		1.62	0.917	3.43	1.942
	1.85	1.767	1.66	0.934	2.70	1.528
	1.65		1.73	0.979	2.13	1.206
*hd*MO1	2.28		3.48	1.570	3.47	1.565
	2.25	2.217	5.47	2.468	4.01	1.809
	2.12		4.93	2.224	3.45	1.556
uninjected	1.62		2.31	1.423	2.33	1.435
	1.40	1.623	2.39	1.472	2.34	1.441
	1.85		2.59	1.595	3.19	1.965

Quantitative PCR data corresponding to Figure 5.7. Quantitative PCR (performed by S. Dayan) was used to assess levels of *tfr1a* and *tfr1b* transcripts (relative to *acta1* transcript levels) in *hd*MO1-treated, *mc*MO1-treated and uninjected embryos. The experiment was performed on three independent occasions (Experiment 1, 2 and 3). In every experiment, each embryo sample was run in triplicate, to account for pipetting error and/or apparatus variability in plate reading. Raw values presented in the tables above represent arbitrary units of RNA transcript, resulting from using the relative standard curve method for quantification (as set out by Applied Biosciences). Two values (shown in brackets) were considered obvious outliers and were omitted from subsequent statistical analyses. Triplicate values for *acta1* were averaged (excluding the outlier), and each *tfr1a* and *tfr1b* value was then normalised to the average *acta1* value for that particular sample. The normalised values are presented graphically in Chapter 5, Figure 5.7.

References

1. **Myers, R.H., Marans, K.S. and MacDonald, M.E.** (1998) Huntington's Disease. In Wells, R.D. and Warren, S.T. (eds.), *Genetic Instabilities and Hereditary Neurological Diseases*. Academic Press, pp. 301-323.

2. **Huntington's Disease Collaborative Research Group** (1993) A novel gene containing a trinucleotide repeat that is expanded and unstable on Huntington's disease chromosomes. *Cell,* **72,** 971-83.

3. **Ambrose, C.M., Duyao, M.P., Barnes, G., Bates, G.P., Lin, C.S., Srinidhi, J., Baxendale, S., Hummerich, H., Lehrach, H. and Altherr, M.** (1994) Structure and expression of the Huntington's disease gene: evidence against simple inactivation due to an expanded CAG repeat. *Somatic Cell and Molecular Genetics,* **20,** 27-38.

4. **Lin, B., Nasir, J., Kalchman, M.A., McDonald, H., Zeisler, J., Goldberg, Y.P. and Hayden, M.R.** (1995) Structural analysis of the 5' region of mouse and human Huntington disease genes reveals conservation of putative promoter region and di- and trinucleotide polymorphisms. *Genomics,* **25,** 707-15.

5. **Lin, B., Rommens, J.M., Graham, R.K., Kalchman, M., MacDonald, H., Nasir, J., Delaney, A., Goldberg, Y.P. and Hayden, M.R.** (1993) Differential 3' polyadenylation of the Huntington disease gene results in two mRNA species with variable tissue expression. *Human Molecular Genetics,* **2,** 1541-5.

6. **Strong, T.V., Tagle, D.A., Valdes, J.M., Elmer, L.W., Boehm, K., Swaroop, M., Kaatz, K.W., Collins, F.S. and Albin, R.L.** (1993) Widespread expression of the human and rat Huntington's disease gene in brain and nonneural tissues. *Nat Genet,* **5,** 259-65.

7. **Li, S.H., Schilling, G., Young, W.S., 3rd, Li, X.J., Margolis, R.L., Stine, O.C., Wagster, M.V., Abbott, M.H., Franz, M.L., Ranen, N.G. et al.** (1993) Huntington's disease gene (IT15) is widely expressed in human and rat tissues. *Neuron,* **11,** 985-93.

8. **Sharp, A.H., Loev, S.J., Schilling, G., Li, S.H., Li, X.J., Bao, J., Wagster, M.V., Kotzuk, J.A., Steiner, J.P., Lo, A. et al.** (1995) Widespread expression of Huntington's disease gene (IT15) protein product. *Neuron,* **14,** 1065-74.

9. **DiFiglia, M., Sapp, E., Chase, K., Schwarz, C., Meloni, A., Young, C., Martin, E., Vonsattel, J.P., Carraway, R., Reeves, S.A. et al.** (1995) Huntingtin is a cytoplasmic protein associated with vesicles in human and rat brain neurons. *Neuron,* **14,** 1075-81.

10. **Bhide, P.G., Day, M., Sapp, E., Schwarz, C., Sheth, A., Kim, J., Young, A.B., Penney, J., Golden, J., Aronin, N. and DiFiglia, M.** (1996) Expression of normal and mutant huntingtin in the developing brain. *J Neurosci,* **16,** 5523-35.

11. **Gourfinkel-An, I., Cancel, G., Trottier, Y., Devys, D., Tora, L., Lutz, Y., Imbert, G., Saudou, F., Stevanin, G., Agid, Y., Brice, A., Mandel, J.L. and Hirsch, E.C.** (1997) Differential distribution of the normal and mutated forms of huntingtin in the human brain. *Ann Neurol,* **42,** 712-9.

12. **Nance, M.A., Mathias-Hagen, V., Breningstall, G., Wick, M.J. and McGlennen, R.C.** (1999) Analysis of a very large trinucleotide repeat in a patient with juvenile Huntington's disease. *Neurology,* **52,** 392-4.

13. **Rubinsztein, D.C., Leggo, J., Coles, R., Almqvist, E., Biancalana, V., Cassiman, J.J., Chotai, K., Connarty, M., Crauford, D., Curtis, A., Curtis, D., Davidson, M.J., Differ, A.M., Dode, C., Dodge, A., Frontali, M., Ranen, N.G., Stine, O.C., Sherr, M., Abbott, M.H., Franz, M.L., Graham, C.A., Harper, P.S., Hedreen, J.C., Hayden, M.R. et al.** (1996) Phenotypic characterization of individuals with 30-40 CAG repeats in the Huntington disease (HD) gene reveals HD cases with 36 repeats and apparently normal elderly individuals with 36-39 repeats. *Am J Hum Genet,* **59,** 16-22.

14. **Sieradzan, K., Mann, D.M. and Dodge, A.** (1997) Clinical presentation and patterns of regional cerebral atrophy related to the length of trinucleotide repeat expansion in patients with adult onset Huntington's disease. *Neuroscience Letters,* **225,** 45-8.

15. **Telenius, H., Kremer, B., Goldberg, Y.P., Theilmann, J., Andrew, S.E., Zeisler, J., Adam, S., Greenberg, C., Ives, E.J., Clarke, L.A. et al.** (1994) Somatic and gonadal mosaicism of the Huntington disease gene CAG repeat in brain and sperm. *Nat Genet,* **6,** 409-14.

16. **The U.S.-Venezuela Collaborative Research Project and Wexler, N.S.** (2004) Venezuelan kindreds reveal that genetic and environmental factors modulate Huntington's disease age of onset. *Proc Natl Acad Sci U S A.,* **101,** 3498-503.

17. **Vonsattel, J.P., Myers, R.H., Stevens, T.J., Ferrante, R.J., Bird, E.D. and Richardson, E.P., Jr.** (1985) Neuropathological classification of Huntington's disease. *J Neuropathol Exp Neurol,* **44,** 559-77.

18. **Kolb, B. and Whishaw, I.Q.** (1996) *Fundamentals of Human Neuropsychology.* Fourth ed. W. H. Freeman and Company, New York.

19. **Graveland, G.A., Williams, R.S. and DiFiglia, M.** (1985) Evidence for degenerative and regenerative changes in neostriatal spiny neurons in Huntington's disease. *Science,* **227,** 770-3.

20. **Deng, Y.P., Albin, R.L., Penney, J.B., Young, A.B., Anderson, K.D. and Reiner, A.** (2004) Differential loss of striatal projection systems in Huntington's disease: a quantitative immunohistochemical study. *J Chem Neuroanat,* **27,** 143-64.

21. **Reiner, A., Albin, R.L., Anderson, K.D., D'Amato, C.J., Penney, J.B. and Young, A.B.** (1988) Differential loss of striatal projection neurons in Huntington disease. *Proc Natl Acad Sci U S A,* **85,** 5733-7.

22. **Albin, R.L., Qin, Y., Young, A.B., Penney, J.B. and Chesselet, M.F.** (1991) Preproenkephalin messenger RNA-containing neurons in striatum of patients with symptomatic and presymptomatic Huntington's disease: an in situ hybridization study. *Ann Neurol,* **30,** 542-9.

23. **Sapp, E., Ge, P., Aizawa, H., Bird, E., Penney, J., Young, A.B., Vonsattel, J.P. and DiFiglia, M.** (1995) Evidence for a preferential loss of enkephalin immunoreactivity in the external globus pallidus in low grade Huntington's disease using high resolution image analysis. *Neuroscience,* **64,** 397-404.

24. **Richfield, E.K., Maguire-Zeiss, K.A., Vonkeman, H.E. and Voorn, P.** (1995) Preferential loss of preproenkephalin versus preprotachykinin neurons from the striatum of Huntington's disease patients. *Ann Neurol,* **38,** 852-61.

25. **Glass, M., Dragunow, M. and Faull, R.L.** (2000) The pattern of neurodegeneration in Huntington's disease: a comparative study of cannabinoid, dopamine, adenosine and GABA(A) receptor alterations in the human basal ganglia in Huntington's disease. *Neuroscience,* **97,** 505-19.

26. **Richfield, E.K. and Herkenham, M.** (1994) Selective vulnerability in Huntington's disease: preferential loss of cannabinoid receptors in lateral globus pallidus. *Ann Neurol.,* **36,** 577-84.

27. **Young, A.B., Greenamyre, J.T., Hollingsworth, Z., Albin, R., D'Amato, C., Shoulson, I. and Penney, J.B.** (1988) NMDA receptor losses in putamen from patients with Huntington's disease. *Science,* **241,** 981-3.

28. **Albin, R.L., Young, A.B., Penney, J.B., Handelin, B., Balfour, R., Anderson, K.D., Markel, D.S., Tourtellotte, W.W. and Reiner, A.** (1990) Abnormalities of striatal projection neurons and N-methyl-D-aspartate receptors in presymptomatic Huntington's disease. *N Engl J Med.,* **322,** 1293-8.

29. **Trushina, E., Dyer, R.B., Badger, J.D., 2nd, Ure, D., Eide, L., Tran, D.D., Vrieze, B.T., Legendre-Guillemin, V., McPherson, P.S., Mandavilli, B.S., Van Houten, B., Zeitlin, S., McNiven, M., Aebersold, R., Hayden, M., Parisi, J.E., Seeberg, E., Dragatsis, I., Doyle, K., Bender, A., Chacko, C. and McMurray, C.T.** (2004) Mutant huntingtin impairs axonal trafficking in mammalian neurons in vivo and in vitro. *Mol Cell Biol,* **24,** 8195-209.

30. **Ferrante, R.J., Kowall, N.W., Beal, M.F., Martin, J.B., Bird, E.D. and Richardson, E.P., Jr.** (1987) Morphologic and histochemical characteristics of a spared subset of striatal neurons in Huntington's disease. *J Neuropathol Exp Neurol.,* **46,** 12-27.

31. **Rosas, H.D., Liu, A.K., Hersch, S., Glessner, M., Ferrante, R.J., Salat, D.H., van der Kouwe, A., Jenkins, B.G., Dale, A.M. and Fischl, B.** (2002) Regional and progressive thinning of the cortical ribbon in Huntington's disease. *Neurology.,* **58,** 695-701.

32. **Mann, D.M., Oliver, R. and Snowden, J.S.** (1993) The topographic distribution of brain atrophy in Huntington's disease and progressive supranuclear palsy. *Acta Neuropathol (Berl),* **85,** 553-9.

33. **Cudkowicz, M. and Kowall, N.W.** (1990) Degeneration of pyramidal projection neurons in Huntington's disease cortex. *Ann Neurol.,* **27,** 200-4.

34. **Wagster, M.V., Hedreen, J.C., Peyser, C.E., Folstein, S.E. and Ross, C.A.** (1994) Selective loss of [3H]kainic acid and [3H]AMPA binding in layer VI of frontal cortex in Huntington's disease. *Exp Neurol.,* **127,** 70-5.

35. **Sotrel, A., Paskevich, P.A., Kiely, D.K., Bird, E.D., Williams, R.S. and Myers, R.H.** (1991) Morphometric analysis of the prefrontal cortex in Huntington's disease. *Neurology.,* **41,** 1117-23.

36. **Hedreen, J.C., Peyser, C.E., Folstein, S.E. and Ross, C.A.** (1991) Neuronal loss in layers V and VI of cerebral cortex in Huntington's disease. *Neurosci Lett.,* **133,** 257-61.

37. **Heinsen, H., Strik, M., Bauer, M., Luther, K., Ulmar, G., Gangnus, D., Jungkunz, G., Eisenmenger, W. and Gotz, M.** (1994) Cortical and striatal neurone number in Huntington's disease. *Acta Neuropathol (Berl).* **88,** 320-33.

38. **Kremer, H.P., Roos, R.A., Dingjan, G., Marani, E. and Bots, G.T.** (1990) Atrophy of the hypothalamic lateral tuberal nucleus in Huntington's disease. *J Neuropathol Exp Neurol.,* **49,** 371-82.

39. **Byers, R.K., Gilles, F.H. and Fung, C.** (1973) Huntington's disease in children. Neuropathologic study of four cases. *Neurology,* **23,** 561-9.

40. **Jeste, D.V., Barban, L. and Parisi, J.** (1984) Reduced Purkinje cell density in Huntington's disease. *Exp Neurol,* **85,** 78-86.

41. **Rodda, R.A.** (1981) Cerebellar atrophy in Huntington's disease. *J Neurol Sci,* **50,** 147-57.

42. **Spargo, E., Everall, I.P. and Lantos, P.L.** (1993) Neuronal loss in the hippocampus in Huntington's disease: a comparison with HIV infection. *J Neurol Neurosurg Psychiatry,* **56,** 487-91.

43. **Antonini, A., Leenders, K.L., Spiegel, R., Meier, D., Vontobel, P., Weigell-Weber, M., Sanchez-Pernaute, R., de Yebenez, J.G., Boesiger, P., Weindl, A. and Maguire, R.P.** (1996) Striatal glucose metabolism and dopamine D2 receptor binding in asymptomatic gene carriers and patients with Huntington's disease. *Brain.,* **119,** 2085-95.

44. **Grafton, S.T., Mazziotta, J.C., Pahl, J.J., St George-Hyslop, P., Haines, J.L., Gusella, J., Hoffman, J.M., Baxter, L.R. and Phelps, M.E.** (1992) Serial changes of cerebral glucose metabolism and caudate size in persons at risk for Huntington's disease. *Arch Neurol.,* **49,** 1161-7.

45. **Kuwert, T., Lange, H.W., Boecker, H., Titz, H., Herzog, H., Aulich, A., Wang, B.C., Nayak, U. and Feinendegen, L.E.** (1993) Striatal glucose consumption in chorea-free subjects at risk of Huntington's disease. *J Neurol.,* **241,** 31-6.

46. **Tabrizi, S.J., Cleeter, M.W., Xuereb, J., Taanman, J.W., Cooper, J.M. and Schapira, A.H.** (1999) Biochemical abnormalities and excitotoxicity in Huntington's disease brain. *Ann Neurol,* **45,** 25-32.

47. **Gu, M., Gash, M.T., Mann, V.M., Javoy-Agid, F., Cooper, J.M. and Schapira, A.H.** (1996) Mitochondrial defect in Huntington's disease caudate nucleus. *Ann Neurol,* **39,** 385-9.

48. **Browne, S.E., Bowling, A.C., MacGarvey, U., Baik, M.J., Berger, S.C., Muqit, M.M., Bird, E.D. and Beal, M.F.** (1997) Oxidative damage and metabolic dysfunction in Huntington's disease: selective vulnerability of the basal ganglia. *Ann Neurol,* **41,** 646-53.

49. **Butterworth, J., Yates, C.M. and Reynolds, G.P.** (1985) Distribution of phosphate-activated glutaminase, succinic dehydrogenase, pyruvate dehydrogenase and gamma-glutamyl transpeptidase in post-mortem brain from Huntington's disease and agonal cases. *J Neurol Sci.,* **67,** 161-71.

50. **Jenkins, B.G., Koroshetz, W.J., Beal, M.F. and Rosen, B.R.** (1993) Evidence for impairment of energy metabolism in vivo in Huntington's disease using localized 1H NMR spectroscopy. *Neurology.,* **43,** 2689-95.

51. **Jenkins, B.G., Rosas, H.D., Chen, Y.C., Makabe, T., Myers, R., MacDonald, M., Rosen, B.R., Beal, M.F. and Koroshetz, W.J.** (1998) 1H NMR spectroscopy studies of Huntington's disease: correlations with CAG repeat numbers. *Neurology.,* **50,** 1357-65.

52. **Browne, S.E. and Beal, M.F.** (2004) The energetics of Huntington's disease. *Neurochem Res.,* **29,** 531-46.

53. **Borlongan, C.V., Koutouzis, T.K. and Sanberg, P.R.** (1997) 3-Nitropropionic acid animal model and Huntington's disease. *Neurosci Biobehav Rev.,* **21,** 289-93.

54. **Novelli, A., Reilly, J.A., Lysko, P.G. and Henneberry, R.C.** (1988) Glutamate becomes neurotoxic via the N-methyl-D-aspartate receptor when intracellular energy levels are reduced. *Brain Res,* **451,** 205-12.

55. **Albin, R.L. and Greenamyre, J.T.** (1992) Alternative excitotoxic hypotheses. *Neurology,* **42,** 733-8.

56. **Beal, M.F., Ferrante, R.J., Swartz, K.J. and Kowall, N.W.** (1991) Chronic quinolinic acid lesions in rats closely resemble Huntington's disease. *J Neurosci,* **11,** 1649-59.

57. **Beal, M.F., Kowall, N.W., Ellison, D.W., Mazurek, M.F., Swartz, K.J. and Martin, J.B.** (1986) Replication of the neurochemical characteristics of Huntington's disease by quinolinic acid. *Nature,* **321,** 168-71.

58. **Huang, Q., Zhou, D., Sapp, E., Aizawa, H., Ge, P., Bird, E.D., Vonsattel, J.P. and DiFiglia, M.** (1995) Quinolinic acid-induced increases in calbindin D28k immunoreactivity in rat striatal neurons in vivo and in vitro mimic the pattern seen in Huntington's disease. *Neuroscience,* **65,** 397-407.

59. **Browne, S.E., Ferrante, R.J. and Beal, M.F.** (1999) Oxidative stress in Huntington's disease. *Brain Pathol,* **9,** 147-63.

60. **Dexter, D.T., Carayon, A., Javoy-Agid, F., Agid, Y., Wells, F.R., Daniel, S.E., Lees, A.J., Jenner, P. and Marsden, C.D.** (1991) Alterations in the levels of iron, ferritin and other trace metals in Parkinson's disease and other neurodegenerative diseases affecting the basal ganglia. *Brain,* **114 (Pt 4),** 1953-75.

61. **Dexter, D.T., Jenner, P., Schapira, A.H. and Marsden, C.D.** (1992) Alterations in levels of iron, ferritin, and other trace metals in neurodegenerative diseases affecting the basal ganglia. The Royal Kings and Queens Parkinson's Disease Research Group. *Ann Neurol,* **32 Suppl,** S94-100.

62. **Chen, J.C., Hardy, P.A., Kucharczyk, W., Clauberg, M., Joshi, J.G., Vourlas, A., Dhar, M. and Henkelman, R.M.** (1993) MR of human postmortem brain tissue: correlative study between T2 and assays of iron and ferritin in Parkinson and Huntington disease. *AJNR Am J Neuroradiol.,* **14,** 275-81.

63. **Bartzokis, G., Cummings, J., Perlman, S., Hance, D.B. and Mintz, J.** (1999) Increased basal ganglia iron levels in Huntington disease. *Arch Neurol,* **56,** 569-74.

64. **Bartzokis, G. and Tishler, T.A.** (2000) MRI evaluation of basal ganglia ferritin iron and neurotoxicity in Alzheimer's and Huntingon's disease. *Cell Mol Biol (Noisy-le-grand),* **46,** 821-33.

65. **Ke, Y. and Ming Qian, Z.** (2003) Iron misregulation in the brain: a primary cause of neurodegenerative disorders. *Lancet Neurol,* **2,** 246-53.

66. **Nakamura, K., Jeong, S.Y., Uchihara, T., Anno, M., Nagashima, K., Nagashima, T., Ikeda, S., Tsuji, S. and Kanazawa, I.** (2001) SCA17, a novel autosomal dominant cerebellar ataxia caused by an expanded polyglutamine in TATA-binding protein. *Hum Mol Genet,* **10,** 1441-8.

67. **Zoghbi, H.Y. and Orr, H.T.** (2000) Glutamine repeats and neurodegeneration. *Annual Review of Neuroscience,* **23,** 217-47.

68. **La Spada, A.R., Wilson, E.M., Lubahn, D.B., Harding, A.E. and Fischbeck, K.H.** (1991) Androgen receptor gene mutations in X-linked spinal and bulbar muscular atrophy. *Nature,* **352,** 77-9.

69. **Zhuchenko, O., Bailey, J., Bonnen, P., Ashizawa, T., Stockton, D.W., Amos, C., Dobyns, W.B., Subramony, S.H., Zoghbi, H.Y. and Lee, C.C.** (1997) Autosomal dominant cerebellar ataxia (SCA6) associated with small polyglutamine expansions in the alpha 1A-voltage-dependent calcium channel. *Nat Genet,* **15,** 62-9.

70. **Gatchel, J.R. and Zoghbi, H.Y.** (2005) Diseases of unstable repeat expansion: mechanisms and common principles. *Nat Rev Genet,* **6,** 743-55.

71. **Mangiarini, L., Sathasivam, K., Seller, M., Cozens, B., Harper, A., Hetherington, C., Lawton, M., Trottier, Y., Lehrach, H., Davies, S.W. and Bates, G.P.** (1996) Exon 1 of the HD gene with an expanded CAG repeat is sufficient to cause a progressive neurological phenotype in transgenic mice. *Cell,* **87,** 493-506.

72. **Ordway, J.M., Tallaksen-Greene, S., Gutekunst, C.A., Bernstein, E.M., Cearley, J.A., Wiener, H.W., Dure, L.S., Lindsey, R., Hersch, S.M., Jope, R.S., Albin, R.L. and Detloff, P.J.** (1997) Ectopically expressed CAG repeats cause intranuclear inclusions and a progressive late onset neurological phenotype in the mouse. *Cell,* **91,** 753-63.

73. **Faber, P.W., Alter, J.R., MacDonald, M.E. and Hart, A.C.** (1999) Polyglutamine-mediated dysfunction and apoptotic death of a Caenorhabditis elegans sensory neuron. *Proceedings of the National Academy of Sciences of the United States of America,* **96,** 179-84.

74. **Miller, V.M., Nelson, R.F., Gouvion, C.M., Williams, A., Rodriguez-Lebron, E., Harper, S.Q., Davidson, B.L., Rebagliati, M.R. and Paulson, H.L.** (2005) CHIP suppresses polyglutamine aggregation and toxicity in vitro and in vivo. *J Neurosci,* **25,** 9152-61.

75. **Jackson, G.R., Salecker, I., Dong, X., Yao, X., Arnheim, N., Faber, P.W., MacDonald, M.E. and Zipursky, S.L.** (1998) Polyglutamine-expanded human huntingtin transgenes induce degeneration of Drosophila photoreceptor neurons. *Neuron,* **21,** 633-42.

76. **Warrick, J.M., Paulson, H.L., Gray_Board, G.L., Bui, Q.T., Fischbeck, K.H., Pittman, R.N. and Bonini, N.M.** (1998) Expanded polyglutamine protein forms nuclear inclusions and causes neural degeneration in Drosophila. *Cell,* **93,** 939-49.

77. **Meriin, A.B., Zhang, X., He, X., Newnam, G.P., Chernoff, Y.O. and Sherman, M.Y.** (2002) Huntingtin toxicity in yeast model depends on polyglutamine aggregation mediated by a prion-like protein Rnq1. *J Cell Biol,* **157,** 997-1004.

78. **Arrasate, M., Mitra, S., Schweitzer, E.S., Segal, M.R. and Finkbeiner, S.** (2004) Inclusion body formation reduces levels of mutant huntingtin and the risk of neuronal death. *Nature,* **431,** 805-10.

79. **Reddy, P.H., Williams, M., Charles, V., Garrett, L., Pike_Buchanan, L., Whetsell, W.O., Miller, G. and Tagle, D.A.** (1998) Behavioural abnormalities and selective neuronal loss in HD transgenic mice expressing mutated full-length HD cDNA. *Nature Genetics,* **20,** 198-202.

80. **Hodgson, J.G., Agopyan, N., Gutekunst, C.A., Leavitt, B.R., LePiane, F., Singaraja, R., Smith, D.J., Bissada, N., McCutcheon, K., Nasir, J., Jamot, L., Li, X.J., Stevens, M.E., Rosemond, E., Roder, J.C., Phillips, A.G., Rubin, E.M., Hersch, S.M. and Hayden, M.R.** (1999) A YAC mouse model for Huntington's disease with full-length mutant huntingtin, cytoplasmic toxicity, and selective striatal neurodegeneration. *Neuron,* **23,** 181-92.

81. **Martindale, D., Hackam, A., Wieczorek, A., Ellerby, L., Wellington, C., McCutcheon, K., Singaraja, R., Kazemi_Esfarjani, P., Devon, R., Kim, S.U., Bredesen, D.E., Tufaro, F. and Hayden, M.R.** (1998) Length of huntingtin and its polyglutamine tract influences localization and frequency of intracellular aggregates. *Nature Genetics,* **18,** 150-4.

82. **Marsh, J.L., Walker, H., Theisen, H., Zhu, Y.Z., Fielder, T., Purcell, J. and Thompson, L.M.** (2000) Expanded polyglutamine peptides alone are intrinsically cytotoxic and cause neurodegeneration in Drosophila. *Human Molecular Genetics,* **9,** 13-25.

83. **Davies, S.W., Turmaine, M., Cozens, B.A., DiFiglia, M., Sharp, A.H., Ross, C.A., Scherzinger, E., Wanker, E.E., Mangiarini, L. and Bates, G.P.** (1997) Formation of neuronal intranuclear inclusions underlies the neurological dysfunction in mice transgenic for the HD mutation. *Cell,* **90,** 537-48.

84. **Sapp, E., Penney, J., Young, A., Aronin, N., Vonsattel, J.P. and DiFiglia, M.** (1999) Axonal transport of N-terminal huntingtin suggests early pathology of corticostriatal projections in Huntington disease. *J Neuropathol Exp Neurol,* **58,** 165-73.

85. **DiFiglia, M., Sapp, E., Chase, K.O., Davies, S.W., Bates, G.P., Vonsattel, J.P. and Aronin, N.** (1997) Aggregation of huntingtin in neuronal intranuclear inclusions and dystrophic neurites in brain. *Science,* **277,** 1990-3.

86. **Aronin, N., Kim, M., Laforet, G. and DiFiglia, M.** (1999) Are there multiple pathways in the pathogenesis of Huntington's disease? *Philos Trans R Soc Lond B Biol Sci,* **354,** 995-1003.

87. **Scherzinger, E., Lurz, R., Turmaine, M., Mangiarini, L., Hollenbach, B., Hasenbank, R., Bates, G.P., Davies, S.W., Lehrach, H. and Wanker, E.E.** (1997) Huntingtin-encoded polyglutamine expansions form amyloid-like protein aggregates in vitro and in vivo. *Cell,* **90,** 549-58.

88. **Aronin, N., Chase, K., Young, C., Sapp, E., Schwarz, C., Matta, N., Kornreich, R., Landwehrmeyer, B., Bird, E., Beal, M.F. et al.** (1995) CAG expansion affects the expression of mutant Huntingtin in the Huntington's disease brain. *Neuron,* **15,** 1193-201.

89. **Calabresi, V., Guida, S., Servadio, A. and Jodice, C.** (2001) Phenotypic effects of expanded ataxin-1 polyglutamines with interruptions in vitro. *Brain Research Bulletin,* **56,** 337-42.

90. **Trottier, Y., Lutz, Y., Stevanin, G., Imbert, G., Devys, D., Cancel, G., Saudou, F., Weber, C., David, G., Tora, L., Agid, Y., Brice, A. and Mandel, J.L.** (1995) Polyglutamine expansion as a pathological epitope in Huntington's disease and four dominant cerebellar ataxias. *Nature,* **378,** 403-6.

91. **White, J.K., Auerbach, W., Duyao, M.P., Vonsattel, J.P., Gusella, J.F., Joyner, A.L. and MacDonald, M.E.** (1997) Huntingtin is required for neurogenesis and is not impaired by the Huntington's disease CAG expansion. *Nature Genetics,* **17,** 404-10.

92. **Rubinsztein, D.C. and Carmichael, J.** (2003) Huntington's disease: molecular basis of neurodegeneration. *Expert Rev Mol Med.,* **2003,** 1-21.

93. **Sisodia, S.S.** (1998) Nuclear inclusions in glutamine repeat disorders: are they pernicious, coincidental, or beneficial? *Cell.,* **95,** 1-4.

94. **Kuemmerle, S., Gutekunst, C.A., Klein, A.M., Li, X.J., Li, S.H., Beal, M.F., Hersch, S.M. and Ferrante, R.J.** (1999) Huntington aggregates may not predict neuronal death in Huntington's disease. *Ann Neurol,* **46,** 842-9.

95. **Orr, H.T.** (2001) Beyond the Qs in the polyglutamine diseases. *Genes Dev,* **15,** 925-32.

96. **La Spada, A.R. and Taylor, J.P.** (2003) Polyglutamines placed into context. *Neuron.,* **38,** 681-4.

97. **Emamian, E.S., Kaytor, M.D., Duvick, L.A., Zu, T., Tousey, S.K., Zoghbi, H.Y., Clark, H.B. and Orr, H.T.** (2003) Serine 776 of ataxin-1 is critical for polyglutamine-induced disease in SCA1 transgenic mice. *Neuron,* **38,** 375-87.

98. **Katsuno, M., Adachi, H., Kume, A., Li, M., Nakagomi, Y., Niwa, H., Sang, C., Kobayashi, Y., Doyu, M. and Sobue, G.** (2002) Testosterone reduction prevents phenotypic expression in a transgenic mouse model of spinal and bulbar muscular atrophy. *Neuron,* **35,** 843-54.

99. **Schmidt, B.J., Greenberg, C.R., Allingham-Hawkins, D.J. and Spriggs, E.L.** (2002) Expression of X-linked bulbospinal muscular atrophy (Kennedy disease) in two homozygous women. *Neurology,* **59,** 770-2.

100. **Matsuyama, Z., Wakamori, M., Mori, Y., Kawakami, H., Nakamura, S. and Imoto, K.** (1999) Direct alteration of the P/Q-type Ca2+ channel property by polyglutamine expansion in spinocerebellar ataxia 6. *J Neurosci,* **19,** RC14.

101. **Restituito, S., Thompson, R.M., Eliet, J., Raike, R.S., Riedl, M., Charnet, P. and Gomez, C.M.** (2000) The polyglutamine expansion in spinocerebellar ataxia type 6 causes a beta subunit-specific enhanced activation of P/Q-type calcium channels in Xenopus oocytes. *J Neurosci,* **20,** 6394-403.

102. **Frontali, M.** (2001) Spinocerebellar ataxia type 6: channelopathy or glutamine repeat disorder? *Brain Res Bull,* **56,** 227-31.

103. **Dejager, S., Bry-Gauillard, H., Bruckert, E., Eymard, B., Salachas, F., LeGuern, E., Tardieu, S., Chadarevian, R., Giral, P. and Turpin, G.** (2002) A comprehensive endocrine description of Kennedy's disease revealing androgen insensitivity linked to CAG repeat length. *J Clin Endocrinol Metab,* **87,** 3893-901.

104. **Quigley, C.A., De Bellis, A., Marschke, K.B., el-Awady, M.K., Wilson, E.M. and French, F.S.** (1995) Androgen receptor defects: historical, clinical, and molecular perspectives. *Endocr Rev,* **16,** 271-321.

105. **Cattaneo, E., Zuccato, C. and Tartari, M.** (2005) Normal huntingtin function: an alternative approach to Huntington's disease. *Nat Rev Neurosci.,* **6,** 919-30.

106. **Harjes, P. and Wanker, E.E.** (2003) The hunt for huntingtin function: interaction partners tell many different stories. *Trends Biochem Sci,* **28,** 425-33.

107. **Schmitt, I., Bachner, D., Megow, D., Henklein, P., Hameister, H., Epplen, J.T. and Riess, O.** (1995) Expression of the Huntington disease gene in rodents: cloning the rat homologue and evidence for downregulation in non-neuronal tissues during development. *Human Molecular Genetics,* **4,** 1173-82.

108. **Landwehrmeyer, G.B., McNeil, S.M., Dure, L.S.t., Ge, P., Aizawa, H., Huang, Q., Ambrose, C.M., Duyao, M.P., Bird, E.D., Bonilla, E. et al.** (1995) Huntington's disease gene: regional and cellular expression in brain of normal and affected individuals. *Ann Neurol,* **37,** 218-30.

109. **Dure, L.S.t., Landwehrmeyer, G.B., Golden, J., McNeil, S.M., Ge, P., Aizawa, H., Huang, Q., Ambrose, C.M., Duyao, M.P., Bird, E.D. et al.** (1994) IT15 gene expression in fetal human brain. *Brain Res.,* **659,** 33-41.

110. **Zeitlin, S., Liu, J.P., Chapman, D.L., Papaioannou, V.E. and Efstratiadis, A.** (1995) Increased apoptosis and early embryonic lethality in mice nullizygous for the Huntington's disease gene homologue. *Nat Genet,* **11,** 155-63.

111. **Duyao, M.P., Auerbach, A.B., Ryan, A., Persichetti, F., Barnes, G.T., McNeil, S.M., Ge, P., Vonsattel, J.P., Gusella, J.F., Joyner, A.L. and MacDonald, M.E.** (1995) Inactivation of the mouse Huntington's disease gene homolog Hdh. *Science,* **269,** 407-10.

112. **Nasir, J., Floresco, S.B., O_Kusky, J.R., Diewert, V.M., Richman, J.M., Zeisler, J., Borowski, A., Marth, J.D., Phillips, A.G. and Hayden, M.R.** (1995) Targeted disruption of the Huntington's disease gene results in embryonic lethality and behavioral and morphological changes in heterozygotes. *Cell,* **81,** 811-23.

113. **Rigamonti, D., Bauer, J.H., De-Fraja, C., Conti, L., Sipione, S., Sciorati, C., Clementi, E., Hackam, A., Hayden, M.R., Li, Y., Cooper, J.K., Ross, C.A., Govoni, S., Vincenz, C. and Cattaneo, E.** (2000) Wild-type huntingtin protects from apoptosis upstream of caspase-3. *J Neurosci,* **20,** 3705-13.

114. **Dragatsis, I., Efstratiadis, A. and Zeitlin, S.** (1998) Mouse mutant embryos lacking huntingtin are rescued from lethality by wild-type extraembryonic tissues. *Development,* **125,** 1529-39.

115. **O'Kusky, J.R., Nasir, J., Cicchetti, F., Parent, A. and Hayden, M.R.** (1999) Neuronal degeneration in the basal ganglia and loss of pallido-subthalamic synapses in mice with targeted disruption of the Huntington's disease gene. *Brain Res,* **818,** 468-79.

116. **Gottfried, M., Lavine, L. and Roessmann, U.** (1981) Neuropathological findings in Wolf-Hirschhorn (4p-) syndrome. *Acta Neuropathol (Berl).* **55,** 163-5.

117. **Wexler, N.S., Young, A.B., Tanzi, R.E., Travers, H., Starosta-Rubinstein, S., Penney, J.B., Snodgrass, S.R., Shoulson, I., Gomez, F., Ramos Arroyo, M.A. et al.** (1987) Homozygotes for Huntington's disease. *Nature.,* **326,** 194-7.

118. **Myers, R.H., Leavitt, J., Farrer, L.A., Jagadeesh, J., McFarlane, H., Mastromauro, C.A., Mark, R.J. and Gusella, J.F.** (1989) Homozygote for Huntington disease. *Am J Hum Genet.,* **45,** 615-8.

119. **Dragatsis, I., Levine, M.S. and Zeitlin, S.** (2000) Inactivation of Hdh in the brain and testis results in progressive neurodegeneration and sterility in mice. *Nat Genet,* **26,** 300-6.

120. **Metzler, M., Chen, N., Helgason, C.D., Graham, R.K., Nichol, K., McCutcheon, K., Nasir, J., Humphries, R.K., Raymond, L.A. and Hayden, M.R.** (1999) Life without huntingtin: normal differentiation into functional neurons. *J Neurochem,* **72,** 1009-18.

121. **Metzler, M., Helgason, C.D., Dragatsis, I., Zhang, T., Gan, L., Pineault, N., Zeitlin, S.O., Humphries, R.K. and Hayden, M.R.** (2000) Huntingtin is required for normal hematopoiesis. *Human Molecular Genetics,* **9,** 387-94.

122. **Reiner, A., Del Mar, N., Meade, C.A., Yang, H., Dragatsis, I., Zeitlin, S. and Goldowitz, D.** (2001) Neurons lacking huntingtin differentially colonize brain and survive in chimeric mice. *J Neurosci,* **21,** 7608-19.

123. **Van Raamsdonk, J.M., Pearson, J., Rogers, D.A., Bissada, N., Vogl, A.W., Hayden, M.R. and Leavitt, B.R.** (2005) Loss of wild-type huntingtin influences motor dysfunction and survival in the YAC128 mouse model of Huntington disease. *Hum Mol Genet.,* **14,** 1379-92.

124. **Ho, L.W., Brown, R., Maxwell, M., Wyttenbach, A. and Rubinsztein, D.C.** (2001) Wild type Huntingtin reduces the cellular toxicity of mutant Huntingtin in mammalian cell models of Huntington's disease. *J Med Genet,* **38,** 450-2.

125. **Leavitt, B.R., Guttman, J.A., Hodgson, J.G., Kimel, G.H., Singaraja, R., Vogl, A.W. and Hayden, M.R.** (2001) Wild-type huntingtin reduces the cellular toxicity of mutant huntingtin in vivo. *Am J Hum Genet,* **68,** 313-24.

126. **Hoffner, G., Kahlem, P. and Djian, P.** (2002) Perinuclear localization of huntingtin as a consequence of its binding to microtubules through an interaction with beta-tubulin: relevance to Huntington's disease. *J Cell Sci,* **115,** 941-8.

127. **Tao, T. and Tartakoff, A.M.** (2001) Nuclear relocation of normal huntingtin. *Traffic,* **2,** 385-94.

128. **Gutekunst, C.A., Levey, A.I., Heilman, C.J., Whaley, W.L., Yi, H., Nash, N.R., Rees, H.D., Madden, J.J. and Hersch, S.M.** (1995) Identification and localization of huntingtin in brain and human lymphoblastoid cell lines with anti-fusion protein antibodies. *Proc Natl Acad Sci U S A,* **92,** 8710-4.

129. **Trottier, Y., Devys, D., Imbert, G., Saudou, F., An, I., Lutz, Y., Weber, C., Agid, Y., Hirsch, E.C. and Mandel, J.L.** (1995) Cellular localization of the Huntington's disease protein and discrimination of the normal and mutated form. *Nat Genet,* **10,** 104-10.

130. **Kegel, K.B., Meloni, A.R., Yi, Y., Kim, Y.J., Doyle, E., Cuiffo, B.G., Sapp, E., Wang, Y., Qin, Z.H., Chen, J.D., Nevins, J.R., Aronin, N. and DiFiglia, M.** (2002) Huntingtin is present in the nucleus, interacts with the transcriptional corepressor C-terminal binding protein, and represses transcription. *The Journal of Biological Chemistry,* **277,** 7466-76.

131. **Sapp, E., Schwarz, C., Chase, K., Bhide, P.G., Young, A.B., Penney, J., Vonsattel, J.P., Aronin, N. and DiFiglia, M.** (1997) Huntingtin localization in brains of normal and Huntington's disease patients. *Annals of Neurology,* **42,** 604-12.

132. **Hoogeveen, A.T., Willemsen, R., Meyer, N., de Rooij, K.E., Roos, R.A., van Ommen, G.J. and Galjaard, H.** (1993) Characterization and localization of the Huntington disease gene product. *Hum Mol Genet,* **2,** 2069-73.

133. **De Rooij, K.E., Dorsman, J.C., Smoor, M.A., Den Dunnen, J.T. and Van Ommen, G.J.** (1996) Subcellular localization of the Huntington's disease gene product in cell lines by immunofluorescence and biochemical subcellular fractionation. *Hum Mol Genet,* **5,** 1093-9.

134. **Tukamoto, T., Nukina, N., Ide, K. and Kanazawa, I.** (1997) Huntington's disease gene product, huntingtin, associates with microtubules in vitro. *Brain Res Mol Brain Res,* **51,** 8-14.

135. **Block-Galarza, J., Chase, K.O., Sapp, E., Vaughn, K.T., Vallee, R.B., DiFiglia, M. and Aronin, N.** (1997) Fast transport and retrograde movement of huntingtin and HAP 1 in axons. *Neuroreport,* **8,** 2247-51.

136. **Velier, J., Kim, M., Schwarz, C., Kim, T.W., Sapp, E., Chase, K., Aronin, N. and DiFiglia, M.** (1998) Wild-type and mutant huntingtins function in vesicle trafficking in the secretory and endocytic pathways. *Exp Neurol,* **152,** 34-40.

137. **Kegel, K.B., Sapp, E., Yoder, J., Cuiffo, B., Sobin, L., Kim, Y.J., Qin, Z.H., Hayden, M.R., Aronin, N., Scott, D.L., Isenberg, G., Goldmann, W.H. and DiFiglia, M.** (2005) Huntingtin associates with acidic phospholipids at the plasma membrane. *J Biol Chem.,* **280,** 36464-73.

138. **Choo, Y.S., Johnson, G.V., MacDonald, M., Detloff, P.J. and Lesort, M.** (2004) Mutant huntingtin directly increases susceptibility of mitochondria to the calcium-induced permeability transition and cytochrome c release. *Hum Mol Genet,* **13,** 1407-20.

139. **Hilditch-Maguire, P., Trettel, F., Passani, L.A., Auerbach, A., Persichetti, F. and MacDonald, M.E.** (2000) Huntingtin: an iron-regulated protein essential for normal nuclear and perinuclear organelles. *Hum Mol Genet,* **9,** 2789-97.

140. **Matsuyama, N., Hadano, S., Onoe, K., Osuga, H., Showguchi-Miyata, J., Gondo, Y. and Ikeda, J.E.** (2000) Identification and characterization of the miniature pig Huntington's disease gene homolog: evidence for conservation and polymorphism in the CAG triplet repeat. *Genomics,* **69,** 72-85.

141. **Karlovich, C.A., John, R.M., Ramirez, L., Stainier, D.Y. and Myers, R.M.** (1998) Characterization of the Huntington's disease (HD) gene homologue in the zebrafish Danio rerio. *Gene,* **217,** 117-25.

142. **Lin, B., Nasir, J., MacDonald, H., Hutchinson, G., Graham, R.K., Rommens, J.M. and Hayden, M.R.** (1994) Sequence of the murine Huntington disease gene: evidence for conservation, alternate splicing and polymorphism in a triplet (CCG) repeat [corrected]. *Hum Mol Genet,* **3,** 85-92.

143. **Baxendale, S., Abdulla, S., Elgar, G., Buck, D., Berks, M., Micklem, G., Durbin, R., Bates, G., Brenner, S. and Beck, S.** (1995) Comparative sequence analysis of the human and pufferfish Huntington's disease genes. *Nat Genet,* **10,** 67-76.

144. **Barnes, G.T., Duyao, M.P., Ambrose, C.M., McNeil, S., Persichetti, F., Srinidhi, J., Gusella, J.F. and MacDonald, M.E.** (1994) Mouse Huntington's disease gene homolog (Hdh). *Somat Cell Mol Genet,* **20,** 87-97.

145. **Li, Z., Karlovich, C.A., Fish, M.P., Scott, M.P. and Myers, R.M.** (1999) A putative Drosophila homolog of the Huntington's disease gene. *Human Molecular Genetics,* **8,** 1807-15.

146. **Kauffman, J.S., Zinovyeva, A., Yagi, K., Makabe, K.W. and Raff, R.A.** (2003) Neural expression of the Huntington's disease gene as a chordate evolutionary novelty. *J Exp Zoolog B Mol Dev Evol,* **297,** 57-64.

147. **Takano, H. and Gusella, J.F.** (2002) The predominantly HEAT-like motif structure of huntingtin and its association and coincident nuclear entry with dorsal, an NF-kB/Rel/dorsal family transcription factor. *BMC Neurosci,* **3,** 15.

148. **Rao, A.U., Carta, L.K., Lesuisse, E. and Hamza, I.** (2005) Lack of heme synthesis in a free-living eukaryote. *Proc Natl Acad Sci U S A,* **102,** 4270-5.

149. **Andrew, S.E., Goldberg, Y.P., Theilmann, J., Zeisler, J. and Hayden, M.R.** (1994) A CCG repeat polymorphism adjacent to the CAG repeat in the Huntington disease gene: implications for diagnostic accuracy and predictive testing. *Hum Mol Genet,* **3,** 65-7.

150. **Gerber, H.P., Seipel, K., Georgiev, O., Hofferer, M., Hug, M., Rusconi, S. and Schaffner, W.** (1994) Transcriptional activation modulated by homopolymeric glutamine and proline stretches. *Science,* **263,** 808-11.

151. **Andrade, M.A. and Bork, P.** (1995) HEAT repeats in the Huntington's disease protein. *Nature Genetics,* **11,** 115-6.

152. **Neuwald, A.F. and Hirano, T.** (2000) HEAT repeats associated with condensins, cohesins, and other complexes involved in chromosome-related functions. *Genome Res,* **10,** 1445-52.

153. **Xia, J., Lee, D.H., Taylor, J., Vandelft, M. and Truant, R.** (2003) Huntingtin contains a highly conserved nuclear export signal. *Hum Mol Genet,* **12,** 1393-403.

154. **Steffan, J.S., Agrawal, N., Pallos, J., Rockabrand, E., Trotman, L.C., Slepko, N., Illes, K., Lukacsovich, T., Zhu, Y.Z., Cattaneo, E., Pandolfi, P.P., Thompson, L.M. and Marsh, J.L.** (2004) SUMO modification of Huntingtin and Huntington's disease pathology. *Science,* **304,** 100-4.

155. **Yanai, A., Huang, K., Kang, R., Singaraja, R.R., Arstikaitis, P., Gan, L., Orban, P.C., Mullard, A., Cowan, C.M., Raymond, L.A., Drisdel, R.C., Green, W.N., Ravikumar, B., Rubinsztein, D.C., El-Husseini, A. and Hayden, M.R.** (2006) Palmitoylation of huntingtin by HIP14is essential for its trafficking and function. *Nat Neurosci.,* **9,** 824-31.

156. **Huang, K., Yanai, A., Kang, R., Arstikaitis, P., Singaraja, R.R., Metzler, M., Mullard, A., Haigh, B., Gauthier-Campbell, C., Gutekunst, C.A., Hayden, M.R. and El-Husseini, A.** (2004) Huntingtin-interacting protein HIP14 is a palmitoyl transferase involved in palmitoylation and trafficking of multiple neuronal proteins. *Neuron,* **44,** 977-86.

157. **Humbert, S., Bryson, E.A., Cordelieres, F.P., Connors, N.C., Datta, S.R., Finkbeiner, S., Greenberg, M.E. and Saudou, F.** (2002) The IGF-1/Akt pathway is neuroprotective in Huntington's disease and involves Huntingtin phosphorylation by Akt. *Dev Cell,* **2,** 831-7.

158. **Luo, S., Vacher, C., Davies, J.E. and Rubinsztein, D.C.** (2005) Cdk5 phosphorylation of huntingtin reduces its cleavage by caspases: implications for mutant huntingtin toxicity. *J Cell Biol,* **169,** 647-56.

159. **Wellington, C.L., Ellerby, L.M., Hackam, A.S., Margolis, R.L., Trifiro, M.A., Singaraja, R., McCutcheon, K., Salvesen, G.S., Propp, S.S., Bromm, M., Rowland, K.J., Zhang, T., Rasper, D., Roy, S., Thornberry, N., Pinsky, L., Kakizuka, A., Ross, C.A., Nicholson, D.W., Bredesen, D.E. and Hayden, M.R.** (1998) Caspase cleavage of gene products associated with triplet expansion disorders generates truncated fragments containing the polyglutamine tract. *Journal of Biological Chemistry,* **273,** 9158-67.

160. **Wellington, C.L., Singaraja, R., Ellerby, L., Savill, J., Roy, S., Leavitt, B., Cattaneo, E., Hackam, A., Sharp, A., Thornberry, N., Nicholson, D.W., Bredesen, D.E. and Hayden, M.R.** (2000) Inhibiting caspase cleavage of huntingtin reduces toxicity and aggregate formation in neuronal and nonneuronal cells. *The Journal of Biological Chemistry,* **275,** 19831-8.

161. **Gafni, J. and Ellerby, L.M.** (2002) Calpain activation in Huntington's disease. *J Neurosci,* **22,** 4842-9.

162. **Gafni, J., Hermel, E., Young, J.E., Wellington, C.L., Hayden, M.R. and Ellerby, L.M.** (2004) Inhibition of calpain cleavage of huntingtin reduces toxicity: accumulation of calpain/caspase fragments in the nucleus. *J Biol Chem,* **279,** 20211-20.

163. **Ona, V.O., Li, M., Vonsattel, J.P., Andrews, L.J., Khan, S.Q., Chung, W.M., Frey, A.S., Menon, A.S., Li, X.J., Stieg, P.E., Yuan, J., Penney, J.B., Young, A.B., Cha, J.H. and Friedlander, R.M.** (1999) Inhibition of caspase-1 slows disease progression in a mouse model of Huntington's disease. *Nature,* **399,** 263-7.

164. **Graham, R.K., Deng, Y., Slow, E.J., Haigh, B., Bissada, N., Lu, G., Pearson, J., Shehadeh, J., Bertram, L., Murphy, Z., Warby, S.C., Doty, C.N., Roy, S., Wellington, C.L., Leavitt, B.R., Raymond, L.A., Nicholson, D.W. and Hayden, M.R.** (2006) Cleavage at the caspase-6 site is required for neuronal dysfunction and degeneration due to mutant huntingtin. *Cell,* **125,** 1179-91.

165. **Warby, S.C., Chan, E.Y., Metzler, M., Gan, L., Singaraja, R.R., Crocker, S.F., Robertson, H.A. and Hayden, M.R.** (2005) Huntingtin phosphorylation on serine 421 is significantly reduced in the striatum and by polyglutamine expansion in vivo. *Hum Mol Genet,* **14,** 1569-77.

166. **Faber, P.W., Barnes, G.T., Srinidhi, J., Chen, J., Gusella, J.F. and MacDonald, M.E.** (1998) Huntingtin interacts with a family of WW domain proteins. *Hum Mol Genet,* **7,** 1463-74.

167. **Peters, M.F. and Ross, C.A.** (2001) Isolation of a 40-kDa Huntingtin-associated protein. *J Biol Chem,* **276,** 3188-94.

168. **Holbert, S., Denghien, I., Kiechle, T., Rosenblatt, A., Wellington, C., Hayden, M.R., Margolis, R.L., Ross, C.A., Dausset, J., Ferrante, R.J. and Neri, C.** (2001) The Gln-Ala repeat transcriptional activator CA150 interacts with huntingtin: neuropathologic and genetic evidence for a role in Huntington's disease pathogenesis. *Proc Natl Acad Sci U S A,* **98,** 1811-6.

169. **Steffan, J.S., Kazantsev, A., Spasic-Boskovic, O., Greenwald, M., Zhu, Y.Z., Gohler, H., Wanker, E.E., Bates, G.P., Housman, D.E. and Thompson, L.M.** (2000) The Huntington's disease protein interacts with p53 and CREB-binding protein and represses transcription. *Proc Natl Acad Sci U S A,* **97,** 6763-8.

170. **Chai, Y., Wu, L., Griffin, J.D. and Paulson, H.L.** (2001) The role of protein composition in specifying nuclear inclusion formation in polyglutamine disease. *J Biol Chem,* **276,** 44889-97.

171. **Holbert, S., Dedeoglu, A., Humbert, S., Saudou, F., Ferrante, R.J. and Neri, C.** (2003) Cdc42-interacting protein 4 binds to huntingtin: Neuropathologic and biological evidence for a role in Huntington's disease. *Proc Natl Acad Sci U S A,* **25,** 25.

172. **Hattula, K. and Peranen, J.** (2000) FIP-2, a coiled-coil protein, links Huntingtin to Rab8 and modulates cellular morphogenesis. *Curr Biol,* **10,** 1603-6.

173. **Horn, S.C., Lalowski, M., Goehler, H., Droge, A., Wanker, E.E. and Stelzl, U.** (2006) Huntingtin interacts with the receptor sorting family protein GASP2. *J Neural Transm,* **113,** 1081-90.

174. **Goehler, H., Lalowski, M., Stelzl, U., Waelter, S., Stroedicke, M., Worm, U., Droege, A., Lindenberg, K.S., Knoblich, M., Haenig, C., Herbst, M., Suopanki, J., Scherzinger, E., Abraham, C., Bauer, B., Hasenbank, R., Fritzsche, A., Ludewig, A.H., Buessow, K., Coleman, S.H., Gutekunst, C.A., Landwehrmeyer, B.G., Lehrach, H. and Wanker, E.E.** (2004) A protein interaction network links GIT1, an enhancer of huntingtin aggregation, to Huntington's disease. *Mol Cell,* **15,** 853-65.

175. **Liu, Y.F., Deth, R.C. and Devys, D.** (1997) SH3 domain-dependent association of huntingtin with epidermal growth factor receptor signaling complexes. *The Journal of Biological Chemistry,* **272,** 8121-4.

176. **Li, X.J., Li, S.H., Sharp, A.H., Nucifora, F.C., Jr., Schilling, G., Lanahan, A., Worley, P., Snyder, S.H. and Ross, C.A.** (1995) A huntingtin-associated protein enriched in brain with implications for pathology. *Nature,* **378,** 398-402.

177. **Pal, A., Severin, F., Lommer, B., Shevchenko, A. and Zerial, M.** (2006) Huntingtin-HAP40 complex is a novel Rab5 effector that regulates early endosome motility and is up-regulated in Huntington's disease. *J Cell Biol.,* **172,** 605-18.

178. **Kalchman, M.A., Koide, H.B., McCutcheon, K., Graham, R.K., Nichol, K., Nishiyama, K., Kazemi-Esfarjani, P., Lynn, F.C., Wellington, C., Metzler, M., Goldberg, Y.P., Kanazawa, I., Gietz, R.D. and Hayden, M.R.** (1997) HIP1, a human homologue of S. cerevisiae Sla2p, interacts with membrane-associated huntingtin in the brain. *Nat Genet,* **16,** 44-53.

179. **Wanker, E.E., Rovira, C., Scherzinger, E., Hasenbank, R., Walter, S., Tait, D., Colicelli, J. and Lehrach, H.** (1997) HIP-I: a huntingtin interacting protein isolated by the yeast two-hybrid system. *Hum Mol Genet,* **6,** 487-95.

180. **Kalchman, M.A., Graham, R.K., Xia, G., Koide, H.B., Hodgson, J.G., Graham, K.C., Goldberg, Y.P., Gietz, R.D., Pickart, C.M. and Hayden, M.R.** (1996) Huntingtin is ubiquitinated and interacts with a specific ubiquitin-conjugating enzyme. *J Biol Chem,* **271,** 19385-94.

181. **Singaraja, R.R., Hadano, S., Metzler, M., Givan, S., Wellington, C.L., Warby, S., Yanai, A., Gutekunst, C.A., Leavitt, B.R., Yi, H., Fichter, K., Gan, L., McCutcheon, K., Chopra, V., Michel, J., Hersch, S.M., Ikeda, J.E. and Hayden, M.R.** (2002) HIP14, a novel ankyrin domain-containing protein, links huntingtin to intracellular trafficking and endocytosis. *Hum Mol Genet,* **11,** 2815-2828.

182. **Ducker, C.E., Stettler, E.M., French, K.J., Upson, J.J. and Smith, C.D.** (2004) Huntingtin interacting protein 14 is an oncogenic human protein: palmitoyl acyltransferase. *Oncogene,* **23,** 9230-7.

183. **Boutell, J.M., Thomas, P., Neal, J.W., Weston, V.J., Duce, J., Harper, P.S. and Jones, A.L.** (1999) Aberrant interactions of transcriptional repressor proteins with the Huntington's disease gene product, huntingtin. *Human Molecular Genetics,* **8,** 1647-55.

184. **Modregger, J., DiProspero, N.A., Charles, V., Tagle, D.A. and Plomann, M.** (2002) PACSIN 1 interacts with huntingtin and is absent from synaptic varicosities in presymptomatic Huntington's disease brains. *Hum Mol Genet,* **11,** 2547-58.

185. **Sun, Y., Savanenin, A., Reddy, P.H. and Liu, Y.F.** (2001) Polyglutamine-expanded huntingtin promotes sensitization of N-methyl-D-aspartate receptors via post-synaptic density 95. *J Biol Chem,* **276,** 24713-8.

186. **Sittler, A., Walter, S., Wedemeyer, N., Hasenbank, R., Scherzinger, E., Eickhoff, H., Bates, G.P., Lehrach, H. and Wanker, E.E.** (1998) SH3GL3 associates with the Huntingtin exon 1 protein and promotes the formation of polygln-containing protein aggregates. *Molecular Cell,* **2,** 427-36.

187. **Li, S.H., Cheng, A.L., Zhou, H., Lam, S., Rao, M., Li, H. and Li, X.J.** (2002) Interaction of Huntington disease protein with transcriptional activator Sp1. *Mol Cell Biol,* **22,** 1277-87.

188. **Dunah, A.W., Jeong, H., Griffin, A., Kim, Y.M., Standaert, D.G., Hersch, S.M., Mouradian, M.M., Young, A.B., Tanese, N. and Krainc, D.** (2002) Sp1 and TAFII130 transcriptional activity disrupted in early Huntington's disease. *Science,* **296,** 2238-43.

189. **Lopes-Cendes, I., Maciel, P., Kish, S., Gaspar, C., Robitaille, Y., Clark, H.B., Koeppen, A.H., Nance, M., Schut, L., Silveira, I., Coutinho, P., Sequeiros, J. and Rouleau, G.A.** (1996) Somatic mosaicism in the central nervous system in spinocerebellar ataxia type 1 and Machado-Joseph disease. *Ann Neurol,* **40,** 199-206.

190. **Tanaka, F., Reeves, M.F., Ito, Y., Matsumoto, M., Li, M., Miwa, S., Inukai, A., Yamamoto, M., Doyu, M., Yoshida, M., Hashizume, Y., Terao, S., Mitsuma, T. and Sobue, G.** (1999) Tissue-specific somatic mosaicism in spinal and bulbar muscular atrophy is dependent on CAG-repeat length and androgen receptor--gene expression level. *Am J Hum Genet,* **65,** 966-73.

191. **Hashida, H., Goto, J., Suzuki, T., Jeong, S., Masuda, N., Ooie, T., Tachiiri, Y., Tsuchiya, H. and Kanazawa, I.** (2001) Single cell analysis of CAG repeat in brains of dentatorubral-pallidoluysian atrophy (DRPLA). *J Neurol Sci,* **190,** 87-93.

192. **Chong, S.S., McCall, A.E., Cota, J., Subramony, S.H., Orr, H.T., Hughes, M.R. and Zoghbi, H.Y.** (1995) Gametic and somatic tissue-specific heterogeneity of the expanded SCA1 CAG repeat in spinocerebellar ataxia type 1. *Nature Genetics,* **10,** 344-50.

193. **Richards, R.I.** (2001) Dynamic mutations: a decade of unstable expanded repeats in human genetic disease. *Human Molecular Genetics,* **10,** 2187-94.

194. **Benitez, J., Robledo, M., Ramos, C., Ayuso, C., Astarloa, R., Garcia Yebenes, J. and Brambati, B.** (1995) Somatic stability in chorionic villi samples and other Huntington fetal tissues. *Hum Genet.,* **96,** 229-32.

195. **Mangiarini, L., Sathasivam, K., Mahal, A., Mott, R., Seller, M. and Bates, G.P.** (1997) Instability of highly expanded CAG repeats in mice transgenic for the Huntington's disease mutation. *Nature Genetics,* **15,** 197-200.

196. **Wheeler, V.C., Auerbach, W., White, J.K., Srinidhi, J., Auerbach, A., Ryan, A., Duyao, M.P., Vrbanac, V., Weaver, M., Gusella, J.F., Joyner, A.L. and MacDonald, M.E.** (1999) Length-dependent gametic CAG repeat instability in the Huntington's disease knock-in mouse. *Human Molecular Genetics,* **8,** 115-22.

197. **Kennedy, L. and Shelbourne, P.F.** (2000) Dramatic mutation instability in HD mouse striatum: does polyglutamine load contribute to cell-specific vulnerability in Huntington's disease? *Hum Mol Genet,* **9,** 2539-44.

198. **Ishiguro, H., Yamada, K., Sawada, H., Nishii, K., Ichino, N., Sawada, M., Kurosawa, Y., Matsushita, N., Kobayashi, K., Goto, J., Hashida, H., Masuda, N., Kanazawa, I. and Nagatsu, T.** (2001) Age-dependent and tissue-specific CAG repeat instability occurs in mouse knock-in for a mutant Huntington's disease gene. *J Neurosci Res,* **65,** 289-97.

199. **Kennedy, L., Evans, E., Chen, C.M., Craven, L., Detloff, P.J., Ennis, M. and Shelbourne, P.F.** (2003) Dramatic tissue-specific mutation length increases are an early molecular event in Huntington disease pathogenesis. *Hum Mol Genet,* **12,** 3359-67.

200. **Rolfsmeier, M.L. and Lahue, R.S.** (2000) Stabilizing effects of interruptions on trinucleotide repeat expansions in Saccharomyces cerevisiae. *Molecular and Cellular Biology,* **20,** 173-80.

201. **Quan, F., Janas, J. and Popovich, B.W.** (1995) A novel CAG repeat configuration in the SCA1 gene: implications for the molecular diagnostics of spinocerebellar ataxia type 1. *Hum Mol Genet,* **4,** 2411-3.

202. **Matsuyama, Z., Izumi, Y., Kameyama, M., Kawakami, H. and Nakamura, S.** (1999) The effect of CAT trinucleotide interruptions on the age at onset of spinocerebellar ataxia type 1 (SCA1). *J Med Genet,* **36,** 546-8.

203. **Frontali, M., Novelletto, A., Annesi, G. and Jodice, C.** (1999) CAG repeat instability, cryptic sequence variation and pathogeneticity: evidence from different loci. *Philos Trans R Soc Lond B Biol Sci,* **354,** 1089-94.

204. **Kimmel, C.B., Ballard, W.W., Kimmel, S.R., Ullmann, B. and Schilling, T.F.** (1995) Stages of embryonic development of the zebrafish. *Dev Dyn,* **203,** 253-310.

205. **de Jong, J.L. and Zon, L.I.** (2005) Use of the zebrafish system to study primitive and definitive hematopoiesis. *Annu Rev Genet.,* **39,** 481-501.

206. **Watase, K., Venken, K.J., Sun, Y., Orr, H.T. and Zoghbi, H.Y.** (2003) Regional differences of somatic CAG repeat instability do not account for selective neuronal vulnerability in a knock-in mouse model of SCA1. *Hum Mol Genet,* **2,** 2.

207. **Sen, S., Dash, D., Pasha, S. and Brahmachari, S.K.** (2003) Role of histidine interruption in mitigating the pathological effects of long polyglutamine stretches in SCA1: A molecular approach. *Protein Sci.,* **12,** 953-62.

208. **Turner, D.L. and Weintraub, H.** (1994) Expression of achaete-scute homolog 3 in Xenopus embryos converts ectodermal cells to a neural fate. *Genes Dev,* **8,** 1434-47.

209. **Westin, J. and Lardelli, M.** (1997) Three novel Notch genes in zebrafish: Implications for vertebrate Notch gene evolution and function. *Dev. Genes Evol.,* **207,** 51-63.

210. **Sambrook, J., Fritsch, E.F. and Maniatis, T.** (1989) *Molecular Cloning: A laboratory manual.* 2nd edition ed. Cold Spring Harbor Laboratory Press.

211. **Laccone, F., Maiwald, R. and Bingemann, S.** (1999) A fast polymerase chain reaction-mediated strategy for introducing repeat expansions into CAG-repeat containing genes. *Hum Mutat,* **13,** 497-502.

212. **Michalik, A., Kazantsev, A. and Van_Broeckhoven, C.** (2001) Method to introduce stable, expanded, polyglutamine-encoding CAG/CAA trinucleotide repeats into CAG repeat-containing genes. *Biotechniques,* **31,** 250-2, 254.

213. **Westerfield, M.** (1995) *The Zebrafish Book: A guide to the laboratory use of Zebrafish (Danio rerio).* 3 ed. University of Oregon Press, Eugene.

214. **Jowett, T.** (1997) *Tissue in Situ Hybridization: Methods in Animal Development*. Wiley, New York.

215. **Cole, L.K. and Ross, L.S.** (2001) Apoptosis in the developing zebrafish embryo. *Dev Biol,* **240,** 123-42.

216. **Lieschke, G.J., Oates, A.C., Crowhurst, M.O., Ward, A.C. and Layton, J.E.** (2001) Morphologic and functional characterization of granulocytes and macrophages in embryonic and adult zebrafish. *Blood,* **98,** 3087-96.

217. **Sundberg, R.D. and Broman, H.** (1955) The application of the Prussian blue stain to previously stained films of blood and bone marrow. *Blood,* **10,** 160-6.

218. **Pearson, C.E., Edamura, K.N. and Cleary, J.D.** (2005) Repeat instability: mechanisms of dynamic mutations. *Nat Rev Genet.,* **6,** 729-42.

219. **Menalled, L.B. and Chesselet, M.F.** (2002) Mouse models of Huntington's disease. *Trends Pharmacol Sci,* **23,** 32-9.

220. **Rubinsztein, D.C.** (2002) Lessons from animal models of Huntington's disease. *Trends in Genetics,* **18,** 202-9.

221. **Detrich III, H.W., Westerfield, M. and Zon, L.I.** (1999) *The Zebrafish: Biology*. Academic Press, San Diego.

222. **Cartharius, K., Frech, K., Grote, K., Klocke, B., Haltmeier, M., Klingenhoff, A., Frisch, M., Bayerlein, M. and Werner, T.** (2005) MatInspector and beyond: promoter analysis based on transcription factor binding sites. *Bioinformatics,* **21,** 2933-42.

223. **Holzmann, C., Maueler, W., Petersohn, D., Schmidt, T., Thiel, G., Epplen, J.T. and Riess, O.** (1998) Isolation and characterization of the rat huntingtin promoter. *Biochem J,* **336 (Pt 1),** 227-34.

224. **Watase, K., Weeber, E.J., Xu, B., Antalffy, B., Yuva-Paylor, L., Hashimoto, K., Kano, M., Atkinson, R., Sun, Y., Armstrong, D.L., Sweatt, J.D., Orr, H.T., Paylor, R. and Zoghbi, H.Y.** (2002) A long CAG repeat in the mouse Sca1 locus replicates SCA1 features and reveals the impact of protein solubility on selective neurodegeneration. *Neuron,* **34,** 905-19.

225. **Thisse, B., Heyer, V., Lux, A., Alunni, V., Degrave, A., Seiliez, I., Kirchner, J., Parkhill, J.P. and Thisse, C.** (2004) Spatial and temporal expression of the zebrafish genome by large-scale in situ hybridization screening. *Methods Cell Biol,* **77,** 505-19.

226. **Eisenberg, E. and Levanon, E.Y.** (2003) Human housekeeping genes are compact. *Trends Genet,* **19,** 362-5.

227. **Funk, W.D. and Wright, W.E.** (1992) Cyclic amplification and selection of targets for multicomponent complexes: myogenin interacts with factors recognizing binding sites for basic helix-loop-helix, nuclear factor 1, myocyte-specific enhancer-binding factor 2, and COMP1 factor. *Proc Natl Acad Sci U S A,* **89,** 9484-8.

228. **Chon, H., Bluyssen, H.A., Holstege, F.C., Koomans, H.A., Joles, J.A. and Braam, B.** (2005) Gene expression of energy and protein metabolism in hearts of hypertensive nitric oxide- or GSH-depleted mice. *Eur J Pharmacol,* **513,** 21-33.

229. **Bertolino, E., Reimund, B., Wildt-Perinic, D. and Clerc, R.G.** (1995) A novel homeobox protein which recognizes a TGT core and functionally interferes with a retinoid-responsive motif. *J Biol Chem,* **270,** 31178-88.

230. **Yang, Y., Hwang, C.K., D'Souza, U.M., Lee, S.H., Junn, E. and Mouradian, M.M.** (2000) Three-amino acid extension loop homeodomain proteins Meis2 and TGIF differentially regulate transcription. *J Biol Chem,* **275,** 20734-41.

231. **Bertolino, E., Wildt, S., Richards, G. and Clerc, R.G.** (1996) Expression of a novel murine homeobox gene in the developing cerebellar external granular layer during its proliferation. *Dev Dyn,* **205,** 410-20.

232. **Wallis, D. and Muenke, M.** (2000) Mutations in holoprosencephaly. *Hum Mutat,* **16,** 99-108.

233. **Heasman, J.** (2002) Morpholino oligos: making sense of antisense? *Developmental Biology,* **243,** 209-14.

234. **Scheid, P., Pelster, B. and Kobayashi, H.** (1990) Gas exchange in the fish swimbladder. *Adv Exp Med Biol.,* **277,** 735-42.

235. **Pelster, B. and Burggren, W.W.** (1996) Disruption of hemoglobin oxygen transport does not impact oxygen-dependent physiological processes in developing embryos of zebra fish (Danio rerio). *Circ Res,* **79,** 358-62.

236. **Ransom, D.G., Haffter, P., Odenthal, J., Brownlie, A., Vogelsang, E., Kelsh, R.N., Brand, M., van Eeden, F.J., Furutani-Seiki, M., Granato, M., Hammerschmidt, M., Heisenberg, C.P., Jiang, Y.J., Kane, D.A., Mullins, M.C. and Nusslein-Volhard, C.** (1996) Characterization of zebrafish mutants with defects in embryonic hematopoiesis. *Development,* **123,** 311-9.

237. **Weinstein, B.M., Schier, A.F., Abdelilah, S., Malicki, J., Solnica-Krezel, L., Stemple, D.L., Stainier, D.Y., Zwartkruis, F., Driever, W. and Fishman, M.C.** (1996) Hematopoietic mutations in the zebrafish. *Development,* **123,** 303-9.

238. **Wingert, R.A., Brownlie, A., Galloway, J.L., Dooley, K., Fraenkel, P., Axe, J.L., Davidson, A.J., Barut, B., Noriega, L., Sheng, X., Zhou, Y. and Zon, L.I.** (2004) The chianti zebrafish mutant provides a model for erythroid-specific disruption of transferrin receptor 1. *Development,* **131,** 6225-35.

239. **Donovan, A., Brownlie, A., Dorschner, M.O., Zhou, Y., Pratt, S.J., Paw, B.H., Phillips, R.B., Thisse, C., Thisse, B. and Zon, L.I.** (2002) The zebrafish mutant gene chardonnay (cdy) encodes divalent metal transporter 1 (DMT1). *Blood,* **100,** 4655-9.

240. **Donovan, A., Brownlie, A., Zhou, Y., Shepard, J., Pratt, S.J., Moynihan, J., Paw, B.H., Drejer, A., Barut, B., Zapata, A., Law, T.C., Brugnara, C., Lux, S.E., Pinkus, G.S., Pinkus, J.L., Kingsley, P.D., Palis, J., Fleming, M.D., Andrews, N.C. and Zon, L.I.** (2000) Positional cloning of zebrafish ferroportin1 identifies a conserved vertebrate iron exporter. *Nature,* **403,** 776-81.

241. **Huang, X. and Saint-Jeannet, J.P.** (2004) Induction of the neural crest and the opportunities of life on the edge. *Dev Biol,* **275,** 1-11.

242. **Furutani-Seiki, M., Jiang, Y.J., Brand, M., Heisenberg, C.P., Houart, C., Beuchle, D., van Eeden, F.J., Granato, M., Haffter, P., Hammerschmidt, M., Kane, D.A., Kelsh, R.N., Mullins, M.C., Odenthal, J. and Nusslein-Volhard, C.** (1996) Neural degeneration mutants in the zebrafish, Danio rerio. *Development,* **123,** 229-39.

243. **Bonilla, E., Estevez, J., Suarez, H., Morales, L.M., Chacin de Bonilla, L., Villalobos, R. and Davila, J.O.** (1991) Serum ferritin deficiency in Huntington's disease patients. *Neurosci Lett,* **129,** 22-4.

244. **Morrison, P.J. and Nevin, N.C.** (1994) Serum iron, total iron binding capacity and ferritin in early Huntington disease patients. *Ir J Med Sci,* **163,** 236-7.

245. **Schultz, R.M. and Liebman, M.N.** (1993) Proteins II: Structure-Function Relationship of Protein Families. In Devlin, T.M. (ed.), *Textbook of Biochemistry; with Clinical Correlations.* Third ed. Wiley-Liss, New York, pp. 91-134.

246. **Shaw, G.C., Cope, J.J., Li, L., Corson, K., Hersey, C., Ackermann, G.E., Gwynn, B., Lambert, A.J., Wingert, R.A., Traver, D., Trede, N.S., Barut, B.A., Zhou, Y., Minet, E., Donovan, A., Brownlie, A., Balzan, R., Weiss, M.J., Peters, L.L., Kaplan, J., Zon, L.I. and Paw, B.H.** (2006) Mitoferrin is essential for erythroid iron assimilation. *Nature,* **440,** 96-100.

247. **Brownlie, A., Donovan, A., Pratt, S.J., Paw, B.H., Oates, A.C., Brugnara, C., Witkowska, H.E., Sassa, S. and Zon, L.I.** (1998) Positional cloning of the zebrafish sauternes gene: a model for congenital sideroblastic anaemia. *Nat Genet,* **20,** 244-50.

248. **Brownlie, A., Hersey, C., Oates, A.C., Paw, B.H., Falick, A.M., Witkowska, H.E., Flint, J., Higgs, D., Jessen, J., Bahary, N., Zhu, H., Lin, S. and Zon, L.** (2003) Characterization of embryonic globin genes of the zebrafish. *Dev Biol,* **255,** 48-61.

249. **Wingert, R.A., Galloway, J.L., Barut, B., Foott, H., Fraenkel, P., Axe, J.L., Weber, G.J., Dooley, K., Davidson, A.J., Schmid, B., Paw, B.H., Shaw, G.C., Kingsley, P., Palis, J., Schubert, H., Chen, O., Kaplan, J. and Zon, L.I.** (2005) Deficiency of glutaredoxin 5 reveals Fe-S clusters are required for vertebrate haem synthesis. *Nature,* **436,** 1035-39.

250. **Halliwell, B. and Gutteridge, J.M.** (1990) Role of free radicals and catalytic metal ions in human disease: an overview. *Methods Enzymol,* **186,** 1-85.

251. **Aisen, P., Enns, C. and Wessling-Resnick, M.** (2001) Chemistry and biology of eukaryotic iron metabolism. *Int J Biochem Cell Biol,* **33,** 940-59.

252. **Papanikolaou, G. and Pantopoulos, K.** (2005) Iron metabolism and toxicity. *Toxicol Appl Pharmacol,* **202,** 199-211.

253. **Fleming, M.D., Trenor, C.C., 3rd, Su, M.A., Foernzler, D., Beier, D.R., Dietrich, W.F. and Andrews, N.C.** (1997) Microcytic anaemia mice have a mutation in Nramp2, a candidate iron transporter gene. *Nat Genet,* **16,** 383-6.

254. **Gunshin, H., Mackenzie, B., Berger, U.V., Gunshin, Y., Romero, M.F., Boron, W.F., Nussberger, S., Gollan, J.L. and Hediger, M.A.** (1997) Cloning and characterization of a mammalian proton-coupled metal-ion transporter. *Nature,* **388,** 482-8.

255. **McKie, A.T., Barrow, D., Latunde-Dada, G.O., Rolfs, A., Sager, G., Mudaly, E., Mudaly, M., Richardson, C., Barlow, D., Bomford, A., Peters, T.J., Raja, K.B., Shirali, S., Hediger, M.A., Farzaneh, F. and Simpson, R.J.** (2001) An iron-regulated ferric reductase associated with the absorption of dietary iron. *Science,* **291,** 1755-9.

256. **Shayeghi, M., Latunde-Dada, G.O., Oakhill, J.S., Laftah, A.H., Takeuchi, K., Halliday, N., Khan, Y., Warley, A., McCann, F.E., Hider, R.C., Frazer, D.M., Anderson, G.J., Vulpe, C.D., Simpson, R.J. and McKie, A.T.** (2005) Identification of an intestinal heme transporter. *Cell.,* **122,** 789-801.

257. **Vulpe, C.D., Kuo, Y.M., Murphy, T.L., Cowley, L., Askwith, C., Libina, N., Gitschier, J. and Anderson, G.J.** (1999) Hephaestin, a ceruloplasmin homologue implicated in intestinal iron transport, is defective in the sla mouse. *Nat Genet,* **21,** 195-9.

258. **Aisen, P.** (2004) Transferrin receptor 1. *Int J Biochem Cell Biol,* **36,** 2137-43.

259. **Kawabata, H., Yang, R., Hirama, T., Vuong, P.T., Kawano, S., Gombart, A.F. and Koeffler, H.P.** (1999) Molecular cloning of transferrin receptor 2. A new member of the transferrin receptor-like family. *J Biol Chem,* **274,** 20826-32.

260. **Dautry-Varsat, A.** (1986) Receptor-mediated endocytosis: the intracellular journey of transferrin and its receptor. *Biochimie,* **68,** 375-81.

261. **Nishi, T. and Forgac, M.** (2002) The vacuolar (H+)-ATPases--nature's most versatile proton pumps. *Nat Rev Mol Cell Biol,* **3,** 94-103.

262. **Ohgami, R.S., Campagna, D.R., Greer, E.L., Antiochos, B., McDonald, A., Chen, J., Sharp, J.J., Fujiwara, Y., Barker, J.E. and Fleming, M.D.** (2005) Identification of a ferrireductase required for efficient transferrin-dependent iron uptake in erythroid cells. *Nat Genet.,* **37,** 1264-9.

263. **Fleming, M.D., Romano, M.A., Su, M.A., Garrick, L.M., Garrick, M.D. and Andrews, N.C.** (1998) Nramp2 is mutated in the anemic Belgrade (b) rat: evidence of a role for Nramp2 in endosomal iron transport. *Proc Natl Acad Sci U S A.,* **95,** 1148-53.

264. **Ponka, P.** (1997) Tissue-specific regulation of iron metabolism and heme synthesis: distinct control mechanisms in erythroid cells. *Blood,* **89,** 1-25.

265. **Brzoska, K., Meczynska, S. and Kruszewski, M.** (2006) Iron-sulfur cluster proteins: electron transfer and beyond. *Acta Biochim Pol,* **53,** 685-91.

266. **Atamna, H., Walter, P.B. and Ames, B.N.** (2002) The role of heme and iron-sulfur clusters in mitochondrial biogenesis, maintenance, and decay with age. *Arch Biochem Biophys,* **397,** 345-53.

267. **Fitzpatrick, P.F.** (1999) Tetrahydropterin-dependent amino acid hydroxylases. *Annu Rev Biochem,* **68,** 355-81.

268. **Harrison, P.M. and Arosio, P.** (1996) The ferritins: molecular properties, iron storage function and cellular regulation. *Biochim Biophys Acta,* **1275,** 161-203.

269. **Ajioka, R.S., Phillips, J.D. and Kushner, J.P.** (2006) Biosynthesis of heme in mammals. *Biochim Biophys Acta,* **3,** 3.

270. **Wang, H., Long, Q., Marty, S.D., Sassa, S. and Lin, S.** (1998) A zebrafish model for hepatoerythropoietic porphyria. *Nat Genet.,* **20,** 239-43.

271. **Childs, S., Weinstein, B.M., Mohideen, M.A., Donohue, S., Bonkovsky, H. and Fishman, M.C.** (2000) Zebrafish dracula encodes ferrochelatase and its mutation provides a model for erythropoietic protoporphyria. *Curr Biol.,* **10,** 1001-4.

272. **Baravalle, G., Schober, D., Huber, M., Bayer, N., Murphy, R.F. and Fuchs, R.** (2005) Transferrin recycling and dextran transport to lysosomes is differentially affected by bafilomycin, nocodazole, and low temperature. *Cell Tissue Res,* **320,** 99-113.

273. **Daro, E., van der Sluijs, P., Galli, T. and Mellman, I.** (1996) Rab4 and cellubrevin define different early endosome populations on the pathway of transferrin receptor recycling. *Proc Natl Acad Sci U S A.,* **93,** 9559-64.

274. **McGraw, T.E., Dunn, K.W. and Maxfield, F.R.** (1993) Isolation of a temperature-sensitive variant Chinese hamster ovary cell line with a morphologically altered endocytic recycling compartment. *J Cell Physiol.,* **155,** 579-94.

275. **Engelender, S., Sharp, A.H., Colomer, V., Tokito, M.K., Lanahan, A., Worley, P., Holzbaur, E.L. and Ross, C.A.** (1997) Huntingtin-associated protein 1 (HAP1) interacts with the p150Glued subunit of dynactin. *Hum Mol Genet,* **6,** 2205-12.

276. **Li, S.H., Gutekunst, C.A., Hersch, S.M. and Li, X.J.** (1998) Interaction of huntingtin-associated protein with dynactin P150Glued. *J Neurosci,* **18,** 1261-9.

277. **Gauthier, L.R., Charrin, B.C., Borrell-Pages, M., Dompierre, J.P., Rangone, H., Cordelieres, F.P., De Mey, J., MacDonald, M.E., Lessmann, V., Humbert, S. and Saudou, F.** (2004) Huntingtin controls neurotrophic support and survival of neurons by enhancing BDNF vesicular transport along microtubules. *Cell,* **118,** 127-38.

278. **Gunawardena, S., Her, L.S., Brusch, R.G., Laymon, R.A., Niesman, I.R., Gordesky-Gold, B., Sintasath, L., Bonini, N.M. and Goldstein, L.S.** (2003) Disruption of axonal transport by loss of huntingtin or expression of pathogenic polyQ proteins in Drosophila. *Neuron,* **40,** 25-40.

279. **Zerial, M. and McBride, H.** (2001) Rab proteins as membrane organizers. *Nat Rev Mol Cell Biol.,* **2,** 107-17.

280. **Drake, B.L. and Head, J.R.** (1990) Transferrin receptor expression in early postimplantation mouse trophoblast and associated tissues. *Placenta,* **11,** 535-47.

281. **Young, D., Klemm, A.R., Beckman, D.A., Brent, R.L. and Lloyd, J.B.** (1997) Uptake and processing of 59Fe-labelled and 125I-labelled rat transferrin by early organogenesis rat conceptuses in vitro. *Placenta,* **18,** 553-62.

282. **Adamson, E.D.** (1982) The location and synthesis of transferrin in mouse embryos and teratocarcinoma cells. *Dev Biol,* **91,** 227-34.

283. **Liew, Y.F., Shaw, N.S., Li, X., Li, F., Liao, Q., Konstantinova, S.G., Jordanova, N.G., Russanov, E.M., Oexle, H., Gnaiger, E. and Weiss, G.** (2005) Mitochondrial cysteine desulfurase iron-sulfur cluster S and aconitase are post-transcriptionally regulated by dietary iron in skeletal muscle of rats. *J Nutr.,* **135,** 2151-8.

284. **Arenas, J., Campos, Y., Ribacoba, R., Martin, M.A., Rubio, J.C., Ablanedo, P. and Cabello, A.** (1998) Complex I defect in muscle from patients with Huntington's disease. *Ann Neurol,* **43,** 397-400.

285. **Lipschitz, D.A., Cook, J.D. and Finch, C.A.** (1974) A clinical evaluation of serum ferritin as an index of iron stores. *N Engl J Med.,* **290,** 1213-6.

286. **Koroshetz, W.J., Jenkins, B.G., Rosen, B.R. and Beal, M.F.** (1997) Energy metabolism defects in Huntington's disease and effects of coenzyme Q10. *Ann Neurol.,* **41,** 160-5.

287. **Lodi, R., Schapira, A.H., Manners, D., Styles, P., Wood, N.W., Taylor, D.J. and Warner, T.T.** (2000) Abnormal in vivo skeletal muscle energy metabolism in Huntington's disease and dentatorubropallidoluysian atrophy. *Ann Neurol.,* **48,** 72-6.

288. **Saft, C., Zange, J., Andrich, J., Muller, K., Lindenberg, K., Landwehrmeyer, B., Vorgerd, M., Kraus, P.H., Przuntek, H. and Schols, L.** (2005) Mitochondrial impairment in patients and asymptomatic mutation carriers of Huntington's disease. *Mov Disord,* **20,** 674-9.

289. **Seong, I.S., Ivanova, E., Lee, J.M., Choo, Y.S., Fossale, E., Anderson, M., Gusella, J.F., Laramie, J.M., Myers, R.H., Lesort, M. and MacDonald, M.E.** (2005) HD CAG repeat implicates a dominant property of huntingtin in mitochondrial energy metabolism. *Hum Mol Genet.,* **14,** 2871-80.

290. **Oexle, H., Gnaiger, E. and Weiss, G.** (1999) Iron-dependent changes in cellular energy metabolism: influence on citric acid cycle and oxidative phosphorylation. *Biochim Biophys Acta.,* **1413,** 99-107.

291. **Browne, S.E., Wheeler, V., White, J.K., Fuller, S.W., MacDonald, M. and Beal, M.F.** (1999) Dose-dependent alterations in local cerebral glucose use associated with the huntingtin mutation in Hdh CAG knock-in transgenic mice. *Soc. Neurosci. Abstr.,* **25**.

292. **Gregorio, J., DiMauro, J.-P.P., Narr, S., Fuller, S.W. and Browne, S.E.** (2002) Cerebral metabolism defects in HD: Glucose utilization abnormalities in multiple HD mouse models. *Soc. Neurosci. Abstr.,* **28**.

293. **Feigin, A., Leenders, K.L., Moeller, J.R., Missimer, J., Kuenig, G., Spetsieris, P., Antonini, A. and Eidelberg, D.** (2001) Metabolic network abnormalities in early Huntington's disease: an [(18)F]FDG PET study. *J Nucl Med.,* **42,** 1591-5.

294. **Kuwert, T., Lange, H.W., Langen, K.J., Herzog, H., Aulich, A. and Feinendegen, L.E.** (1990) Cortical and subcortical glucose consumption measured by PET in patients with Huntington's disease. *Brain.,* **113,** 1405-23.

295. **Kuhl, D.E., Markham, C.H., Metter, E.J., Riege, W.H., Phelps, M.E. and Mazziotta, J.C.** (1985) Local cerebral glucose utilization in symptomatic and presymptomatic Huntington's disease. *Res Publ Assoc Res Nerv Ment Dis.,* **63,** 199-209.

296. **Mancuso, M., Davidzon, G., Kurlan, R.M., Tawil, R., Bonilla, E., Di Mauro, S. and Powers, J.M.** (2005) Hereditary ferritinopathy: a novel mutation, its cellular pathology, and pathogenetic insights. *J Neuropathol Exp Neurol.,* **64,** 280-94.

297. **Curtis, A.R., Fey, C., Morris, C.M., Bindoff, L.A., Ince, P.G., Chinnery, P.F., Coulthard, A., Jackson, M.J., Jackson, A.P., McHale, D.P., Hay, D., Barker, W.A., Markham, A.F., Bates, D., Curtis, A. and Burn, J.** (2001) Mutation in the gene encoding ferritin light polypeptide causes dominant adult-onset basal ganglia disease. *Nat Genet,* **28,** 350-4.

298. **Levi, S., Cozzi, A. and Arosio, P.** (2005) Neuroferritinopathy: a neurodegenerative disorder associated with L-ferritin mutation. *Best Pract Res Clin Haematol.,* **18,** 265-76.

299. **Pandolfo, M.** (2002) Iron metabolism and mitochondrial abnormalities in Friedreich ataxia. *Blood Cells Mol Dis,* **29,** 536-47; discussion 548-52.

300. **Rotig, A., de Lonlay, P., Chretien, D., Foury, F., Koenig, M., Sidi, D., Munnich, A. and Rustin, P.** (1997) Aconitase and mitochondrial iron-sulphur protein deficiency in Friedreich ataxia. *Nat Genet.,* **17,** 215-7.

301. **Seznec, H., Simon, D., Bouton, C., Reutenauer, L., Hertzog, A., Golik, P., Procaccio, V., Patel, M., Drapier, J.C., Koenig, M. and Puccio, H.** (2005) Friedreich ataxia: the oxidative stress paradox. *Hum Mol Genet.,* **14,** 463-74.

302. **Wilson, R.B., Lynch, D.R., Farmer, J.M., Brooks, D.G. and Fischbeck, K.H.** (2000) Increased serum transferrin receptor concentrations in Friedreich ataxia. *Ann Neurol.,* **47,** 659-61.

303. **Szebenyi, G., Morfini, G.A., Babcock, A., Gould, M., Selkoe, K., Stenoien, D.L., Young, M., Faber, P.W., MacDonald, M.E., McPhaul, M.J. and Brady, S.T.** (2003) Neuropathogenic forms of huntingtin and androgen receptor inhibit fast axonal transport. *Neuron,* **40,** 41-52.

304. **Wheeler, V.C., White, J.K., Gutekunst, C.A., Vrbanac, V., Weaver, M., Li, X.J., Li, S.H., Yi, H., Vonsattel, J.P., Gusella, J.F., Hersch, S., Auerbach, W., Joyner, A.L. and MacDonald, M.E.** (2000) Long glutamine tracts cause nuclear localization of a novel form of huntingtin in medium spiny striatal neurons in HdhQ92 and HdhQ111 knock-in mice. *Human Molecular Genetics,* **9,** 503-13.

305. **Trettel, F., Rigamonti, D., Hilditch-Maguire, P., Wheeler, V.C., Sharp, A.H., Persichetti, F., Cattaneo, E. and MacDonald, M.E.** (2000) Dominant phenotypes produced by the HD mutation in STHdh(Q111) striatal cells. *Hum Mol Genet,* **9,** 2799-809.

306. **Presley, J.F., Mayor, S., McGraw, T.E., Dunn, K.W. and Maxfield, F.R.** (1997) Bafilomycin A1 treatment retards transferrin receptor recycling more than bulk membrane recycling. *J Biol Chem,* **272,** 13929-36.

307. **van Weert, A.W., Dunn, K.W., Gueze, H.J., Maxfield, F.R., Stoorvogel, W., Johnson, L.S., Pytowski, B. and McGraw, T.E.** (1995) Transport from late endosomes to lysosomes, but not sorting of integral membrane proteins in endosomes, depends on the vacuolar proton pump. *J Cell Biol.,* **130,** 821-34.

308. **Tabrizi, S.J., Workman, J., Hart, P.E., Mangiarini, L., Mahal, A., Bates, G., Cooper, J.M. and Schapira, A.H.** (2000) Mitochondrial dysfunction and free radical damage in the Huntington R6/2 transgenic mouse. *Ann Neurol,* **47,** 80-6.

309. **Haacke, E.M., Cheng, N.Y., House, M.J., Liu, Q., Neelavalli, J., Ogg, R.J., Khan, A., Ayaz, M., Kirsch, W. and Obenaus, A.** (2005) Imaging iron stores in the brain using magnetic resonance imaging. *Magn Reson Imaging,* **23,** 1-25.

310. **Amsterdam, A., Nissen, R.M., Sun, Z., Swindell, E.C., Farrington, S. and Hopkins, N.** (2004) Identification of 315 genes essential for early zebrafish development. *Proc Natl Acad Sci U S A,* **101,** 12792-7.